Mitigation techniques of seismic hazard effects on art objects

Dissertation

submitted to and approved by the

Department of Architecture, Civil Engineering and Environmental Sciences
University of Braunschweig – Institute of Technology

and the

Department of Civil and Environmental Engineering
University of Florence

in candidacy for the degree of a
Doktor-Ingenieur (Dr.-Ing.) /
Dottore di Ricerca in Civil and Environmental Engineering*)

by
Sebastiano Baggio
Born 23.07.1985
from San Martino di Lupari, Italy

Submitted on	01/09/2016
Oral examination on	09/11/2016
Professorial advisors	Prof. Anna Saetta Prof. Martin Empelmann

2018

*) Either the German or the Italian form of the title may be used.

Dedicated to my Family and to all my old and new Friends:
with their help no road is too long
and no goal is too far.

Mitigation techniques of seismic hazard effects on art objects

Short Abstract: In this thesis the problem of preservation of art objects from seismic hazard is dealt with, in particular by defining the seismic demand, the seismic capacity and finally by proposing an adequate methodology for mitigation intervention. Amongst seismic mitigation techniques, seismic isolation, and in particular the use of friction isolator devices, is considered as an effective retrofitting strategy for art objects. Specific tools are developed for optimizing the design phase of the isolation characteristics for Double Concave Curved Surface Sliders (DCCSS), also with the help of numerical simulations. Finally, the entire proposed methodology is applied to a case study concerning the study and design of a seismic isolated base for the *Bust of Francesco I D'Este*, a sculpture carved by Gian Lorenzo Bernini in the 17th century, and housed at the *Palazzo dei Musei in Modena (Italy)*.

Keywords: *Art objects, Cultural Heritage, Sculptures, Seismic hazard, Seismic mitigation techniques*

Acknowledgments

(…) Ci fu un vento impetuoso e gagliardo da spaccare i monti
e spezzare le rocce davanti al Signore, ma il Signore non era nel vento.
Dopo il vento ci fu un terremoto, ma il Signore non era nel terremoto.
Dopo il terremoto ci fu un fuoco, ma il Signore non era nel fuoco.
Dopo il fuoco ci fu il mormorio di un vento leggero.
(1Re 19,11-12)

(…) Now there was a great wind, so strong that it was splitting mountains
and breaking rocks in pieces before the Lord, but the Lord was not in the wind;
and after the wind an earthquake, but the Lord was not in the earthquake;
and after the earthquake a fire, but the Lord was not in the fire;
and after the fire a sound of sheer silence.
(1Kings 19,11-12)

I would like to express my gratitude to all the people involved in this Joint Doctorate: these years I spent in the research field helped me to grow, both culturally and personally.
I gratefully thank the coordinators of this Doctorate, Prof. Fabio Castelli and Prof. Klaus Thiele, for giving me the chance to join this school and to challenge myself in this International experience.
Profound gratitude goes to my tutors, Prof. Martin Empelmann for the patience and the precious advices and to Prof. Anna Saetta for the kind help, the patience and the irreplaceable support.
I thank also Prof. Renato Vitaliani for his clear view of engineering and life, Dr. Luisa Berto for the tireless support to this work and the profitable discussion about it. Thanks to former students of the Ph.D. school, Tommaso, Diego and Irene for their precious support and help.
Also thanks to Eng. Irene Rocca, that helped me a lot during the crucial phases of my work.
Thanks to Dr. Eng. Maria Gabriella Castellano, and Dr. Eng. Samuele Infanti of *FIP Industriale*, for the material support and the knowledge shared during our collaboration.
My last thank is the most important and goes to my family and to all my friends: without their support, I could not take on these three challenging years of studies.

Pictures of Test at FIP facilities are available with courtesy of *FIP Industriale*; pictures and details of tests at *Galleria Estense* of Modena with courtesy of *Galleria Estense* di Modena.

Abstract

In this thesis the preservation of art objects from Seismic Hazard is dealt with, in particular by defining seismic demand, seismic capacity for this kind of object and finally by proposing an adequate methodology for mitigation intervention.

In order to develop suitable mitigation procedures, in particular seismic isolation techniques, the thesis follows the ensuing framework:

- study of seismic demand for art objects which are often located in the upper floors of the hosting building;
- study of seismic capacity of this kind of objects;
- study and review of seismic mitigation techniques, with particular attention to seismic isolator devices as friction isolators;
- development of tools for optimizing the choice of the isolation characteristics for double concave friction pendulum and for the calibration and validation of the numerical model of the friction sliders, with help of numerical simulations;
- development of a case study, concerning the study and design of a seismic isolated base for the Bust of Francesco I d'Este.

Concerning the seismic vulnerability assessment of the art objects, the definition of seismic demand for this kind of objects is not straightforward, since they are often exposed at the upper floors of the hosting building. This leads to the amplification of the seismic action due to the "filter effect" of the building and the height of the object from the ground floor. In this work, Eurocode 8 and NTC 2008 prescriptions about the amplification of the seismic demand for non-structural components (to which the art object is assimilated) are analysed and reviewed with some original contributions of the author.

Concerning the definition of seismic capacity of art objects, different approaches for rigid or for deformable bodies are presented. For the first ones, the rocking and overturning phenomena are briefly recalled. For the second ones, stress analysis approach is discussed.

Once defined the seismic vulnerability, a brief review of the "state of the art" of seismic mitigation intervention is given. For the objectives of this thesis, a particular attention is devoted to seismic isolation systems, among them friction isolators are considered as a valid and promising retrofitting technology for such kind of application. In this study a specific seismic isolation device is studied, i.e. Double Concave Curved Surface Sliders

(DCCSS in the following), usually employed in civil constructions. In particular, due to the needs of Museum exhibitions, the devices have to be properly rescaled: therefore, in depth analysis and numerical simulations of the behaviour of the isolation system are needed. In this thesis, it is taken advantage of the extensive experimental campaign performed in Caltrans Laboratories in University of California – San Diego (detailed in Favaretto, 2012) in collaboration with *FIP Industriale*. The main outcome of this phase of the research is the proposal of a suitable calibration process for the main parameters of the DCCSS. Finite Elements simulations of the isolated system under different seismic inputs are also presented with the aim of validating the proposed calibration methods.

To validate the entire proposed methodology, the case study of the seismic isolation intervention of the Bust of *Francesco I d'Este* in Modena is presented and carried out. Evaluation of the seismic input at both ground and second floor, by considering also the influence of the building, vulnerability assessment of the object, mitigation of the seismic hazard with application of the isolation system are therefore presented and discussed. The sculpture, carved by Gian Lorenzo Bernini in the 17th century, is the most valuable piece in the collection of the *Galleria Estense*, located at the second floor of *Palazzo dei Musei*, in Modena city hit by the seismic events of May 2012. Given its geometrical and inertial characteristics, the statue is prone to overturning and a seismic mitigation intervention is needed to prevent damages given by further earthquakes, while matching the stringent requirements of museum exhibitions.

The outcomes of this research may be useful for facing the hot issue of seismic assessments of artistic assets. It is worth mentioning the significant and effective collaboration with *FIP Industriale*, concerning some operative phases of the seismic isolation intervention of the Bust of *Francesco I d'Este*.

Finally, the main results of the whole research are summarized and discussed. In particular, the methodology developed within this research and the tools proposed and validated in the thesis are re-elaborated, with the aim to provide a support to assess and mitigate the seismic hazard effects on art objects, evidencing the main original contribution of the author.

Index of contents

Index of figures

Index of tables

1 Introduction

1.1 Motivation and scope of the research

Safeguard of Cultural Heritage from seismic events is nowadays a compelling task, especially in countries, such as Italy, with a rich artistic asset, often situated in seismic areas (e.g. Lowry et al. 2008, Augusti and Ciampoli 1996).

Indeed, recent seismic events of L'Aquila in 2009 and of Emilia Romagna in 2012 demonstrated once again the importance of dealing with the seismic protection of art objects. Actually, such objects are often housed in ancient buildings with great architectural and cultural value, for which the enhancement of the seismic behaviour with traditional interventions are conflicting with the conservation principia.

The main goal of the proposed research project is to evaluate seismic response and vulnerability level of cultural objects in order to develop suitable mitigation procedures and techniques with particular attention to isolation techniques.

The reference Standards are the "*Italian Guidelines for evaluation and mitigation of seismic-risk to cultural heritage*" (D.P.C.M. 2011), which so far are specifically devoted to masonry constructions and have been re-formulated in Berto et al. (2012), Favaretto (2012) with the aim of extending their principia and the approaches to art and cultural objects.

In this thesis a further development and enhancement of such Standards is proposed with focus on the seismic mitigation aspect.

According to this methodology aimed to evaluate and reduce the seismic risk of the art objects, the following steps are dealt with: 1) the knowledge path, which involves historical research, geometrical survey and material characterization; 2) the characterization of the seismic action of the site; 3) the development of specific methods of analysis, according to the characteristics of the objects and to the required level of accuracy,4) design of suitable intervention for seismic protection (retrofitting strategies) of art objects.

In detail, *vulnerability assessment and seismic risk mitigation* are the main aspects to deal with in this thesis, and the case study of the *Bust of Francesco I d'Este* in Modena is used to validate the entire proposed methodology, and it is believed that the outcomes of this research may be of interest for further seismic assessments of artistic assets.

Concerning the phase of definition of the retrofitting strategy, it is necessary to find a compromise between the structural safety and the conservation principles. In this

research, among the risk mitigation techniques, solutions based on isolation systems are considered as a valid retrofit strategy for art objects. These strategies, which allow to reduce the transferred seismic actions, have been used so far mostly on new constructions throughout the world, but some examples of their application to existing construction and artefacts represent an interesting perspective.
The research takes advantages from the collaboration with *FIP Industriale,* an international firm leader in the production of anti-seismic devices, for the part concerning the seismic isolation intervention of the *Bust of Francesco I d'Este*.

1.2 Overview of the thesis

The contents of each chapter of the thesis are here presented.

Chapter 2 concerns the vulnerability assessment of cultural and art objects and is subdivided in two parts: Demand and Capacity issues. In the first part different methods for the evaluation of seismic action at ground floor are presented, with an overview of the major literature works and the principal Technical standards. In particular, Eurocode and NTC 2008 prescriptions, as well as the reconstruction of the seismic history of the sites are here presented. Moreover, since the art objects are often exposed at the upper floors of the hosting building, the amplification of the seismic action due to the "filter effect" of the building is also discussed, explaining the importance of dealing with such a problem, and introducing different methods for the assessment of the action with some original contributions of the author. Part of the chapter is devoted to the review of the different methods exposed.
In the second part of the chapter, the problem of the correct assessment of the seismic performance of art object is presented, distinguishing different approaches for rigid or for deformable bodies. For the first ones, the mechanisms at the base of rocking and overturning phenomena are presented. For the second ones, stress analysis is discussed.

In ***Chapter 3*** a brief survey of the "state of the art" of isolation devices used for statues and the similar objects (in terms of mass and dimensions) is given. Therefore, the chapter presents some insights into the validation a specific isolation device, i.e. Double Concave Curved Surface Sliders, specifically re-designed to fit the peculiar situation of lightweight objects, with particular reference to Michelangelo's Prigioni Sculptures located at the *Galleria dell'Accademia* in Florence. These devices are carefully studied, in order to

accurately assess the performance of the seismic isolation, taking advantages of the results of an extensive experimental campaign performed in Caltrans Laboratories in University of California – San Diego (detailed in Favaretto, 2012). In particular, a suitable calibration process of the main parameters for the numerical analyses is here proposed and validated. Finally, FE simulations of the isolated system under different seismic inputs are presented.

Chapter 4 shows the case study of the isolation intervention developed, studied and realized for the *Bust of Francesco I d'Este*. The sculpture, carved by Gian Lorenzo Bernini in the 17th century, is the most valuable piece in the collection of the *Galleria Estense*, located at the second floor of *Palazzo dei Musei*, in Modena. The statue is characterized by high centre of mass, therefore is prone to overturning. This case study allows to validate the entire proposed methodology: assessment of the seismic input at both ground and second floor, evaluation of the influence of the building, which act as filter, on the seismic action, numerical simulations of seismic events, mitigation of the seismic hazard with application of the isolation system.

Finally, in ***Chapter 5***, main results of the whole research are summarized and discussed. In particular, the methodology developed within this research and the tools proposed and validated in the previous chapter are re-elaborated, with the aim to provide a support to assess and mitigate the seismic hazard effects on art objects.

2 Vulnerability Assessment

2.1 Foreword

In this chapter a brief outline of the principal methods for vulnerability assessment of art objects is presented. In particular, both the evaluation of the demand and of the capacity are dealt with.

Concerning the Demand, after a description of the seismic action at the ground level according to the approach proposed by the European Standards and particularly NTC 2008, seismic demand is primarily presented in terms of response spectra and seismic signals generation in order to be representative of the characteristics of the site. Since the art object can be placed inside a building, at a height different from the ground level, the assessment of the "filter effect" due to the characteristics of the building is here presented, both according to the current standard and to more sophisticated approaches.

Regarding the seismic capacity of art objects, two different approaches for the definition of suitable models to evaluate their capacity have to be followed: the first one belongs to the framework of the rigid body mechanics to evaluate the stability condition, the second one considers the deformability of the object to evaluate its stress state. The first approach should be applied when the sculpture is not restrained to the floor, and investigations about its global stability conditions must be carried out, considering the onset of possible motion phenomena. In most cases an acceptable approximation assumes that the sculpture may be idealized as a rigid block, for which a number of researches can be found in literature. In particular, the response of a rigid block subjected to a random ground motion has been widely studied by several authors dealing with different features of this complex phenomenon, which is characterized by different options of behaviour e.g. (Housner 1963, Ishiyama 1982, Shenton 1995). The second approach should be followed when both rocking and overturning phenomena are prevented. In this case the stress level induced by the earthquake should be investigated and compared with the material strength. To this aim Finite Element models of the art object can be assembled, and subjected to seismic acceleration, in order to evaluate the stress level of the body.

2.2 Demand

2.2.1 Seismic history

Analysing the seismic history of the site where the art object is located is essential for correct seismic hazard assessment. Seismic history could be obtained by studying

earthquake catalogues and events based on macroseismic data (e.g. intensity or magnitude and distance from the source). It is worth noting that the accurate understanding of the seismicity of the site represents a crucial phase of the knowledge path, especially for high cultural value art object.

Concerning the Italian Territory, seismic data can be easily retrieved in two databases, respectively ITACA 2.0 (*Italian Accelerometric Archive*) and ISIDe (*Italian Seismological Instrumental and Parametric Data basE*):

- ITACA 2.0 (http://itaca.mi.ingv.it) is the Italian accelerometric database, with data collected from 1972 to January 2015, and consists of accelerograms, seismograms (for velocity and displacement) and response spectra for over 1200 seismic events with Magnitude ≥ 3, recorded by the Italian Strong-motion Network (RAN – Rete Accelerometrica Nazionale), operated by the Italian Civil Protection Department - Presidency of the Council of Ministers (DPC) and by the National Seismic Network (Rete Sismometrica Nazionale), operated by "Istituto Nazionale di Geofisica e Vulcanologia" (INGV). Most of the signals given by the database are already processed and the characterising parameters of the specific event are reported (Peak Ground Acceleration, epicentre distance, Intensity, Magnitude, etc.), with the recording station, the respective accelerogram or seismogram;
- ISIDe (http://iside.rm.ingv.it/) is a seismological catalogue edited by "Unità Funzionale – Analisi Dati per la Sismologia", the research unit, part of INGV, deputed to develop procedures for real-time and deferred analysis of seismic events, and to provide verified information on current seismicity as soon as it becomes available, along with updated information on past seismicity. This catalogue provides the earthquake parameters obtained by integrating data from locations performed in near-real time with data from the Italian Seismic Bulletin (in Italian, Bollettino Sismico). Its archive consists of seismic data collected from year 1983 by the Seismic Bulletin, and since year 1000 AD by the Parametric Catalogue of the Italian Earthquakes (Catalogo Parametrico dei Terremoti Italiani).

2.2.2 Safety Requirements and definition of the seismic action according to Eurocode 8

As stated in Eurocode 8 Part 1 (EN 1998-1, in the following: EC8), primary scope of

seismic regulations is to ensure that, in the event of earthquakes:

- *Human lives are protected;*
- *Damage is limited; and*
- *Structures important for civil protection remain operational.*

The Eurocode, as well as the Italian Building Code (NTC 2008), acknowledges the random nature of seismic events and the limited resources available to counter their effects, and therefore recognizes that the attainment of such goals is only partially possible and only measurable in probabilistic terms. According to a probabilistic approach, the regulations prescribe different requirements for the structures to be met with an adequate level of reliability: to this aim the reference seismic action is associated with a reference probability of exceedance, or a reference return period.

In particular, according to EC8 and referring to civil constructions, two fundamental requirements need to be satisfied:

- *"No-collapse requirement"*. The structure shall be designed and constructed to withstand the design seismic action without local or global collapse, thus retaining its structural integrity and a residual load bearing capacity after the seismic events. The design seismic action is expressed in terms of: a) the reference seismic action associated with a reference probability of exceedance, P_{NCR}, in 50 years or a reference return period, T_{NCR}, and b) the importance factor γ_I to take into account reliability differentiation.
- *"Damage limitation requirement"*. The structure shall be designed and constructed to withstand a seismic action having a larger probability of occurrence than the design seismic action, without the occurrence of damage and the associated limitations of use, the costs of which would be disproportionately high in comparison with the costs of the structure itself. The seismic action to be taken into account for the "damage limitation requirement" has a probability of exceedance, P_{DLR}, in 10 years and a return period, T_{DLR}.

The compliance of these fundamental requirements imposes the satisfaction of the so defined limit states:

- *"Ultimate limit states" (ULS), associated with collapse or other forms of structural failure which may endanger the safety of the people*;
- *"Damage limitation states" (DLS), associated with damage beyond which specified service requirements are no longer met.*

In other words, different elastic response spectra related to different levels of the seismic

action are defined to be used in the design and verification of civil structures. Such representation can vary in the national territories, according to the definition of seismic zones in which the hazard is assumed to be constant. EC8 transfers to each of the National Authorities the responsibility for defining the seismic zonation. In this standard, a single parameter defines the local seismicity: i.e. the value of the reference Peak Ground Acceleration on type A ground, a_{gR} (also referred as PGA). Reference peak ground acceleration corresponds to the reference return Period T_{NCR} of the seismic action for the no collapse requirements. Basic representation of seismic action, within the scope of EC8, is the elastic ground acceleration response spectrum, or *"elastic response spectrum"*. Shape of the elastic response spectra is the same for the two levels of seismic action (described in Sect. 3.2.2.2 of EC8): in particular Type 1 and Type 2 elastic response spectra are defined by fixed parameters distinct by soil category. This peculiarity means that, in spite of the seismic zonation defined by national authorities, different places in Europe can be characterized by the same spectral shape without reference to important characteristics as, for example, epicentral distance from the nearest seismic source, fault mechanism, propagation mechanism. It can be observed that in such way the spectral shape is only indirectly correlated to the local seismicity, raising some doubts to the actual capability to represent the local seismic action of a specific place or territory.

2.2.3 Safety requirements according to Italian Standards

2.2.3.1 Italian Building code – NTC 2008

Italian Building code – *"Norme Tecniche per le Costruzioni 2008"* – (NTC 2008) is based on the same principles of safeguarding human lives and limiting the damage of structures expressed in EC8 and briefly recalled in Sect. 2.2.2. Unlike EC8, NTC 2008 proposes four different limit states, the first two of which belong to the category of *"Damage limitation states"* and the remaining classified as *"Ultimate limit states"*, related to different exceedance probability.

According to Sect. 3.2.1 of NTC 2008, Serviceability Limit States (SLS) are:

- *Immediate Occupancy Limit State (in Italian Stato Limite di Operatività – SLO)*, following the earthquake the whole construction, including structural and non-structural elements and relevant equipment, should not be damaged and without significant disruptions of the use of the building;
- *Damage Limitation Limit State (in Italian Stato Limite di Danno – SLD)*, following the earthquake the whole construction, including the structural and non-

structural elements and the relevant equipment, withstands damage that would not attempt the safety of the users and does not significantly compromise the resilience and stiffness towards vertical and horizontal actions, remaining immediately usable even though part of the equipment suffers an interruption of use.

while Ultimate Limit State (ULS) are:

- *Life Safety Limit State (in Italian Stato Limite di Salvaguardia della Vita – SLV)*, following the earthquake, the building undergoes fractures and collapses of the non-structural components and equipment, along with significant damage of structural components which is associated with a substantial loss of stiffness against horizontal actions; the construction instead retains enough strength and stiffness for vertical actions and a margin of safety against collapse due to horizontal seismic actions;
- *Near Collapse Limit State (in Italian Stato Limite di Collasso – SLC)*, following the earthquake the building undergoes serious fractures and collapses of the non-structural components and equipment and very serious damage to structural components; the building still retains a margin of safety for vertical actions and a limited capacity against collapse due to horizontal seismic actions.

2.2.3.2 D.P.C.M. 2011 – Proposal for Art Objects

Since the investigation of this study is the assessment of the seismic behaviour of statues and artistic assets, it is necessary to redefine the limit states in accordance with the specificities of such objects. To this aim "*D.P.C.M. 9 febbraio 2011 – Guidelines for assessment and mitigation of seismic risk of cultural heritage*" (D.P.C.M. 2011) meets the specific need of preservation of statues and art objects with the definition of a further limit state, while maintaining the respect of the prescriptions given by NTC 2008 for the safeguard of human lives.

In detail, according to D.P.C.M. 2011, life safety and protection against seismic risk are guaranteed when verifications are held in compliance with three limit states:

- *Ultimate Limit States*: for the safety against rare earthquakes of high intensity, in order to safeguard human lives, with usually reference to *Life Safety Limit State (in Italian SLV);*
- *Serviceability Limit States*: for less intense but more frequent earthquakes with the aim of reconciling economic and functional aspects, reference is made to the

Damage Limitation Limit State (in Italian SLD);

- *Artistic Limit States* (*in Italian SLA – Stato Limite Artistico*): is introduced to take into account special conditions in order to limit the damage on art objects to a remediable level with actual conservative techniques, for those situation in which the damage on the building, or on the object itself, represents an invaluable loss with an irreversible impact on the cultural heritage.

Verification for SLA is therefore suggested in specific cases, exclusively at a local level, for the parts of the building in which elements with particular historical and artistic value are present. With particular reference to art objects, it is worth noting that SLA, in most of the cases, must be checked according to the seismic action related to the Ultimate Limit State (SLV), since it considers the global loss of equilibrium, which irreparably compromise the conservation of the object itself. Also Museum Institutions or National Authorities may require a different and more severe seismic protection level, in relation to the historical and artistic importance of the art objects, and thus taking into account, for the most significant cases, the seismic action for the SLV. In these situations, it must be checked whether the satisfaction of the ULS implies directly the satisfaction of the ALS and vice versa. For example, the two limit states of rocking (oscillation around a corner of a statue) and overturning (complete loss of equilibrium) can have different thresholds, even though they consider the same reference seismic action. Indeed, if while analysing the equilibrium conditions of an object, the reference seismic action implies the oscillation but not the overturning, it can be asserted that the SLA is not verified because the triggering of oscillations can lead to uncontrollable damage for the object, while the ULS is satisfied since no overturning occurs. Despite this fact there are situations in which different levels of seismic protection can be designed for the ALS that can be referred to less strong but more frequent earthquakes. In these situations, partial damages to the art objects can be accepted as long as they are restorable and a global conservation is provided.

2.2.4 Definition of the seismic action according to NTC 2008

Similarly to EC8 prescription, the definition of the seismic action is related to different elastic response spectra, according to the most recent official probabilistic seismic hazard maps (MPS04) published by INGV for the Italian territory and acknowledged by the National Authorities in the Italian Building Code NTC 2008. Seismic classification of the Italian Territory evolved through the years to acknowledge the most recent studies held

by INGV. In particular, it is interesting to briefly recall the process that in the last decade led to the actual seismic classification.

2.2.4.1 Seismic hazard maps

The current classification of the Italian territory is based on the criteria for seismic classification published in 2003 and based on scientific studies held by INGV and in particular on the analysis of the seismic hazard of a territory defined as the probability that a territory may be affected by an event that exceeds a given intensity or magnitude threshold, during a given time interval (generally 50 years). According to the classification proposed and enforced in the Italian regulations with the O.P.C.M. 3274 of March 20th 2003, Italian territory is subdivided into four zones:

- Zone 1 - The most dangerous area, where major earthquakes may occur;
- Zone 2 - Municipalities in this area may be affected by quite strong earthquakes;
- Zone 3 - Municipalities in this area may be subject to modest shocks;
- Zone 4 - It is the least dangerous. Municipalities of this area have a low probability of seismic damages.

Each zone is characterized by a value of the seismic action, expressed in terms of maximum acceleration at the bedrock, a_g (Zone 1=0,35 g, Zone 2=0,25 g, Zone 3=0,15 g, zone 4=0,05 g). Further improvements of the zonation were introduced in the Italian regulations with OPCM 3519 of 28th of April 2006 which acknowledges the studies carried out by INGV, Reluis, Eucentre research groups, and also the update of the study on seismic hazard by the work of "Gruppo di Lavoro 2004". In Figure 1 is reported the proposed seismic hazard map for the Italian territory in which the seismic hazard is presented as intervals of bedrock acceleration (a_g), with a probability of exceeding the threshold equal to 10% in 50 years: every specific site is therefore characterized by its own ground acceleration.

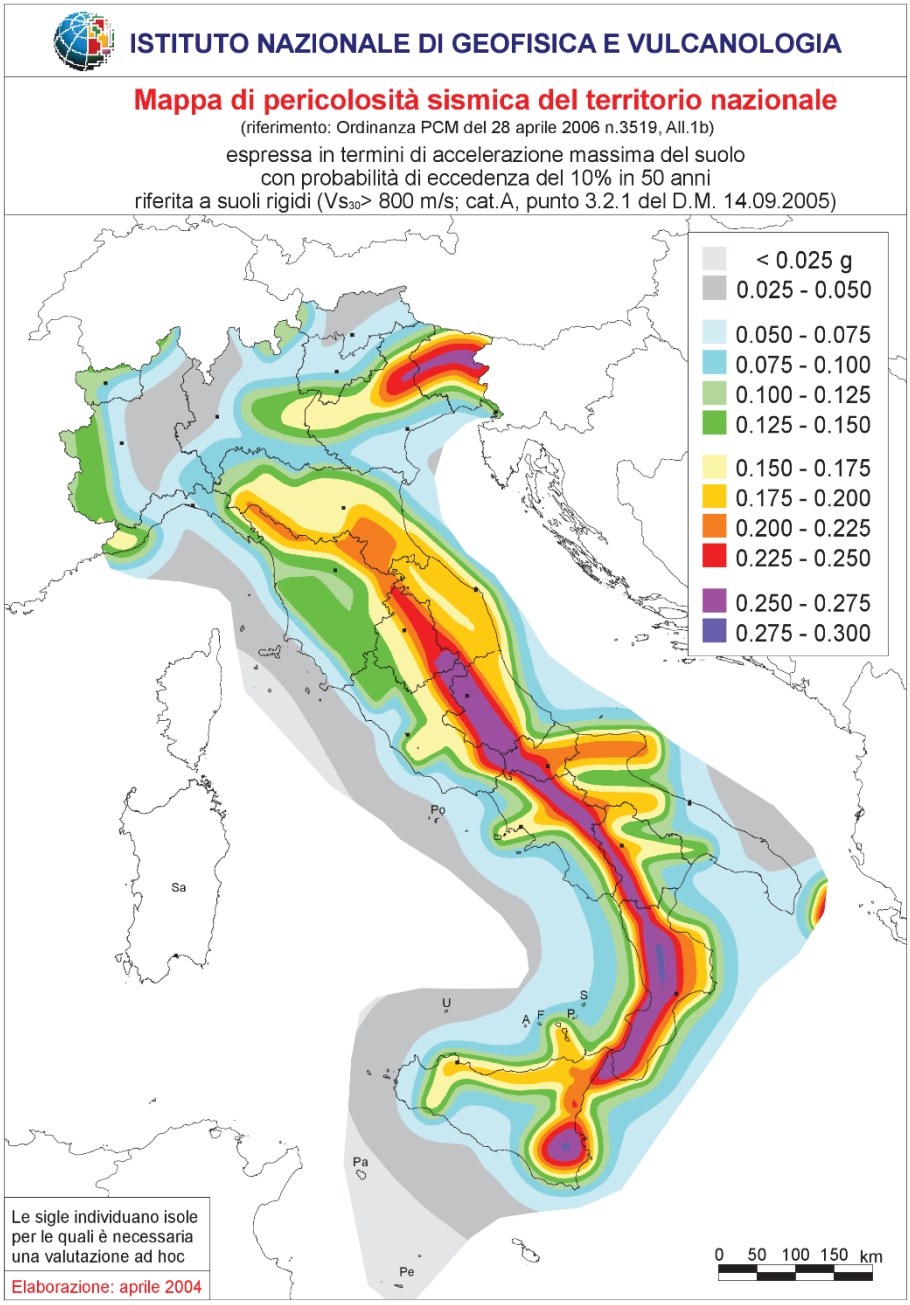

Figure 1 – Seismic hazard map of the Italian territory

For operational needs, OPCM 3519 defined broader intervals of bedrock acceleration (a_g), with a probability of exceeding the threshold equal to 10% in 50 years, to be assigned to the 4 seismic areas:

- Zone 1 – $a_g > 0{,}25$
- Zone 2 – $0{,}15 < a_g \leq 0{,}25$
- Zone 3 – $0{,}05 < a_g \leq 0{,}15$
- Zone 4 – $a_g \leq 0{,}05$

Seismic zonation according to these criteria and updated to 2015 is given in Figure 2.

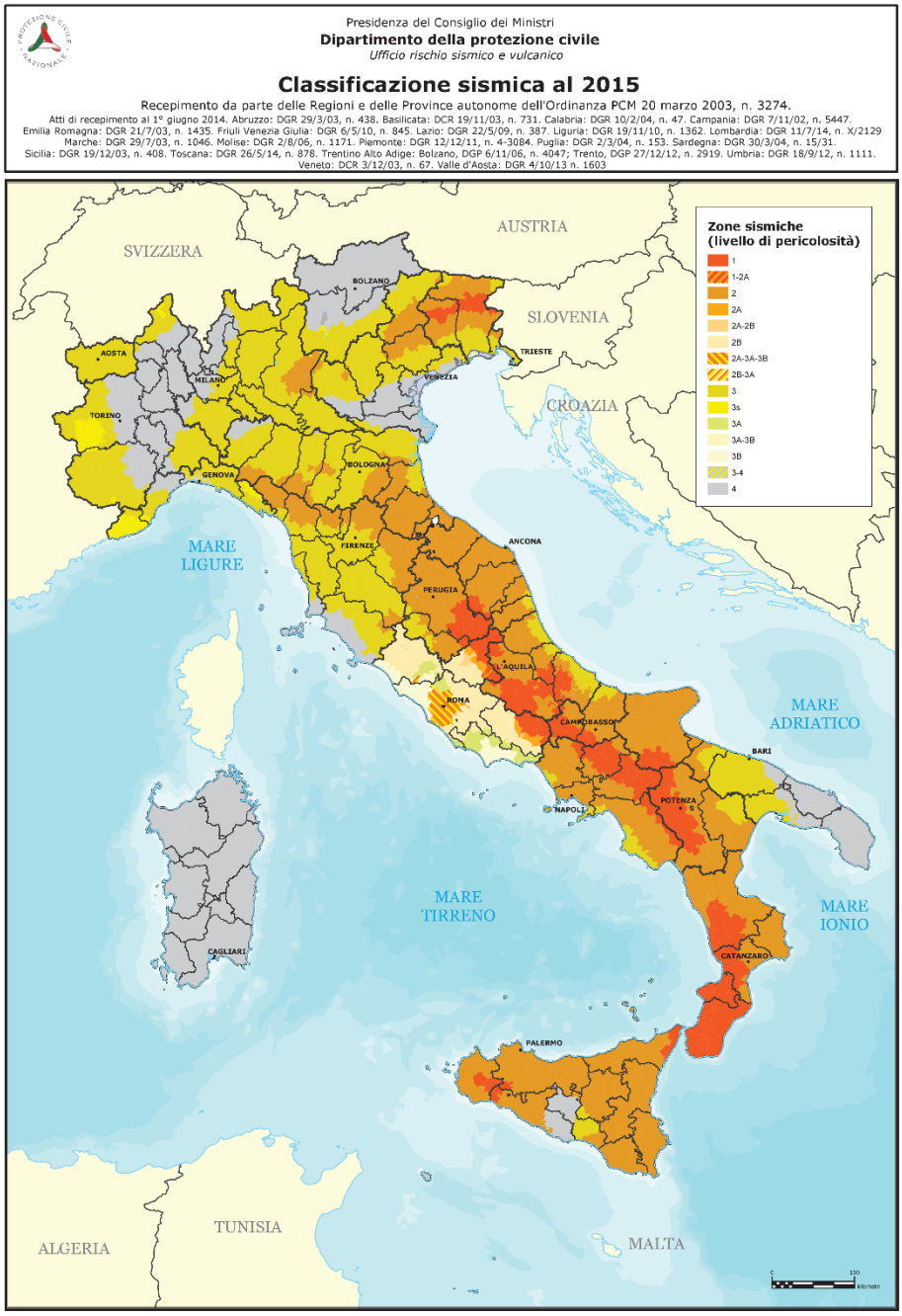

Figure 2 – Seismic zonation of the Italian territory as 2015

Finally, the 1st of July 2009, the latest revision of the Italian Building Code, NTC 2008, came into force. NTC 2008 fully adopted the seismic classification proposed by "*Gruppo di lavoro* 2004": each site can be characterized by its own acceleration, according to its geographical coordinates and to the nominal design life the seismic hazard, then, can be defined for each point of the national territory.

The probabilistic seismic hazard maps display, for each point of a regular grid spaced by 0.05°, the horizontal peak ground acceleration on stiff soil (a_g) and the spectral acceleration (S_a) for different return periods (T_r) corresponding to 9 probabilities of exceedance in 50 years, from 2% (T_r = 2475 years) to 81% (T_r = 30 years). The values

are evaluated on three percentiles (16th, 50th, 84th). For a_g values the associated disaggregation analysis is also available. For example, Figure 3 shows the Interactive Seismic Hazard maps for the territory around the city of Modena. It is possible to observe the regular grid of points in which the ground acceleration is defined, to every colour corresponds a different value of the peak ground acceleration on stiff soil (a_g).

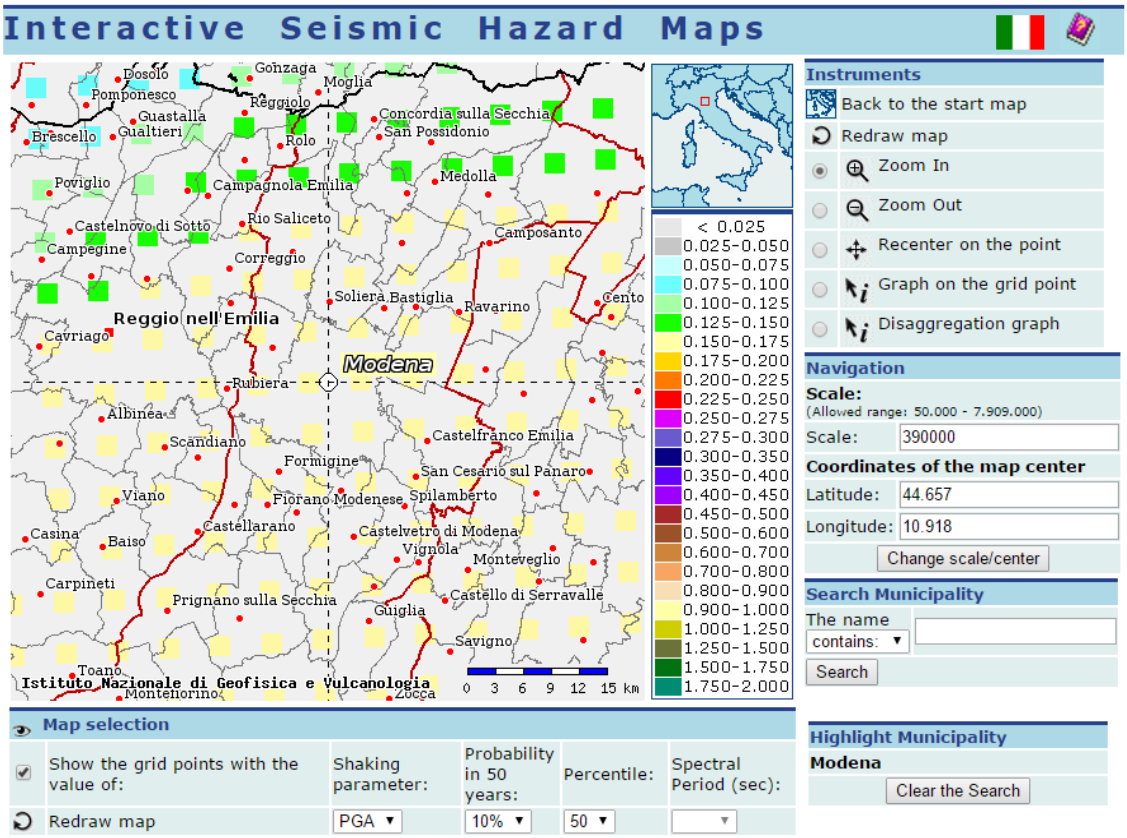

Figure 3 – Interactive Seismic Hazard maps for the territory of Modena

For the points pertaining to the grid, it is also possible to ask for the disaggregation of the seismic hazard according to a certain probability of exceedance and return period, for both epicentral distance and magnitude (Figure 4).

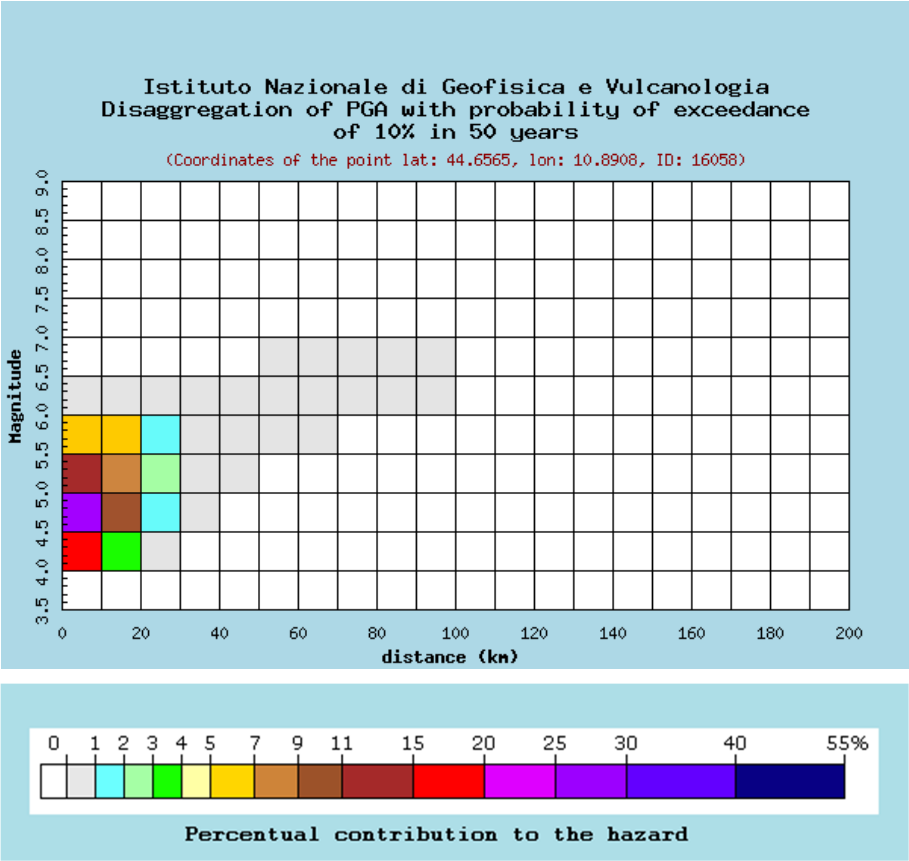

Figure 4 – Disaggregation of PGA for the territory of Modena

With such detailed definition of the seismic hazard, seismic classification with uniform hazard zone, as intended by the previous iteration of the building code, is thus useful only for planning management and territorial control by relevant boards (Local administrations, *Genio Civile*, etc.).

2.2.4.2 Seismic spectrum according NTC 2008

One of the most compelling task to deal with is the correct representation of the seismic action according to the characteristics of the site in which the structure is placed. In this sense the elastic response spectrum plays an important role in giving a first accurate assessment of the seismic acceleration of the site. Definition of a meaningful response spectrum is also necessary to the extraction and selection of seismic accelerograms for Time Histories analysis.

NTC 2008 defines seismic hazard for a specific site in terms of the maximum horizontal acceleration expected in free field condition on a rigid soil (soil type A), as well as the corresponding elastic spectral shape, with reference to a given exceedance probability P_{VR} (as defined in Sect. 3.2.1, NTC 2008), in a given reference period V_R.

According to Sect. 3.2.3, NTC 2008, seismic motion is defined by three translational

components, two horizontal and one vertical, denoted as X, Y and Z, and represented in different ways, one of which is given by the maximum expected acceleration and the related seismic elastic response spectrum. Spectral shapes of horizontal $S_e(T)$ and vertical $S_{Ve}(T)$ components are given respectively in Sect. 3.2.3.2.1 and 3.2.3.2.2 of NTC 2008. Both spectral shapes are unique for the site which is characterized for each of the exceedance probability P_{VR} by the following three parameters:

- a_g: maximum horizontal acceleration expected at the site;
- F_0: maximum value of the spectral amplification factor of the horizontal acceleration;
- T_C^*: period related to the attainment of the constant velocity branch of the response spectrum.

It is worth noting that the three parameters are related to the probability of exceedance P_{VR} of a certain seismic event, in a given return period T_R, and therefore to the reference period for the seismic action V_R, as defined in 2.4.3 NTC 2008:

$$V_R = V_N \cdot C_U \quad [years] \qquad (1)$$

where:

- V_N is the nominal life of the object of the analysis (building, civil structure or in this case an art object), in most of the cases for ordinary construction equal to 50 years;
- C_U is the "Class of Use" factor, given to civil constructions and related to the consequences of service interruption, or even the collapse (Table 1).

Nominal life	***Reference Period V_R***			
	Class of Use			
V_N	***I*** $C_U = 0,7$	***II*** $C_U = 1,0$	***III*** $C_U = 1,5$	***IV*** $C_U = 2,0$
≤ 10	35	35	35	35
≤ 50	≥ 35	≥ 50	≥ 75	≥ 100
≤ 100	≥ 70	≥ 100	≥ 150	≥ 200

Table 1 – Reference Period according nominal life and class of use

With such definition of the reference Period V_R, it is possible to obtain the exceedance probability related to a certain limit state in Table 2.

Limit States		*P_{VR}: Probability of Exceedance in the Reference Period V_R*
Serviceability Limit States	***SLO***	*81%*
	SLD	*63%*
Ultimate Limit States	***SLV***	*10%*
	SLC	*5%*

Table 2 – Probability of exceedance according to the limit state

Taking into consideration the reference period V_R and the considered limit state, associated to a specific probability of exceeding P_{VR} in the reference period, the return period T_R of the seismic action can be assessed. For example, for ordinary buildings in cases of Class of Use III, for the Ultimate Limit State (ULS - SLV), the return period to be assumed is equal to T_R = 712 years, which is an event with a 10% probability of being exceeded in the reference period V_R= *75 yrs*.

With the aim of a correct assessment of the seismic demand and capacity of the art object, in addition to the seismic acceleration parameters, it is necessary to define also the elastic displacement response spectrum $S_{De}(T)$ and the peak ground velocity (PGV).

According to NTC 2008, the seismic displacement response spectrum $S_{De}(T)$ is given by the following expression, starting from the seismic acceleration response spectra $S_e(T)$:

$$S_{De}(T) = S_e(T) \cdot \left(\frac{T}{2\pi}\right)^2 \quad [m] \qquad (2)$$

that correspond to an integration of the seismic acceleration spectrum as well the considered period does not exceed T_E = 6 s in case of C, D, E type soil.

Regarding the horizontal peak ground velocity value v_g (PGV), it may be taken directly related to PGA via the period T_c, which is the period corresponding to the beginning of the constant velocity branch of the response spectrum (e.g. Bommer et al., 2000). In this work, the following relationship proposed by NTC 2008 was assumed:

$$v_g = 0{,}16 \cdot S \cdot a_g \cdot T_C \quad [m/s] \qquad (3)$$

where:

- a_g is the maximum horizontal acceleration
- S is a coefficient that takes into account the characteristics of the soil.

In the following studies, reference is made only to NTC 2008 prescription since it represents the more refined definition of the seismic action proposed by the Italian Building Code, with the identification of specific parameters, representative of the site.

2.2.4.3 Seismic Accelerograms

Sect. 3.2.3.6 of NTC 2008 defines the conditions under which the use of seismic accelerograms is made possible to perform Time History analyses for the verification of ULS and SLS limit states. Three different types of seismic accelerograms are allowed:

- *Artificial accelerograms* generated to match target response spectra;
- *Synthetic accelerograms* generated from models of seismic fault rupture;
- *Real accelerograms* recorded in earthquakes.

About the use of seismic accelerograms, Bommer (2002) offers a brief summary of the principal characteristics of the different types of accelerograms. The paper proposes also a brief review of the principal methods to obtain seismic accelerograms. Concerning the generation of *Artificial Accelerograms*, several methods are available such as the SIMQKE method of Gasparini and Vanmarcke (1976). These methods are considered by Bommer the most convenient and attractive for design code applications, since the required input, a response spectrum, is always defined and therefore the criteria for the generation of the records are very easily specified. However, the use of artificial records presents some shortcomings; in particular they tend to have unrealistically high duration and numbers of cycles of motion, especially for inelastic analysis (Naeim & Lew, 1995). The problems are primarily due to the fact that the smoothed response spectra used in design do not generally correspond to the expected motion from a single realistic earthquake scenario. It is worth mentioning, among the methods for generation of Synthetic Accelerograms, the ray method, the empirical Green's functions method and stochastic methods. All these methods are reviewed by Lam et al. (2000) and require an earthquake scenario to be defined, at least in terms of size (magnitude or seismic moment) and distance from the site. On this premise, these methods appear all quite complex, and their application requires a fairly advanced understanding of seismology.

The last method reviewed by Bommer (2002) consists in the *Selection of Recorded Seismic Accelerograms*, obtained by National and European Databases (e.g. ESD) and scaled properly according to the seismic characteristics of the site. Although the article focuses primarily on the regulatory requirements for the use of accelerograms in Time History analyses, it is worth noting that Bommer (2002) suggests the selection of recorded seismic accelerograms to overcome the inherent problems in the use of the other two methods.

In the present work, the selection of *Real Accelerograms* can be considered the most reliable method to obtain a suite of seismic signal representative of the seismicity of the

site, because of the above mentioned drawbacks of *Artificial* or *Synthetic Accelerograms*. To perform the correct selection of *Real Accelerograms* it is necessary to define the criteria for such choice. NTC 2008 in Sect. 3.2.3.6 provides the characteristics to which the set of accelerograms should comply with:

a) *Duration of the artificial accelerograms must be chosen on the basis of the magnitude and the other physical parameters that determine the peak ground acceleration and the stratigraphic coefficient, without specific studies the duration of the pseudo-stationary part must be longer than 10 seconds, preceded and followed by parts of increasing amplitude until the final duration is not shorter than 25 seconds;*

b) *The response spectrum of the artificial accelerogram must match the 5% damping elastic response spectrum adopted for the site, no value of the mean elastic spectrum, calculated from all time histories, should be less than 90% of the corresponding value spectrum in the range of periods between 0,2T and 2T, where T is the fundamental period of the structure for ULS verification;*

c) *In case of seismic isolated structures, the range of periods between $0{,}2T_{is}$ and $1{,}2\ T_{is}$ has to be taken into account as spectrum compatibility interval;*

d) *Use of registered real seismic records is allowed, on the condition that their choice is representative of the seismicity of the site and adequately justified by the characteristics of the seismic source, site condition, magnitude, distance from the source, and maximum expected horizontal acceleration at the site.*

It is important to underline that the given prescriptions are principally oriented to the use of artificial accelerograms, since the generation of artificial accelerograms appears to be the most convenient and attractive for design code applications. This results in a series of compliance characteristics for the use of Artificial Accelerograms.

Following the approach proposed by Iervolino et al. (2010), the same prescriptions given for the generation of artificial accelerograms are adopted for the selection and scaling of real recorded earthquakes. As mentioned before, Italian standards, as also EC8, allow the use of artificially generated accelerograms and real recorded earthquakes, the latter obtainable by the use of REXEL (Iervolino et al., 2010), software developed and distributed by Reluis (*Rete Laboratori Universitari di Ingegneria Sismica* – Seismic engineering laboratories network). This software allows the search for a natural set of accelerograms compatible with the acceleration spectrum defined in accordance with the instructions of NTC 2008, EC8, or arbitrarily defined by the user. In the following, an example of selection and scaling of spectrum compatible accelerograms by means of REXEL is shown, with a step by step procedure. Elastic response spectrum in acceleration for the site is determined by entering the coordinates of the location, longitude and

latitude, and specifying Soil Category, Topographic Category, Design Life, Importance Class and Limit State. It is also necessary to specify the components of the seismic action that are to be considered: the two independent orthogonal horizontal components, X and Y, which are characterized by the same response spectrum, and/or the vertical component Z, characterized by a specific spectrum as shown in Figure 5.

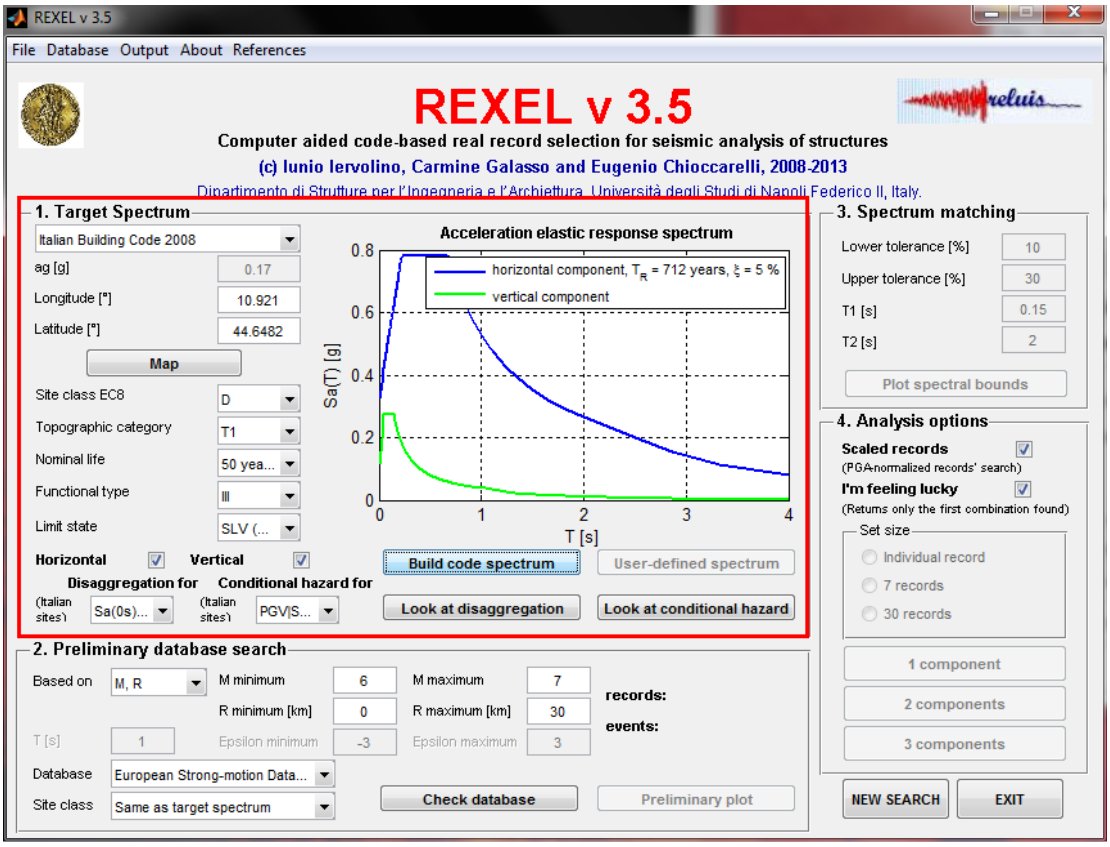

Figure 5 – Target Spectrum definition

The acceleration records, among which the search can be performed, belong to the European Strong Motion Database (ESD) or to the Italian Accelerometric Archive (ITACA 2.0). The user can choose from which one of these databases the subsets of accelerograms are extracted. Such sets are coherent to a specific combination of Moment Magnitude/Epicentral distance of interest, in addition to an assigned local geology. The intervals of magnitude (M_{min}, M_{max}) and distance (R_{min}, R_{max}) should be chosen on the bases of the characteristics of the earthquake relevant to the site, and given by the analysis of the seismic risk disaggregation. About the choice of the soil category, two alternatives for selecting the events are given: the option "*Same as target spectrum*" restricts the search to accelerograms only from sites with the same soil type, otherwise "*Any site class*" extends the search to other accelerograms from sites of any soil category class (Figure 6). Once provided these values, Rexel returns the number of records available and characterized by these features and among which the software will perform the extraction

of the spectrum-compatible sets.

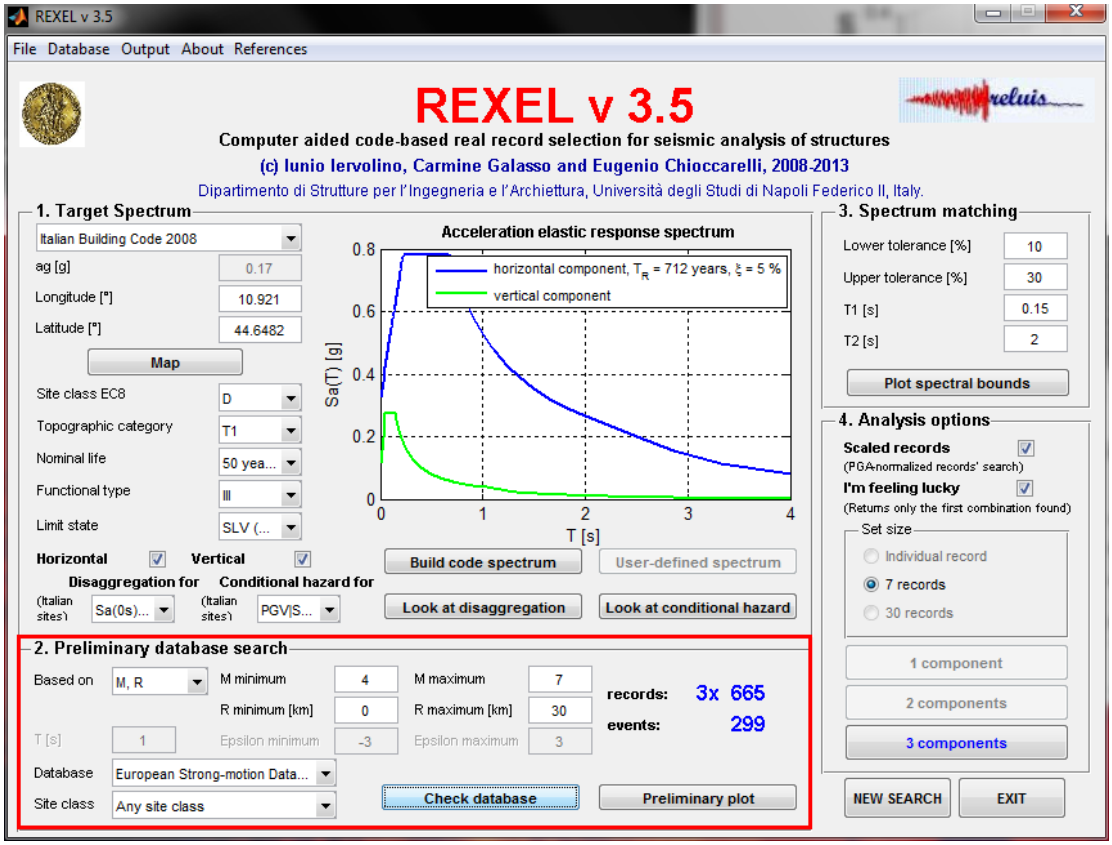

Figure 6 – Database search

Once defined the research, it is necessary to specify the range of spectrum-compatibility (T_1, T_2), between 0s and 4s, and the tolerance with which the average spectrum of the combination of 7 accelerograms must respect the target spectrum in the desired period range. More precisely, the percent difference is specified for the lower and the upper limit of the average spectrum of the set of accelerograms compared to the reference spectrum (Figure 7).

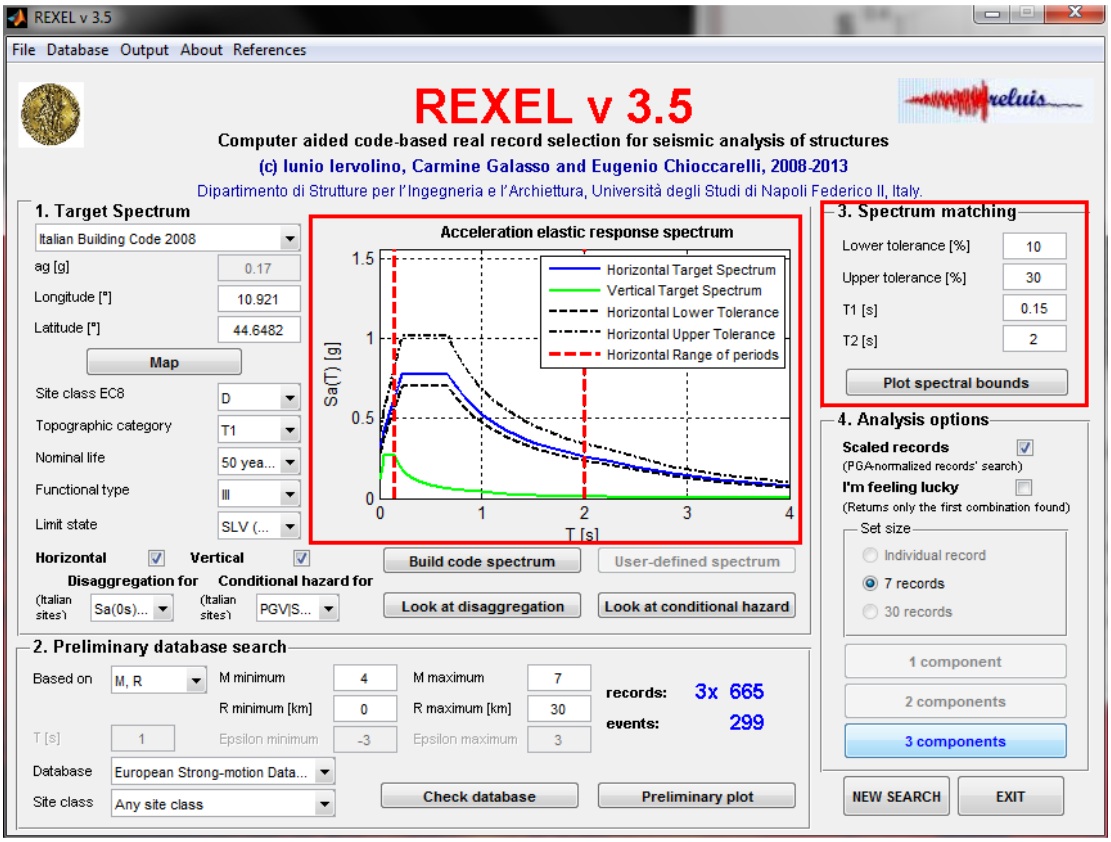

Figure 7 – Spectrum-compatibility interval and tolerance

All the possible combinations of 7 spectra, that can be assembled with records found in the database and compatible with the defined Magnitude and Epicentral Distance, are then analysed, in order to check their compatibility with the reference spectrum.

The combinations consist of 7 groups of accelerograms that include two horizontal components and a vertical component. In this case, the software proceeds to the automatic selection in two successive steps: first the spectrum-compatible combinations are extracted checking the horizontal component of the spectrum (7 pairs); then, the program analyses the obtained combinations and verifies the spectrum-compatibility of the vertical component, asking the user to specify the tolerance limits with the target spectrum and the period range of interest for the vertical component.

In Figure 8, it is shown the graphic outputs of the combination of 7 groups of accelerograms provided by Rexel, whose average spectrum is compatible with both horizontal and vertical target spectra.

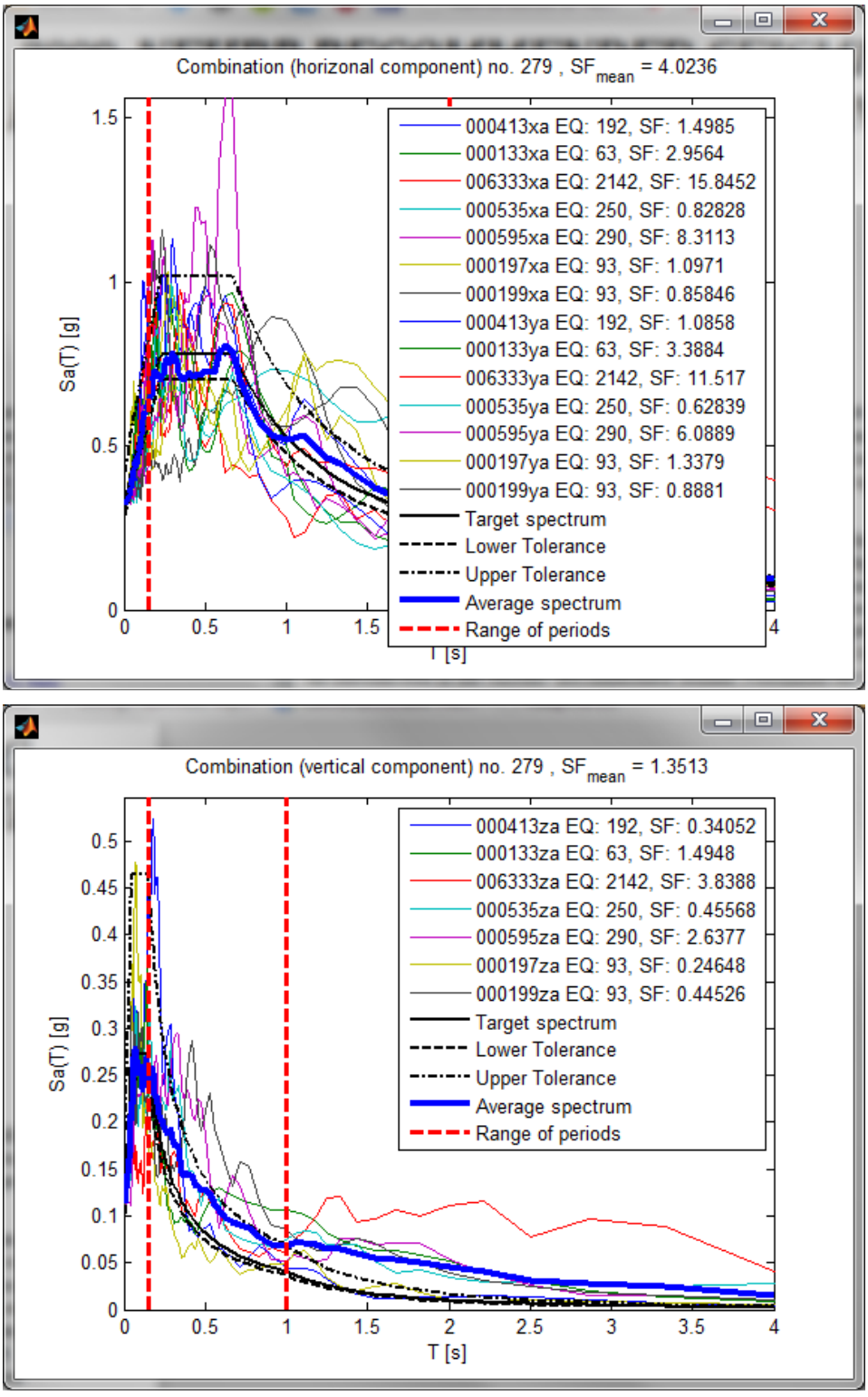

Figure 8 – Spectrum-compatible combination of 7 groups of accelerograms

Starting from this brief outline on the use of REXEL, some critical aspects can be recalled, underlined also by the author and supported by the hints given by Bommer et al. (2002) and Iervolino (2010):

- It can be notice that the constraints of compatibility are acceptable on the average, but very questionable for individual earthquakes;

- The actual effect of the vertical seismic component is returned with difficulty, since in order to find spectrum-compatible sets of accelerograms with the vertical component, the tolerance on upper limit is usually set very high and the range of periods is usually of small interest;
- ESD and ITACA 2.0 database are most lacking for soil categories C and D, compared to B. This means that for such sites the only way to get an acceptable number of sets records from the database is to consider the option “Any site class” in the soil category selection. But this choice, implicitly makes losing the requirement of "full representation of the seismicity of the site" (see NTC 2008 Sect. 3.2.3.6);
- The uncertainty in the definition of the interval of interest for the spectrum-compatibility: it is unclear whether or not it is to prefer the choice of a wide range of periods (for example, in order to include also the periods of isolation devices) to the drawback of the resulting combinations of accelerograms whose spectra are less “close” to the design spectrum (in order to meet the constraints of compatibility in a longer interval);

It is therefore suggested strong caution in the use of such software.

2.2.5 Seismic action at higher levels

2.2.5.1 General overview

To determine the seismic action acting on any object (i.e. which can be defined as secondary system) contained within buildings, it is important to take account that the structure filters the seismic signal, modifying, with its response, the frequency content and the amplification of the strong motion applied to the base. To consider this effect, different approaches can be followed.

Two basic approaches currently exist which provide the basis for engineering analysis and response calculations for secondary systems. They are the combined primary-secondary system approach, which consider the coupling of the two systems, and the cascading analysis methods, in which the primary and secondary systems are decoupled and analysed individually. The most popular cascading approach is the conventional floor response spectrum approach, on which some design codes are based.

In cascading approaches, the response behaviour of the primary system at the support points of a secondary system is first determined while neglecting the effect of the secondary system. The response spectra at the support points (i.e. the floor response

spectra), that is the signals obtained at the floor level, are then used as input to the secondary system. Then the secondary system response behaviour can be determined by using time domain analysis or by using one of several modal combination rules.

Even if the Floor Response Method can provide a simple procedure for the assessment of the seismic response of the secondary systems, some criticism can be raised. In particular, it is worth noting that the interaction between primary and secondary systems is neglected. In fact, Floor Response Method gives acceptable results for secondary systems with relatively small masses and with frequencies which are not tuned to a frequency of the primary structural system (resonance). Otherwise, when the masses of the secondary systems are not negligible or when resonance occurs, a significant error can result in the estimation of the secondary system seismic response. In this case, the application of the Floor Response Method is inappropriate, and the accurate determination of the floor seismic action has to be performed carrying out dynamic analysis of the coupled system structure-object, with reference also to the connecting system. In this thesis, due to the small mass of the secondary system (i.e. statues) with respect to the building, and the different frequencies of the two systems, cascade approaches are considered a reliable and suitable method to assess the seismic action at the base of the pedestal of the artwork.

2.2.5.2 Floor response spectrum approach according to current Standards: direct generation

Within the framework of cascading analysis methods, current building codes provide simplified formulas for assessing the seismic action on non-structural elements in terms of acceleration amplification with the height, i.e. by using the direct generation of Floor Response Spectra. Given the ground response spectrum and knowing the main dynamic parameters of the structure (e.g. height, vibration period), this method makes possible to obtain the floor response spectrum of higher levels of the building by using simple mathematical expressions. The schematic representation of the direct generation of the Floor Response spectra is given in Figure 9.

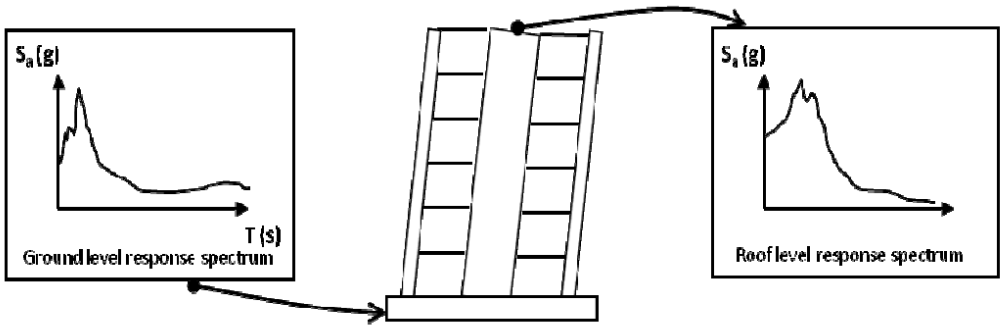

Figure 9 – Direct Generation of Floor Response Spectra, Calvi (2014)

It is worth noting that the floor response spectrum approach represents a research field still in development that leads also to the formulation of Displacement Floor Spectra, proposed by Lagomarsino (2014), and also adopted in CNR DT 212/2013, evaluated starting from the corresponding ground floor spectra and modified by the height to which the object is placed, the parameters that characterize the seismic response of the structure (periods, modal shapes and participation coefficients of the most representative modes, damping) and damping of the object.

2.2.5.2.1 European Standards: Eurocode 8 and NTC 2008

In order to evaluate the amplification of the acceleration due to the art object location in the building, the simplified method proposed by EC8 and NTC 2008 for non-structural elements can be used. Maximum acceleration S_a (in [g]) to which the element is exposed, is evaluated as:

$$S_a = \alpha \cdot S \left[\frac{3 \cdot (1 + Z/H)}{1 + (1 - T_a/T_1)^2} - 0.5 \right] \geq \alpha \cdot S \quad [g] \qquad (4)$$

where:

- α is the ratio between PGA on a soil type A for the considered Limit State and the gravitational acceleration g;
- S is the coefficient that takes into account the soil type and topography condition;
- T_a is the fundamental period of the non-structural element;
- T_1 is the fundamental period of the structure in the considered direction;
- z is the height of the center of gravity of the non-structural element measured from the foundation level;
- h is the height of the building measured from the foundation level.

The factor:

$$Amp = \left[\frac{3 \cdot (1 + z/h)}{1 + (1 - T_a/T_1)^2} - 0.5\right] \geq 1 \quad [-] \qquad (5)$$

can be considered as an "Acceleration Amplification coefficient", Figure 10.

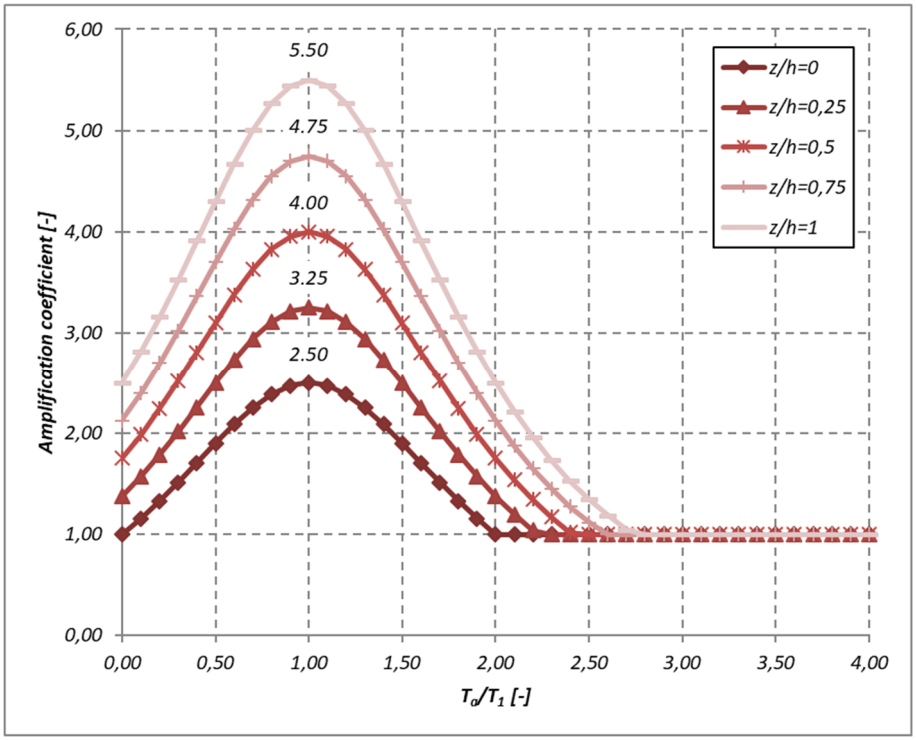

Figure 10 – Amplification coefficient for the acceleration

It is worth noting that for long periods EC8 provides an estimation of the amplification effect particularly onerous and to the safe side, due to the limitation in the Eq. (4), which corresponds to assume the value of PGA as lower bound of the floor acceleration instead of the more reasonable spectral value at ground level (NTC 2008 ground spectrum).

2.2.5.2.2 CNR Guidelines

Concerning the displacement induced by seismic action, which is crucial for the design of the seismic isolation system, the suggested approach follows the guidelines of CNR-DT 212/2013. According to this formulation the displacement response spectrum at level z of the building is given by:

$$S_{dZ}(T) = max\left[S_d(T);\ \sum_{k=1}^{r} S_{dZ,k}(T)\right] \quad [m] \qquad (6)$$

where $S_d(T)$ is the displacement response spectrum of the ground motion, r is the number of the considered modes of the building, and $S_{dZ,k}(T)$ for the kth mode is expressed as:

$$S_{dZ,k}(T,z) = \begin{cases} S_d(T_k)\dfrac{\gamma_k|\psi_k(z)|\left(\dfrac{T}{T_k}\right)^2}{\sqrt{\left(1-\dfrac{T}{T_k}\right)^2+\dfrac{0.05}{\left(\eta(\xi)\eta(\xi_b)\right)^2}\dfrac{T}{T_k}}} & T < T_k \\ S_d(T_k)\dfrac{\eta(\xi)\eta(\xi_b)\gamma_k|\psi_k(z)|\left(\dfrac{T}{T_k}\right)^2}{\sqrt{\left(1-\dfrac{T}{T_k}\right)^2+0.05\dfrac{T}{T_k}}} & T_k \le T \le 1.9T_k \\ 3.8\cdot S_d(T_k)\cdot\gamma_k\cdot|\psi_k(z)|\cdot\eta(\xi)\cdot\eta(\xi_b) & T > 1.9T_k \end{cases} \quad (7)$$

with T the period of the object and T_k the period of the kth building mode, $|\psi_k(z)|$ the value of the mode-shape of the building at the height z, $\gamma_k$the modal participation factor, $\eta(\xi)$ and $\eta(\xi_b)$ respectively the damping correction factors for the object and the structure, calculated according to the well known expression $\eta = \sqrt{10/(5+\xi)}$.

It is worth noting that, since $S_d(T_k)$ is the spectral value of the displacement calculated for the k^{th} period of the structure, the remaining part of the equation may be considered as an amplification coefficient. In this way the three equations reported in (8) can be rewritten as:

$$S_{dz,k}(T,z) = \alpha_{amp,k}\left(\frac{T}{T_k}, z, \xi_b, \xi\right)\cdot S_d(T_k) \quad [m] \quad (8)$$

where the amplification factor may be seen as the product of two distinct factors:

$$\alpha_{amp,k} = \alpha'_{amp,k}\left(\frac{T}{T_k}, \xi_b, \xi\right)\cdot \alpha''_{amp,k}(z) \quad [-] \quad (9)$$

the first depends on the ratio T/T_k (defining the relationship between the periods of structure and of the object) and the second on the height z of the object from the ground (and therefore from the adopted modal shape).

The value of $\alpha'_{amp,k}(T/T_k)$ is shown in Figure 11 for different values of the damping of the object. According to the cited guidelines, an approximated estimation of the displacement may be obtained referring only to the first mode and assuming:

$$\gamma_1 = 3n/(2n+1) \quad (10)$$

with n number of floors of the building. For the mode-shape, it is possible to apply the formula:

$$\psi(z) = (z/H)^{\kappa} \quad (11)$$

approximating the first mode-shape as linear when κ=1.

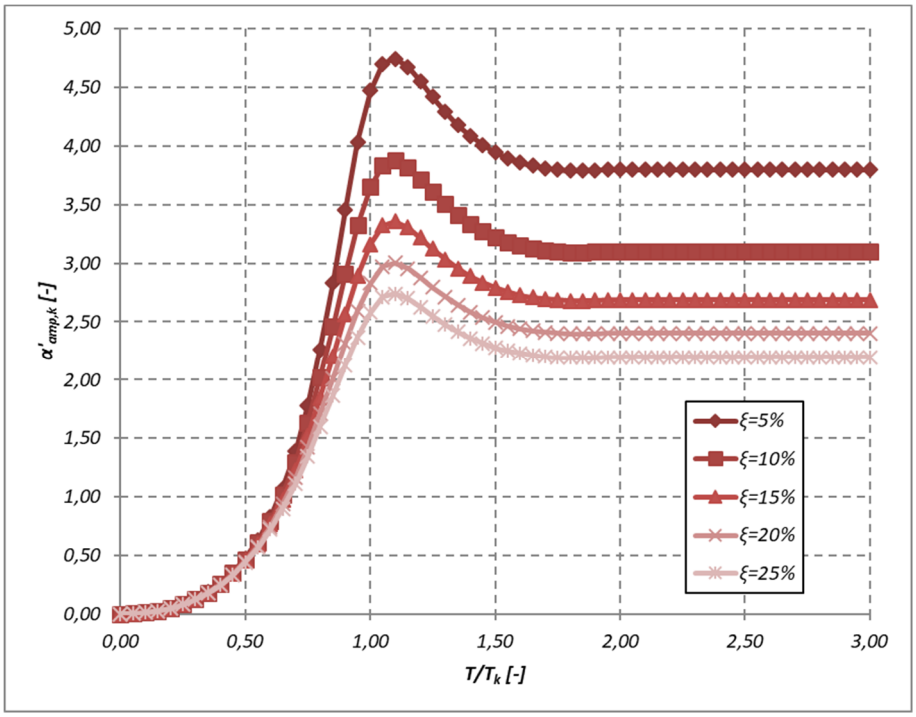

Figure 11 – Amplification coefficient $\alpha'_{amp,k}(T/T_k)$

2.2.5.3 *Cascading analysis methods. Direct generation of input signal at floor level and Floor Response Spectrum approach*

Along with simplified approaches, given by current regulations and technical documents, other kind of approaches for the determination of the seismic acceleration acting at higher floors can be found in literature. In particular, it is possible to compute the modification and amplification of the seismic signals by the stiffness and height of the building containing the art object by means of a Numerical analysis. According to the cascading analysis method, seismic signals at the ground floor are applied to the base of the F.E. model of the building, and acceleration time histories are registered at a node of the floor where the object is placed. Due to the high number of analyses and the discretization of the F.E. model the procedure can be considered quite computationally expensive. A conceptual scheme of this method is presented in Figure 12, in which the effect of the building is represented by the "floor seismic signal" in the upper right corner.

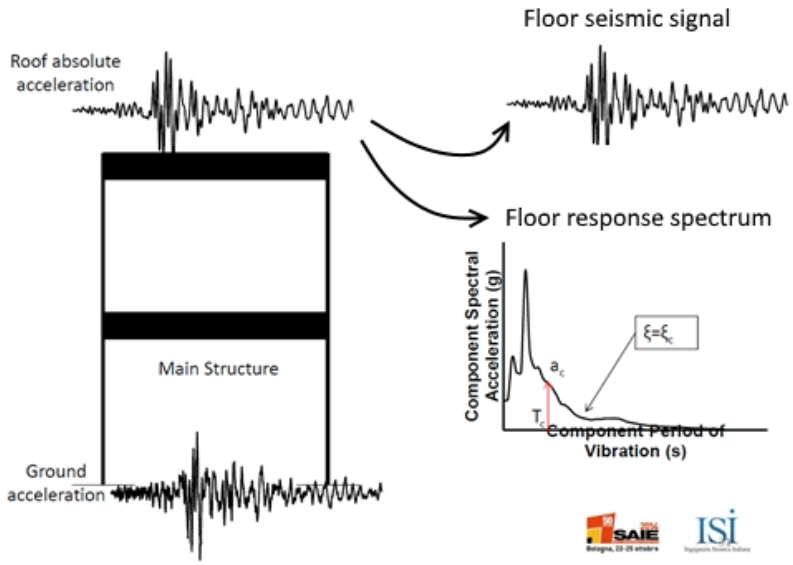

Figure 12 – Floor Response spectra approach, Calvi (2014) – (modified)

To overcome this kind of numerical difficulties associated with the analysis of large dimensional F.E. models, substructuring or structural partitioning is considered a profitable approach to reduce the computational time, without compromising the reliability of the analyses. Substructuring refers to the division of a complex architecture into a number of substructures whose boundaries can be suitably specified.

It is preferable to make the structural partitioning corresponding to physical partitioning. If the stiffness or flexibility properties of each secondary system can be determined, then each can be treated as a complex structural element. Numerical methods can then be used for the partitioned structure. Once the displacements and/or forces on the boundaries of a substructure are found, then each substructure can be analysed separately under known boundary conditions, Chen (1988).

A representative substructure of the building hosting the art object has to be analysed, by defining appropriate distribution of boundary constraints to simulate the presence of the remaining part of the building. In particular, four conditions can be considered, two of them are limit conditions:

- Absence of constraints, which represents the limit situation in which the portion of the building is not affected by the presence of the adjacent parts, and then analysed as a separated building;
- Presence of translational spring with low stiffness, which represents the condition in which the portion of the building is poorly bound to the adjacent parts;
- Presence of translational springs characterized by high stiffness, which represents

the situation in which the portion of the building is strongly bound to the adjacent parts;

- Presence of fixed constraints, which represents the limit situation in which the portion of the building is rigidly constrained at the nodes on the sides.

The determination of the elastic constant to be attributed to the springs elements can be carried out according to the process shown below, which estimates the stiffness on the basis of the plausible periods of the adjacent portions of the building next to the analysed substructure.

The classical relationship between the period T, the mass m and the stiffness k is:

$$T = 2\pi \cdot \sqrt{\frac{m}{k}} \quad [s] \tag{12}$$

from which the stiffness can be derived as

$$k = \left(\frac{2\pi}{T}\right)^2 \cdot m \quad [N/m] \tag{13}$$

This last equation gives an estimation of the global stiffness of the building, which is assumed to be proportional to the pertaining masses and inversely proportional to the square of the Period of vibration. With these hypotheses it is possible to assess the stiffness of the remaining parts of the building, next to the considered substructure.

Once determined the main parameters of the model in term of stiffness and constraint, the seven couples of seismic signals, obtained according 2.2.4.3, are applied at the base of the primary system and the acceleration time history at the base of the secondary system is registered. In particular, since a full set of seven couples of seismic signals are applied twice in the combinations longitudinal/lateral direction and then in the lateral/longitudinal direction, fourteen seismic floor response signals can be extracted. Therefore, the analysis of the secondary system can be carried out in two different ways: with the direct application of the fourteen floor seismic inputs to the secondary system, or by calculating of the floor response spectra from the floor seismic signals.

In the direct analysis, a dynamic time history analysis of the secondary system is carried out by applying the seven couples of floor seismic signals at its base, and the performance of the system in terms of material stresses, acceleration and displacement can be assessed.

It is worth noting, that strong caution is given to the analysis of the results of the Time History analysis. Indeed, seven couples of seismic inputs are given, made up of a longitudinal and a lateral direction: in this case the analysis is performed by applying the

two acceleration input, first according the X-Y direction and then switching the directions. This caution is due to the remaining uncertainties in the principal direction of the forthcoming earthquakes, and it is prudently assumed to observe the behaviour of the building and the statue itself in both the cases. At the end of this process it is possible to observe different behaviours of the primary-secondary system and define the most dangerous in terms of material stresses, acceleration and displacement, as aforementioned before.

2.3 Capacity

2.3.1 Characterization of the objects: from reality to model

The geometrical survey is fundamental for defining the model to be used in the analysis phase; the level of accuracy required by the survey has to be related to the adopted methods of analysis and to the aims of the analysis itself.

In this thesis different geometrical surveys, with highly different detail level, were described and used in the case studies:

1) a rough survey based on the measurement of the most significant geometrical dimensions (i.e. maximum depth, width, and height of the object) can be performed in order to obtain the necessary data for a preliminary stability analysis;
2) the high accurate 3D digital representation of each object obtained with laser scanner technology. Such a survey allows to compute accurately some fundamental geometrical properties, such as the volume of the statue, its height, and the position of the centre of gravity.

Before introducing the more sophisticated methods for the geometrical survey, it is appropriate to recall the importance of direct survey with manual measurement with measuring tape or yardstick. The simplest art objects, as for example stone pedestals or compact statues, can be conveniently measured without need of more complex methods, which are always very expensive. Direct measurement is also useful to add information to detailed surveys as the relative position of adjacent bodies (e.g. a statue with its pedestal).

Some examples of such procedure are given in the following, by using case studies which may also serve as examples on how to address similar issues in analogous heritage assets. Figure 13 shows the pedestals of the statues exhibited in *Galleria dell'Accademia* in Firenze with the measurement used to establish the position of the statues on the pedestal. Similarly, Figure 14 shows some phases of the direct survey performed on the pedestal of the Bust of *Francesco I d'Este*: since its simple geometry, it was possible to correctly represent a geometrical and then numerical model, starting from the measured dimensions.

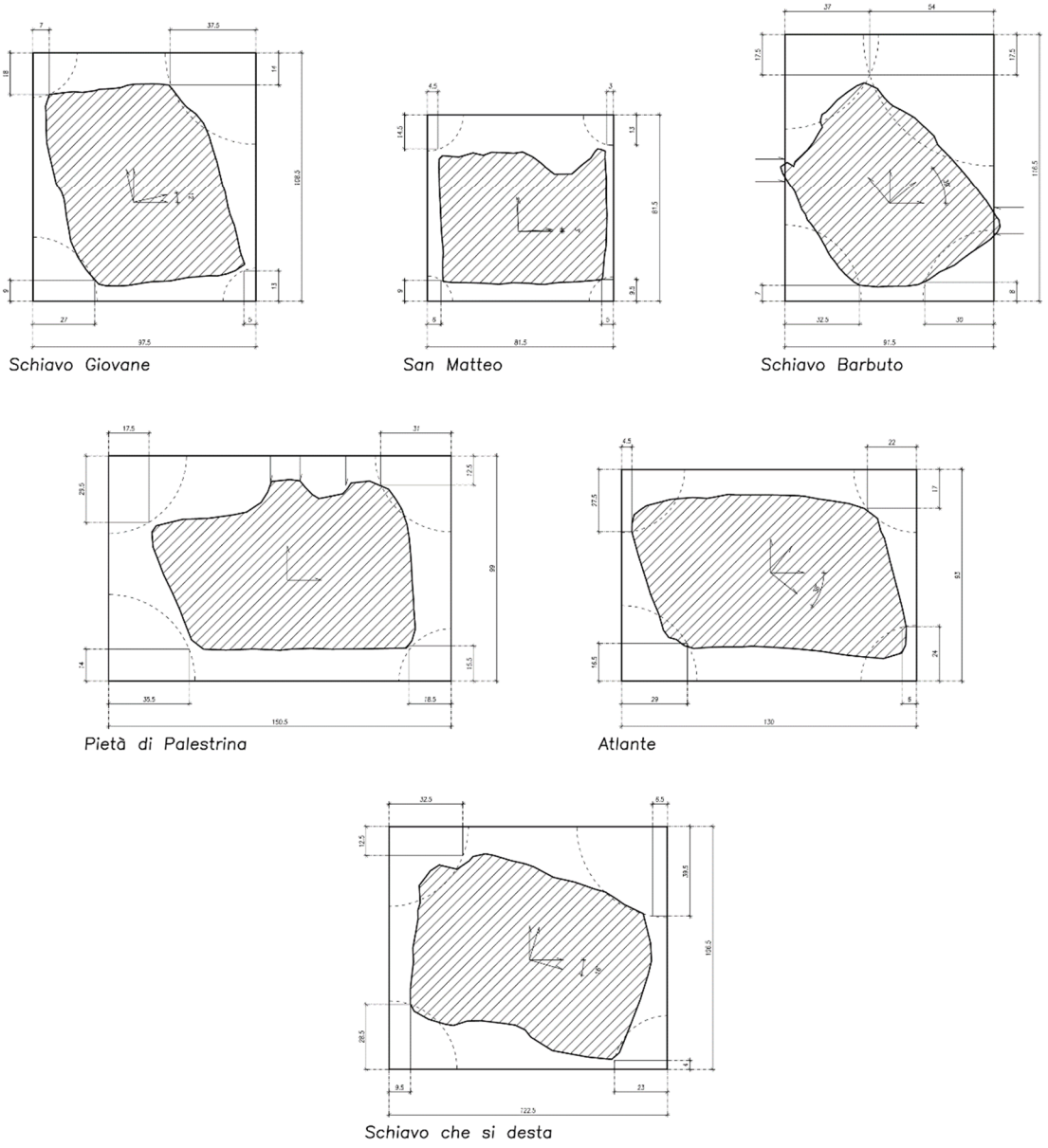

Figure 13 – Measurement of the pedestals and relative position of the Michelangelo's sculptures exhibited in Galleria dell'Accademia – Firenze

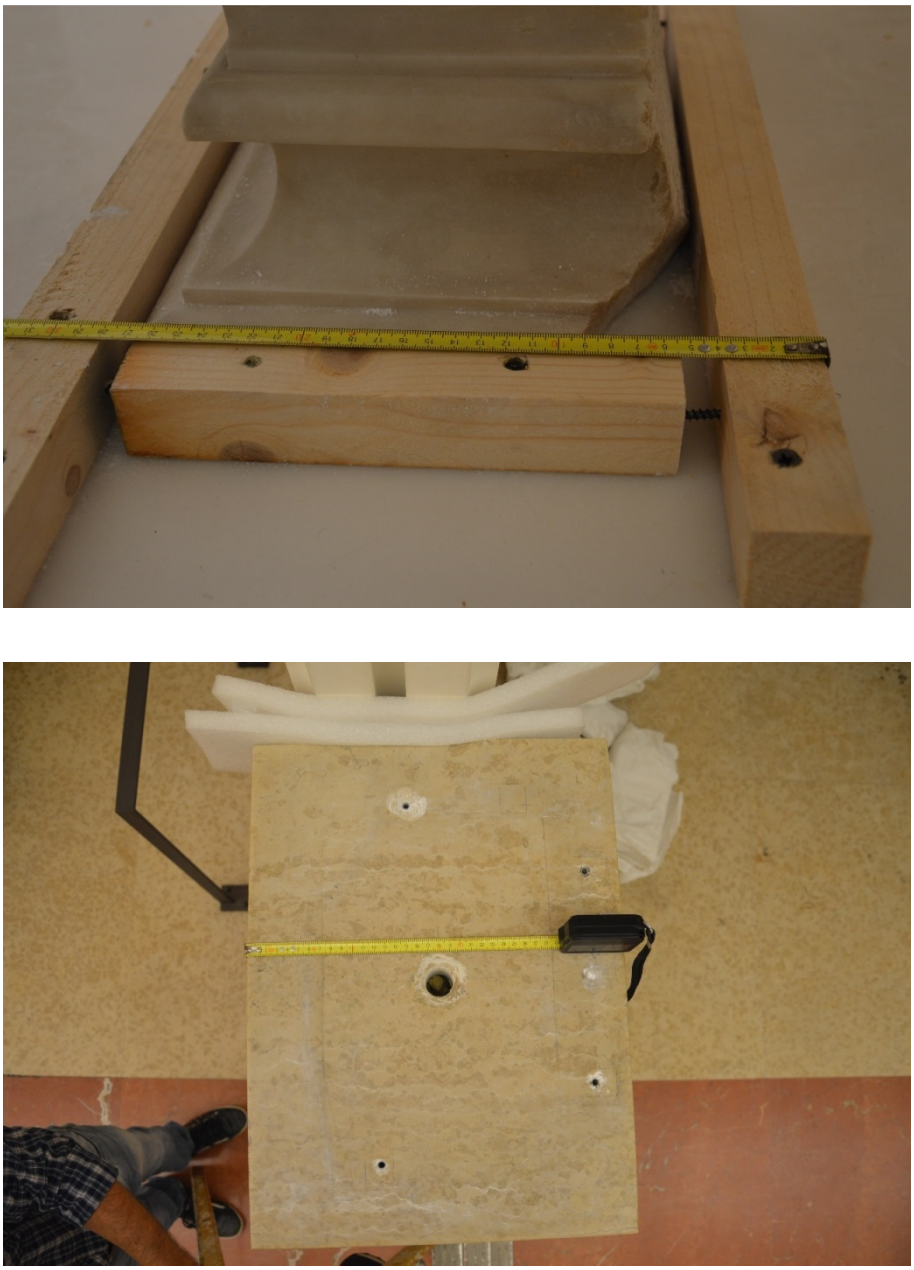

Figure 14 – Direct measurement of pedestal of statues with measuring tape

In addition to the direct measure of the geometry of the statues, the photographic survey can help to define other important characteristics as the approximate position of the centre of gravity of the statue.

In Figure 15 an example of the approximated determination of the centre of Gravity of Michelangelo's San Matteo is shown, in particular an equivalent block approximating the real geometry of the statue is presented.

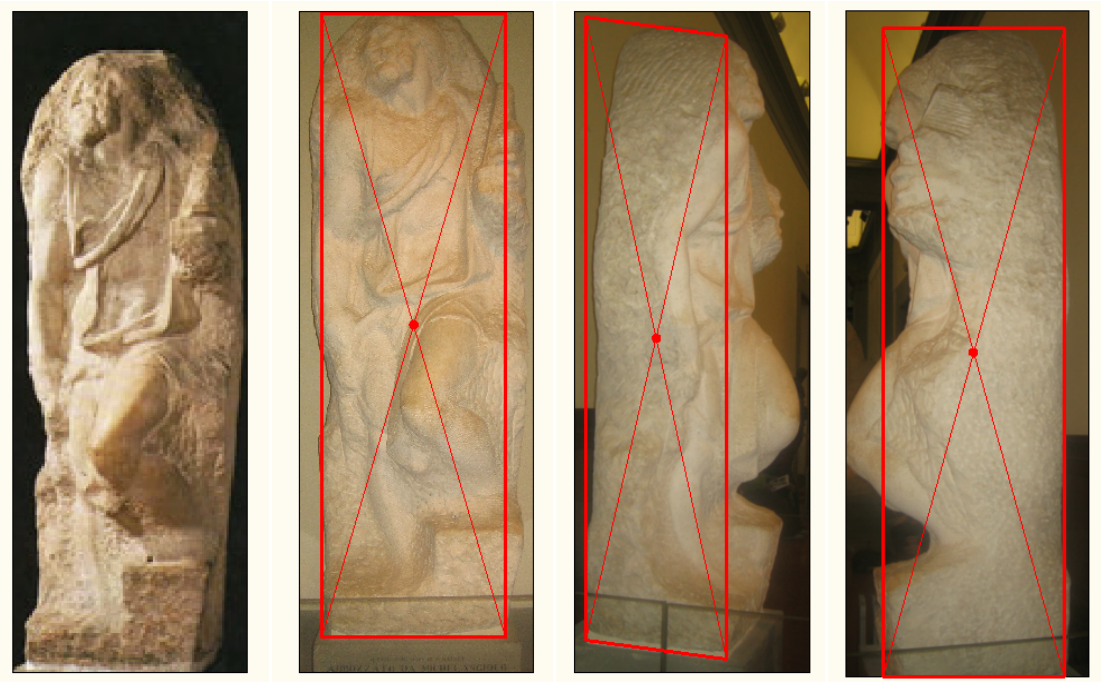

Figure 15 – San Matteo: Determination of an equivalent block and the centre of gravity, Berto et. al (2011)

Another kind of simplified model with a different degree of accuracy and elaboration can be given by the simplification of the 3D laser scanner survey, as shown in Favaretto (2012). In Figure 16 the process of simplification of the laser scan survey is shown. In detail, Figure 16 (a) shows the assessment of the centre of gravity, starting from the lateral measures and the definition of an equivalent parallelepiped, and (b) the multi block approach, that consist in approximating a complex geometry with a certain number of blocks in order to achieve a better accuracy.

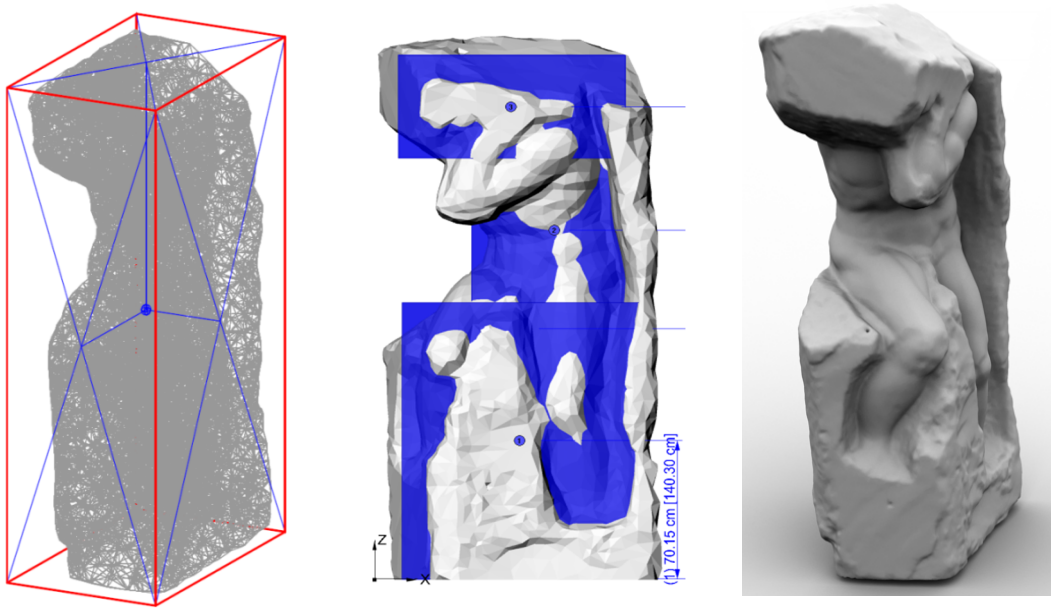

(a) (b) (c)

Figure 16 – Geometrical characteristics of Prigione Atlante (a) approximate block (b) multiple blocks (c) 3D laser scan survey

About the most recent technologies for geometrical survey and numerical modelling of art objects, some interesting examples can be found in Berto et al. (2012) and also in Borri and Grazini (2006). Both works describe the process of vulnerability assessment of statues and they acknowledge the need of a reliable geometrical survey in order to perform simple to advanced analyses to assess the capacity of the artwork to withstand static and dynamic (also seismic) actions. In Berto et al. (2012) the vulnerability assessment of the statues pertaining to the Statuary group of *"Prigioni"*, along with *San Matteo and "Pietà di Palestrina"*, sculpted by Michelangelo Buonarroti and exposed in *Galleria dell'Accademia* in Firenze is presented. To perform this work, geometrical survey proved to be fundamental to define the models to be used in the analysis phase. The used data were obtained by above mentioned two kind of geometrical surveys: the rough survey based on the measurement of the main geometrical dimensions, and the high accurate 3D digital representation of each sculpture obtained with laser scanner technology by the Visual Computing Laboratory, ISTI-CNR. Since the high (often excessive for computational purpose) accuracy of the 3D laser scan geometrical survey, the original precision was reduced and a surface with around 50 k faces was chosen. With such resolution it was possible to obtain reliable results with an acceptable computational time.

In Figure 17 are reported the digital models, reconstructed from the laser scanner survey, of three statues exposed in *Galleria dell'Accademia* in Firenze: San Matteo, Prigione

Barbuto and Prigione Atlante.

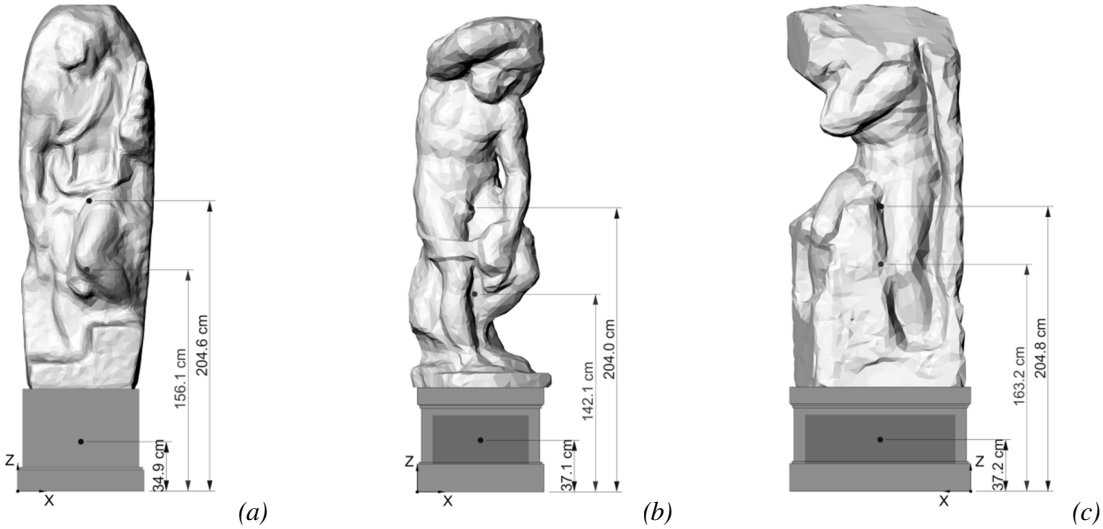

San Matteo *Prigione Barbuto* *Prigione Atlante*

Figure 17 – Digital model and geometrical data of Michelangelo's San Matteo (a), Prigione Barbuto (b) and Prigione Atlante (c)

Thanks to the surveys, it was possible to evaluate seismic capacity of the sculptures in terms of rocking and overturning, with the analysis of rigid body models, and in terms of stress state with the analysis the solid meshes for the Finite Element Analyses, created from the 3D geometry of the statues.

A famous example of the use of Laser Scanner Survey in order to perform extensive F.E. analysis is presented in Borri and Grazini (2006), where the results of the vulnerability analysis of Michelangelo's David is presented. Various numerical models of *David* were constructed, at varying levels of sophistication and detail. The most relevant one was obtained from a survey using laser-scan technology done by the ISTI-CNR (Matteini, 2004), in collaboration with Stanford University. The laser scanner survey provided also in this case a very detailed geometrical model, made by a surface composed of over 50 million triangles (Figure 18).

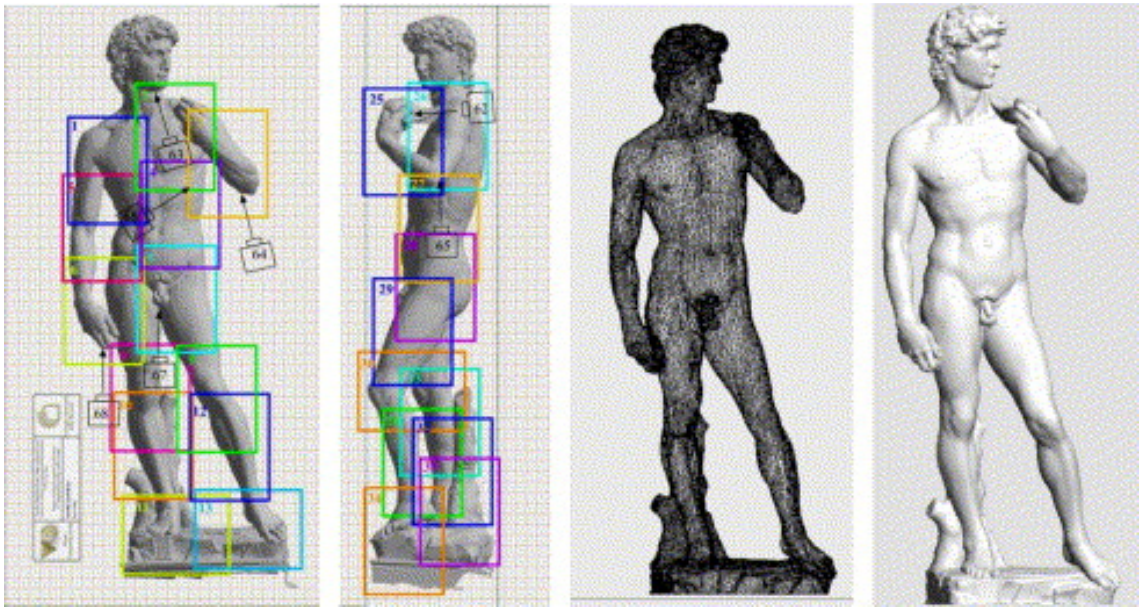

Figure 18 – Digital model of Michelangelo's David – Borri and Grazini (2006)

Also in this case the detailed geometrical survey provided the basis for further simplified models with 20,000, 50,000 and 100,000 triangles to facilitate structural analysis computations (see Figure 19). Starting from these surfaces, appropriately treated and made regular, the solid of the statue was represented and used to define the numerical model made by over 400,000 finite elements.

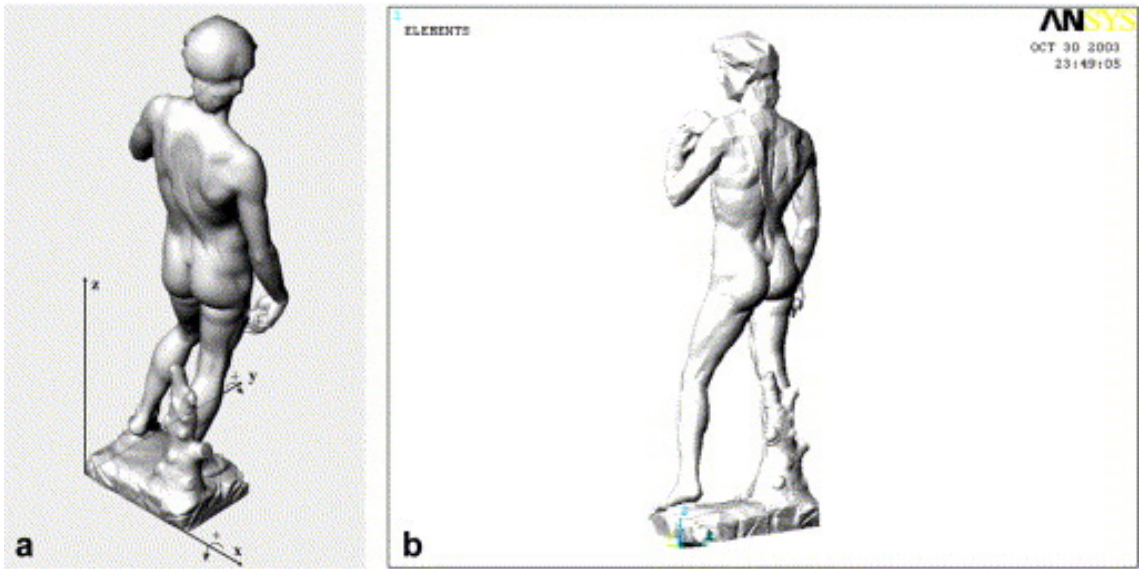

Figure 19 – Simplified model for Numerical analysis – Borri and Grazini (2006)

In present days, new technologies are made easily available to the users for the geometrical survey, in particular using Autodesk 123D Catch, a free software developed and distributed by Autodesk part of a suite of hobbyist CAD and 3D modelling tools based on Autodesk Inventor. The primary intent of such software is to enable users of 123D to create physical objects from their designs using 3D printing technology.

Autodesk's Catch program uses photogrammetry technology to create a 3D model out of multiple pictures taken by the user and support the exportation of STL 3D models. This software connects together images with common visual structures, then asking the user to help connect points that could not be determined through the automatic analyses. Such program can be used to create 3D models in form of a cloud of points and it is therefore particularly interesting for the possibility to represent the geometry of an object without need of expensive and cumbersome equipment as for laser scanner survey. In the perspective of protection of cultural property from the effects of seismic risk, it is therefore possible to easily obtain the real geometry of an object, enabling the rapid estimation of inertial characteristics necessary to the determination of the seismic vulnerability of the asset. In the Autodesk 123D Catch website, a wide gallery of 3D models shows the potential of this program for quick and easy survey of cultural objects, among the most general models generated by amateurs, a good number of scanned art objects are presented and available for download for further 3D modelling (see Figure 20).

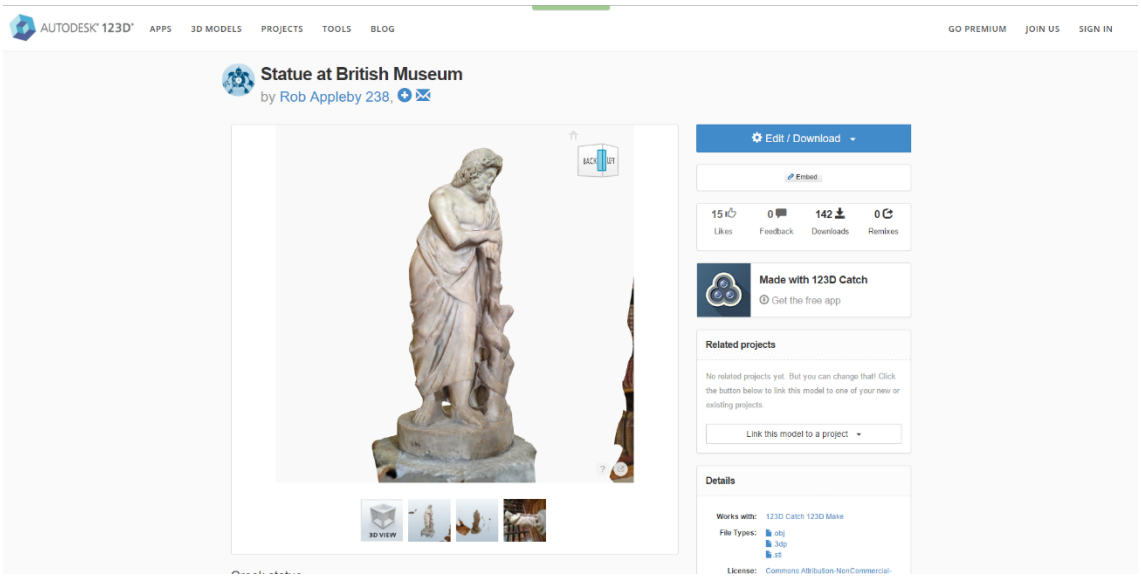

Figure 20 – 123D Catch 3D models gallery, an example of art object

After the preliminary survey phase conducted with Autodesk 123D, it is possible to proceed with the refinement of the raw 3D model with Rhinoceros® 3D, a commercial 3D computer graphics and computer-aided design (CAD) application software, to get a representation of the art object suitable for the numerical analyses.

In Sect. 4, the case study of the seismic mitigation intervention for the Bust of Francesco I D'Este is presented. In particular, more than one hundred photos taken during a photographic survey are elaborated with Autodesk123D Catch to obtain a first

geometrical model and elaborated by mean of Rhinoceros® 3D. In order to model the real geometry of the Bust a first direct measurement of the dimension is performed, then the information is used to adjust the final length, width and depth of the geometrical model prior to the numerical modelling. Some phases of the modelling process are presented in Figure 21, in which the elaboration of the photos is shown and the raw geometry of the bust is made and in Figure 22 where the second phase of refinement of the geometry of the bust is presented.

Figure 21 – Bust of Francesco I D'Este, photos elaboration with Autodesk 123D

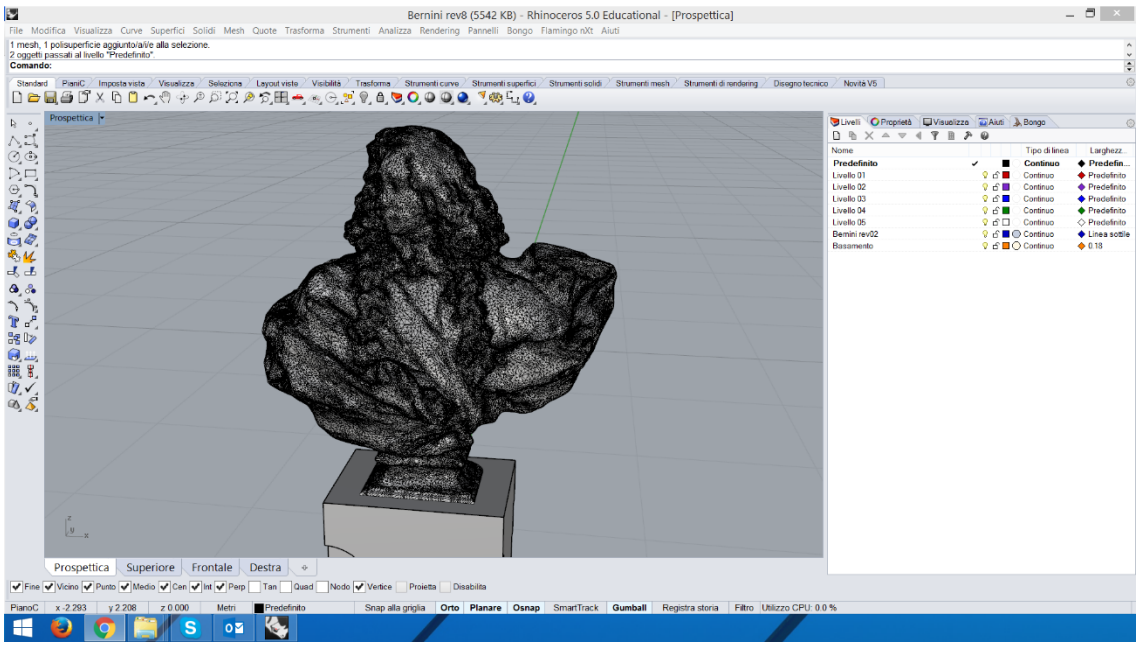

Figure 22 – Bust of Francesco I D'Este, geometry refinement with Rhinoceros® 3D

2.3.2 Rigid Body

The response of a free rigid body on a horizontal rigid floor to earthquake base excitations has been studied by several authors (e.g. Yim et al. 1980, Ishiyama 1982, Housner1963). A detailed description of the types of motions which can occur (rest, sliding motion, rocking motion, sliding-rocking, free flight, impact) can be found in reference Lowry et. al. (2006) and Shenton (1996).

The present study focused on the criteria for triggering of rocking and overturning, which are two very dangerous conditions. Actually the triggering of oscillations could lead to uncontrollable damage of the object while if overturning occurs the safety of the persons which are near the object is not satisfied anymore.

In a preliminary phase the coefficient of friction between the block and the base is assumed to be adequate to prevent the occurrence of sliding phenomenon as the first critical event. Once the minimum values of PGA which cause rocking are calculated some considerations about coherent and reliable values of friction coefficients should be carried out. Also the case of non-symmetric body with respect to the vertical central axis is considered, in addition to the classical one of symmetric rectangular body, which has been studied in depth in literature (e.g. Shenton 1996) and to which the stability analysis of art object is often referred to (e.g. Lowry et. al. 2006).

When a rigid body is subjected to horizontal base acceleration a_g, it will be set into rocking when the overturning moment of the inertia forces around one of its edge exceeds the restoring moment due to the gravitational force, e.g. (Housner 1963, Yim et al. 1980, Augusti and Ciampoli 1996). In such a case the block will oscillate around the base edge, which is assumed as the centre of rotation O or O' depending on the acceleration sign (Figure 23). Hence the critical peak acceleration ($a_{g,c}$) corresponding to the onset of the rocking motion around the point O is given by:

$$\frac{a_{g,c}}{g} = \frac{b}{h} \quad [-] \qquad (14)$$

where g is the gravitational acceleration, b is the distance between the base corner O and the vertical projection of the centre of gravity CG; h is the height of the centre of gravity from the base of body.

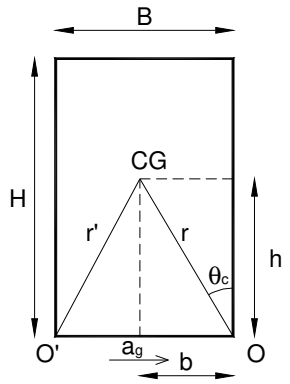

Figure 23 – Geometric parameters of the rigid block

A similar relation may be written for the rotation around the edge O' obtaining a second rocking condition. When the object is non symmetric and may rock on two sides, it is usually sufficient to evaluate the rocking condition corresponding to the minimum value of b. As for the overturning of the block, in this thesis the criterion proposed by (Ishiyama,1982) is applied: the lower limit of the maximum acceleration which can induce overturning is given by the rocking condition (14), while the lower limit v_c of the velocity to overturn a rocking body is given by:

$$v_c \cong 0.4 \sqrt{2 \cdot g \cdot (i^2 + r^2) \cdot (1 - cos\theta_c) \cdot \frac{1}{r \cdot cos\theta_c^2}} \quad [m/s] \qquad (15)$$

where i is the radius of gyration of the block about CG, r is the distance between O and CG and $\theta_c = arctg(b/h)$, as shown in Figure 23.

For slender body with a rectangular form, the overturning criterion may be simplified as:

$$v_c < 0.4 \cdot \sqrt{\frac{4}{3} \cdot \frac{gb^2}{h}} \cdot \cong 14.46 \frac{b}{\sqrt{h}} \quad [cm/s] \qquad (16)$$

In this work the relation (16), valid for rectangular blocks, is applied also for non-symmetrical bodies by replacing h with an equivalent object height h' defined as:

$$h' = \frac{4}{3} \cdot \frac{h^3}{i^2 + r^2} \quad [m] \qquad (17)$$

2.3.3 Deformable body – stress analysis

The simplest solution for preventing the possible body motion is to fix firmly the object to its base, in order to ensure it from rocking or overturning phenomena. This requires to control that the stress level induced in the statues by the seismic action is lower than the strength of the material at any instant. To this aim, a stress analysis of the statue should

be carried out, with models of different degree of accuracy. Many art objects are in fact not strong enough to withstand the dynamic induced forces, as for example glass pieces or tall statues anchored at its feet.

In many cases it is possible to perform a simplified analysis on wireframe models, as described in Borri and Grazini (2006) for the first analyses on Michelangelo's David. In that work a wire frame model of the statue is used to assess the axial forces and the bending moments on the critical section, Figure 24. This kind of model is used to assess the first evaluation of the response of the statue to different earthquakes' simulations without using a more complex 3D model with high computational request. In these analyses the body statue is represented by a model made of different beams connected together, whose geometry approximates the characteristics of the body of the statue.

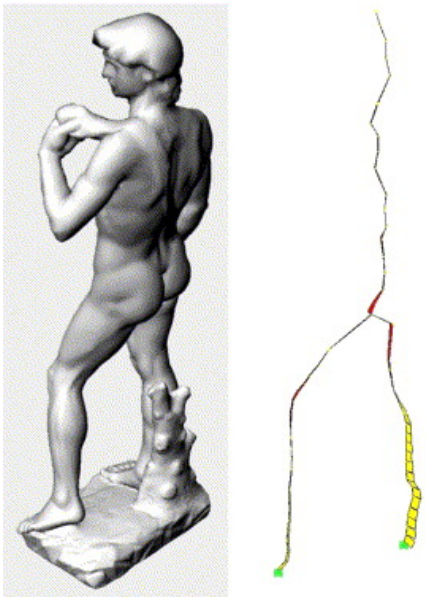

Figure 24 – Wireframe model for Numerical analysis – Borri and Grazini (2006)

On the other hand, to perform accurate analysis, a solid mesh can be created for the art object, e.g. based on a 3D laser scanner survey described at Sect. 2.3.1. Finite element analyses can be performed using different numerical codes (e.g. *midas GEN*, Sap2000, Abacus, Ansys, etc.) in order to evaluate the stress state on the model, see for example Figure 25 where the positive stress of *Prigione Barbuto* are evidenced.

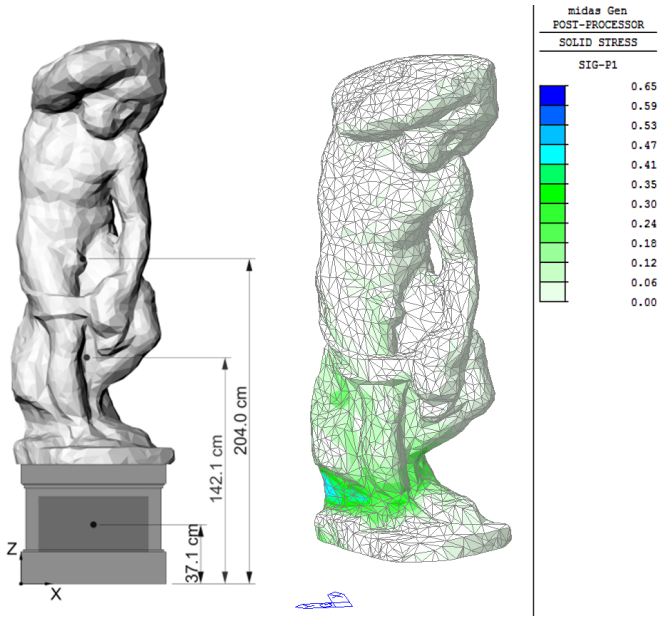

Figure 25 – Prigione Barbuto geometrical and numerical model

The first step of any numerical analyses should always concern linear analyses in order to obtain an overview of the general stress level and a stress pattern of the weakest areas. In this way it is possible to determine, for the statues made by brittle material, which zones are affected by the highest tensile stress and thus which ones could be more vulnerable.

Regarding the material properties, they could be evaluated taking advantage of all the available data from both literature and direct examination of the artworks. For example, in the case of the statuary group of *Galleria dell'Accademia*, the material properties of marble were defined basing on the results of the autoptic examination performed on the external surface of the sculptures, according to the procedure presented in Berto et al. (2011).

More refined non-linear analyses can be performed in case of particular situations, such as tricky conservation condition of the statue itself, as the case of Prigione Barbuto which show the presence of a pass-through fracture on the trunk of the status. Moreover, in case of implementation of a seismic isolation system, non-linear analyses are always necessary.

Some examples of the outcome of the linear and non-linear analyses are given in Sect. 3.3.7.2, with particular reference to statues in non-isolated and isolated condition subjected to the same seismic signals.

3 Seismic Risk Mitigation

3.1 Foreword

Seismic risk mitigation on Museums' contents is a challenging task, that requires a multidisciplinary approach, involving different professional figures in the process, and needs the knowledge of different aspects of artwork preservation. From the simple mount making to the most innovative seismic isolation system, every solution requires the definition of a specific methodology for evaluating the level of safety, since the possible interventions need to find a compromise between safety and conservation requirements, e.g. Agbabian al.et al. (1991). In this sense, seismic isolation is a common and widespread technique for the mitigation of the seismic risk on new buildings and civil constructions, and it can be considered also an interesting retrofitting solution for protecting existing constructions, limiting the transferred action to a tolerated level, safe for the structures. On the other hand, it is worth noting that the isolation of building contents, like museum contents as well as sophisticated medical devices or high performance computer installations, has lagged behind the trend. In this chapter, opportunity and advantages of applying base isolation technologies developed for civil structures to small objects are investigated and some considerations related to the scale effects are discussed. Taking advantage of a series of experimental tests carried out in Caltrans SRMD (Seismic Response Modification Devices) test facility at the University of California San Diego (UCSD), the dynamic response of a system designed to simulate a seismically isolated sculpture is investigated. To this aim, Double Concave Curved Surface Sliders (DCCSS) are specifically re-designed to fit the peculiar situation of "light weight" objects (compared to civil structures). Such prototypes tested in the experimentation were designed accordingly with the specific need of seismic isolation for the six Michelangelo's sculptures placed at the *Galleria dell'Accademia* in Firenze, Italy. To this aim, an experimental set up, made with 4 stackable concrete blocks, was configured to match the geometric and inertia characteristics of Michelangelo's sculptures. More detail about such experimental set – up and the related results can be found in Favaretto (2012). In order to perform an accurate and reliable prediction of the seismic response of the proposed isolated system, the main aspects concerning the numerical simulation are here discussed, also to investigate the efficiency of the existing numerical models, which are developed for traditional devices, when they are applied on such small and particular objects.

A sensitivity analysis on the main parameters of the numerical model of the isolator system was carried out, comparing different calibration to find out the most suitable to numerically reproduce the experimental campaign. In particular, the effect of an enhanced calibration of friction coefficients was presented through the discussion of a number of numerical simulations of both experimental tests and real sculptures under different dynamic conditions.

With this enhancement, the experimental tests results were re-analysed and compared with those obtained for the statues subjected to sinusoidal inputs.

Finally, the sculptures in isolated conditions were subjected to a set of generated accelerograms, compatible with the design spectrum characterizing the Florence site and the main results of the analyses are presented and compared with the case of non-isolated systems. The combined results of this experimental/numerical campaign show a general efficiency of the isolation system in terms of limiting the transferred action and foster the application of this promising technology to art objects. In the conclusion, a close examination of the ripened results is given.

3.2 State of the art of the seismic mitigation techniques

An exhaustive analysis of the seismic mitigation techniques and interventions for art goods is given in Berto et al. (2013), and here reported, with some notes and updates in the latest innovation and implementation on this field.

A first approach to seismic risk mitigation of art objects is the choice of anchoring the object to the structure by means of different support mounts that essentially make it a part of the structure itself, Lowry et al. (2008). However, in this way, the seismic forces will be fully transmitted to the object which often is too brittle to withstand the seismic load. For this reason, in many cases an alternative approach is to be preferred, especially in zones with moderate and high seismicity, for example by adopting base isolation system. This technique is today a widely accepted design philosophy for earthquake resistant design of structural systems as well as sensitive instruments and art objects, e.g. Lowry et al. (2008), Forni et al. (2003), Caliò and Marletta (2004), demonstrating to be an excellent solution, suitable for different types of object, limiting the transferred seismic actions.

Even though the basic concepts and theories that govern the problem are substantially the same, isolation techniques developed for civil structures cannot be directly extended to small objects, but some specific considerations are needed. Small objects involve masses

that are orders of magnitude smaller than those typical of civil structures, hence the interaction with the bearing is significantly different; moreover, such category of objects often cannot withstand even low levels of seismic action. For these reasons the parameters governing the behaviour of the isolation devices need to be adequately recalibrated.

Specifically concerning art objects, a main issue is related to their great historical and cultural value, which requires particular attention in the intervention techniques which have to respect the conservation requirements. Furthermore, the maximum allowed displacement of the system has to be carefully evaluated, since it has to be related both to the required level of protection and to the availability of room in the exhibition area.

One of the most active institutions in the field of art objects protection is the "Getty Conservation Institute" which has provided the first examples of specifically designed anti seismic devices, basically showcases and big statues, mainly exhibited in Getty Villa, in Malibu, Podany (2008). Both rough and low impact techniques, such as mount makings, and seismic isolation systems have been adopted (Lowry et al., 2008); in particular, for the latter solution, sliding bearings have been realized as multiple layers of unidirectional sliders (Figure 26a), made as small carts moving on lubricated spheres along a restrained direction. Characteristics of devices are tailored for each art object and they fit the environment of the museum, (Figure 26b). One of the most famous examples of seismic isolation in the Getty Villa is the one concerning the statue of a Kouros (the Agrigento Youth), which was equipped with a custom seismic isolated base and pedestal based on the technology described above.

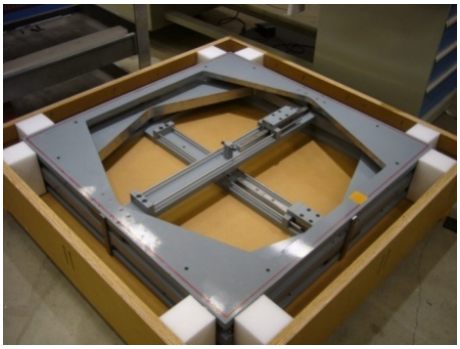

(a)

(b)

Figure 26 – The Getty Conservation Institute - examples of isolation devices (a) multiple layers of unidirectional sliders; (b) in situ installation

A number of other applications have been realized in different seismic countries, but almost all have been carried out by developing specific isolation systems for each object. Some examples of seismic isolation of art objects have been carried out in Italy, e.g. the statue of the Satyr of Mazara del Vallo and the statue of the Imperatore Germanico, which have been isolated by means of laminated rubber bearings; the statues of Nettuno and

Scilla, for which the isolation has been realized by using supports made by steel and Teflon and dampers made of shape memory alloy steel, e.g. (Forni et al., 2003) and (Caliò and Marletta, 2004), and finally the most famous application for the isolation of Bronzes of Riace, for which the first isolation system of the statues was recently replaced with a new special aseismic basement which consists of two great marble blocks supported by four spheres.

It is worth noting that the applications previously described concern art objects isolated by means of specifically studied and designed devices for the situation in which they needed to be applied, according to a tailor-made approach: this optimizes the benefits of isolation, but on the other hand it is not easily applicable to a large number of objects with different characteristics. A smart solution to help the spreading of seismic isolation solution is the application of traditional devices for the protection of art objects, in order to take advantage of the existing technologies.

About this solution it is worth mentioning the statue of Hermes and the Infant Dionysus (h = 2.13 m), the only known surviving work of the sculptor Praxiteles, on display at the Archaeological Museum of Olympia, Koumousis (2007), and isolated by means of the single concave friction pendulum devices.

Following this first example, DCCSS sliders, a kind of friction pendulum bearing widely used in civil applications, are taken in consideration for the seismic isolation of cultural and art object. In particular since the studies by Favaretto (2012), *FIP Industriale* proposed the application of such devices for specific interventions, i.e. the seismic isolation made for the ancient Roman ruins exposed in the archaeological complex of the "*Terme di Diocleziano*" (Baths of Diocletian) in Roma. Figure 27 displays a seismic isolated base made for the restoration of an ancient arch.

Figure 27 – Ancient Roman Arch: the structure is seismically isolated by DCCSS isolators

3.3 Study and in depth analysis of DCCSS isolation device

The sliding bearings isolation system, i.e. the Double Concave Curved Surface Sliders (DCCSS), Fenz and Constantinou (2006), Naeim and Kelly (1999) is considered as a promising and operative solution for seismic risk mitigation of art objects. Such a system is a sliding re-centring device and it is characterized by the fact that the period of oscillation of the structure does not depend upon the mass itself but only on the equivalent radius of the curved surfaces. Moreover, thanks to the intrinsic simplicity, versatility, stability and durability of the dispositive, the isolation by means of curved friction sliders can be considered a particularly valid retrofit strategy, and their employment is especially advantageous in case of irregular or unusual structures with severe performance requirements, including supported equipments and museum sculptures, as suggested by Zayas et al. (1989). Moreover, another important characteristic of these devices is their capacity, once the input is ceased, to re-centre in the initial position, as a combined effect of gravity and curvature. Apparently this characteristic can appear unimportant, but actually it helps the isolated system to safely withstand possible seismic aftershock events.

The idea proposed first in Berto et al. (2013), Baggio et al. (2013) and Baggio et al. (2015a) is to apply the DCCSS, usually adopted for civil applications, to light objects, after a proper re-design and calibration of the devices themselves for the specific case study, and taking advantage of the existing industrial knowhow and technical background, e.g. Infanti et al. (2011). Indeed, as mentioned in Sect. 3.2, seismic isolation by means of friction pendulum bearings (to which also DCCSS belong) has been sussefully realised for the statue of Hermes and the Infant Dionysus, while DCCSS has been already successfully applied for the Ancient Roman ruins in *Terme di Diocleziano* in Roma (*FIP Industriale* latest installations) as mentioned above.

In particular, DCCSS can be considered as an improvement of the friction pendulum bearing for this kind of application. Indeed, compared to other kinds of isolator devices, as elastomeric rubber bearings, or articulated sliders, DCCSSs consent to contain the dimension of the application, in this way respecting the strict specifications of the museums exhibitions.

To prove and validate the use of this kind of seismic isolator, it is taken advantage of the results given by a major research aimed to assess and reduce the seismic vulnerability of art objects (Berto et al. 2012, Berto et al. 2011a, Berto et al. 2011b). Within this research, six Michelangelo's marble sculptures on display at *Galleria dell'Accademia* in Florence,

Italy, (Figure 27) are studied. Indeed, the most significant statues in terms of geometry, mass and conservation state are selected and considered for an in depth look and for further numerical analyses (see Sect. 3.3.7).

Geometrical and inertial characteristics for the six statues are presented in detail in Berto et al., (2011b). These information, useful for vulnerability assessment, are obtained by the acquisition and elaboration of laser scanner surveys (courtesy of ISTI CNR – Pisa) that allowed to assemble the numerical model of the real geometry of the statues. The DCCSS prototypes employed in this procedure are characterized by concave surfaces of equal radius and equal friction coefficient at the two sliding interfaces. The sliding interfaces consist on one side of a proper high-strength thermo-plastic material and on the other side of mirror-polished stainless steel.

The first fundamental step of this work on DCCSS devices is the initial redesign phase: indeed, a simple scaling of the standard devices is not sufficient to provide a reliable solution and it is necessary to perform a complete re-configuration of the mechanical parts of the devices, also considering different materials and constructive technologies. Such an aspect was carried out in Favaretto T. (2012) and Berto L., et al. (2013) in collaboration with *FIP Industriale*, which knowledge and experience on friction isolators is confirmed by its previous work as the supplying of more than 2400 isolation units of the DCCSS type for the buildings in the C.A.S.E. Project in L'Aquila (C.A.S.E. 2010, Infanti et al. 2011).

(a) Prigione Che Si Sveglia *Prigione il Giovane* *Prigione Barbuto* *Prigione Atlante*

(b) San Matteo *(c) Pietà di Palestrina*

Figure 28 – (a) The four Slaves or Prisoners (I Prigioni); (b) San Matteo and (c) Pietà di Palestrina (Florence, Accademia Gallery)

Following this initial design phase, two different series of experimental tests were carried out: the first one at the laboratory of the above mentioned firm aimed to preliminarily identify the mechanical parameters of the devices; the second series of tests, carried out at the Caltrans SRMD test facility, were aimed to verify the preliminary identification and to study the interaction between these new devices and a system simulating the Michelangelo's marble sculptures (further details about the statues of the case study can be found in Berto, et al. (2012) and Berto et al., (2011b)).

In particular, Berto L., et al. (2013) presents the results of the experimental tests performed at the Caltrans SRMD test facility on a model made of four reinforced concrete blocks, whose geometrical configuration and weight are designed to properly represent the body of the statues with adequate accuracy. During the experimental campaign, different tests were performed in order to investigate those aspects that could particularly affect the response of the system, e.g. rocking phenomena, presence of bidirectional and

vertical input, etc. Then, numerical analyses are carried out with the aim to evaluate the possibility to apply the existing numerical models developed for traditional devices also for such kind of light and particular structures (i.e. statues). Therefore, the calibration and validation of the most relevant mechanical parameters were performed: i.e. friction coefficient, initial stiffness and numerical damping.

After this preliminary studies, an enhanced calibration of friction coefficients, which are crucial parameters influencing the behavior of the isolation system, was proposed in this thesis and preliminarily presented in Baggio et al. (2015a) through the discussion of a number of numerical simulations carried out on the experimental tests. In order to validate the behaviour of the isolation system, after the preliminary phase of parameters calibration, an extensive phase of simulation is performed on real geometry models. The isolated statues of *San Matteo*, *Prigione Barbuto* and *Prigione Atlante* (Figure 29) are therefore examined under sinusoidal input (i.e. the input used for the experimental tests) and seismic acceleration inputs.

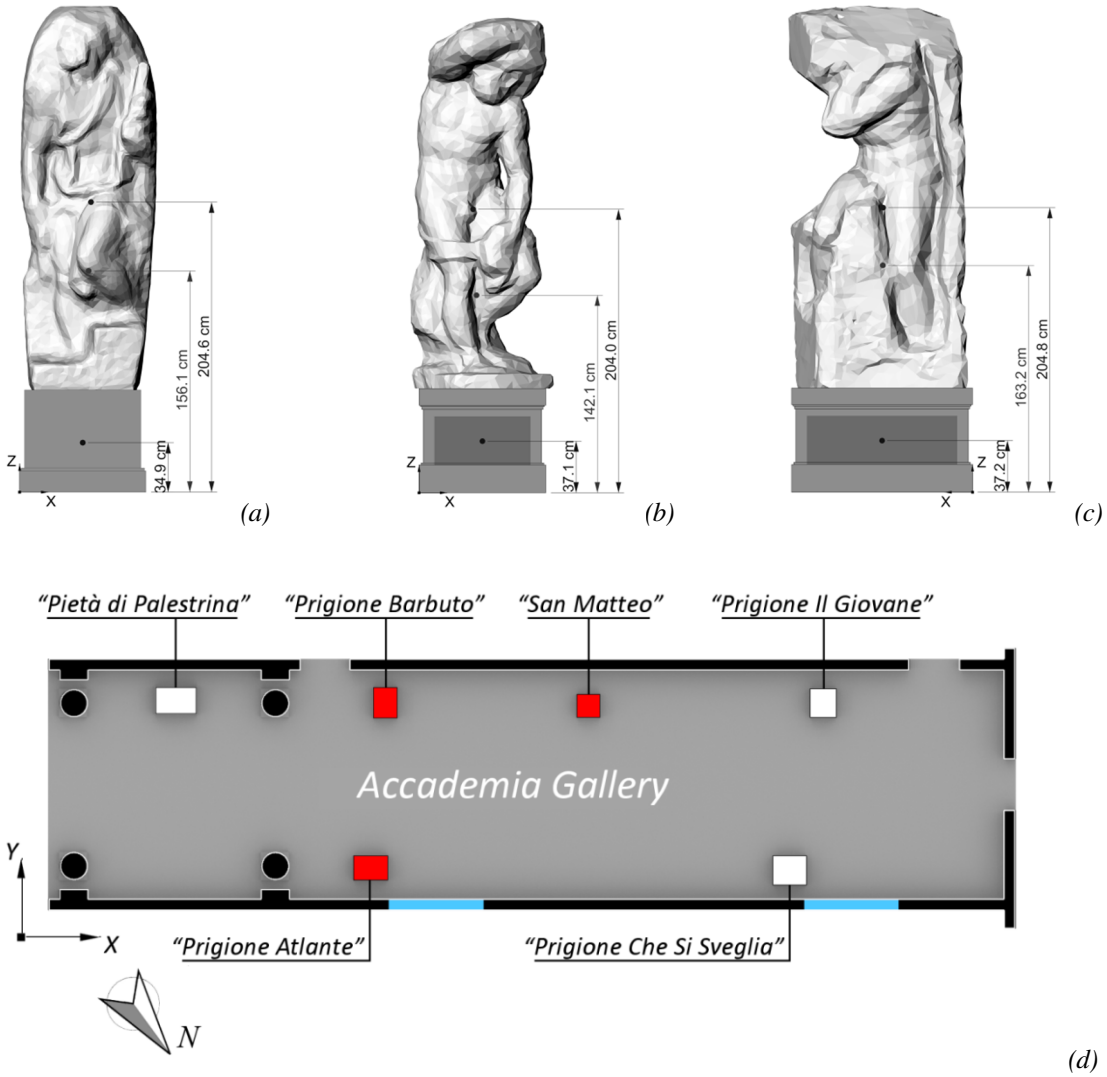

Figure 29 – (a) San Matteo; (b) Prigione Barbuto; (c) Prigione Atlante; (d) location of the sculptures in the gallery (Florence, Accademia Gallery)

3.3.1 Mechanical characteristics of the device

The mechanical behavior of double concave friction pendulum, which has been widely described in Fenz and Constantinou (2006) and in Tsai et al. (2005), is assumed as the reference model for the adopted device. In the following, a brief review of the model proposed by Fenz and Constantinou (2006), for the Double Concave Friction Pendulum Bearing device is presented. In particular, referring to the case of a device with concave surfaces of equal coefficient of friction at the two sliding interfaces, the DCCSS behaviour can be easily represented by an equivalent device where R^* (effective radius of curvature) is calculated as sum of the upper (R_1) and lower (R_2) radius of curvature.

The theoretical Force (F) - Displacement (D) relationship for the device is shown in Figure 30, where W is the vertical load acting on each bearing, μ is the coefficient of friction. In the initial branch, the system is very rigid, with stiffness K_1, until the force $F_0 = \mu W$ is reached, then the restoring force increases proportionally to the displacement, with the stiffness.

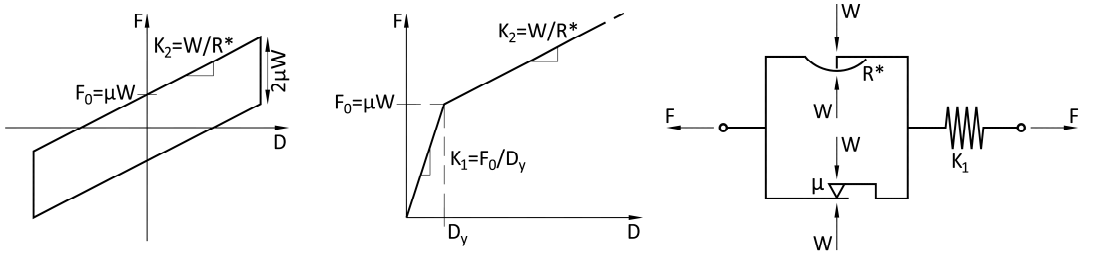

Figure 30 – DCCSS isolation device: (a) theoretical mechanical model; (b) theoretical mechanical model, detail of first branch; (c) schematic representation

The analytical relation between resisting shear force F and the horizontal displacement D along each horizontal direction is therefore:

$$F = \begin{cases} K_1 \cdot D & first\ branch \\ \dfrac{W}{R^*} \cdot D + \mu \cdot W(sign\dot{D}) & second\ branch \end{cases} \qquad (18)$$

In which $\dot{D}$ is the velocity of the motion when sliding occurs. The first term of the second equation is the contribute of the pendulum and it represents the restoring or recentering force developed by the rise of the mass during the motion, offering an horizontal stiffness:

$$K_2 = \frac{W}{R^*} \quad [N/m] \qquad (19)$$

Using such an isolation system, the period of oscillation of the structure does not depend upon the mass itself but only on the equivalent radius R^* of the curved surfaces, according

to the formula, e.g. Infanti et al. (2011), Naeim and Kelly (1999):

$$T = 2\,\pi \sqrt{\frac{1}{g\left(\frac{1}{R^*} + \frac{\mu}{D}\right)}} \quad [s] \qquad (20)$$

where g is the gravity acceleration.

Concerning the friction coefficient, in DCCSS Pendulums device, the attritive properties are expressed with the exponential formula as proposed by Constantinou et al. (1990):

$$\mu(v) = \mu_{fast} - \left(\mu_{fast} - \mu_{slow}\right) \cdot e^{-rv} \quad [-] \qquad (21)$$

where v is the modulus of the sliding velocity vector, r is the evolutive ratio, μ_{fast} and μ_{slow} are the values of the coefficient of friction respectively for high and low sliding velocity.

3.3.2 Characteristics of the prototypes

First prototypes of DCCSS devices suitable for seismic isolation of sculptures are designed and manufactured in collaboration with *FIP Industriale* in 2012, when the studies about this peculiar application started, performing also a specific experimental campaign. Currently, the study on the devices continues with the aim of refining the calibration of the numerical model to represent the dynamic behaviour of seismically isolated statues.

Concerning the geometrical characteristics of the DCCSS used in this research, the dimensions of the devices are scaled with respect to the usual isolators adopted in civil application: in particular, with reference to Figure 31 and Figure 32, the following geometrical characteristics are adopted:

- Height H = 75 mm;
- Diameter ϕ = 270 mm;
- Maximum displacement D_{max} = ± 160 mm;
- Curvature radii R_1=R_2 = 1500 mm
- Equivalent radius $R^* = R_1+R_2$ = 3000 mm.

(a) *(b)*

Figure 31. – DCCSS isolation device for the case study: (a) front view; (b) top view.

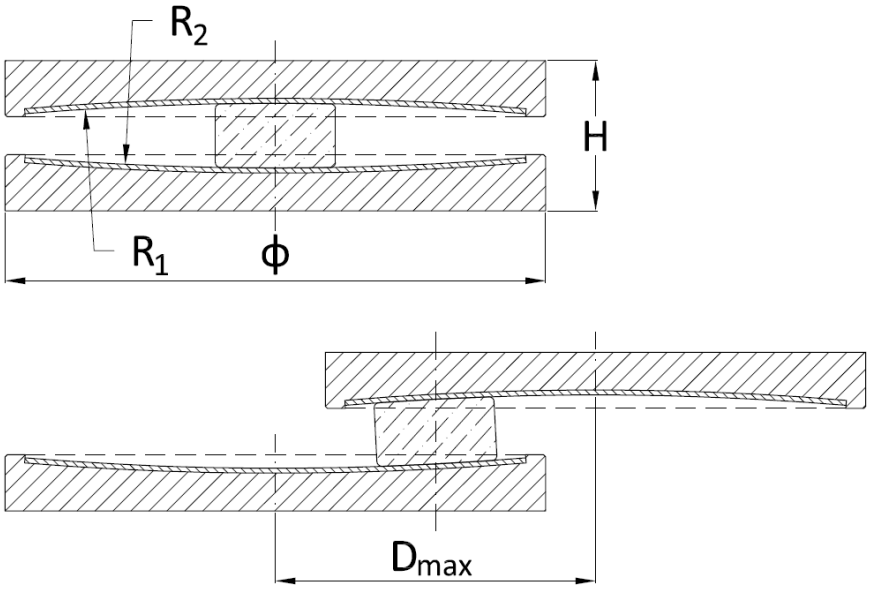

Figure 32. – DCCSS isolation device: geometrical characteristics

The design parameters of the isolators are obtained by considering the seismic action in accordance with the current Italian Standards (NTC 2008, D.P.C.M. 2011) for the site of the *Galleria dell'Accademia* in Florence, assuming a soil type D and a return period T_r = 712 years, Berto et al. (2012), (2013).

Finally, according to the dimensions and the characteristics of mass of the "Prigioni" statues, the reference vertical load W = 10 kN was assumed for each device.

Concerning the other mechanical parameters, it is worth noting that the friction coefficient μ (Sect. 3.3.1 Eq. (21)) is not known a priori, and it is evaluated starting from the results of the tests performed in *FIP Industriale* Research Facility, and considering that, differently to other kind of Friction pendulum devices, a layer of lubricant is applied between the sliders and the sliding surfaces. The lubricant is placed into sliders' cavities, as to reduce the level of transmitted forces to the isolated object.

Figure 31(a) and Figure 31 (b) show one of the DCCSS devices utilized for the case study, with highligthed the small dimensions compared with the standard dimensions of DCCSS used for civil applications, e.g. for the CASE Project devices with h = 112 mm, Φ = 640 mm (C.A.S.E., 2010) have been used.

3.3.3 Experimental tests on the prototype of the device

In order to investigate the dynamic response of isolated art objects, a physical model of the statues on display at the "Galleria dei Prigioni" is designed considering the sculptures of the case study and their geometrical and inertia features. The basic design idea on which this model is built is "modularity", keeping always the possibility to assemble it with a different layout, in order to study different effects, as described below.

The physical model used for the experimental test consists of four reinforced concrete blocks, cast in two different shapes. The lower block, called "footing block" (1.21 x 0.91 x 0.38 m^3 with a weight of 10.65 kN), constitutes the base of the model, while the others, called "body blocks" (all with the same dimensions 0.83 x 0.66 x 0.83 m^3, about 10.5 kN weight), can be put together in different arrangements. The geometrical configuration and the total weight of the equipment are chosen to properly represent the body of the statues with adequate accuracy. Four isolator devices are placed at the corners of the footing block, obtaining the maximum distance between the supports. In Figure 33, three of the five configurations used in the experimental tests are depicted, in particular the three configurations with total weight equal to 41.5 kN, which better approximates the mean weight of the case study, and characterized respectively by low center of mass (Cfg#1), high center of mass (Cfg#4) and high center of mass with eccentricity along lateral direction (Cfg#5).

Test	*Long.*	*Lat.*	*Test Set Up*		*Configuration*
			Long.	*Lat.*	
4	*D1 0_8V1*	-	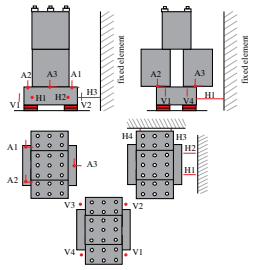		
6	*D1V2*	-			
13	*D1 0_8V1*	-	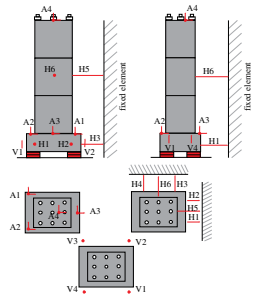		
20	*D1 1_5V2*	*D1 0_8V1*			
24	*D1 1_5V2*	*D1 0_8V1*	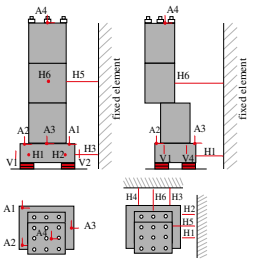		

Figure 33 – Detailed description of a selection of the performed tests: input function, geometrical configuration and layout of the acquisition devices, Berto et al. (2013)

Figure 34 shows the position of the four sliding isolators on the horizontal plane centered on the midpoint of the footing block, together with the points representing the eccentricities of the Cfg#4 (e = 0) and Cfg#5 (e = ± 114 mm). In the same Figure 34 the eccentricities of all the analyzed statues evaluated along the X, Y directions defined in Figure 29, are also shown.

It clearly appears that the *Prigione Atlante* has a marked eccentricity in the lateral direction, which makes this sculpture the more comparable to the CFG#5, while the other statues display smaller eccentricities in both directions.

A horizontal sinusoidal input, with the displacements amplitude D1 equal to 60 mm and different velocities and accelerations obtained with a variation in the frequency input, is applied in the tests, Table 3. Three complete cycles are applied to the system with the exception of two bidirectional tests (test 20 and 24) with eleven cycles.

For the sake of clarity, a complete list of the performed tests is presented in Table 4. In this thesis only some significant tests were selected. Figure 33 summarizes the considered

tests with their main characteristics: input function, direction of application of the input, the test set-up with the layout of the acquisition devices and the geometrical configuration.

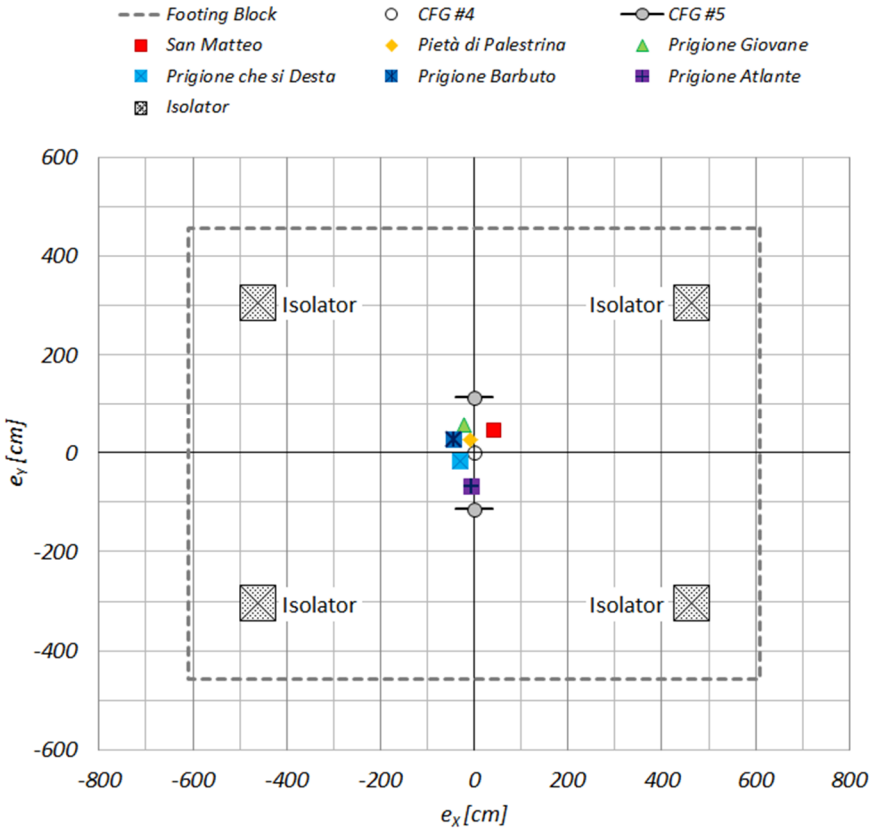

Figure 34 – Plane position of the sculptures' eccentricities compared with the ones of cfg#4 and cfg#5.

Input Name	***Frequency***	***Amplitude (PGD)***	***PGV***	***PGA***	
	[Hz]	*[mm]*	*[mm/s]*	*[mm/s^2]*	*[g]*
D1 0.8 V1	*0.424*	*60.00*	*160.00*	*427*	*0.04*
D1 V2	*0.8*	*60.00*	*300.00*	*1500*	*0.15*
D1 1.5 V2	*1.2*	*60.00*	*450.00*	*3375*	*0.34*

Table 3 – Parameters of the horizontal input tests

Test	*LON*	*LAT*	*VERT*	*PGD*	*PGV*	*PGA*	*CONFIGURATION*					*DIR*
				[mm]	*[mm/s]*	*[g]*	*1 [LCM]*	*2 [LCM2]*	*3 [LCM1]*	*4 [HCM]*	*5 [HCME]*	
1 (*)	*D1V1*			*60*	*200*	*0.07*	*X*					*LON*
2	*D1V1*			*60*	*200*	*0.07*	*X*					*LON*
3	*D1 0_5V1*			*60*	*100*	*0.02*	*X*					*LON*
4	*D1 0_8V1*			*60*	*160*	*0.04*	*X*					*LON*
5		*D1 0_8V1*		*60*	*160*	*0.04*	*X*					*LAT*
6	*D1V2*			*60*	*300*	*0.15*	*X*					*LON*
7	*D1 1_5V2*			*60*	*450*	*0.34*	*X*					*LON*
8		*D1 0_5V1*		*60*	*100*	*0.02*	*X*					*LAT*
9		*D1V2*		*60*	*300*	*0.15*	*X*					*LAT*
10	*D1 0_8V1*			*60*	*160*	*0.04*		*X*				*LON*
11	*D1 0_8V1*			*60*	*160*	*0.04*			*X*			*LON*
12	*D1 0_8V1*			*60*	*160*	*0.04*				*X*		*LON*
13	*D1 0_8V1*			*60*	*160*	*0.04*				*X*		*LON*
14		*D1 0_8V1*		*60*	*160*	*0.04*				*X*		*LAT*
15	*D1 1_5V2*			*60*	*450*	*0.34*				*X*		*LON*
16		*D1 1_5V2*		*60*	*450*	*0.34*				*X*		*LAT*
17	*D1 0_8V1*		*VERT 1*	*60/19.8*	*160/190*	*0.04/0.19*				*X*		*LON*
18	*D1 0_8V1*		*VERT 2*	*60/9.91*	*160/135*	*0.04/0.19*				*X*		*LON*
19	*D1 0_8V1*	*D1 0_8V1*		*60*	*160/160*	*0.04/0.04*				*X*		*2D*
20	*D1 1_5V2*	*D1 0_8V1*		*60*	*300/160*	*0.34/0.04*				*X*		*2D*
21	*D1 0_8V1*			*60*	*160*	*0.04*					*X*	*LON*
22		*D1 0_8V1*		*60*	*160*	*0.04*					*X*	*LAT*
23	*D1 0_8V1*	*D1 0_8V1*		*60*	*160/160*	*0.04/0.04*					*X*	*2D*
24	*D1 1_5V2*	*D1 0_8V1*		*60*	*300/160*	*0.34/0.04*					*X*	*2D*

(*) non lubricated

Table 4 – Detailed description of the performed tests: input function, the geometrical configuration tested and the direction of application of the input

3.3.4 Numerical Modelling of DCCSS

The numerical model of DCCSS is based on Friction Pendulum System (FPS) numerical model, for which (as previously state about the mechanical model) the equivalent Radius of Curvature R*, sum of the upper and lower radius of curvature, is adopted. In commercial F.E. code as SAP2000 and *midas GEN*, "Friction Isolator" element or "Friction Pendulum System" (FPS) represents a Friction Pendulum isolator and recalls the properties described in Sect. 3.3.1, implementing a viscoelastic behaviour, with hardening. The main characteristics of the FPS link are represented by the frictional properties and by the "post-sliding" stiffness given by the radius of curvature for the two shear forces, and by the simulation of the contact (gap element) in axial direction.

Considering a local reference system (x,y,z) with the x direction coincident to the axial direction of the FPS element, the axial behaviour of the link can be expressed as:

$$f_x = P = \begin{cases} k_x d_x & if\ d_x < 0 \\ 0 & otherwise \end{cases} \quad (22)$$

where f_x is the force transmitted, d_x is the displacement component in the vertical direction (positive if upward). In this way just like the real friction isolators, the link is unable to withstand traction.

Regarding the shear behaviour, along the two orthogonal directions, the link shows:

$$\begin{aligned} f_y = f_{yf} + f_{yp} \longrightarrow f_y = -|P|\mu_y\beta_y - |P|\frac{d_y}{R_y} \\ f_z = f_{zf} + f_{zp} \longrightarrow f_z = -|P|\mu_z\beta_z - |P|\frac{d_z}{R_z} \end{aligned} \quad (23)$$

where the terms with the subscript "f" represent the frictional forces acting in the opposite direction to the movement of the isolator and thus determine the energy dissipation of the system, while those with the subscript "p" represent the pendulum behaviour, with resulting in "Restoring Force" that allows the re-centring of the isolator.

In this case, given the characteristics of the device, the same behaviour is assumed in both directions, namely: $\mu_y = \mu_z = \mu$, $R_y = R_z = R$. The parameters β_y and β_z, represent an internal hysteretic variable. Regarding the friction coefficient μ, it depends on the speed of sliding according to (21), and for readers' convenience, properly modified, and here reported:

$$\begin{aligned} \mu_y = \mu_{fast,y} - (\mu_{fast,y} - \mu_{slow,y}) \cdot e^{-rv} \\ \mu_z = \mu_{fast,z} - (\mu_{fast,z} - \mu_{slow,z}) \cdot e^{-rv} \end{aligned} \quad (24)$$

In which velocity is expressed as the square root of the sum of the square velocity components in the two orthogonal directions:

$$v = \sqrt{\dot{d}_y^2 + \dot{d}_z^2} \quad (25)$$

With the evolutive ratio r expressed as:

$$r = \frac{r_y\,\dot{d}_y^2 + r_z\,\dot{d}_z^2}{v^2} \quad (26)$$

inversely proportional to the velocity.

The internal hysteretic variables are defined by:

$$\begin{Bmatrix}\dot{\beta}_y\\ \dot{\beta}_z\end{Bmatrix}=\begin{bmatrix}1-a_y\beta_y^2 & -a_z\beta_y\beta_z\\ -a_z\beta_y\beta_z & 1-a_y\beta_z\end{bmatrix}\begin{Bmatrix}\frac{k_y}{P\mu_y}\dot{d}_y\\ \frac{k_z}{P\mu_z}\dot{d}_z\end{Bmatrix} \quad (27)$$

In which k_y, k_z are the initial stiffness of the isolator before the sliding occurs (also indicated as K_1 in Sect. 3.3.1 – Figure 30), while a_y, a_z are coefficients that assume 0/1 value.

The parameters that need to be accurately calibrate for the correct simulation of the behaviour of the friction pendulum are therefore:

- μ_{slow}, μ_{fast} dynamic friction coefficients at low and high velocity;
- r: evolutive ratio for the equation of dynamic friction;
- K_1: initial stiffness of the isolator before feedback of sliding;
- ξ: numerical damping for the analyses.

3.3.5 Sensitivity analyses of the main parameters

Starting from the results of the experimental campaign (see sect 3.3.3) a sensitivity analysis on the main parameters of the model of the Friction pendulum is performed, and a first estimation for Initial Stiffness, Friction Coefficients and numerical damping is proposed. In order to fully understand the role of the friction on the energy dissipated by the device, more studies were carried out and an enhanced calibration proposed.

3.3.5.1 Sensitivity to stiffness

Stiffness K_1 represents the slope of the initial part of the constitutive law of the device (Figure 30b). The problem of this parameter is that, even though rules of thumb for its evaluation exist, they are derived from experience and they are mainly referred to devices of traditional dimensions. It is important to correctly assess the value of this parameter because analyses showed that it can strongly affect the prediction of the response of the system.

Starting from some of the expressions proposed in literature for the assessment of initial stiffness, (which, as previously stated, are referred to devices with traditional features), the value of initial stiffness K_1 to be assumed in the case study came out as result of a parametric analysis. In particular four proposals were considered: the first two are directly derived from the literature and the other two are specifically proposed in this study.

According to the proposal of Naeim and Kelly (1999), the value of K_1 may be obtained

from the effective stiffness of the system, K_2, evaluated from Eq. (19). For the case study $K_2 = W/R^* = 3.46$ N/mm. The corresponding value of K_1 is given by:

$$K_1 = 51\ K_2 = 176\ N/mm \qquad (28)$$

In Cheng, et al. (2008) and Earthquake Protection Systems Inc. (2003) the initial stiffness is based on the coefficient of friction μ and on a yield displacement which was assumed D_y = 2.54 mm. For the case study, assuming μ = 2%, as obtained from experimental results, K_1 of each device becomes:

$$K_1 = \frac{\mu W}{D_y} = 23.70\ K_2 = 82\ N/mm \qquad (29)$$

The previous expressions are specifically tailored for devices used in civil applications and hence characterized by geometrical dimensions much bigger than those of the devices analysed in this research. Therefore, in this study two different proposals for initial stiffness based on the previous expressions were provided by modifying the coefficients accounting for the reduced dimensions of the new devices:

- Option (A): is based on Eq. (5), assuming μ = 2% and D_y = 0.1 mm, which could be considered a suitably small value for the yield displacement, confirmed also by experimental tests carried out on the proposed small device. The corresponding value of stiffness K_1 is:

$$K_1 = \frac{\mu W}{D_y} = 600\ K_2 = 2076\ N/mm \qquad (30)$$

- Option (B): is based on Eq. (4), where a different multiplier for the value of K_2 was assumed to take into account the reduced dimensions of the devices used in these experimental tests. In particular by considering the dimensional ratios between the standard devices and the proposed one, the multiplier could be assumed equal to 150 and the corresponding value of stiffness K_1 becomes:

$$K_1 = 150\ K_2 = 519\ N/mm; \qquad (31)$$

The graphs shown in Figure 35 depict the relative displacements for test 4 obtained from the numerical tests with the values of K_1 evaluated according to (28)-(31), compared to the corresponding experimental response. The diagrams of Figure 36a show that the experimental results in terms of hysteresis loops are included among the cycles obtained by using values of initial stiffness calculated with Eq. (29) (overestimation) and Option(A) (underestimation). Figure 36b shows an example of the hysteresis loops for one test with high position of the center of mass (test 13), in this case all the numerical curves overestimate the experimental extent of the hysteresis loop (i.e. maximum

displacement and force) and the better results are obtained with Option (A) and (B). The analyses carried out for all the tests lead to conclude that the proposal (B) is the one that best fits the experimental results both in terms of hysteresis loops and of the slope of the unloading branch and therefore it is assumed as reference values for the following analyses.

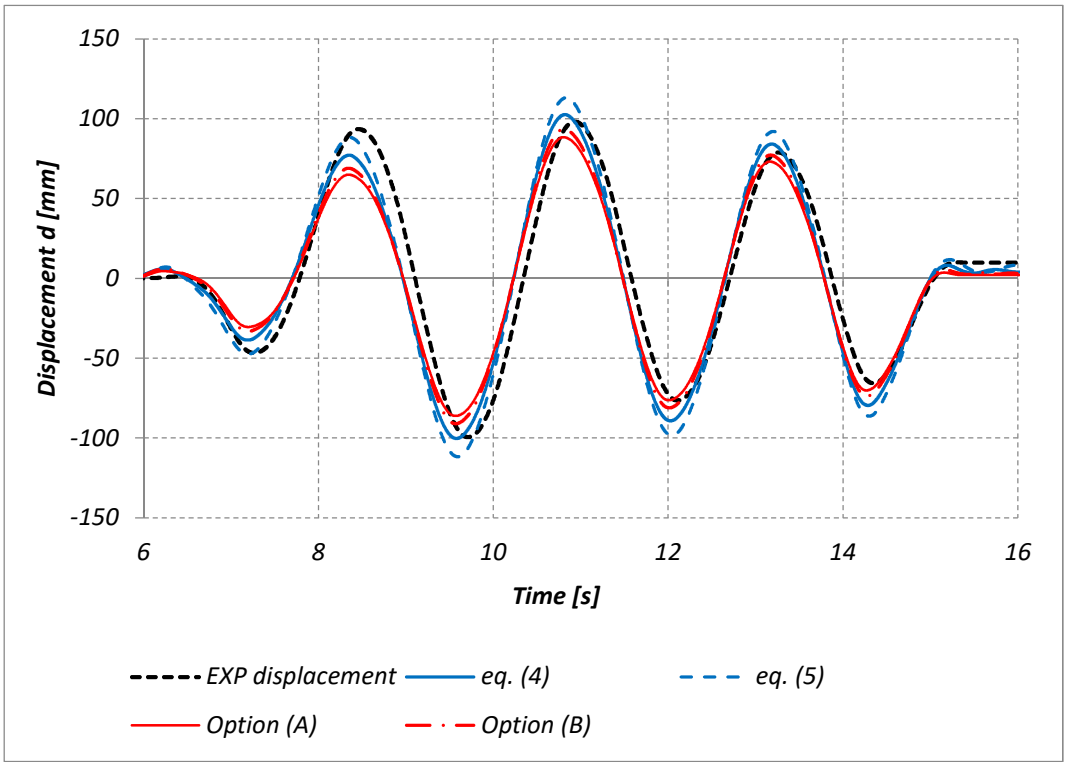

Figure 35 – Comparison between relative displacements obtained from the numerical tests with different value of K_1, and the experimental ones (cfg#1, D1 0.8 V1) – Berto et al. (2013)

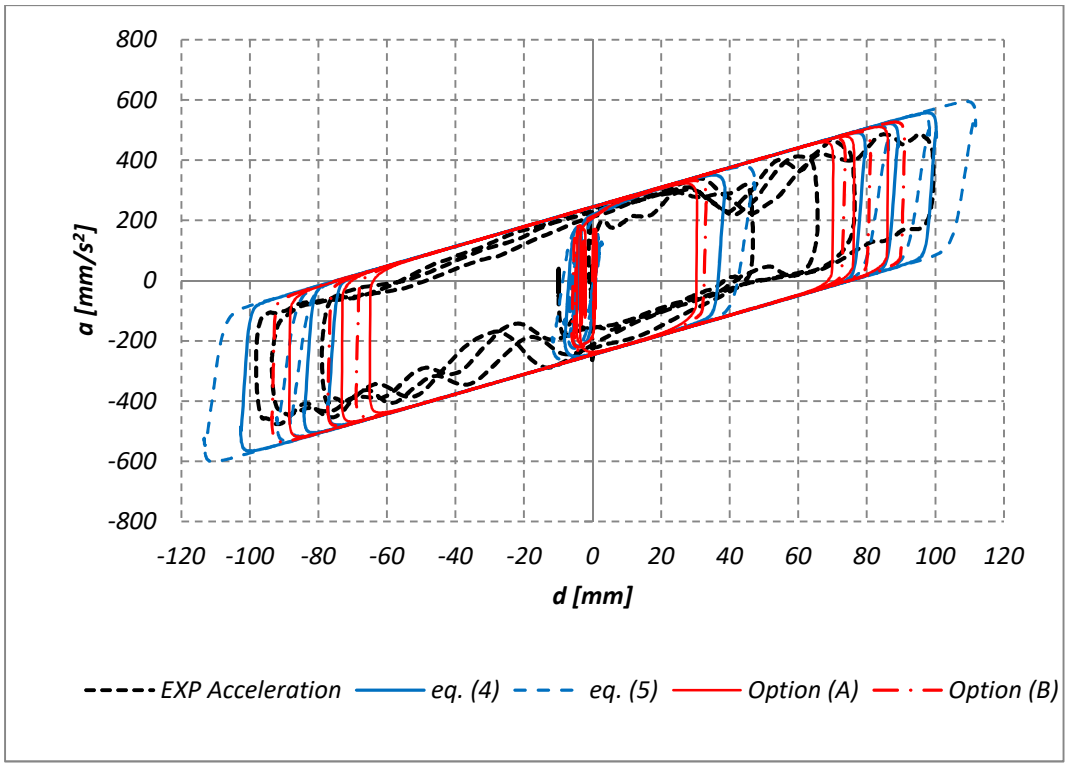

(a)

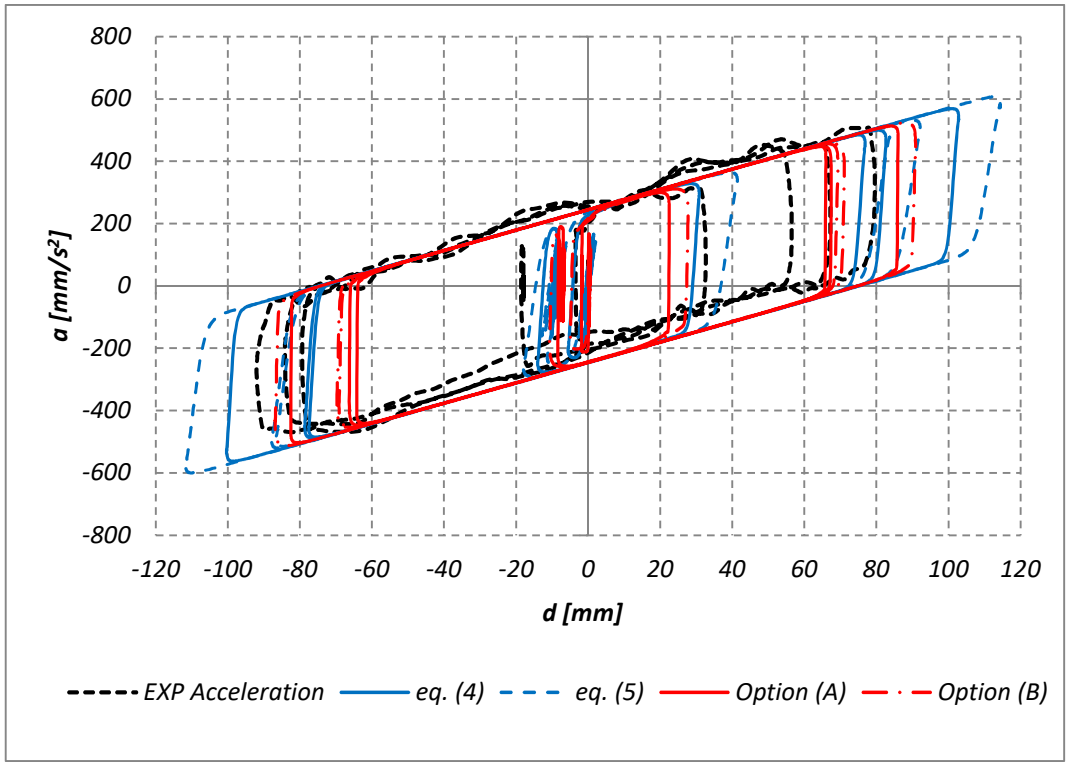

(b)

Figure 36 – Comparison between hysteresis loops of the system obtained from the numerical tests with different value of K1 and the experimental one: (a) cfg#1, D1 0.8 V1; (b) cfg#4, D1 0.8 V1 – Berto et al. (2013)

3.3.5.2 Sensitivity to Friction

The real value of the coefficient of friction depends on a number of factors such as the vertical load acting on the bearing, the material of the slider and of the sliding surfaces and also the relative sliding velocity between the surfaces, as presented in Constantinou

et al. (1990). In this particular case it is also influenced by the presence of the lubricant as previously described. Friction values adopted for traditional devices are in general, according to the producers' details, variable between the 10% -15%. From the results of the experimental tests, the friction coefficient for the devices in analyses emerged to be lower than usual, in particular around 2%-2.5%. For the sensitivity analyses the following parameters were selected:

- initial stiffness K_1 was set according to Option (B)
- friction coefficients μ_s for low sliding velocity was varied between 1% - 1,5%
- friction coefficients μ_f for high sliding velocity was varied between 1% - 3%

Moreover the case of μ_f equal to 5% was considered to evaluate the effect of a value more similar to those used for standard device. These analyses aim to highlight the sensitivity of the numerical solution to a variation of this coefficient and, at the same time, to assess a value that can be properly used to predict the behaviour of a system equipped with such devices.

As an example, Figure 37 compares the numerical and the experimental results for *Test 2*; it is evidenced that the friction coefficient μ_f highly affects the numerical response of the system, while the friction coefficient μ_s has a limited effect on the results. The highest values of μ_f (i.e. 5%) provides a response that underestimates the maximum displacements but, as the coefficient is reduced, the numerical response goes closer to the experimental one; on the other hand, when μ_f =2% is assumed, the displacements are much higher than real, while accelerations may be underestimated. An acceptable result is obtained with a coefficient of friction μ_f =2.5%.

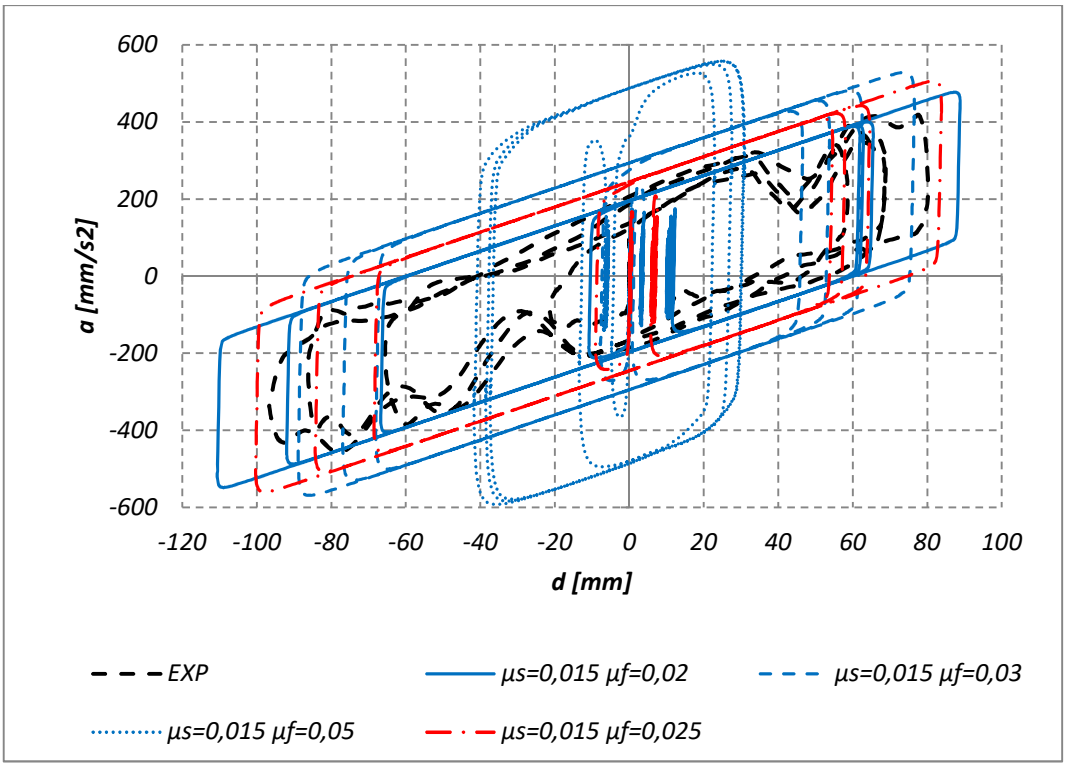

(a)

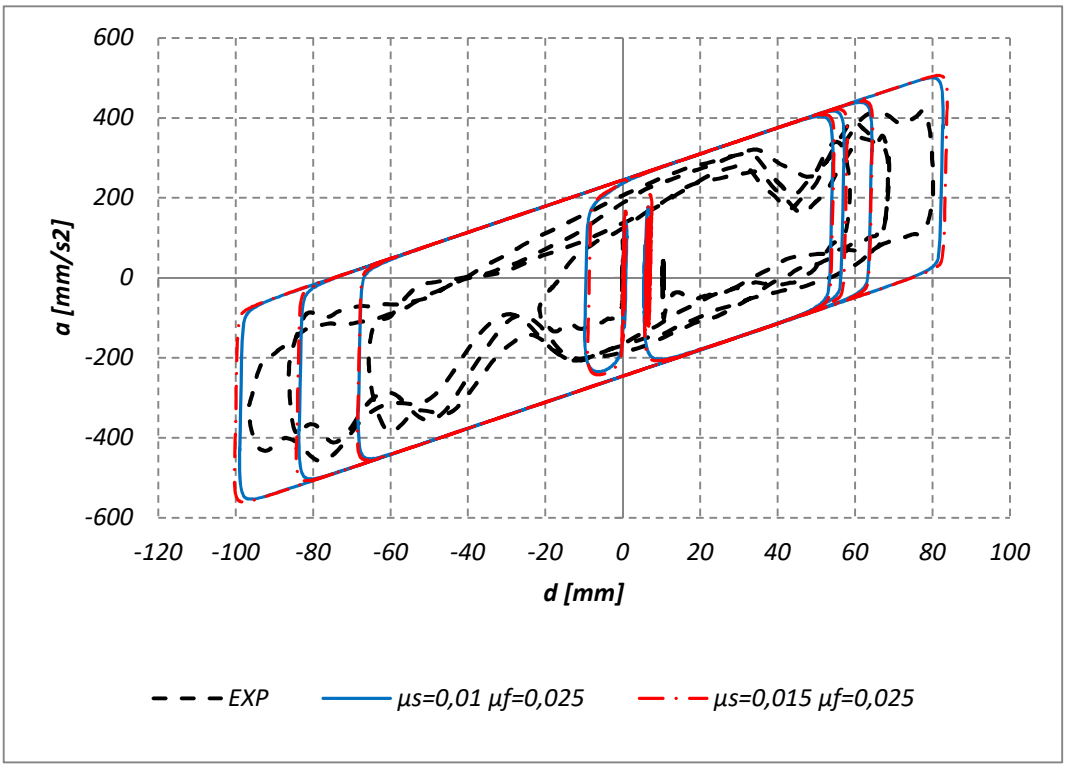

(b)

Figure 37 – Comparison between hysteresis loops of the system obtained from the numerical tests with different value of friction coefficients, and the experimental (cfg#1, D1 V1): (a) sensitivity to μ_f; (b) sensitivity to μ_s – Berto et al. (2013)

3.3.5.3 Sensitivity to numerical damping

Numerical damping influence was investigated assuming K_1 = 519 N/mm (option B) and μ_f = 2.5%, μ_s= 1.5%. Three different values for the damping factor were considered: ξ =0.5%, 2%, 5%.The lower one ξ =0.5% could represent a realistic value for monolithic

rigid sculptures, for which the dissipation of energy is all lumped in the isolators devices, the highest value ξ=5%, is the conventional value assumed in the seismic analysis and represent an indispensable term of comparison for non-rigid objects. As an example of the sensitivity analyses, the comparison between experimental and numerical results in terms of hysteresis loops for the tests in configuration cfg#1 is depicted in Figure 38, for different levels of ground acceleration (i.e. tests 2, 6 and 7) and the three different damping ratios.

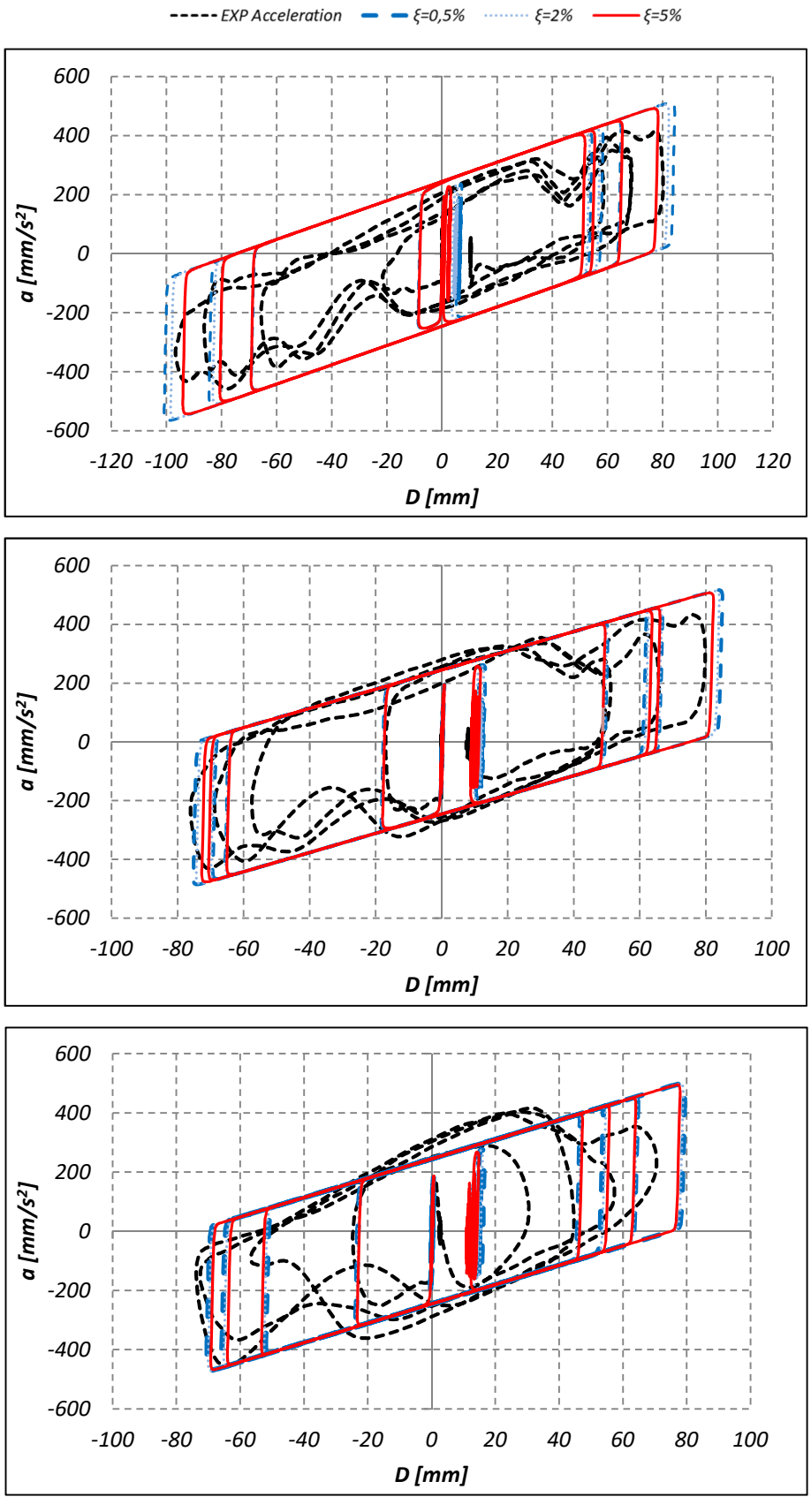

Figure 38 – Comparison between hysteresis loops of the system obtained from the numerical tests with three levels of damping and the experimental one in configuration cfg#1: (a) D1 V1 input, (b) D1 V2 input (c) D1 1.5V2 input – Berto et al. (2013)

The results of the analyses show that the numerical model with $\xi = 5\%$ represents the best compromise between the different experimental results obtained for increasing input. Therefore, it can be concluded that the physical models adopted in this study to represent the statues, which are realized by the superimposition of three blocks, are characterized by a damping ratio higher than a rigid body, probably due to the fact that the dissipation of energy can be also produced by relative displacement between the single blocks. Consequently, a value of damping ratio equal to 5% can be reasonably assumed for modelling the experimental tests, while a value of 0.5% can be considered more reasonable for modelling the statues themselves.

3.3.6 Further investigation on friction coefficients calibration

On the basis of sensitivity analysis, the friction coefficient is identified as the most important parameter influencing the behavior of the isolation system in terms of energy dissipation and, on the numerical side, decisive for the correspondence between experimental tests and simulation. In particular, the analysis focused on the effects of μ_{fast} and μ_{slow}, while the evolutive ratio *r* is assumed around to 0,02 – 0,04 mm/s referring to typical values for friction pendulum systems. The results of this first phase of calibration led to the set of friction parametres (μ_{slow}, μ_{fast}, r) named *Hyp 1* which are recalled in Table 5.

In order to better understand the contribution of the friction coefficient to the behaviour of the seismic isolator, a supplementary series of numerical simulations is carried out for different values of friction parameters. This further analysis has shown a marked variation in energy dissipated per cycle, maximum displacement and maximum value of transmitted shear, also considering, for the evolutive ratio r, a wider range than that assumed in the previous analyses. This confirms the important role of μ_{fast} and μ_{slow} and furthermore highlights the relevance of the parameter r.

Therefore, the parameters μ_{slow}, μ_{fast} and r were evaluated in two steps: firstly by means of an optimization procedure with an Ordinary Least Squares approach and then with a suitable calibration considering the results of the experimental tests obtained with low configuration (LCM) and high configuration (HCM).

In the first step the parameters that fit the experimental results are evaluated minimizing the following cost-function:

$$C = \sqrt{\sum_{i=1}^{n} \left(\mu_i(v_i) - \mu_i^{num}(v_i)\right)^2} \quad [-] \qquad (32)$$

where $\mu_i$and v_i are respectively friction coefficient and velocity of the *n* experimental data, while μ_i^{num} is the numerical value estimated according to (21).

The values of μ_i are obtained starting from the value of experimental acceleration a_i, in the time when the displacement D is zero, in accordance with:

$$\mu_i = \left|\frac{a_i}{g}\right| \quad [-] \qquad (33)$$

which derives from the equation of the shear force (18) for D = 0.

Since each cycle intercepts twice the vertical axis (with zero displacement and maximum velocity), two distinct values of μ_i can be found: μ_{i1} corresponding to the positive value of acceleration, and μ_{i2} corresponding to the negative value. Hence two sets of μ_i can be defined: Set 1 and Set 2 which collects respectively the μ_{i1} and μ_{i2} values. In order to calibrate the friction coefficient, the optimization procedure is applied to both LCM and HCM, considering separately the data corresponding to Set 1 and to Set 2.

In the optimization procedure as initial values of the parameters μ_{slow} and μ_{fast} are assumed respectively the minimum and the maximum value of μ_i, whereas for the evolutive ratio r four values were considered i.e. r = 0.001; 0.005; 0.01; 0.05 [s/mm].

The results of this procedure are shown in Figure 39a for LCM and in Figure 39b for HCM in terms of $\mu - v$ diagram , where the three curves relating to the optimization on Set1, Set2 and Set1+Set 2 are given together with the respective experimental data.

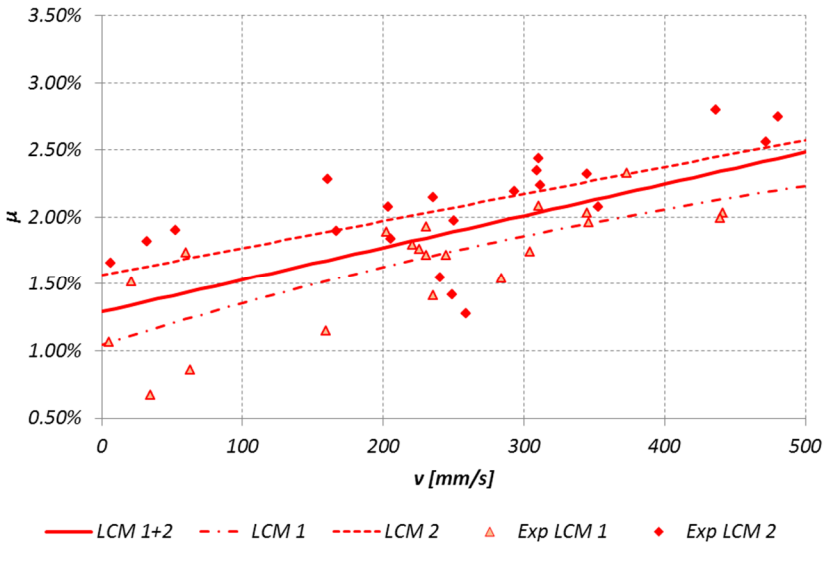

(a)

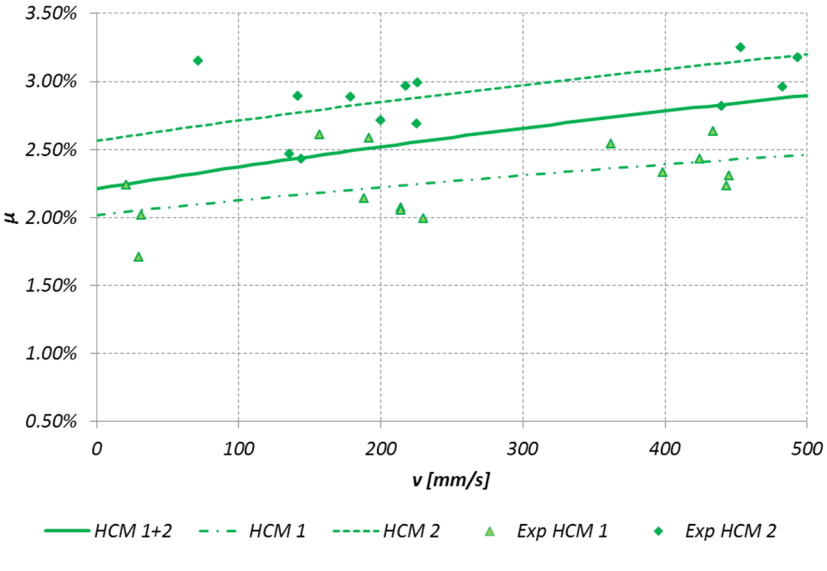

(b)

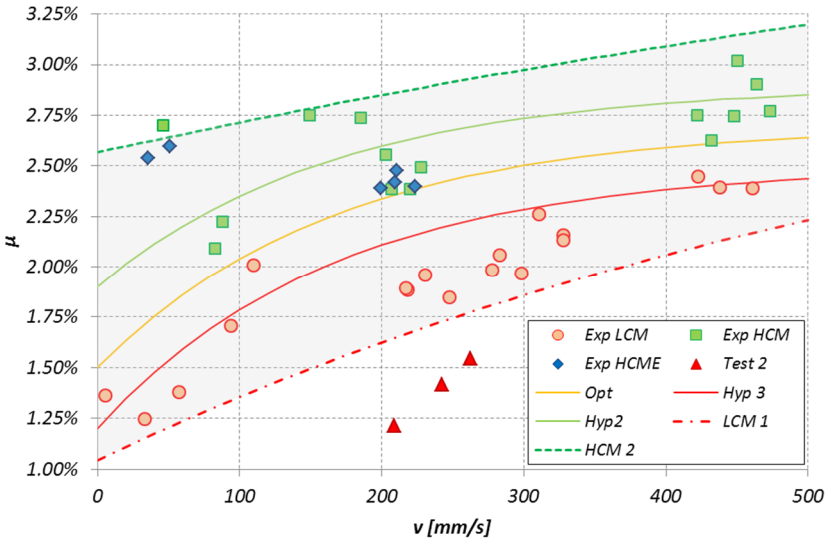

(c)

Figure 39 – Friction coefficient versus velocity. Comparison of the experimental results with the assumed models: (a) optimization on LCM test (Set1 and Set 2); (b) optimization on HCM test (Set1 and Set 2); (c) optimization on all the tests (LCM and HCM)

It is worth noting that for both configurations the obtained curves correspond to unrealistic value of r and μ_{fast}: in fact Constantinou et al. (1990) showed that the sliding value of the coefficient of friction remains constant over a certain value of the sliding velocity, which for the bearings tested by the authors was evaluated between 100 and 200 mm/s.

For this reason, it has been assumed that such curves can not be adopted as the reference ones, but the lowest (LCM1) and the highest (HCM2) curves can be used as the lower and the upper bounds delimiting the zone inside which the suitable calibration has to be searched, dashed area in Figure 39c.

In detail Figure 39c summarizes the results of the second step of calibration, where the experimental data are represented, for an easier view, by the couple of coordinates ($\mu_{i,avg}, v_{i,avg}$) which are the average between μ_{i1} with μ_{i2} and corresponding velocities measured during a cycle of sliding. In this figure the three curves obtained with the calibration procedure are reported: HYP 2 is calibrated considering only HCM data, HYP 3 only LCM data, while the optimum curve (Opt) is calibrated to better represent the whole set of data. As a first validation of this procedure the results of the experimental test carried out in Configuration 5 (HCME), not used for the calibration phase, are also shown in the same Figure, confirming the representativeness of the selected dashed area.

Table 5 summarizes the friction parameters obtained by the calibration procedure compared with the parameters used in previous simulations, here named HYP 1 (Berto et al. 2013, Baggio et al. 2013).

Hypothesis	***Parameters***	***Description***
HYP 1	$\mu_{slow} = 0.015$ $\mu_{fast} = 0.025$ $r = 0.04$	*Data used in Berto et al. 2013, Baggio et al, 2013*
HYP 2	$\mu_{slow} = 0.019$ $\mu_{fast} = 0.029$ $r = 0.006$	*Calibration of cfg#4 set of data (green curve)*
HYP 3	$\mu_{slow} = 0.012$ $\mu_{fast} = 0.025$ $r = 0.006$	*Calibration of cfg#1 set of data (red curve)*
"Opt"	$\mu_{slow} = 0.015$ $\mu_{fast} = 0.027$ $r = 0.006$	*Calibration of all the set of data (yellow curve)*

Table 5 – Friction coefficients obtained by calibration procedure

A number of parametric numerical analyses were performed by means of the general purpose Finite Element program *midas GEN*. The four isolators were modelled with non

linear elements, which combine the non linear behaviour previously described (Sect. 3.3.1, Figure 30) for the shear components with a compression-only behavior for the axial component. The numerical results were then compared to those obtained from the experimental tests in order to validate the selected set of parameters that best fits experimental response.

3.3.6.1 Low configurations tests (LCM)

The results of both unidirectional and bidirectional numerical tests carried out on the low configurations are presented and compared to the experimental data to provide a measure of the efficiency of the numerical simulation of the device behavior, with particular attention to the friction parameters.

In detail Figure 40a presents the acceleration-displacement cycle of Test 4 characterized by low acceleration input: HYP 3 shows a good accordance with numerical results, while HYP 1, adopted in previous works, proves to be less accurate compared to the new calibration. The Opt hypothesis provides a better correspondence in terms of expected acceleration vs displacement, compared to the worse results of HYP 1. In order to confirm that the selected Opt hypothesis is able to reproduce the experimental results also in their temporal evolution, Figure 40b and Figure 40c show the good accordance between experimental and numerical results, both in terms of acceleration vs time and displacement vs time.

Figure 41a depicts the results obtained for Test 6 characterized by higher acceleration input, in which Opt calibration demonstrates strong similarities with HYP3 (calibrated on LCM tests) and a suitable representation of the behavior of the DCCSS during the experimental excitation. Compared to the experimental evidence it was noted a negligible underestimation of the stroke of the tests.

Results in terms of acceleration and displacements are displayed in Figure 41b and Figure 41c, confirming a good accordance between numerical results obtained with Opt calibration and experimental results.

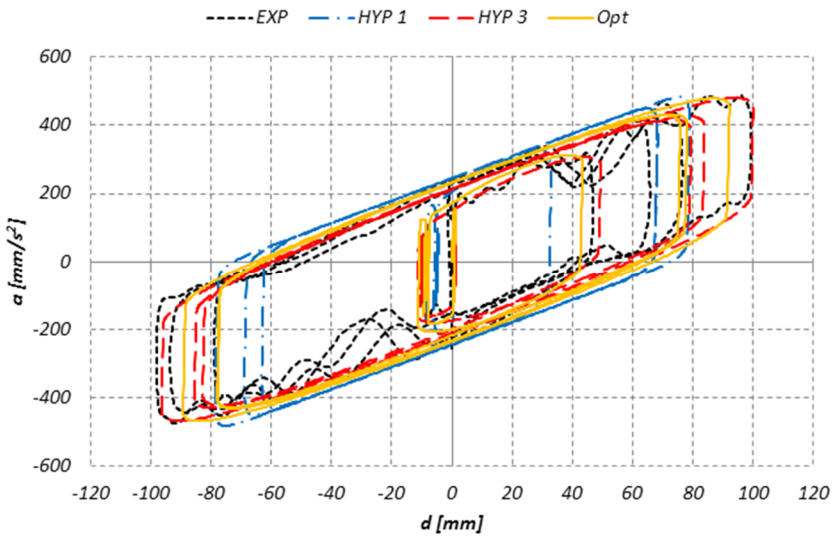

(a)

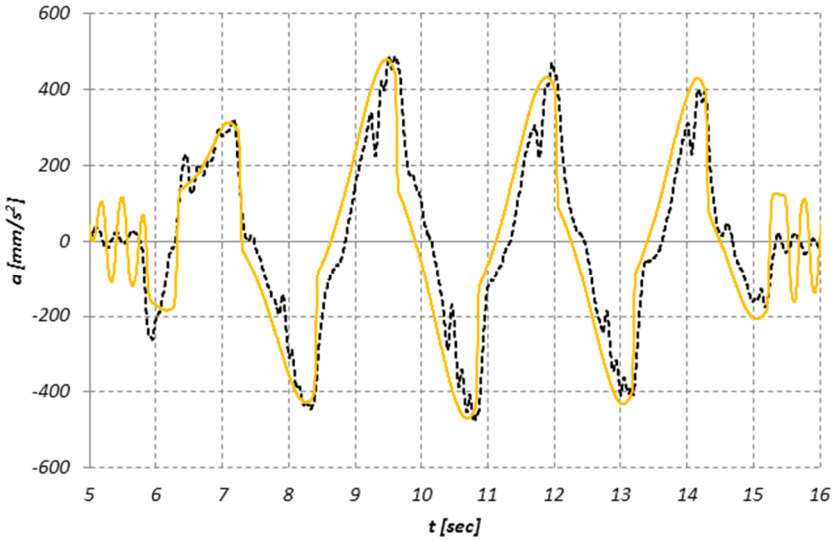

(b)

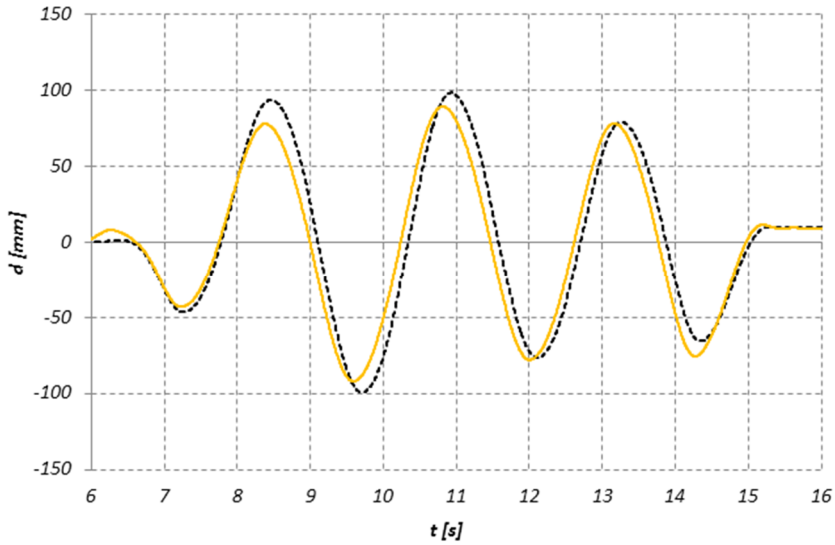

(c)

Figure 40 – Test 4: comparison between experimental and numerical results obtained with different calibration of friction coefficients: (a) acceleration-displacement; (b) acceleration-time; (c) displacement-time

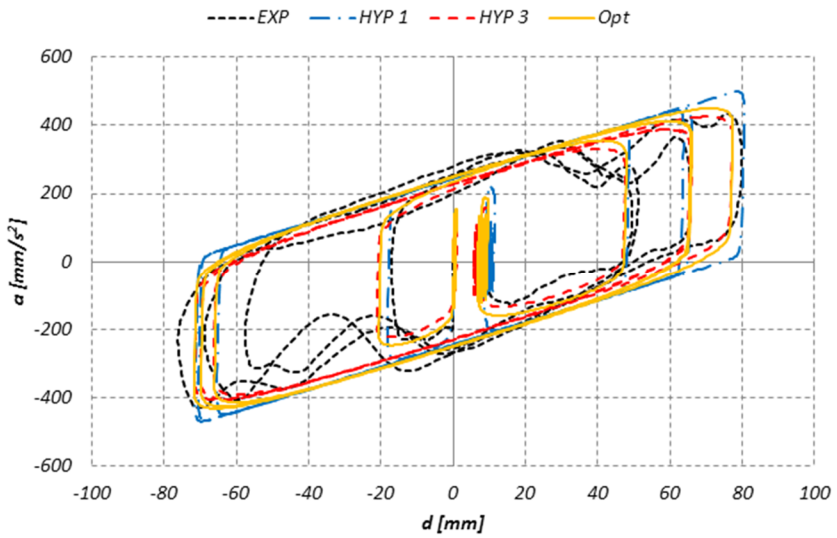

(a)

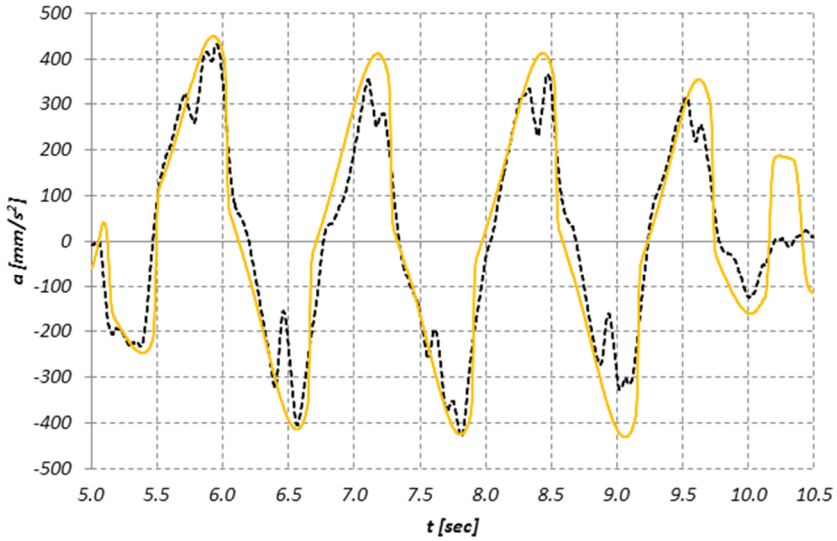

(b)

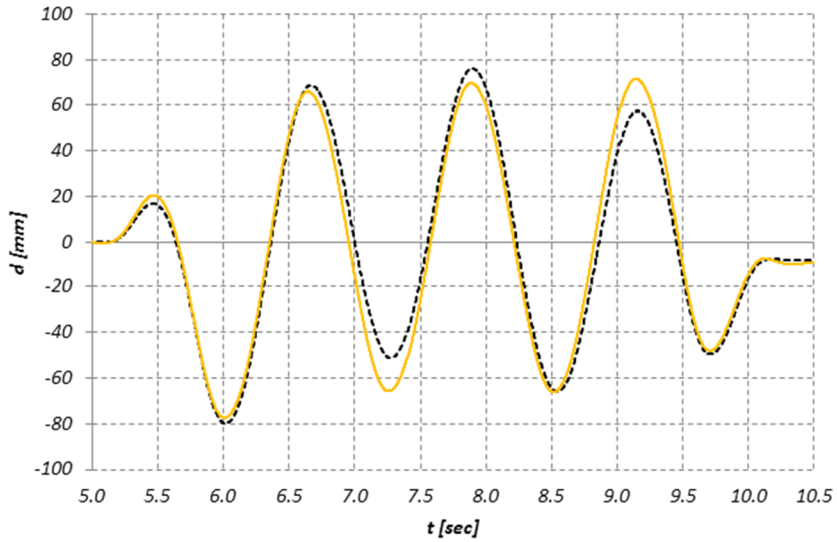

(c)

Figure 41 – Test 6: comparison between experimental and numerical results obtained with different calibration of friction coefficients: (a) acceleration-displacement; (b) acceleration-time; (c) displacement-time

3.3.6.2 High configurations tests (HCM)

Cfg#4

In Figure 42a is reported the acceleration-displacement cycle for Test 13 for HYP1, HYP2 and Opt hypothesis. In this case Opt hypothesis shows an overestimation of the positive experimental displacement, if compared with the other hypotheses, while for the negative one, it demonstrates to be the best approximation. In summary the results obtained by optimum calibration can be considered satisfactory. In particular, as shown in Figure 42b and Figure 42c, both the graphs acceleration vs time and displacement vs time obtained by adopting Opt hypothesis compare quite well with the experimental one.

Figure 43a shows acceleration-displacement cycle for Test 15, in which Opt calibration strongly resembles HYP2, both of them demonstrate to well capture the results in terms of acceleration and displacements vs time, Figure 43b and Figure 43c.

Finally, results of the simulation of the bidirectional *Test 20* are reported in Figure 44a and Figure 44b, which present the acceleration-displacement cycles for the longitudinal and lateral direction compared with the experimental evidence. In Figure 44c is also shown the displacement path observed on the horizontal plane for the test. All these results confirm the good accordance of the numerical simulations with the experimental ones also in case of 2D input.

Cfg#5

The results of the numerical simulation of bidirectional *Test 24*, assuming Opt calibration, are shown in Figure 45, demonstrating the good agreement with the experimental evidences. Moreover the results of the *Test 24* compare quite well with those of the *Test 20* both in terms of displacement and acceleration, confirming the effectiveness of the DCCSS devices in eliminating the torsional motion associated to the eccentricity of mass, see Sect. 3.3.

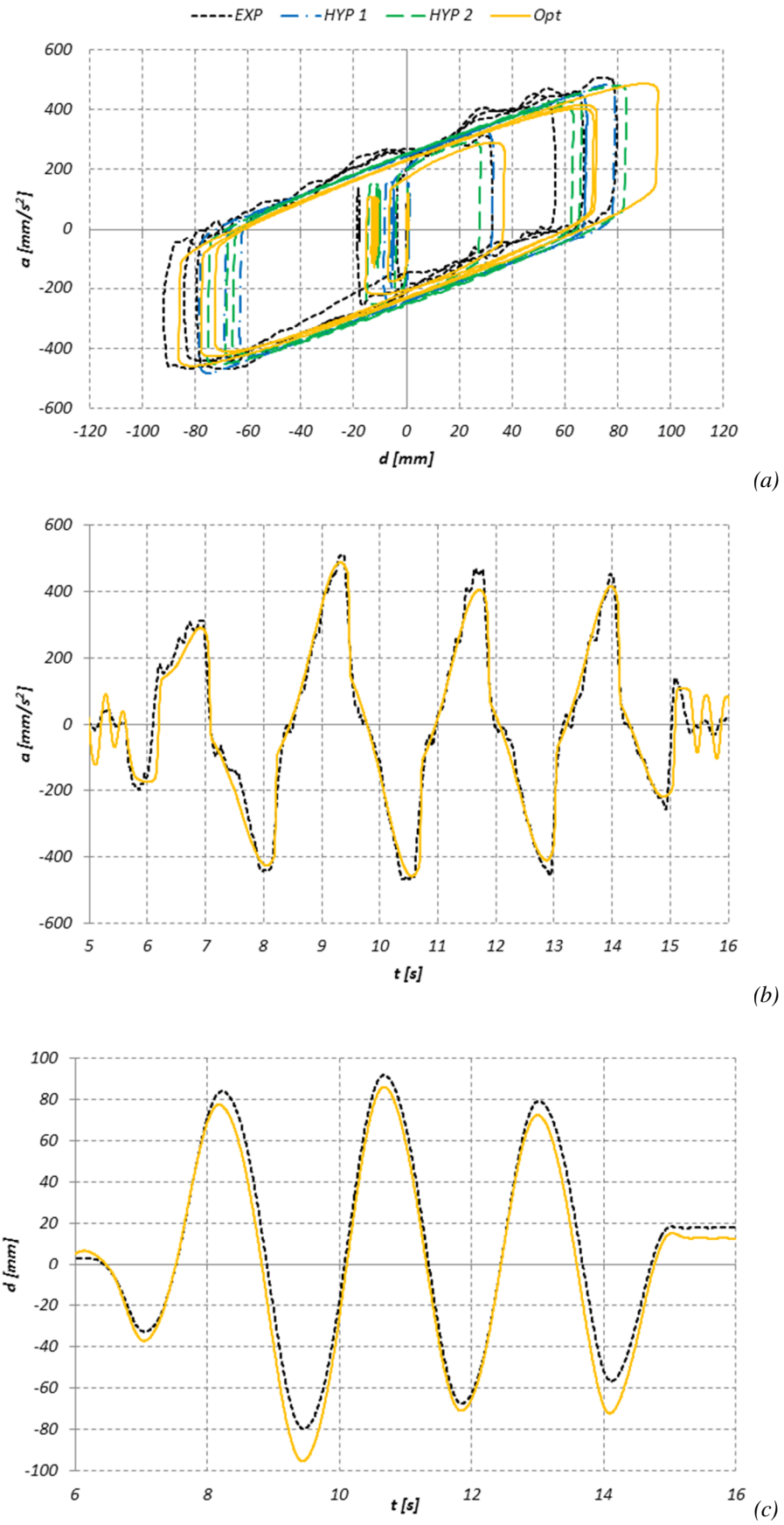

Figure 42 – Test 13: comparison between experimental and numerical results obtained with different calibration of friction coefficients: (a) acceleration-displacement; (b) acceleration-time; (c) displacement-time;

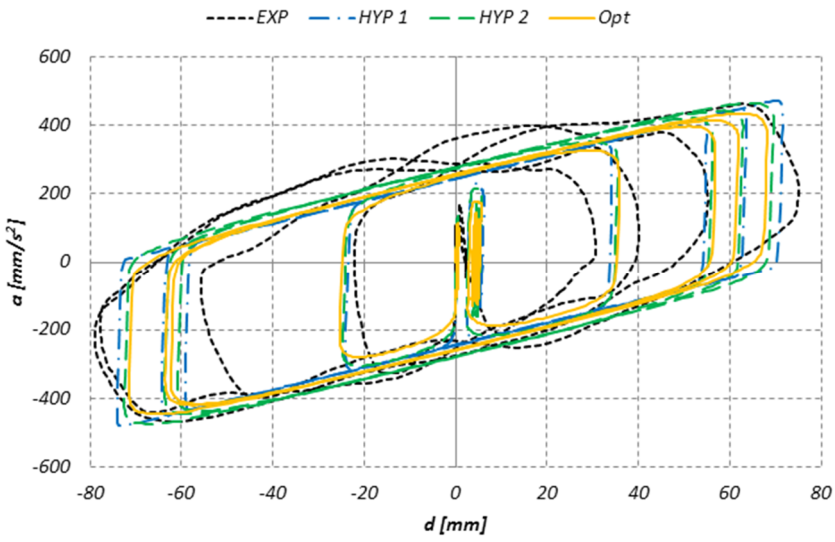

(a)

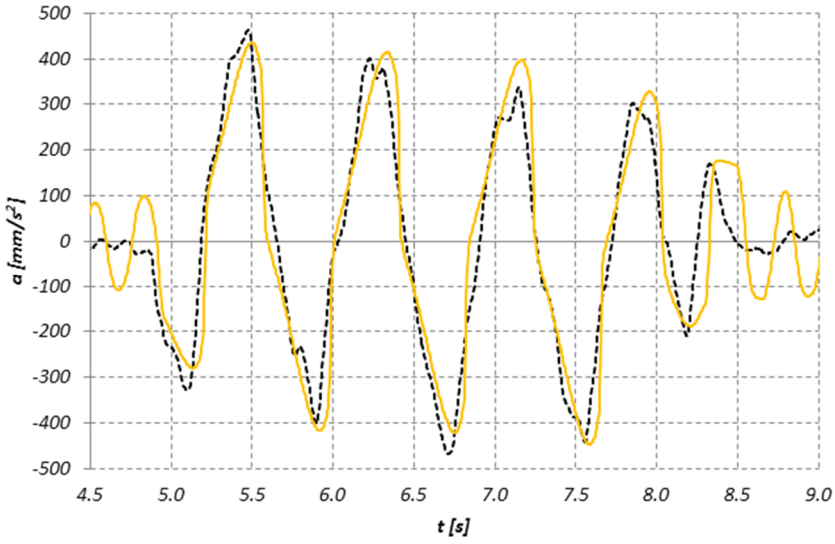

(b)

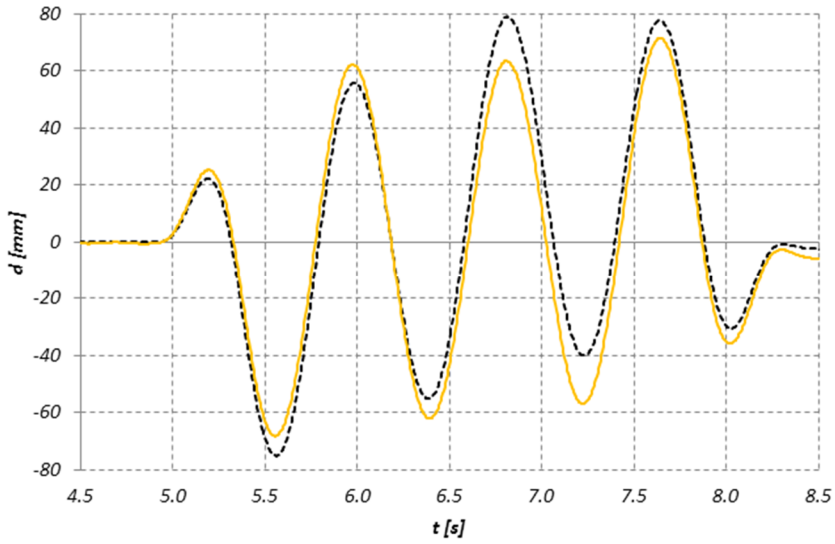

(c)

Figure 43 – Test 15: comparison between experimental and numerical results obtained with different calibration of friction coefficients: (a) acceleration-displacement; (b) acceleration-time; (c) displacement-time

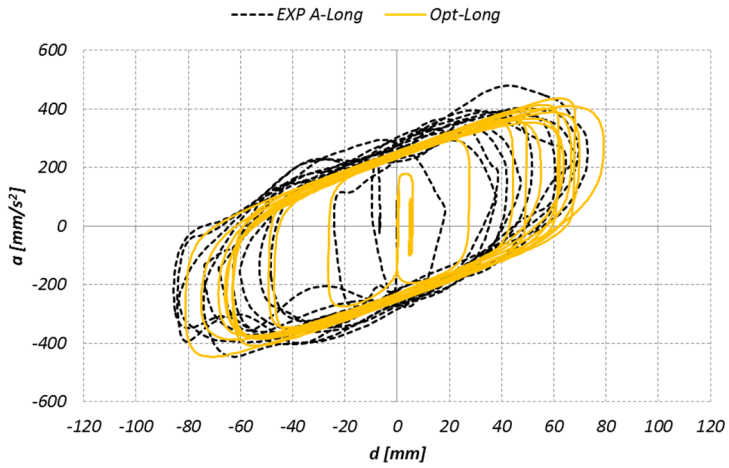

(a)

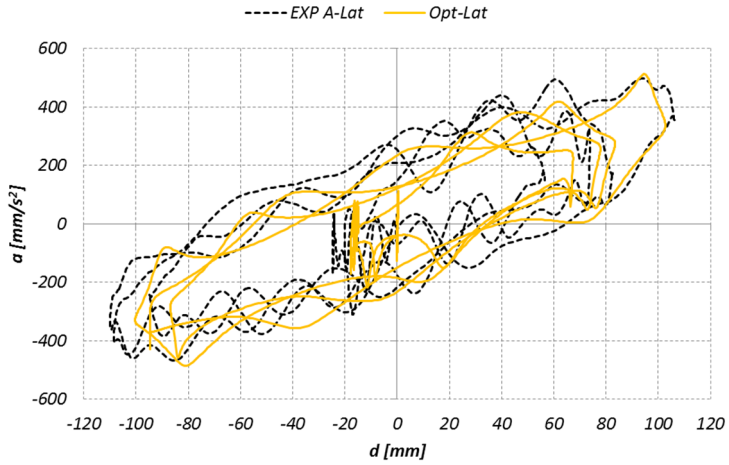

(b)

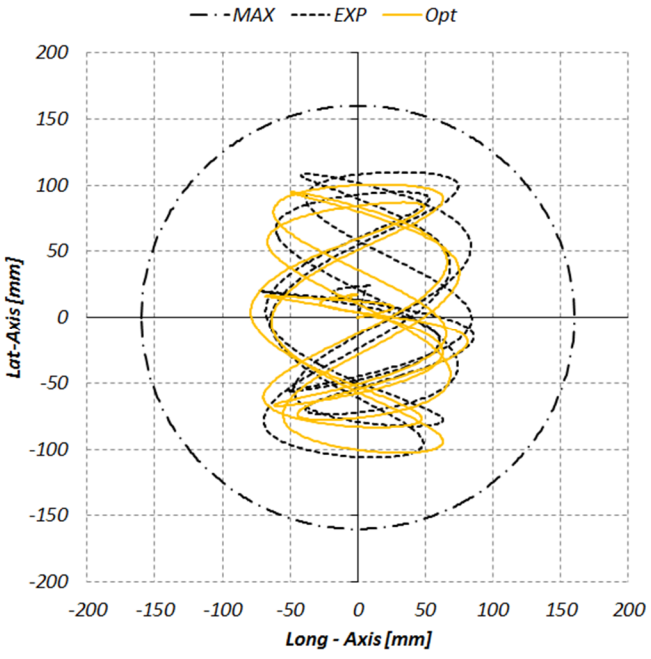

(c)

Figure 44 – Test 20: comparison between experimental and numerical results obtained with the Opt calibration of friction coefficients: (a) acceleration-displacement longitudinal direction; (b) acceleration-displacement lateral direction;(c) displacements on the horizontal plane

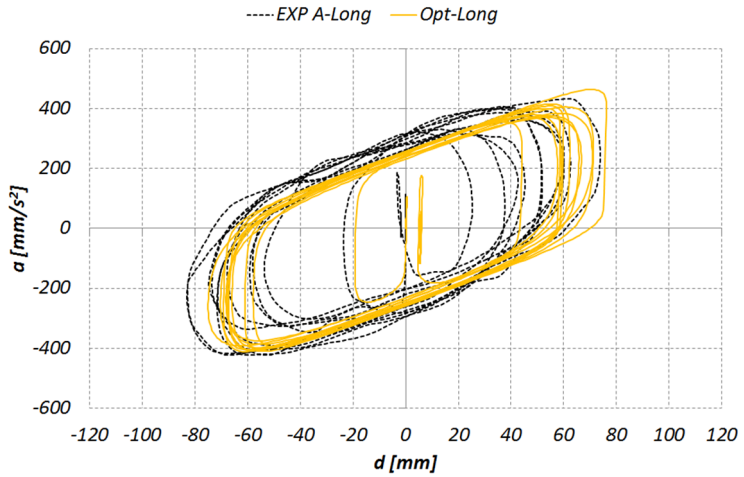

(a)

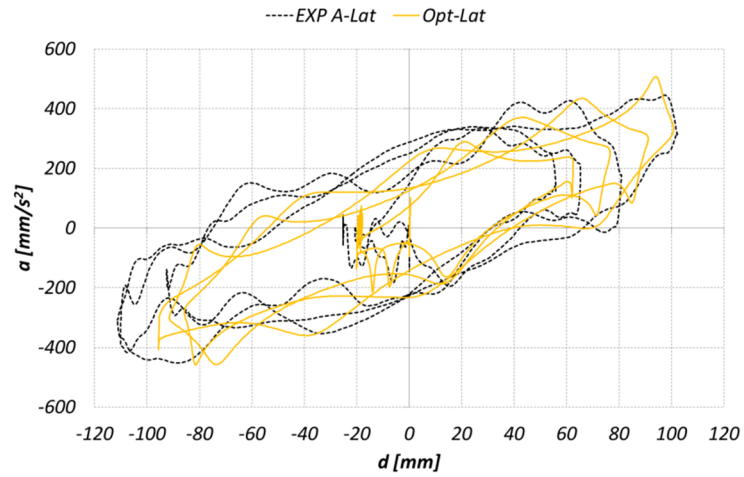

(b)

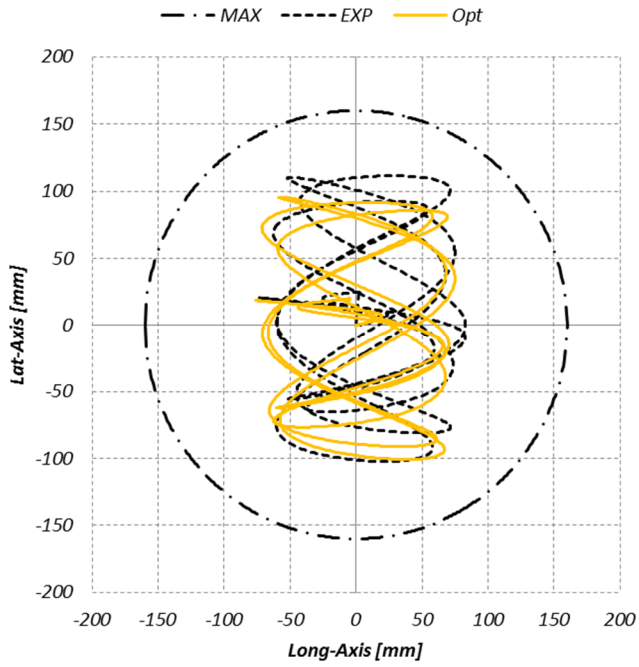

(c)

Figure 45 – Test 24: comparison between experimental and numerical results obtained with the Opt calibration of friction coefficients: (a) acceleration-displacement longitudinal direction; (b) acceleration-displacement lateral direction; (c) displacements on the horizontal plane

3.3.7 Numerical Prediction of the dynamic behaviour of the isolated system

In this section the results of dynamic analyses on three of the Michelangelo's sculptures are reported. In particular, the study concerns the sculptures of *San Matteo*, *Prigione Barbuto* and *Prigione Atlante*, which may be considered the most critical ones with respect to the seismic vulnerability due to both the tendency to rocking and overturning and their intrinsic weakness.

The analyses were performed using general purpose Finite Element programs (*midas GEN*) and the F.E. models were obtained starting from the laser scanner survey of the statues performed by the Visual Computing Laboratory, ISTI-CNR, and then processed by Rhinoceros® in order to obtain a tetrahedral 3D Finite Element mesh. In a first phase of the analysis, an isotropic linear elastic material was assumed for the statues and the underlying pedestals. Four friction isolator links were placed beneath the base with one of the ending restrained to the ground and it was hypothized that the statues were efficiently restrained to the pedestal. The isolators were modeled with the non linear elements described in Sect. 3.3.4. According to Berto et al. (2012), the numerical analyses were carried out assuming for the marble material Young Modulus E = 50000 MPa, Poisson ratio $\nu = 0.2$, and a specific weight of 27 kN/m^3. For the pedestal, made of Pietra Serena, the same values were selected for Young Modulus and Poisson ratio, while 26 kN/m^3 was assumed for the specific weight. It is worth noting that the pedestal of San Matteo is a solid compact block, while the *Prigione Atlante* and *Prigione Barbuto* have a hollow pedestal. The material properties were evaluated based on the observations drawn from the autoptic examination of the external surface of the sculptures and on the reference values of the mechanical characteristics of the best quality Carrara Marble now on the market (i.e. the variety named "Bianco Acquabianca", very likely equivalent to the statuario quarried in antiquity), Berto et al. (2012). To account for the effects of the deterioration concerning *San Matteo* and *Prigione Atlante*, a reduction of about 20% of the mechanical properties was considered.

In order to assess the occurrence of cracking and/or compressive damaging in the statues the stress state obtained by the analysis should be compared with strength properties of the marble, which for the study case are summerized in Table 6 in terms of reasonable minimum and maximum values. Such values were calculated by considering a partial material factor for the marble $\gamma_m = 2$ to account for the uncertainty of the material.

Strength (MPa)	*Good condition*	*Deteriorated condition*
Compression f_{cd}	*31÷72*	*25÷58*
Tension f_{td}	*2÷4,5*	*1,6÷3,6*

Table 6 – Marble sculptures: reference values for the mechanical strength

It is worth noting that, in case the maximum stresses obtained from the numerical analyses exceed the strenght values of Table 6, the hypothesis of linear elastic material for marble should be replaced by a suitable constitutive law, with brittle behaviour in tension and a non linear stress-strain law in compression.

According to the sensitivity analysis (Sect. 3.3.5.3, Berto et al. (2013)) a damping value $\xi = 0.5$ % was adopted for the analysis of the marble statues, which can be considered monolithic rigid blocks.

3.3.7.1 Response to the sinusoidal input

Firstly, the response of the three sculptures to the input used in the experimental tests for HCM configuration was investigated. In this section the results obtained considering the input of test 13 are shown and compared with the experimental and numerical results found for the physical model, Figure 46a. It is evident that the three sculptures behave in very similar way, little difference may be evidenced for "Prigione Atlante" due to the higher weight with respect to the others. The response of the statues displays wider stroke and higher maximum acceleration than that obtained by both the experimental test and the numerical simulation with the Opt calibration of the test 13. This is reasonably due to the fact that, in the experimental set up, a supplementary dissipation of energy may be produced by relative displacement between the single concrete blocks. This is also the reason that has led to adopt a damping ratio $\xi = 5$ % in physical model simulation, Sect 4, instead of the $\xi = 0{,}5$% adopted for real statues. To support such a hypothesis, Figure 46b shows the same comparison of Figure 46a, but adopting also for the statues the damping ratio $\xi = 5$ %. The very good accordance between the numerical results obtained by the physical model and by the statues' FE models, evidences that the main difference between such two models is represented by the damping properties, while the value of the friction coefficient and the initial stiffness of the system obtained with the calibration procedure previously proposed are effective also for the statue simulation.

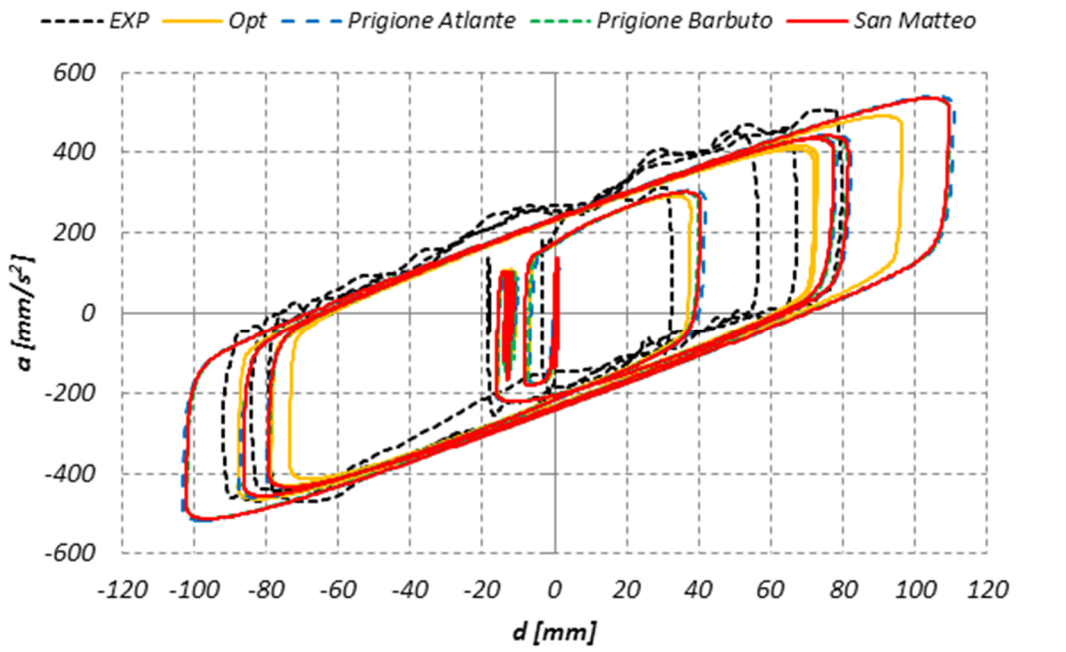

(a)

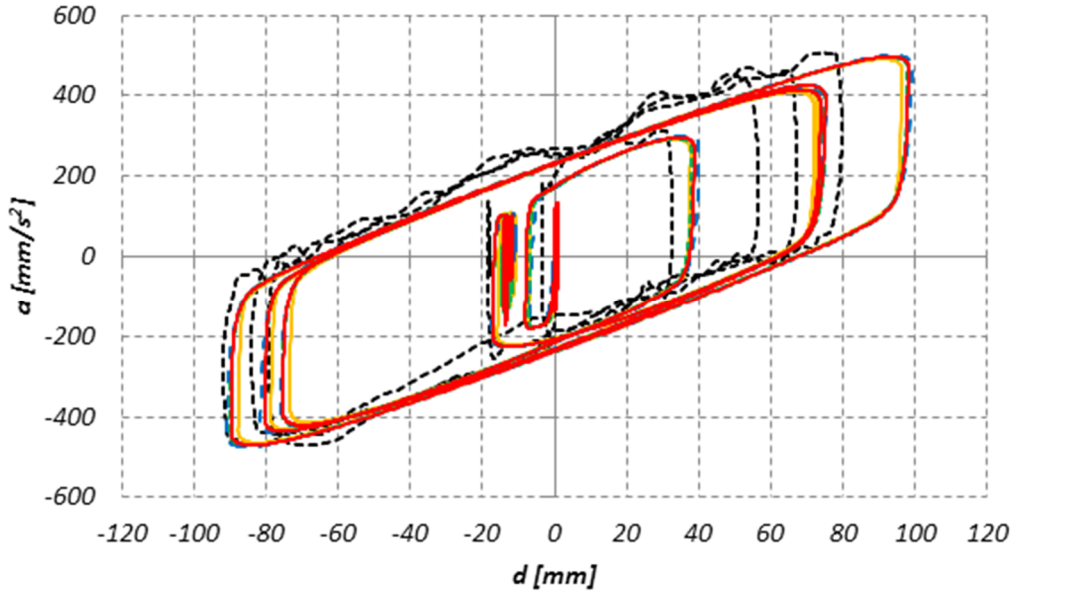

(b)

Figure 46 – Test 13: comparison between the hysteretic loops obtained for the physical model in HCM configuration and the ones found for the examined statues by adopting: (a) ξ = 0.5%; (b) ξ = 5%;

3.3.7.2 Response to the seismic input

The response of the three statues to the seismic excitation was analyzed in two different conditions: statue fixed to the ground and statue isolated by means of the proposed DCCSS devices. In each condition and for each statue, six time history analyses were performed considering three different couples of ground motions acting respectively in X and Y direction (Figure 29). The one causing maximum response in terms of displacement and stress was evaluated, according to the European provisions (EC8).

The three couples of ground motions records were selected from the European Strong Motion Database (ESD) using the software Rexel (Iervolino et al. 2010), with reference to a return period Tr = 712 yrs, with a range of magnitude M= (4÷7) and a source-to-site distance R = (0÷40 km) which correspond to the seismic hazard of the site. In the selection of seismic inputs the compatibility with the design spectrum was ensured within the period range from 0.6 s to 4.0 s, following the provisions of EC8 for isolated structures.

Figure 47 shows the ground acceleration vs time and the acceleration acting at the base of the sculptures in isolated condition for the three couple of seismic records. In particular a_{lat} and a_{long} represent respectively the acceleration in the direction of the shortest and longest side of the basement of each statue (e.g. for the *Prigione Barbuto* and the *San Matteo* a_{lat} is X direction, while for the Prigione Atlante a_{lat} is the Y direction, Figure 29). It is worth noting that, also in this case, the seismic responses for the three sculptures are very similar, i.e. the three graphs are almost overlapping.

The effect of the isolation system is evident: both along longitudinal and lateral directions the peak acceleration is reduced of about 70%.

The maximum effect in terms of displacement response was obtained with the couple of records "E0198". For this case, Figure 48a shows the displacements in the longitudinal – lateral plane compared with the maximum tolerable displacement assumed for the device (i.e. D_{max} = ± 160 mm). Similarly Figure 48b and Figure 48c show the same graphs for the other two seismic records.

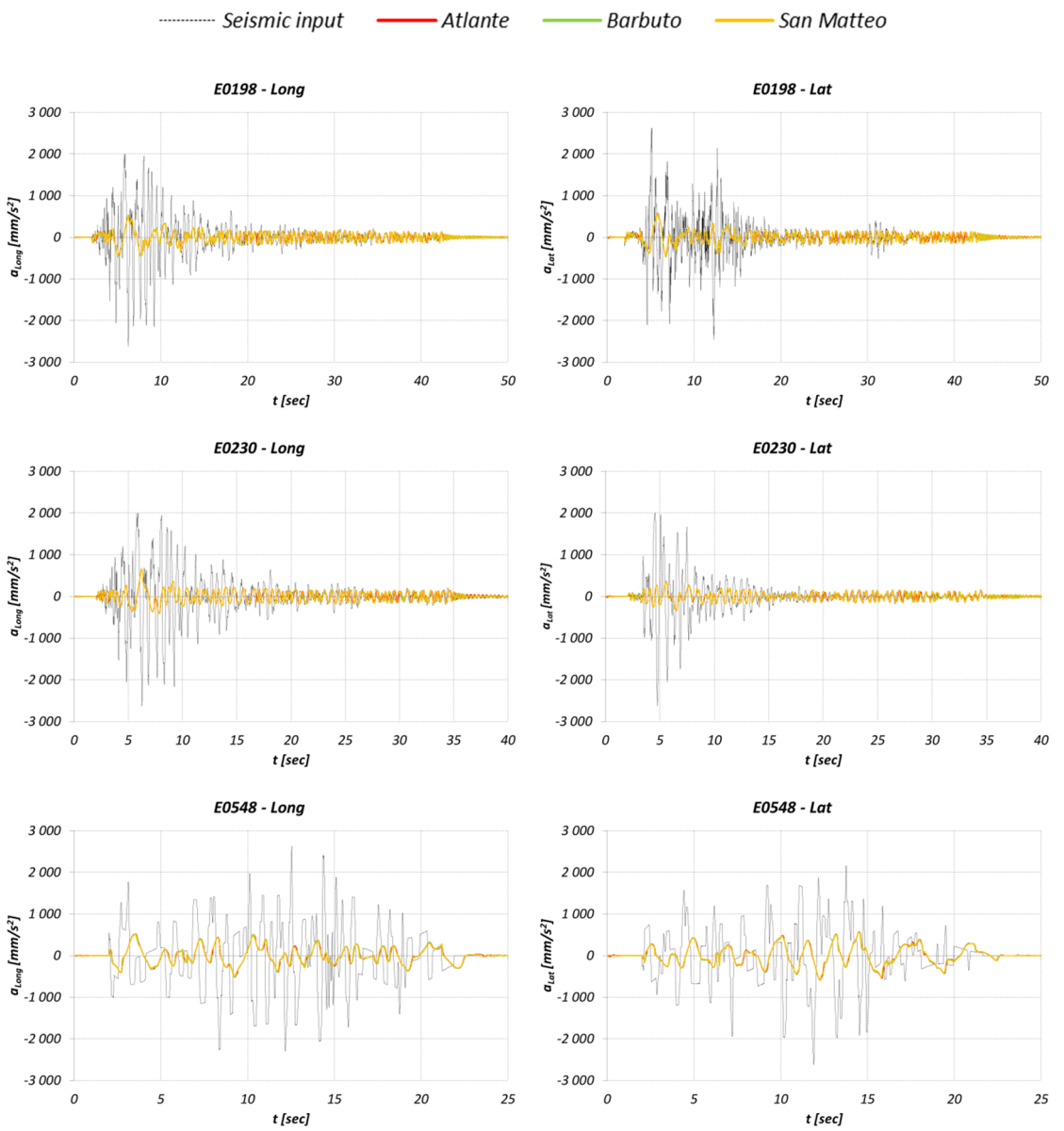

(a) (b)

Figure 47 – Reduction of the seismic acceleration for the three seimic input: (a) longitudinal direction; (b) lateral direction;

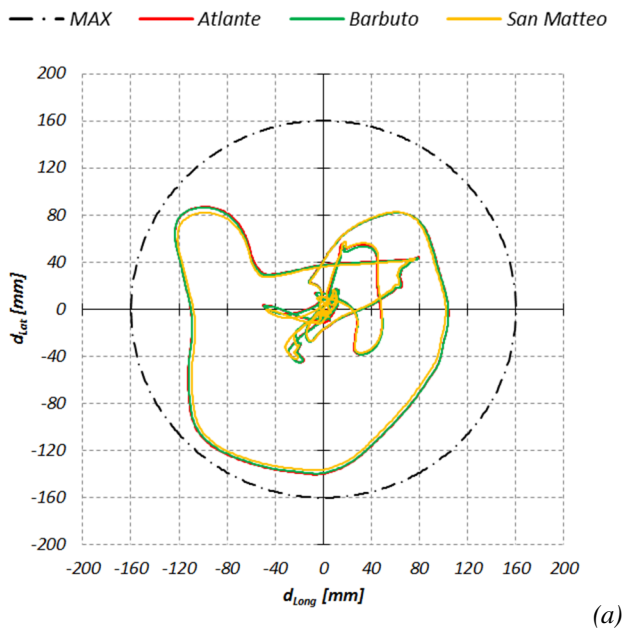

(a)

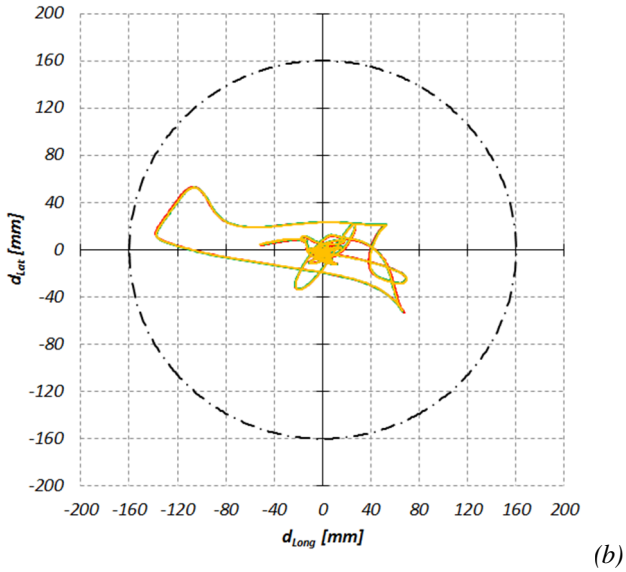

(b)

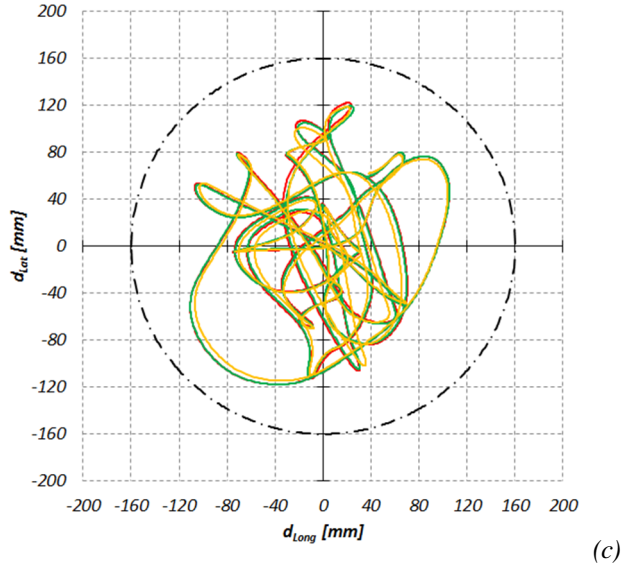

(c)

Figure 48 – Displacements on the horizontal plane for the three statues subjected to seismic input: (a) seismic input E0198; (b) seismic input E0230; (c) seismic input E0548

Finally Figure 49, Figure 50 and Figure 52 show the principal tensile stresses contours obtained with the most demanding seismic records both in fixed and isolated conditions, for the three statues. In all cases the results give evidence of the effectiveness of the devices.

It is worth noting that, also in fixed condition, the maximum stresses are lower than the corresponding strength summarized in Table 6, so confirming that the marble material remains within the linear elestic region. However, the adoption of an isolation system can be considered as convenient and opportune, in particular for the *Prigione Barbuto* for which the introduction of the DCCSS devices allows to reduce more than 80% the state of stress in the zone of the pre-existing fracture, leading to negligible tensile stress, Figure 51.

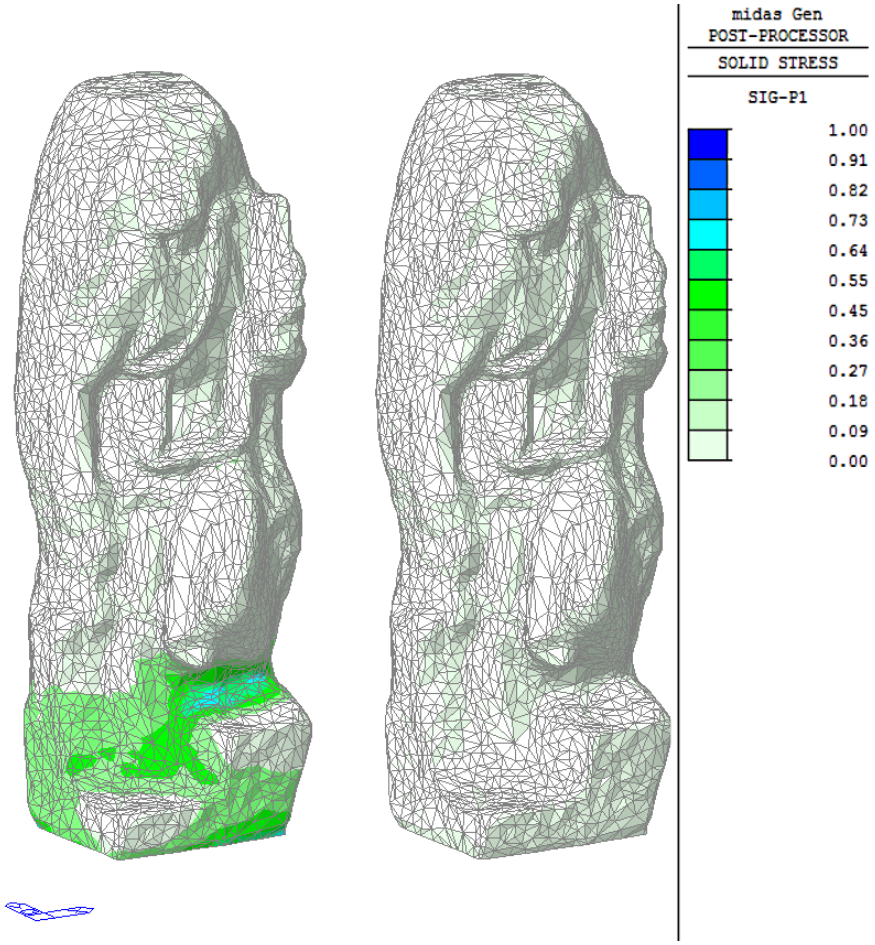

(a) *(b)*

Figure 49 – San Matteo. Maximum principal tensile stresses (MPa) due to seismic action E0548: (a) not isolated case; (b) isolated case;

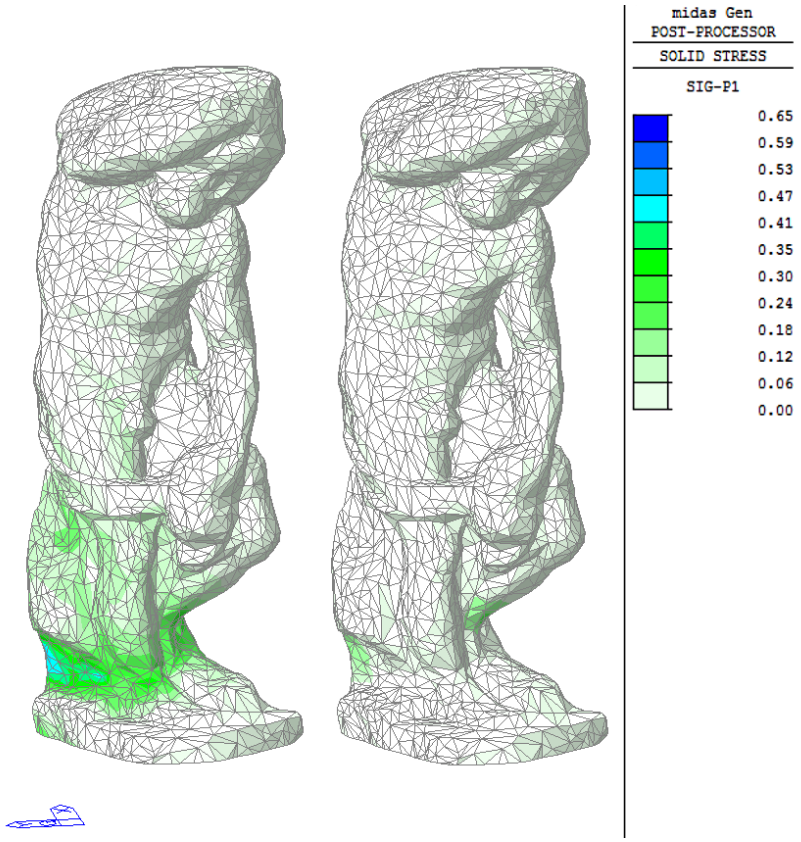

(a) *(b)*

Figure 50 – Prigione Barbuto. Maximum principal tensile stresses (MPa) due to seismic action E0548: (a) not isolated case; (b) isolated case;

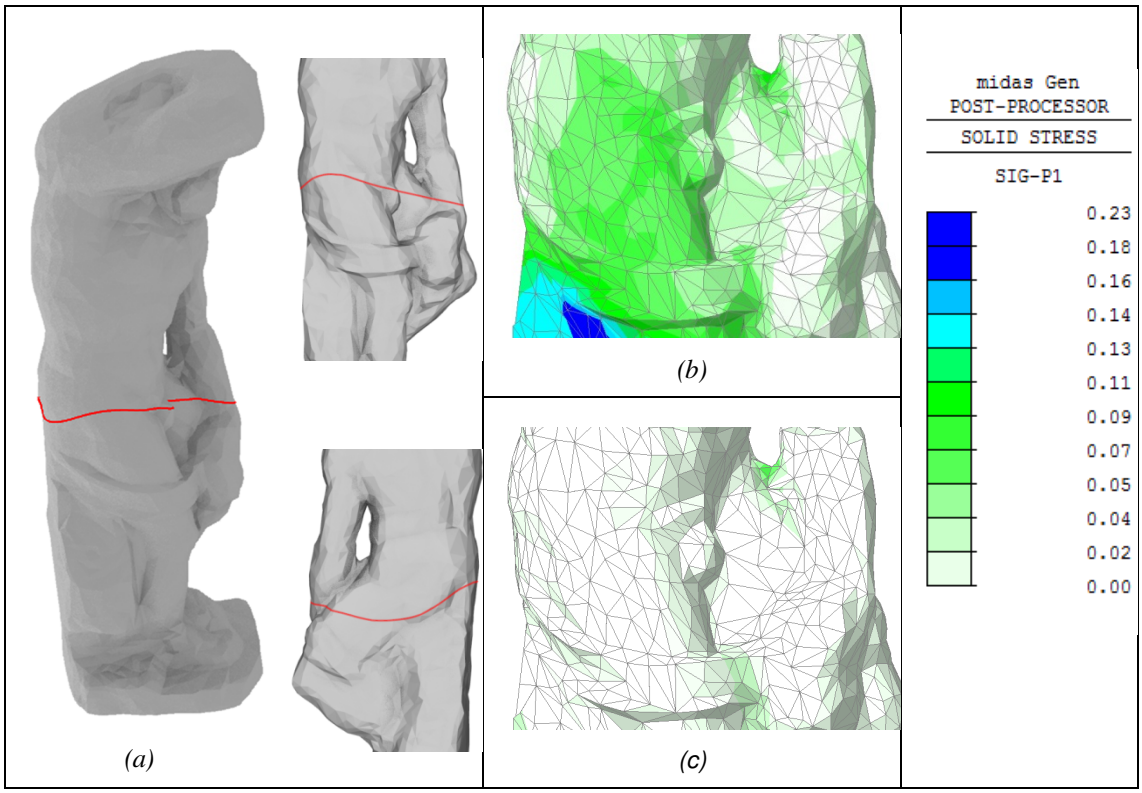

Figure 51 – Prigione Barbuto: (a) localization of the fracture; maps of the principal tensile stresses in proximity of the crack for (b) non isolated case; (c) isolated case;

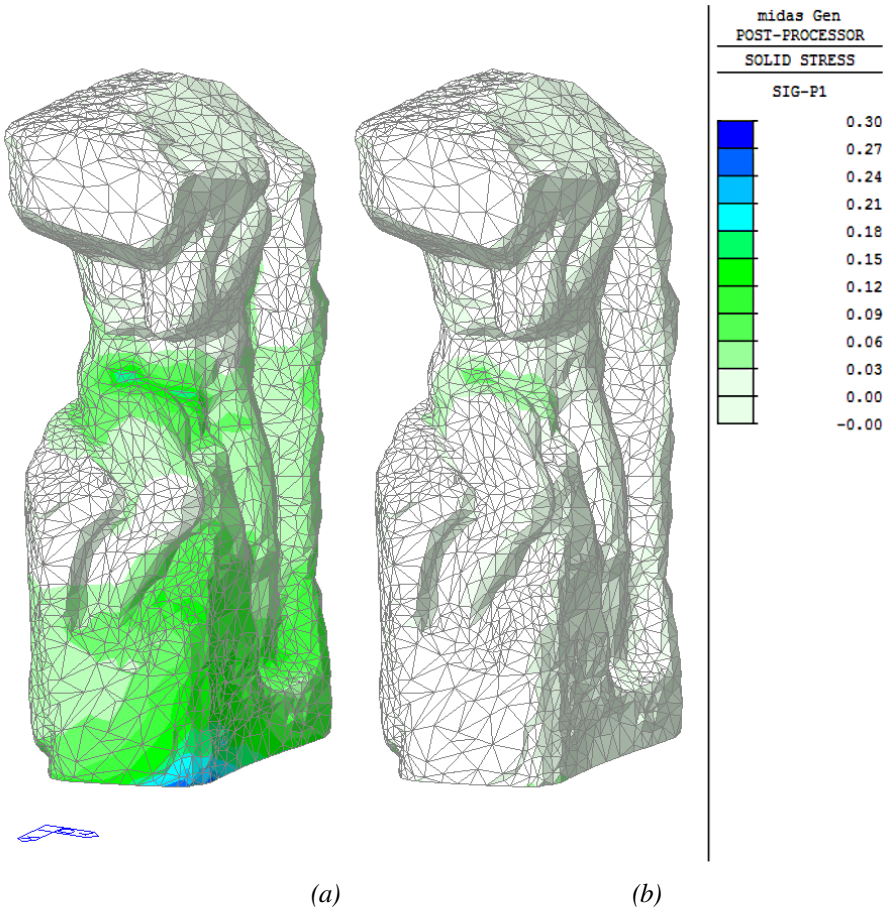

Figure 52 – "Prigione Atlante". Maximum principal tensile stresses (MPa) due to seismic action E0198: (a) not isolated case; (b) isolated case

3.3.8 Comments and conclusions

In Sect. 3.3, the possibility to seismically isolate art objects, i.e. Michelangelo's six marble sculptures exhibited in *Galleria dell'Accademia* in Florence, by means of a traditional DCCSS is investigated. The process of redesign took advantage of the existing industrial know-how and technical background, in collaboration with *FIP Industriale*, which also manufactured the prototypes of these devices. Then a series of experimental tests was carried out at the University of California UCSD with the aim to characterize the prototypes and to investigate their interaction with a physical model, simulating Michelangelo's marble sculptures, analysed in Berto et al. (2012).

The results of the SRMD experimental campaign were firstly analysed in Favaretto (2012), and Berto et al. (2013), in which some comments on the experimentation were proposed, and herein briefly reported.

About unidirectional tests, results highlight a significant reduction of the transferred acceleration, which becomes more effective as the peak ground acceleration of the input increases. The hysteretic curves evidence local oscillations in the output acceleration,

which in some cases induce significant deviations from the expected theoretical behaviour. Such phenomenon, probably due to a non-simultaneous motion of the interfaces, is also affected by the different geometrical layout of the system, the configuration of the bearings and their layout and the intensity of the input. In particular, the increasing input acceleration causes a reduction of local oscillations in the output; likewise, the closer the input accelerations are to the value of static friction coefficient, the higher these effects are and may induce damage to the artefact.

From the experimental results friction coefficient was found to be lower than that assumed for the corresponding traditional ones, generally ranging between the 10%÷15%. For this specific case friction can be reasonably found in the range 1.5÷2.5%.

Results of bidirectional tests show that an approach with simple superposition of unidirectional tests are prone to underestimate the maximum displacement, providing a solution that is not on the safe side and confirm the importance to perform 2D or 3D laboratory tests.

It should be highlighted that tests were conducted with not extremely high levels of acceleration, in fact art objects can often withstand very low levels of stress (also according to their state of conservation), hence the transmitted forces must be very low and the "activation" of the system should be kept at low levels as well. On the other hand, the reduction of forces generates higher displacements, connected to the reduction of friction and dissipation, that must fit the availability of space of the exhibition hall.

Concerning the numerical simulation of the dynamic response of the system, the phase of calibration and validation of the traditional numerical model involved the initial stiffness, the values of the coefficient of friction and the numerical damping. According to experimental results and parametric analyses a modification of the classical formula to assess the value of initial stiffness K_1 accounting for the reduced dimensions of the new devices was implemented. Furthermore, an enhanced calibration of the friction parameters of the DDCCS was performed with a two-steps procedure. The comparison between the experimental results obtained for low and high configurations and the numerical simulations carried out with different values of friction parameters demonstrated that "Opt" calibration is a good compromise among the possible choices for the friction parameters, with a good accordance in terms of global response. Regarding the effectiveness of this seismic mitigation solution, the results of the experimental/numerical campaign show a general efficiency of the isolation system in terms of limiting the transferred action. Moreover, the numerical simulation of the

dynamic and seismic behaviour of the isolated sculptures, proves the effectiveness of the proposed isolation system in reducing the principal tensile stresses in the bodies of the statues, with reduction from 60% to 90% of the tension on the most stressed zones. On the other side, the reduction is accompanied with wide horizontal displacements, which represent a crucial parameter in order to preserve the safety of the isolated good and the viewer. From this point of view, the most demanding seismic event (simulated) in terms of displacement and acceleration for the isolated system is the same for all the statues.
Finally it is worth noting that, thanks to their properties, DCCSS are particularly effective in eliminating the effect of the eccentricity of the masses of the isolated structure and this effect is well captured by the numerical simulation carried out for the case of cfg#5 as well as for the *Prigione Atlante* in isolated condition.

4 Case study, an example of “integrated design”: Bust of Francesco I

4.1 Forewords

In this chapter the case study of the bust of Francesco I d'Este, carved by Gian Lorenzo Bernini between 1651 and 1652, and housed at the *Galleria Estense* of Modena, is presented and both seismic vulnerability assessment and design of a specific intervention of seismic mitigation are performed. First phase of the study is the acquisition of data and information to define an appropriate knowledge path, which includes the definition of geometrical and material properties of the bust and an accurate identification of the host building, required for the proper determination of the seismic action at the base of the sculpture. Actually, to this aim, it is necessary to evaluate the “filter effect” of the building on seismic inputs which may significantly be altered from the ground floor to the second floor.

Then, after the evaluation of seismic vulnerability, it is proposed the adoption of an isolation system based on the DCCSS devices described in Sect 3.3. The results of the analyses, carried out adopting seismic demand given by the Italian Standards (NTC 2008), show a good efficiency of the proposed isolation system in reducing the effects of seismic action and consequently the seismic risk of the bust. It is worth noting that during the design process, a number of requirements on size and shape of the devices are imposed by the aesthetics and the characteristics of the museum exhibition.

4.2 *Palazzo dei Musei* Building

Palazzo dei Musei is a masonry building, built in the second part of the eighteenth century, Figure 53. The building complex is developed around three main courtyards. Roughly 12500 m^2 wide, it is about 25 m tall, with 4 floors. Originally conceived as Augustinian convent and *Albergo dei Poveri* (shelter for poor and homeless people) now it hosts the most important cultural institutions and museums of the City of Modena. The building is located south of *Piazza Sant'Agostino*, a square that is an example of the urban planning for the city commissioned by Francesco III d'Este, Duke of Modena. Here Francesco III built two large buildings with a social purpose: on the north side the hospital, and on the other side the *Albergo dei Poveri*. The construction works started in 1764 and finished in 1771, a few years later the construction of the hospital across Piazza Sant'Agostino. Famous architects of that time worked on the project: *Pietro Termanini, Andrea Tarabusi, Francesco Vandelli and Francesco Croce*. In 1788, however, Duke *Ercole III* decided to turn it into an *Albergo delle Arti*, a place where young people could be educated at various craft activities. In 1881 the building became part of the municipal assets. Finally, in 1883 it was transformed in the present *Palazzo dei Musei* and started hosting the artistic collections of the City of Modena, that just until the year before were in "*Palazzo Ducale*" in Modena.

Figure 53 – Axonometric view of Palazzo dei Musei – courtesy of Mr. Loreno Confortini

Just beyond the entrance, in the courtyard, it is placed the statue of the *Duke of Ferrara Borso d'Este*, surrounded by the marbles of *Museo Lapidario Estense*. The next courtyard preserves other Roman remains, and is closed by a glass canopy. In the bottom right of the main entrance, a sort of secular chapel houses the statue of the architect Luigi Poletti, and gives access to the eponymous art library. The staircase on the right leads to several museums housed here: the Municipal historical archive, the *Libreria Estense* (the City library) , the *Musei Civici archeologico-etnologico e d’arte medievale e moderna*, and at the top floor, the *Galleria Estense*, one of the most important Italian art galleries, preserving artworks by *Tintoretto, Paolo Veronese, Guido Reni, Jacopo Bassano, Correggio, Cosmè Tura, Tommaso da Modena, Lorenzo di Credi, Jacopo Palma il giovane, Dosso Dossi, il Guercino, i fratelli Carracci, i Primitivi Emiliani* and the famous *Trittico by El Greco*. However, the most famous works are the two portraits of the Duke Francesco I d'Este: the marble bust by *Gian Lorenzo Bernini* and the paint by *Diego Velázquez*.

4.2.1 Geometrical survey

Most of the geometrical information about the building came from the digitizing of drawings of the museum plans, kindly provided by the Municipality of Modena.

Figure 54 and Figure 55 show aerial images of *Palazzo dei Musei* where the portion of the building hosting the Bernini's statue is highlighted.

Figure 56 is a view from above of the building, showing the orientation of the bust with respect to north. Figure 57, Figure 58, Figure 59 (kindly supplied by *Arch. Rossella Cadignani*, of the Municipality of Modena) show the plans respectively of the ground, first and second floors of the wing where the bust is located. Figure 60 shows a section at the entrance to the Palazzo, adjacent to the hall containing the bust. Figure 61 and Figure 62 show details of the plan and section of the same hall.

Figure 54 – View of the Northern front of Palazzo dei Musei

Figure 55 – View of the western front of Palazzo dei Musei

Some geometrical data for *Palazzo dei Musei* are given below. This information is useful for later analyses, especially for a simplified evaluation of the seismic action at the base of the sculpture according to the current Standard, see Sect. 2.2.5.2.

- Total height of building: 25.20 m to roof beams (measured from ground level);
- Height of second-storey floor with respect to ground level (on which the pedestal rests): 14.60 m.

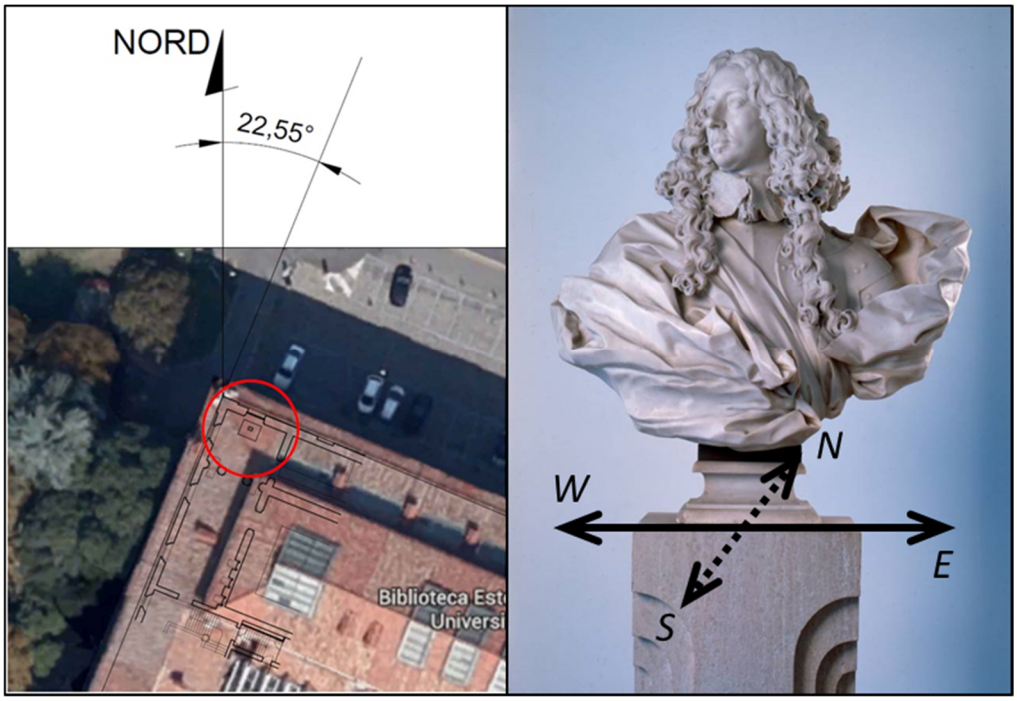

Figure 56 – Orientation of Palazzo dei Musei e position of the bust inside the building

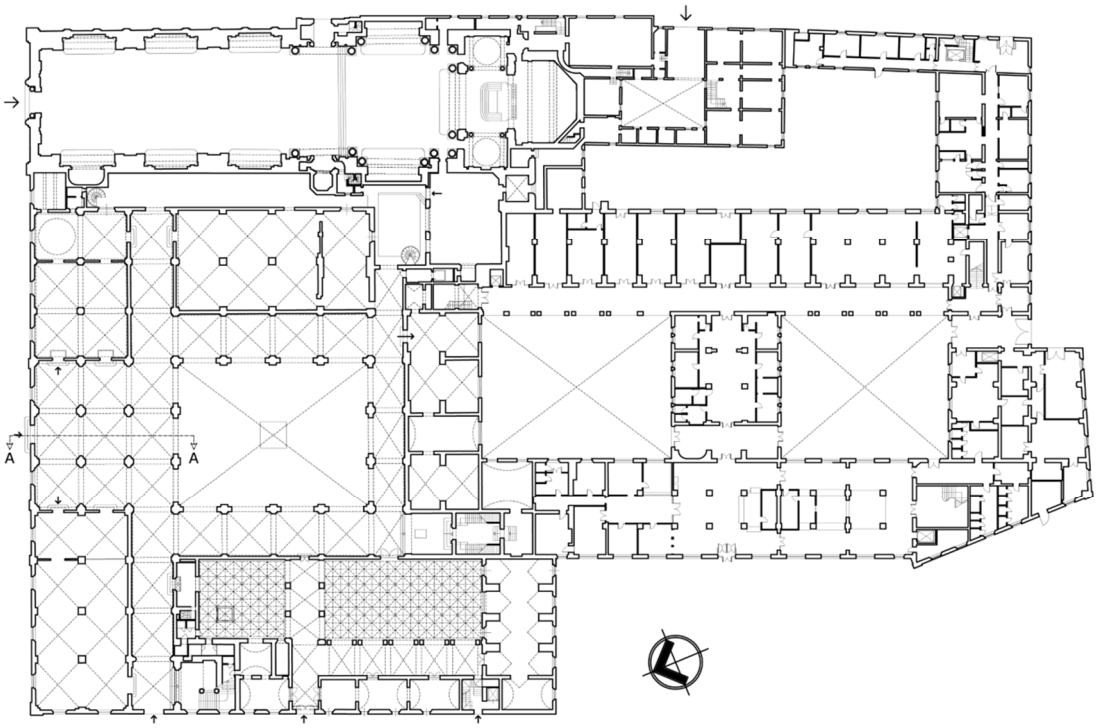

Figure 57 – Ground floor plan, Palazzo dei Musei

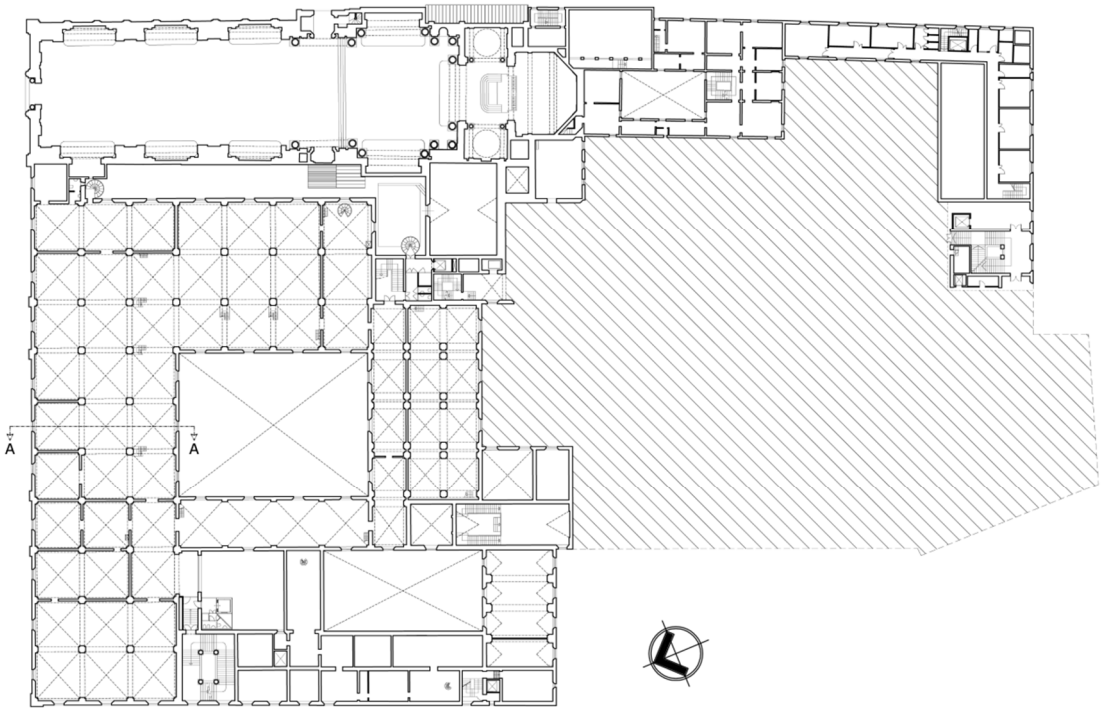

Figure 58 – First floor plan, Palazzo dei Musei

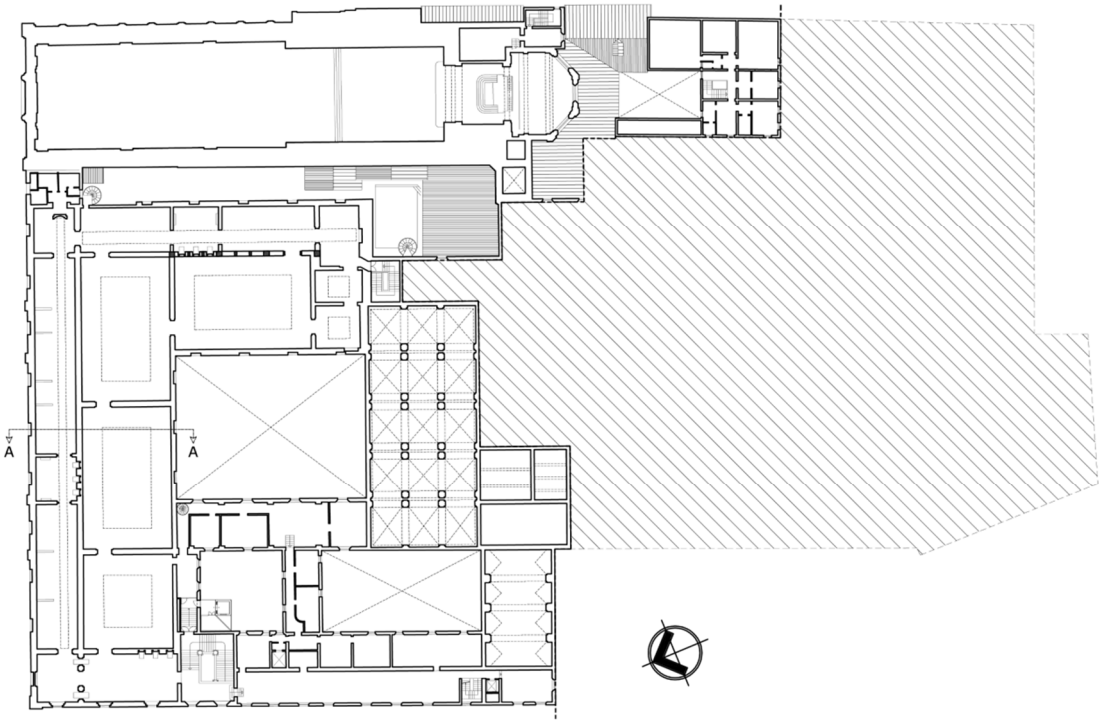

Figure 59 – Second floor plan, Palazzo dei Musei

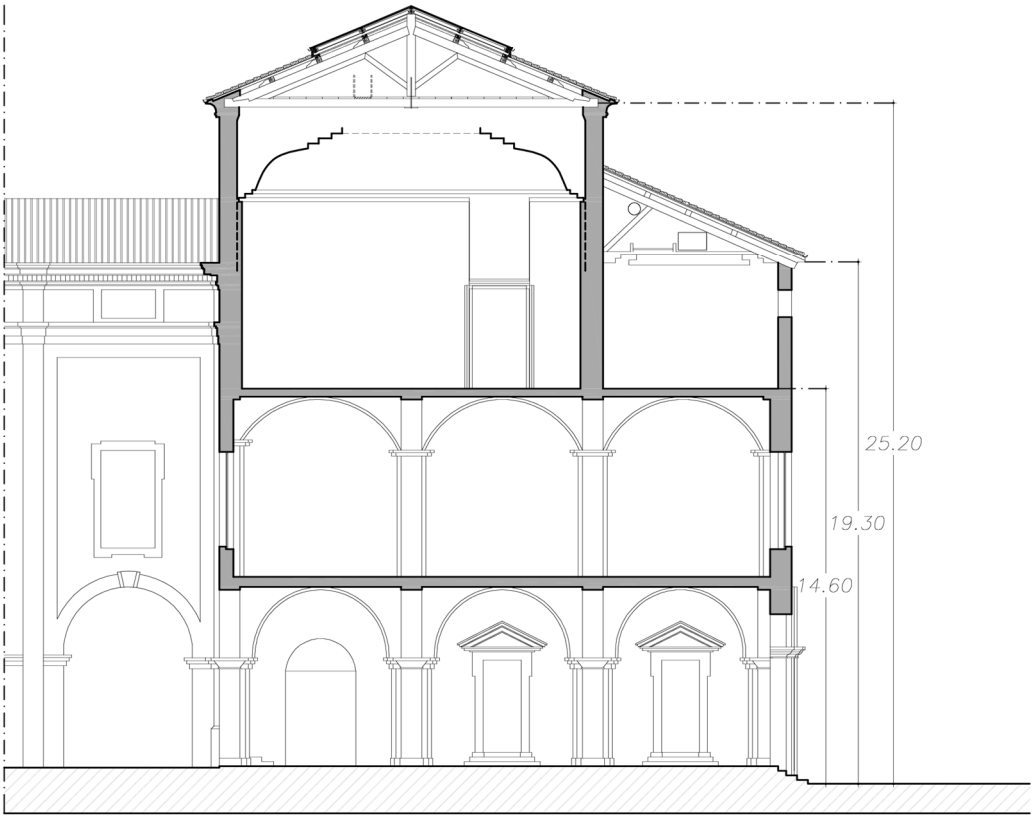

Figure 60 – Cross section of Palazzo dei Musei where the bust is placed

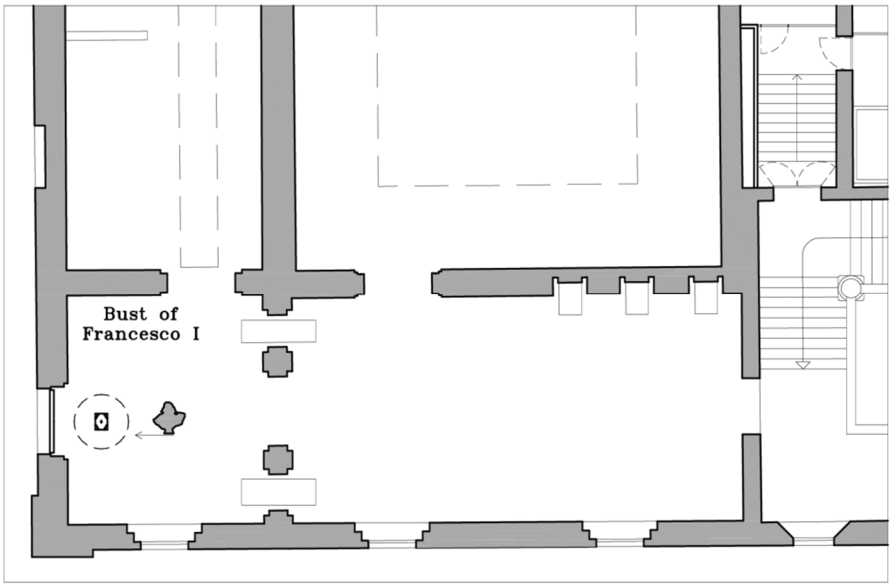

Figure 61 – Close view of the second floor and localization of the bust

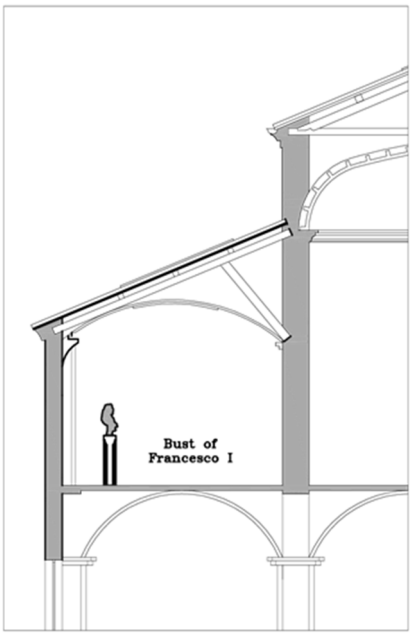

Figure 62 – Cross section of the second floor and localization of the bust, detail

To verify the acquired drawings, a 3D laser scanner survey of the area where the bust is placed has been performed by CIRCE Cartography Lab of IUAV, with particular attention to the part corresponding (underneath) the room in which the bust is placed from the ground level to the top.

Thanks to the survey, the plan dimensions of the room were corrected and updated to the actual ones, whereas the dimensions of the section have been substantially confirmed. Figure 63 and Figure 64 show plans and sections built from the 3D laser scanner survey.

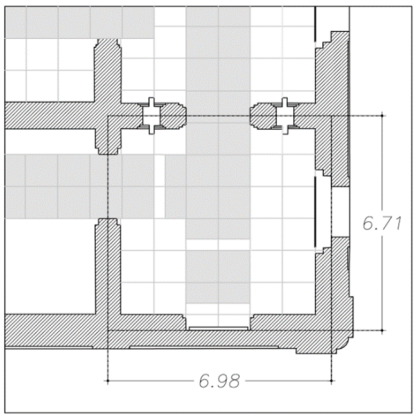

Figure 63 – Graphic rendering of the 3D laser scanner survey (CIRCE –IUAV) - Second Floor

(a) *(b)*

Figure 64 – Graphic rendering of the 3D laser scanner survey (CIRCE –IUAV) – Section N-S (a), section E-W (b)

Finally, also a large portion of the building façade has been measured, with the rendering of the related orthophotos, Figure 65.

(a) *(b)*

Figure 65 – Orthophotos from 3D laser scanner survey - North Façade (a), East Façade (b)

4.2.2 Numerical modelling

In order to assess the seismic input acting at the second floor, a Finite Element model of the Museum is created. Due to the complexity and the huge extension of the whole Building, the F.E. Model represents only the part of the building in which the bust is exposed. In particular, according to the procedure exposed in Sect. 2.2.5.3 a representative substructure of *Palazzo dei Musei* has been analysed, and the appropriate distribution of boundary constraints to simulate the presence of the remaining part of the building has been studied. The North-West corner is represented (red zone in Figure 66), with a size of about 28 m x 21 m from the ground level to the top (Figure 67). The model spans for 4 modules along the East-West direction and 3 modules along the North-South direction, each module is identified by the planar projection of the cross vault of the ceiling (Figure 63).

The geometry of the model has been discretized using shell elements for the masonry walls and for the vaults of first and second floor, while beam elements have been used to discretize the columns.

Figure 67 shows views of the model implemented for the numerical analysis.

Elastic analyses have been performed, both modal to determine the main vibration modes of the structure and time history analyses.

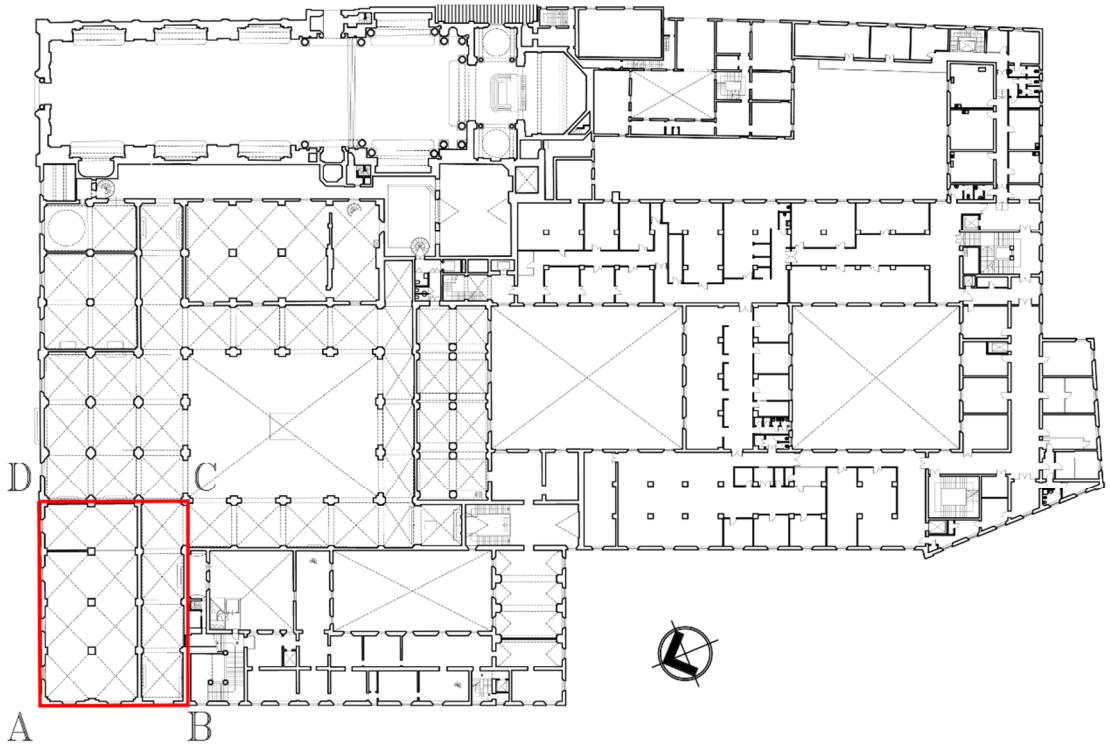

Figure 66 – First floor plan with marked in red the modeled area

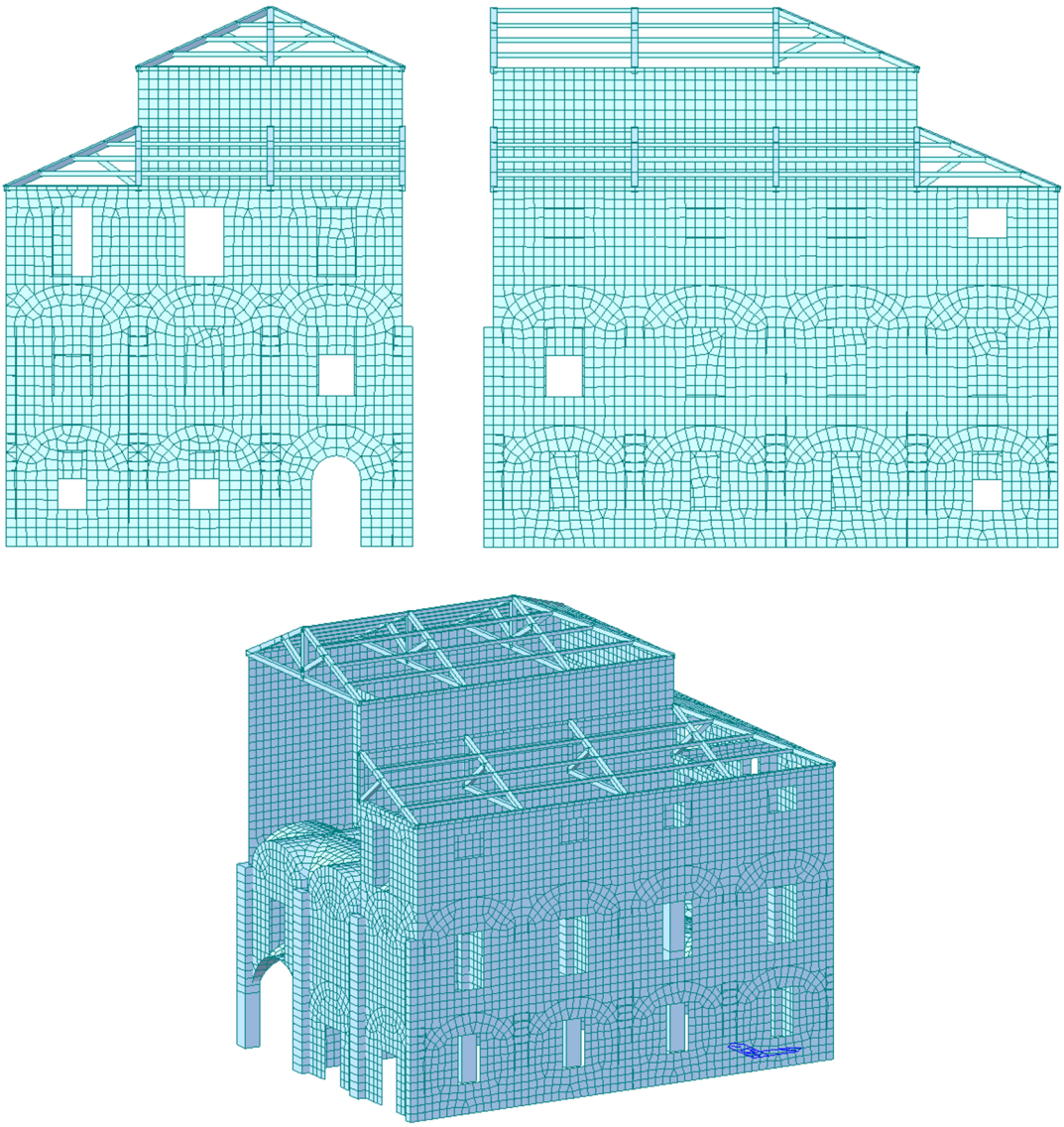

Figure 67 – F.E. Numerical model

4.2.2.1 Mechanical parameters

Without a deeper in situ investigation that could determine the mechanical characteristics of the masonry, reference values of table C8A2.1 (*Circolare applicativa norme tecniche*) associated to “*murature in mattoni pieni e malta di calce*” (solid bricks masonry with lime mortar) have been used. For the analyses two different elastic modules have been considered:

- $E_{MAX} = 1800\ MPa$
- $E_{RID} = 1800 \cdot 0{,}7 = 1260\ MPa$

Which correspond respectively to good or poor mechanical properties. The reduction factor 0,7 corresponds to consider a cracked masonry, therefore resulting in a deterioration of its mechanical characteristics.

4.2.2.2 Boundary conditions: effects on the neighbouring buildings

According to procedure described in paragraph 2.3.3, the model that represents the area ABCD in Figure 68, has fixed boundaries at its base and, in correspondence with the nodes along the two sides BC and CD, presents the previously defined four boundary conditions (ref. Sect. 2.3.3), here recalled for readers' convenience:

- Absence of constraints, which represents the limit situation in which the portion of the building is not affected by the presence of the adjacent parts, and therefore is analysed as a separated building (hereinafter referred as "*FREE*");
- Presence of translational spring with low stiffness, which represents the condition in which the portion of the building is poorly bounded to the adjacent parts (hereinafter referred to "K_{MIN}");
- Presence of translational springs characterized by high stiffness, which represents the situation in which the portion of the building is strongly bounded to the adjacent parts (hereinafter referred to "K_{MAX}");
- Presence of fixed constraints, which represents the limit situation in which the portion of the building is rigidly constrained at the nodes on the sides BC and CD (hereinafter called "*FIX*").

The stiffness of the adjacent parts of the building, next to the considered substructure, can be evaluated according to Eq. (13), which assumes that stiffness is proportional to the pertaining masses and inversely proportional to the square of the Period of vibration.

To this aim, the first step is to evaluate the mass of the adjacent buildings. As simplifying hypotheses, it has been assumed that the mass incidence per area is uniform throughout the whole building, and equal to that of the considered substructure. For this model the total mass, due to the self-weight and the 60% of the live loads, have been calculated and it is equal to 4.644,34 t. With a plan area of 568 m^2, a mass per area $\rho = 8{,}18\ t/m^2$ is obtained, including all the three floors of the building.

With a good approximation, the green and cyan coloured areas shown in Figure 68 may be considered as the adjacent portions to the "partial" model that determine the degree of constraint of the substructure.

In Table 7, the value of the plan area and the corresponding value of the mass are given for those zones, respectively afferent to the sides CD and BC.

As regards the BC side, it has been considered a mass density $\rho = 6{,}135\ t/m^2$, corresponding to 75% of the value calculated above, to take into account that while the green zone may be considered homogeneous with respect to the partial model for height

and size, the blue zone presents a total height lower than that of the ABCD substructure and two internal covered courtyards.

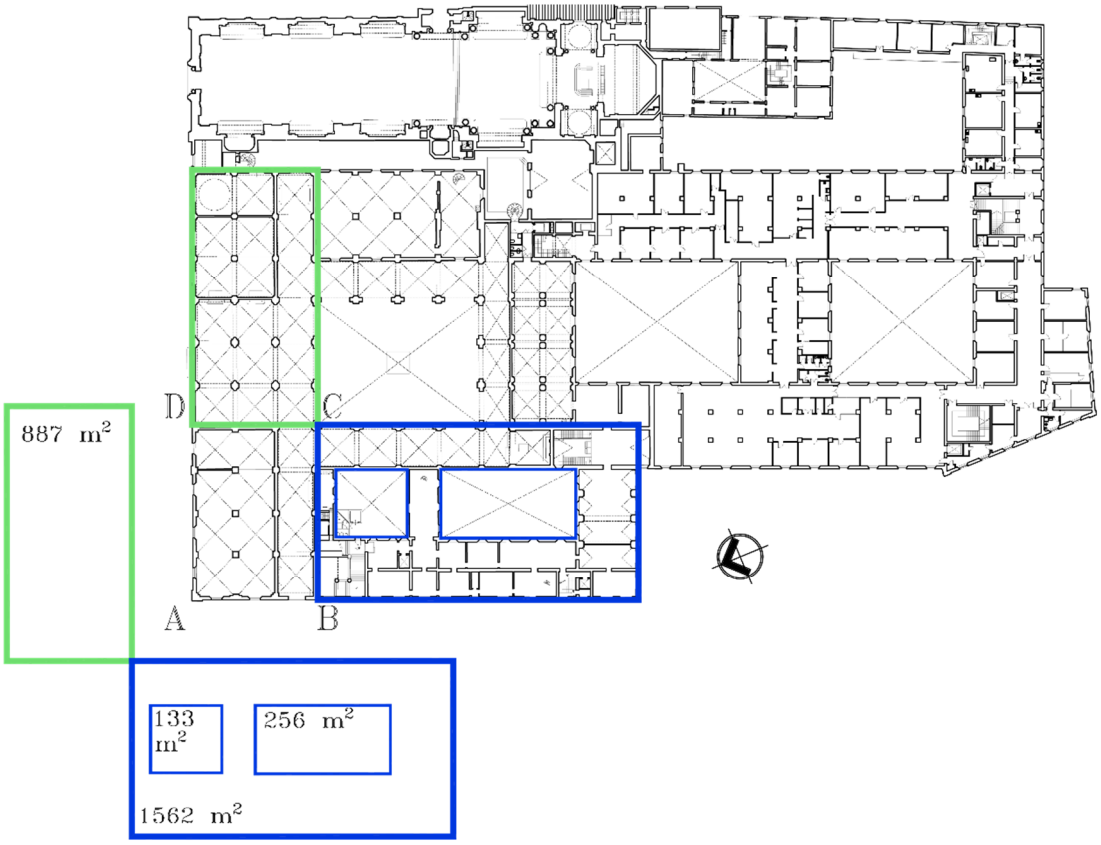

Figure 68 – Entire building and adjacent areas to the considered substructure

	Area (m^2)	***Mass (t)***
Zone afferent to CD	*887*	*7.252,70*
Zone afferent to BC	*1562-(133+256) = 1173*	*7.193,42*

Table 7 – Areas and mass of the zones afferent to the sides CD and BC

It is interesting to note that in this way the value of the total mass calculated for the two zones is comparable, also implying similar value of stiffness.

Considering a reliable range for the fundamental period T of this kind of constructions ($0{,}2\ s \leq T \leq 0{,}8\ s$), from (13) the corresponding value of the stiffness of the adjacent zones has been evaluated, Table 8.

By assuming that the stiffness is uniformly distributed in the nodes of the model at the side BC and DC the values of the corresponding elastic constant of the spring for the condition "K_{MAX}" (corresponding to $T_{min} = 0{,}2s$) and "K_{MIN}" (corresponding to $T_{max} = 0{,}8s$) have been evaluated, Table 9.

	T_{min} = 0,2 s	T_{max} = 0,8 s
Zone afferent to CD	*7.150,87 kN/mm*	*446,9 kN/mm*
Zone afferent to BC	*7.092,42 kN/mm*	*443,3 kN/mm*

Table 8 – Stiffness of the zones adjacent to the substructure

	K_{MAX}	K_{MIN}
Zone afferent to CD (217 nodes)	*32,95 kN/mm*	*2,06 kN/mm*
Zone afferent to BC (214 nodes)	*33,14 kN/mm*	*2,07 kN/mm*

Table 9 – Spring stiffness in correspondence with the nodes

It is worth noting that these values of stiffness have been attributed to the translational springs acting in the direction perpendicular to the restrained side, (i.e. BC and CD). In the orthogonal direction other springs with half the stiffness have been disposed, to take into account the rectangular shape of the two adjacent portions, with ratio between the two sides almost equal to 2. In particular, according to the proposal of ATC3-06 the main period of a structure may be expressed as:

$$T = 0.09\frac{H}{\sqrt{D}} \quad [s] \tag{34}$$

where H(m) is the height of the building and D(m) is the dimension of the building in the considered direction. It follows that the relationship between the stiffness calculated with reference to the two orthogonal directions is given by:

$$\frac{k_1}{k_2} = \frac{\left[\left(\frac{2\pi}{T_1}\right)^2 \cdot m\right]}{\left[\left(\frac{2\pi}{T_2}\right)^2 \cdot m\right]} = \left(\frac{T_2}{T_1}\right)^2 = \frac{\left[0.09\frac{H}{\sqrt{D_2}}\right]}{\left[0.09\frac{H}{\sqrt{D_1}}\right]} = \frac{D_1}{D_2} \tag{35}$$

The boundary condition obtained is schematically represented in Figure 69, in which for the sake of clarity a single spring is indicated for each one of the restrained side.

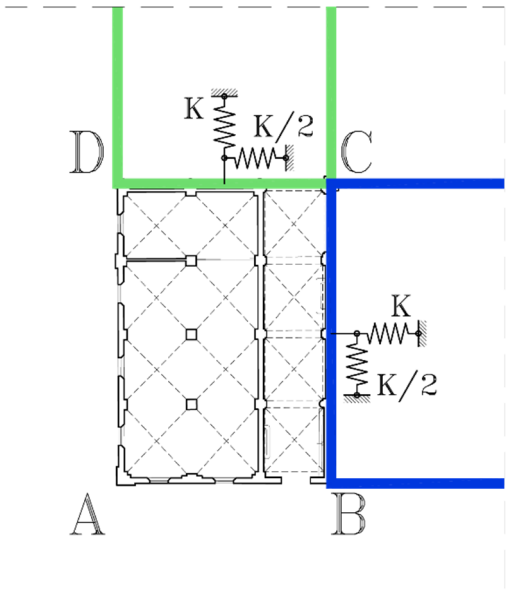

Figure 69 – Schematic representation of the boundaries adopted in the model

4.2.2.3 Results of the modal analysis

In the following, the results of the modal analyses of the substructure are given, assuming the different boundary condition for the lateral restraints. Particularly in Table 10 the main results are summarized in terms of Period of Vibration, participating mass and the relative direction of the principal vibration modes, considering a good mechanical characteristic of the masonry (E_{MAX} = *1800 MPa*). The same results for the reduced elastic modulus (E_{MIN} = *1260 MPa*) are reported in Table 11. In the tables, the modes with participating mass >10% are highlighted. Concerning the adopted reference system, the X direction corresponds to the side BC, while Y is oriented along the side AB of the building (corresponding also to the x and y direction of the Bust/Pedestal system as detailed in Sect. 4.4.1.3).

The natural frequency analysis shows common characteristics for the “FREE” and “K_{MIN}” cases, without significant differences in the behaviour of the structure, but only a diminishing of the fundamental periods by incrementing the stiffness of the boundary conditions. First two modes of vibration are of translational kind, respectively in the Y direction and in the X direction, the third mode is of torsional kind, and the fifth mode is a translational mode with participating mass in the Z – vertical direction. With the increasing of the stiffness of the springs, corresponding to “K_{MAX}” and, at the limit, “FIX”, the modal analysis points out a more complex behaviour in which it becomes impossible to recognize just two principal modes, and a third torsional mode, but multiple modes are found.

	FREE			KMIN			KMAX			FIX		
Vibration mode	Period T [s]	Dir.	Mass [%]	Period T [s]	Dir.	Mass [%]	Period T [s]	Dir.	Mass [%]	Period T [s]	Dir.	Mass [%]
1	0,483	DY	81,45	0,353	DY	84,04	0,176	DY	49,53	0,161	DY	11,47
2	0,286	DX	73,58	0,257	DX	73,84	0,141	DX	54,18	0,119	DZ	32,95
3	0,249	RZ	77,58	0,218	RZ	80,55	0,13	DY DZ	19,84 12,98	0,117	DZ	16,00
4	0,18			0,169			0,12	DZ	29,39	0,115		
5	0,131	DZ	15,65	0,125	DZ	17,15	0,118			0,113		
6	0,123			0,12	DZ	14,42	0,116	RZ	13,16	0,111		
7	0,12	DZ	25,05	0,117			0,115			0,109		
8	0,117			0,115			0,111			0,108		
9	0,115			0,113			0,107	RZ	19,72	0,105		
10	0,111			0,112			0,105			0,105		

Table 10 – Results of modal analysis for the four boundary conditions of lateral restraints (E_{MAX}= 1800 MPa)

	FREE			KMIN			KMAX			FIX		
Vibration mode	Period T [s]	Dir.	Mass [%]	Period T [s]	Dir.	Mass [%]	Period T [s]	Dir.	Mass [%]	Period T [s]	Dir.	Mass [%]
1	0,518	DY	83,90	0,394	DY	83,59	0,191	DY	42,42	0,189	DY	11,71
2	0,335	DX	74,64	0,296	DX	73,66	0,154	DX DZ	45,47 23,59	0,141	DZ	27,39
3	0,289	RZ	80,03	0,248	RZ	80,39	0,144	DY DX	15,28 13,3	0,139	DZ	20,93
4	0,204			0,196			0,14			0,137		
5	0,147	DZ	22,59	0,147	DZ	23,15	0,139			0,132		
6	0,141			0,142			0,137	DZ	11,84	0,131		
7	0,139			0,139			0,132			0,129		
8	0,137			0,138			0,132	RZ	11,04	0,126		
9	0,133	DZ	12,61	0,133			0,132			0,126		
10	0,132	DZ	14,00	0,133			0,129			0,125		

Table 11 – Results of modal analysis for the four boundary conditions of lateral restraints (E_{MIN}= 1260MPa)

In the following analyses only the two cases summarized in Table 12 will be considered, delimiting a plausible range for the real behaviour of the building.

DEF case	STIFF case
$E_{masonry}$ = 1260 MPa	$E_{masonry}$ = 1800 MPa
Boundary condition = KMIN	Boundary condition = KMAX

Table 12 – Reference cases

4.3 Seismic demand

In order to proceed to an intervention for the seismic risk mitigation, it is necessary to correctly define the seismic action at the base of the pedestal, to which the art object is subjected.

Taking into consideration that the bust is displayed at the second floor of the *Palazzo dei Musei*, definition of the seismic action requires firstly the evaluation of the action at the ground floor, then the analysis of the seismic response of the building in order to determine the eventual amplification effect. Seismic action acting at the ground floor has been evaluated according to the current regulation, "Norme Tecniche per le Costruzioni 2008" (NTC 2008). After the analysis of the seismic response of the building, the seismic action at the base of the pedestal has been evaluated in terms of both acceleration and displacement.

4.3.1 Seismic action acting at the ground floor

4.3.1.1 Response spectra according to Technical Standards

A fundamental step for the seismic risk assessment is the evaluation of the seismic demand. As stated in Sect. 2.2.4.2, for the purpose of this work, the seismic input has been evaluated according to the recent Italian building code (NTC 2008).

With reference to Sect. 2.2.4.2 for *Palazzo dei Musei*, and also for the art object, a nominal life V_N = 50 years and a functional class C_U =1,5 has been assumed, which corresponds to a reference period V_R =75 yrs. It leads to a design for the *Ultimate Limit State (ULS)* with a seismic action characterized by a return period T_r = 712 years, that is an event with a 10% probability of being exceeded in a 75 years' period.

In Figure 70 the geographical coordinates of the site of *Palazzo dei Musei* are shown while in Figure 71 the values of the reference parameters a_g, F_0, T_C^* of the seismic action are presented:

- a_g peak horizontal acceleration at the site;
- F_0 maximum value of the amplification factor of the spectrum for horizontal acceleration;
- T_C^* period corresponding to constant velocity of the response spectrum.

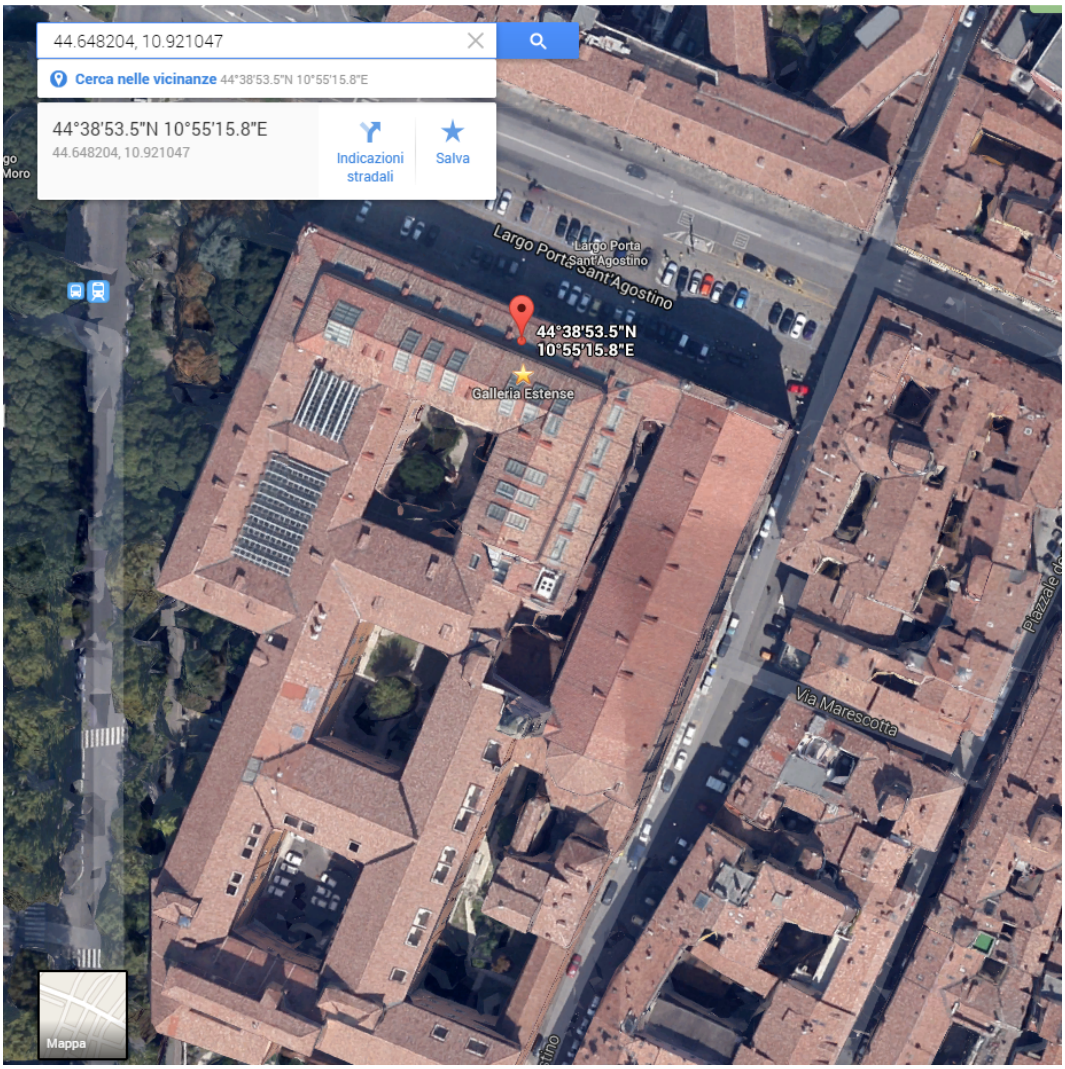

Figure 70 – Coordinates of Palazzo dei Musei (in italian)

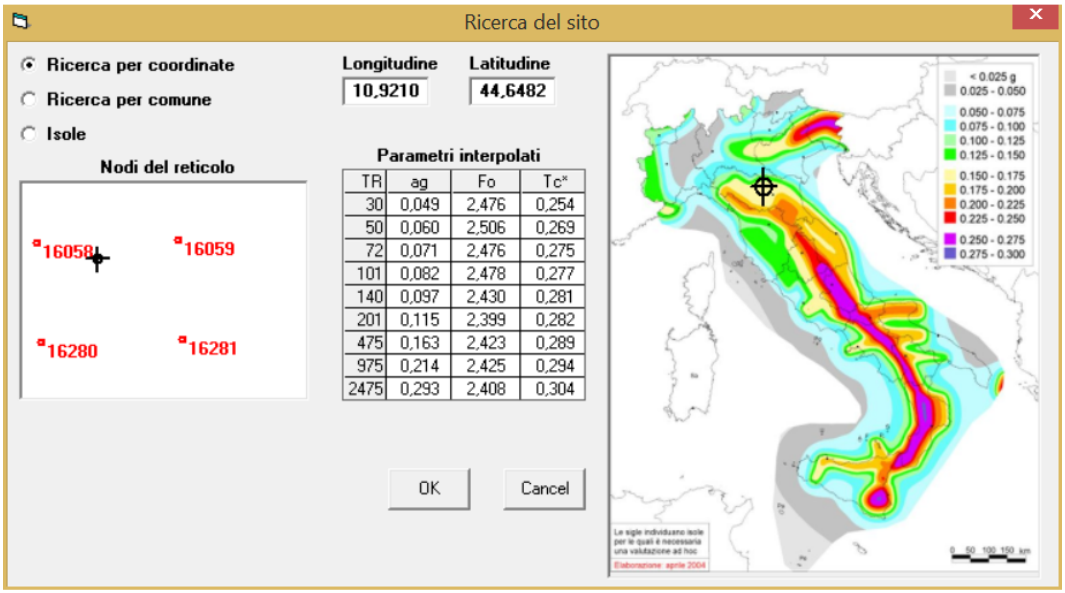

Figure 71 – SIMQKE_GR seismic hazard parameters for Modena (in Italian)

These parameters have been obtained for the city of Modena using SIMQKE_GR, a software developed by Prof. Eng. Piero Gelfi of the University of Brescia.

In the first phase of study due to the lack of data about the soil characterization, the available cartography has been carefully examined. Figure 72 shows an excerpt from the map of geological classification for the Urban plan of the municipality of Modena, in which the areas near the site of the museum complex (highlighted by the dashed line) is classified as: *Clays and predominantly clay soils* (*Argille e terreni prevalentemente argillosi*) that corresponds to Type C soil for the seismic analyses.

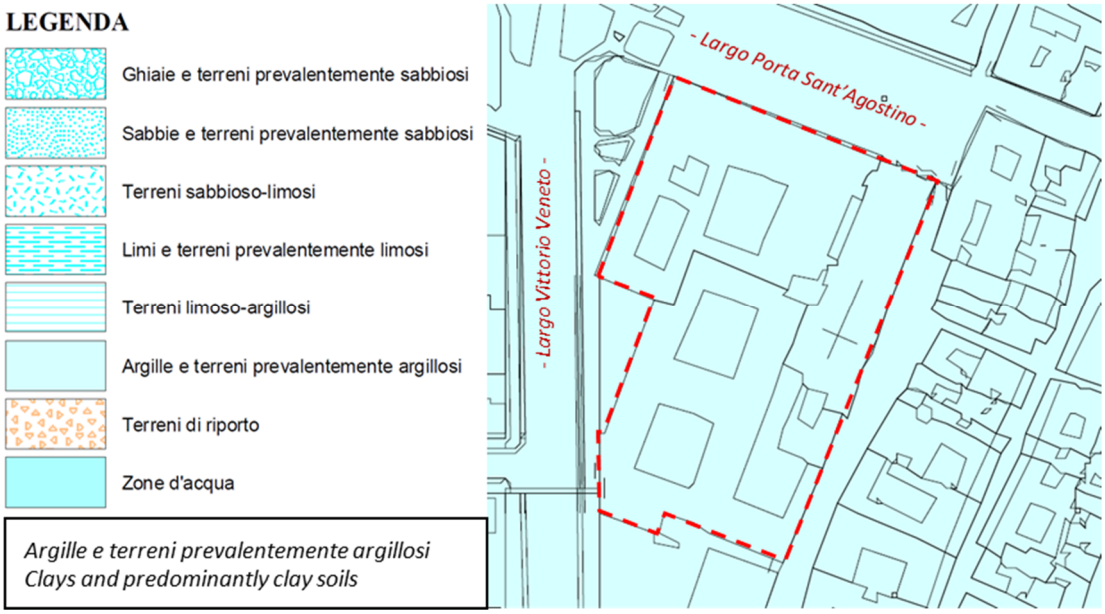

Figure 72 – Excerpt of town “P.R.G.” of Modena (town planning scheme cartography)

After this preliminary phase, the results of in situ testing for geotechnical characterization of the soil performed by the municipality of Modena for the works of restoration of the second floor of the Palace Museum has been made available. In particular, the stratigraphy of the subsoil has been determined by probing, and the "Downhole" sonic test for the characterization of the transmission velocity Vs of shear waves in the subsoil layers to a depth of 30m below the ground level. From the obtained values of V_{s30} derived from this geological study the soil in situ has been classified as of Type C, which corresponds to the coefficient of stratigraphic amplification $S_s = 1{,}421$.

Since *Palazzo dei Musei* is located in a plain site, topographic category T_1 has been adopted (Tab. 3.2.IV NTC 2008 Sect. 3.2.2), so $S_T = 1$.

The value of Peak Ground Acceleration (PGA) for different limit states are listed in Table 13.

Limit State	T_R *(years)*	a_g *(g)*	$PGA = S \cdot a_g$ *(g)*
SLO	*45*	*0,057*	*0,0866*
SLD	*75*	*0,071*	*0,1086*
SLV	*712*	*0,191*	*0,2704*
SLC	*1462*	*0,248*	*0,3298*

Table 13 – Peak acceleration of the seismic action for different Limit States – Soil type C

Acceleration elastic response spectrum is given by a normalized spectral shape referring to a conventional damping of 5%, and multiplied by the value of the maximal horizontal acceleration a_g on a reference site. Both spectral shape and a_g change with the probability of the reference period.

With the above mentioned characteristics, the seismic response spectra for the acceleration acting horizontally is obtained for the ULS with the conventional damping coefficient $\xi = 5\%$. The main parameters are given in Table 14.

Maximum horizontal acceleration in the site	a_g *[g]*	*0,190*
Maximum spectral amplification factor	F_0 *[-]*	*2,424*
Period corresponding to the beginning of constant velocity segment (ground reference)	Tc^* *[s]*	*0,292*
Stratigraphic amplification coefficient	S_s *[-]*	*1,424*
Cc coefficient	C_c *[-]*	*1,576*
Topographic amplification coefficient	S_T *[-]*	*1*
Coefficient S=Ss x S_T	*S [-]*	*1,424*
PGA – Peak Ground Acceleration	a_g *S [g]*	*0,271*
Period corresponding to the beginning of constant acceleration segment	T_B *[s]*	*0,153*
Period corresponding to the beginning of constant velocity segment	T_C *[s]*	*0,460*
Period corresponding to the beginning of constant displacement segment	T_D *[s]*	*2,360*

Table 14 – Seismic action parameters – Modena – Soil type C for T_R*=712 years*

4.3.1.2 Extraction of spectrum compatible accelerograms

In order to perform the dynamic time history analyses, seven couples of ground motions records have been selected from the European Strong-motion Database (ESD) and elaborated by using the software REXEL (Iervolino et al. 2010). In the selection of these records, specific spectrum compatibility requirements are needed.

Current Italian and European standards give a number of requirements to be fulfilled for the spectrum compatibility of Artificial and Synthetic accelerograms. These criteria can be fruitfully extended to the selection and scaling of real natural accelerograms. Anyway, with particular reference with the present case, no prescription is given for the spectrum compatibility of seismically isolated secondary system embedded in other principal system and characterized by a different vibration frequency in comparison with that of the building. For these reasons in this work two different spectrum compatibility ranges were considered, the first with reference to the natural period of the building, and the second one to the natural period of the isolated system as described in the following.

4.3.1.2.1 Spectrum compatibility range with reference to the Building – *RANGE1*

In this first selection, the range of Magnitude M = (4÷6) and the range of source-to-site distance R = (0÷20) km were considered on the basis of the disaggregation analyses provided by INGV. As recommended by the EC8 and NTC 2008, the records were properly scaled to the value of PGA expected for the site. Following the prescriptions proposed by the regulations, the compatibility with the design response spectrum of the site is given in the period range (0,15 s – $2T_1$), where T_1 is the main period of vibration of the structure, estimated from the results of modal analysis, see. Sect. 4.2.2.3. In particular, the numerical modelling of the building in the two cases (i.e. the *DEF* and *STIFF* cases), leads to a value of main period respectively equal to:

DEF $$T_1 = 0{,}39\ s \qquad (36)$$

STIFF $$T_1 = 0{,}18\ s \qquad (37)$$

For the following calculation, the maximum value of the main period (*DEF* case) structure is chosen, which leads to the interval for spectrum compatibility equal to: 0,15 s – 0,78 s (rounded to 0,8 s).

Figure 73 summarizes the data input used for the signal extraction in REXEL, while Figure 74 shows the result of such procedure in terms of individual spectra of the accelerogram combination and average spectrum.

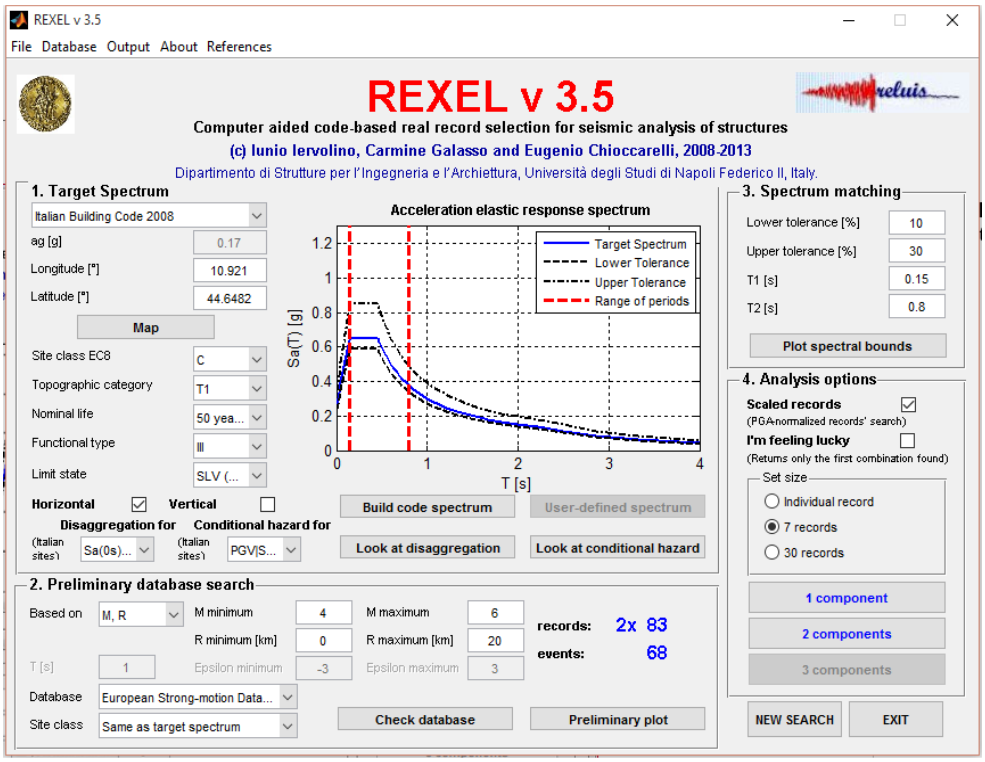

Figure 73 – REXEL data input – Building Period interval

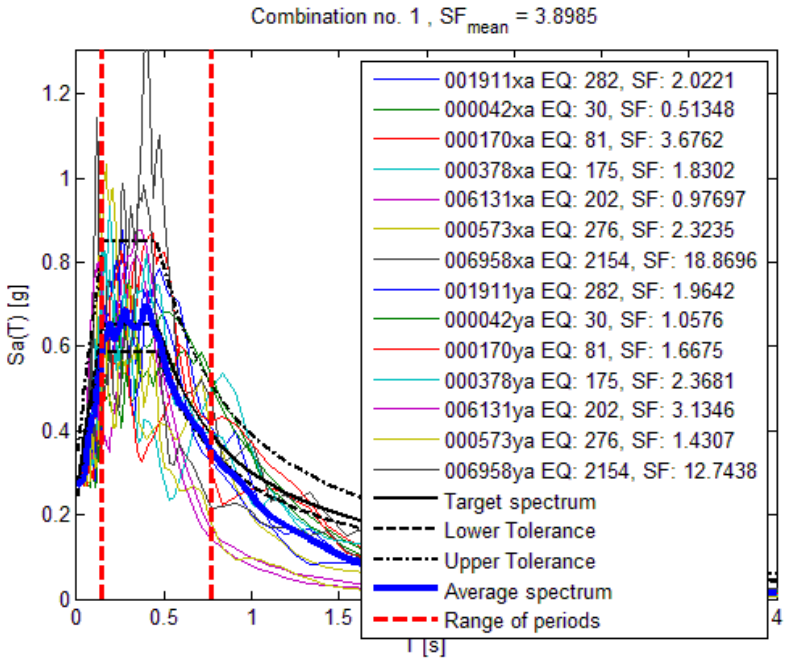

Figure 74 – Individual spectra of the combination and average spectrum given by REXEL

As an example, in Figure 75 the most demanding couple of spectrum-compatible accelerograms (i.e. couple 6958) is given.

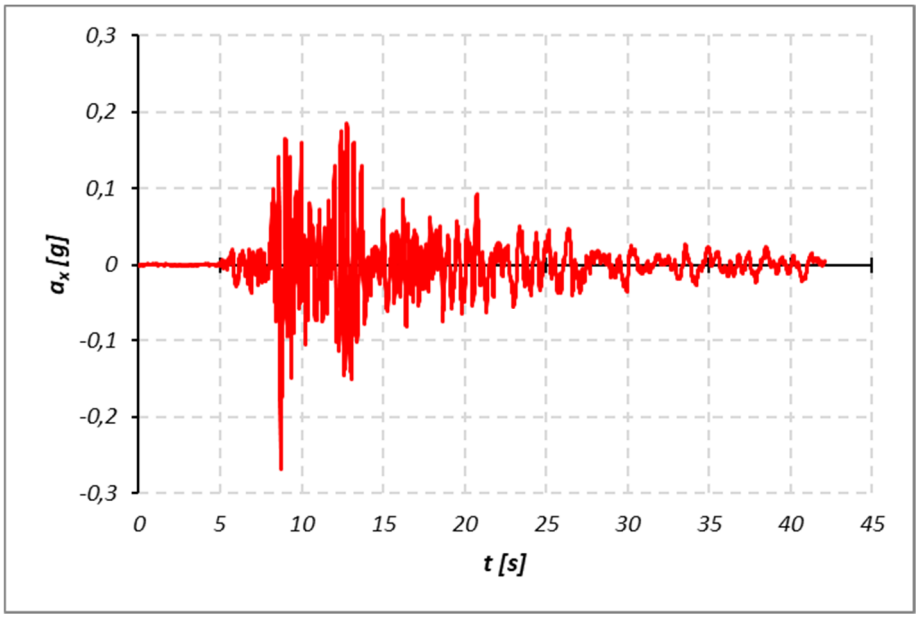

(a)

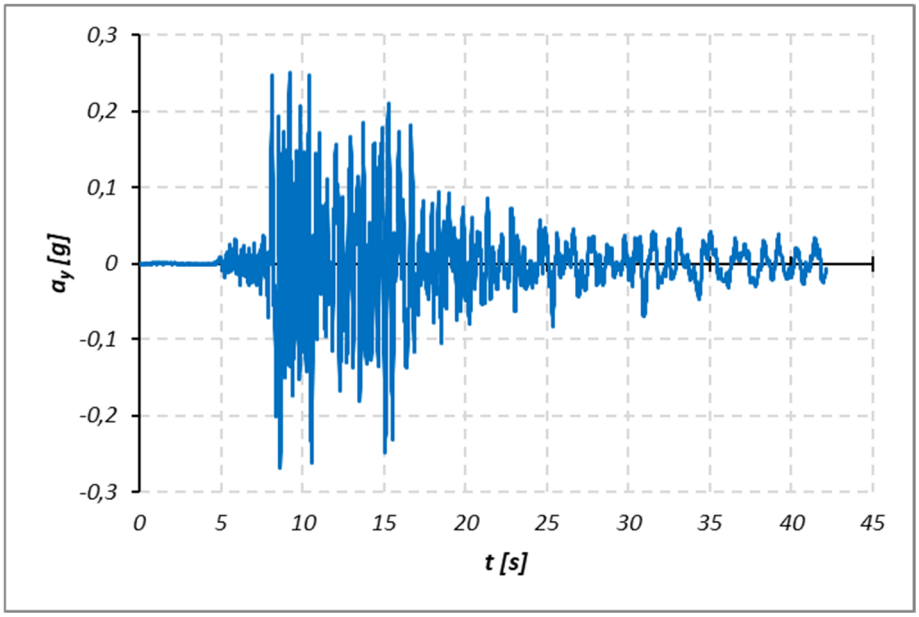

(b)

Figure 75 – Couple of spectrum compatible accelerograms (006958): (a) “X” direction (b) “Y” direction

4.3.1.2.2 Spectrum compatibility range with reference to the isolation system – RANGE2

The second selection of spectrum compatible accelerograms is carried out taking into consideration a wider range of periods, in order to ensure an adequate representation of the seismic action near to the period of the seismic isolation system T_{is}. In particular, in this case, a value of T_{is} = 2,36 sec can be assumed, as first estimation and ideal target for the period of the isolation system. Considering T_{is}, the spectrum compatibility is given between (0,15 s ÷ 1,2T_{is}), i.e. 0,15 and 2,85 seconds, comprising both fundamental periods of the primary and secondary structures (building and art object).

In order to fulfil the spectrum compatibility, larger ranges of Magnitude M = (4÷7) and of source-to-site distance R = (0÷30) km were considered instead of the previous parameters. Considering these variations on M and R parameters, Iervolino and Cornell (2005) noted that no consistent evidence suggests that it is strictly necessary to take great care in the selection of records with respect to such factors. Also in Iervolino et al. (2010), the spectral shape is considered as the most important proxy for earthquake damage potential on structures, more than event parameters as M and R.

Figure 76 summarizes the data input used for the signal extraction in REXEL, while Figure 77 shows the result of such procedure in terms of individual spectra of the accelerogram combination and average spectrum of the extracted spectra.

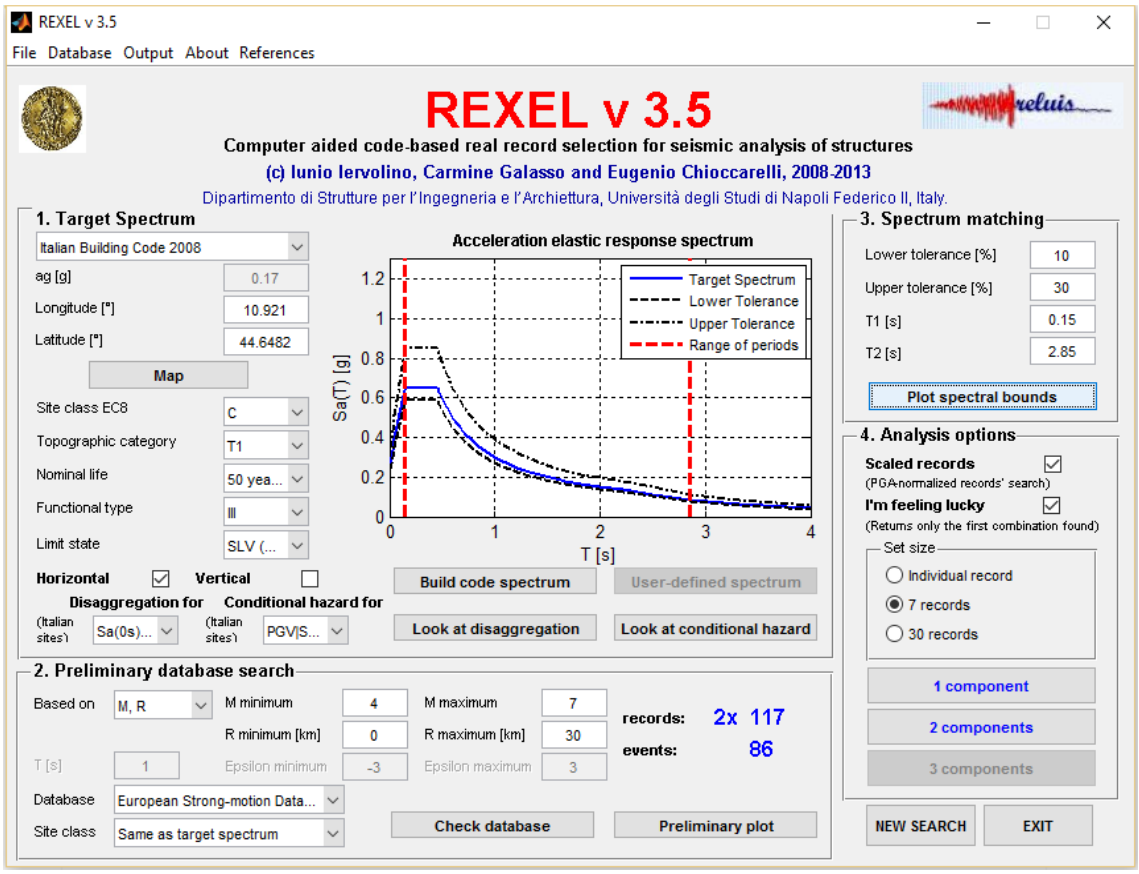

Figure 76 – REXEL data input – Isolation System Period interval

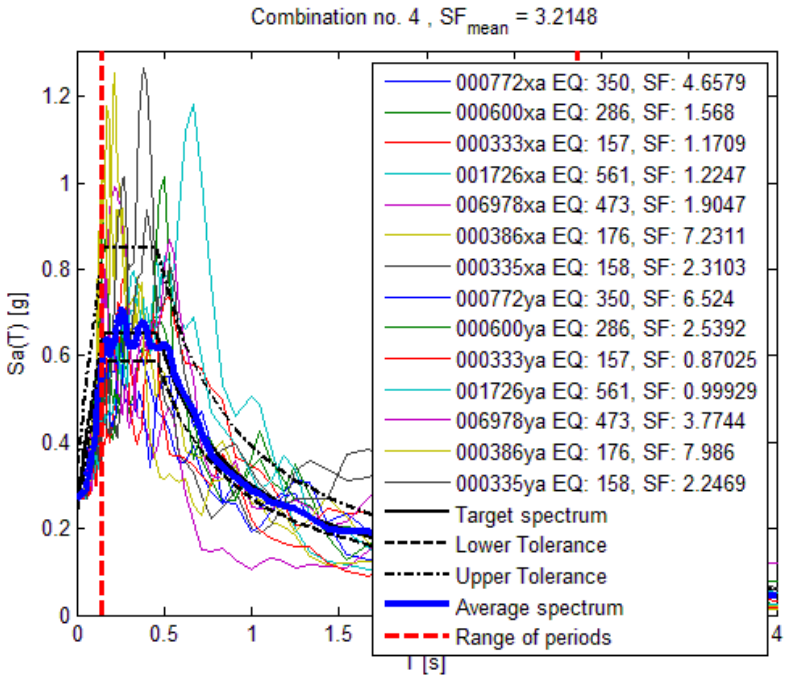

Figure 77 – Individual spectra of the combination and average spectrum given by REXEL

Similarly to *RANGE1*, also in this case, the most demanding couple of spectrum-compatible accelerograms (i.e. couple 0335) is given in Figure 78.

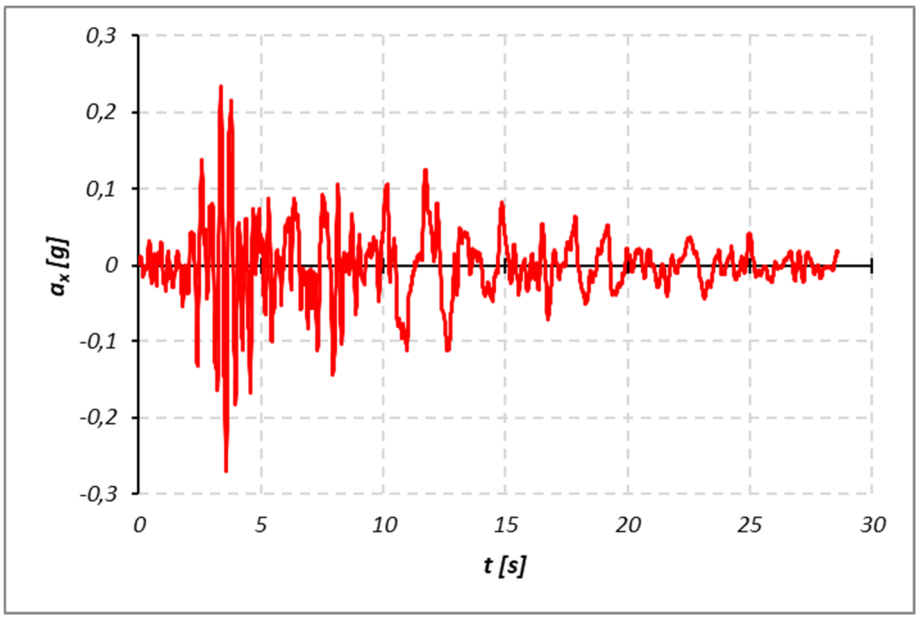

(a)

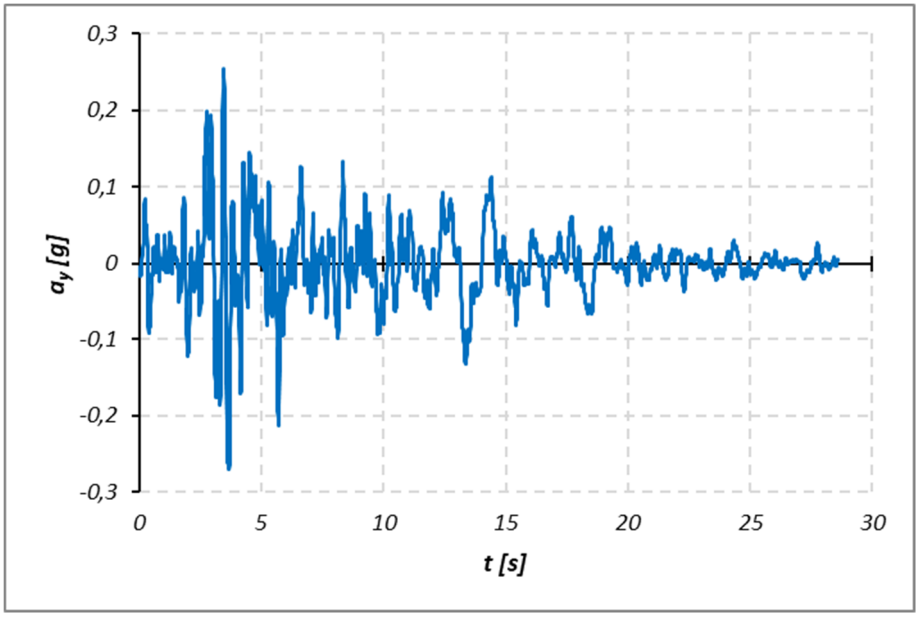

(b)

Figure 78 – Couple of spectrum compatible accelerograms (000335): (a) “X” direction (b) “Y” direction

4.3.1.2.3 Comparison and comments

Figure 79 and Figure 80 show the comparison between the mean spectra respectively in terms of ground acceleration and ground displacement for *RANGE1*, *RANGE2* and the reference spectra given by NTC 2008.

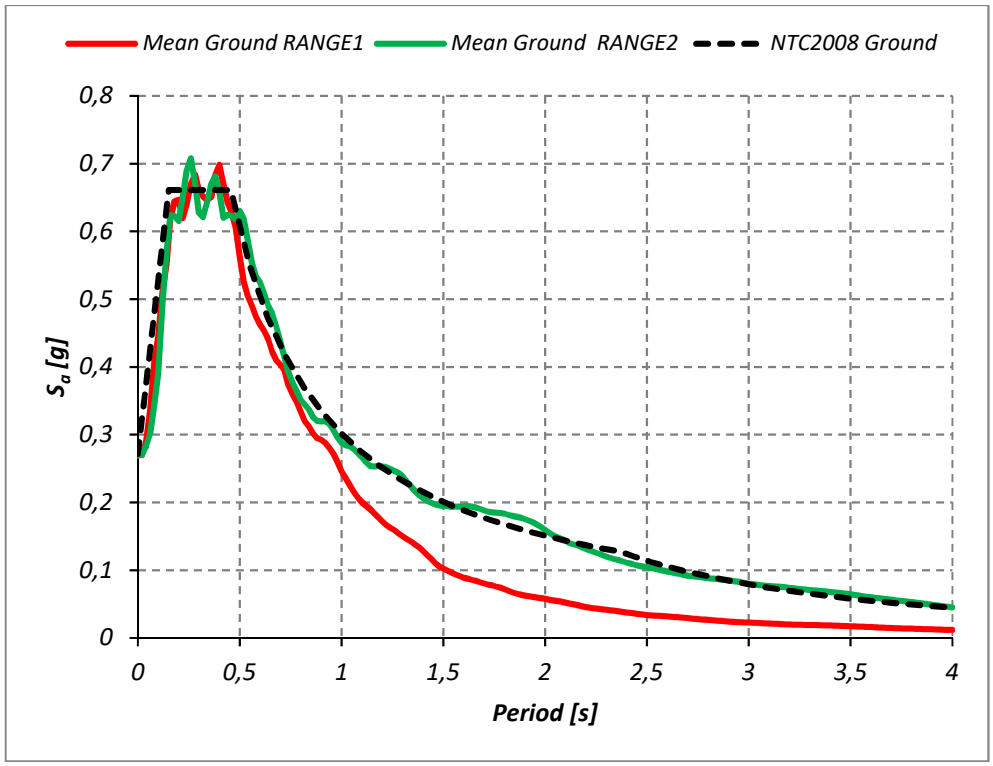

Figure 79 – Comparison between Mean Acceleration spectra given by RANGE1, RANGE2 and Technical Standars NTC 2008

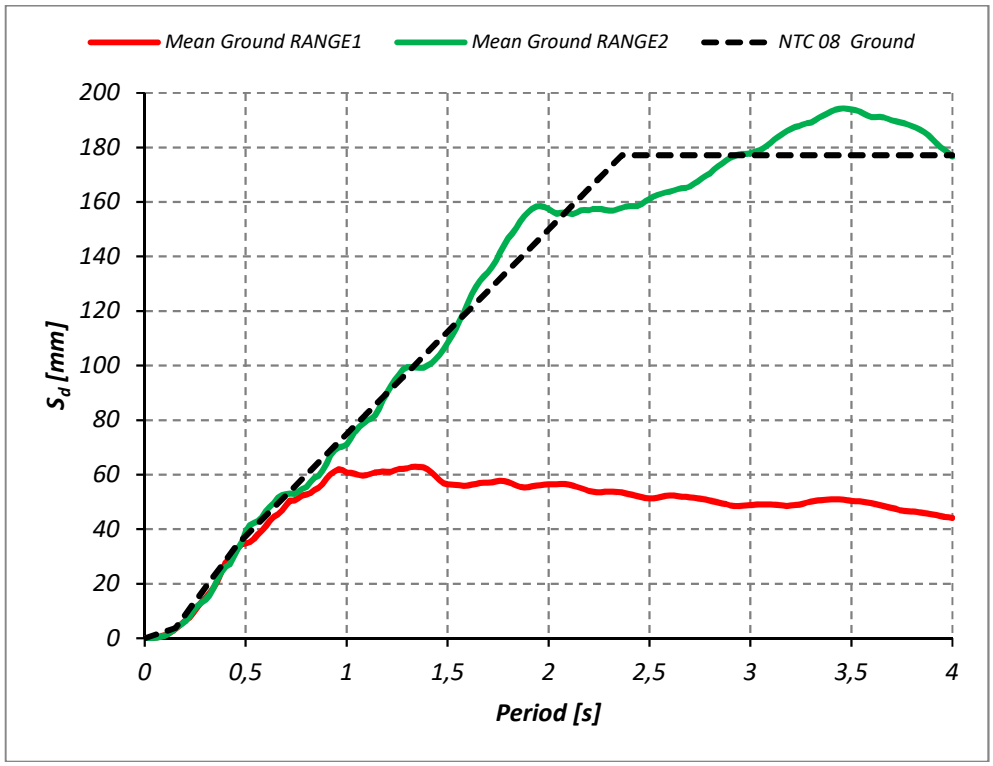

Figure 80 – Comparison between Mean Displacement spectra given by RANGE1, RANGE2 and Technical Standars NTC 2008

As evident the set of accelerograms corresponding to *RANGE2* provides the better matching with the NTC 2008 spectra, also for long period (which interests the Seismic Isolation system).

4.3.1.3 Seismic History

When evaluating the vulnerability of significant works (e.g. belonging to the historical and cultural heritage), it is fundamental to collect as much information as possible about the "seismic history" of the site, i.e., knowledge of previous seismic events which took place in the area, is essential. These data may be found in ITACA 2.0 (Italian Accelerometric Archive) and ISIDe (Italian Seismological Instrumental and parametric Database). Further details about the two databases are given in Sect. 2.2.1.

Referring to the seismic history of Modena from the year 1470 to 2004, Table 15 lists the main seismic events of intensity Is ≥ 5 (Mercalli scale), taken from the ISIDe catalogue. The table also shows the values corresponding to moment magnitude M_w at the epicentre, intensity I_0 on the Mercalli scale at the epicentre, and the number of survey points N_p.

Seismic history of Modena [44.647, 10.925]

Total number of earthquakes: 139

Effects	***Earthquake occurred:***				
I_s			***Np***	***I_0***	***Mw***
6	*1474 03 11 20:30*	*Modena*	*12*	*5*	*4.30 ±0.34*
7-8	*1501 06 05 10:00*	*Appennino modenese*	*20*	*9*	*5.98 ±0.32*
6	*1504 12 31 04:00*	*Bolognese*	*15*		
6	*1505 01 03 02:00*	*Bolognese*	*31*	*8*	*5.57 ±0.25*
5	*1505 01 20 23:50*	*Bolognese*	*11*		
5	*1505 01 27 02:40*	*Bolognese*	*2*		
5	*1536 08 17 00:05*	*Appennino tosco-emiliano?*	*10*	*6-7*	*5.29 ±0.56*
6	*1547 02 10 13:20*	*Reggio Emilia*	*13*	*7*	*5.14 ±0.34*
4	*1570 11 70 19:10*	*Ferrara*	*60*	*7-8*	*5.46 ±0.25*
6-7	*1661 03 21 23:00*	*Modenese*	*4*	*6-7*	*4.93 ±0.34*
7	*1671 06 20 10:00*	*Modena-Reggio Emilia*	*8*	*7*	*5.25 ±0.72*
5	*1811 07 15 22:44*	*Sassuolo*	*21*	*6-7*	*5.25 ±0.40*
7	*1832 03 13 03:30*	*Reggiano*	*98*	*7-8*	*5.53 ±0.18*
5	*1834 10 04 19:00*	*Bolognese*	*12*	*6*	*4.85 ±0.43*
5	*1837 04 11 17:00*	*Alpi Apuane*	*60*	*9*	*5.81 ±0.20*
6	*1850 09 18 06:20*	*Modenese*	*7*	*5*	*4.30 ±0.34*
6	*1869 06 25 13:58*	*Media valle del Reno*	*18*	*7-8*	*5.42 ±0.48*
5	*1873 05 16 19:35*	*Reggiano*	*15*	*6-7*	*5.09 ±0.59*
5	*1873 06 29 03:58*	*Bellunese*	*199*	*9-10*	*6.32 ±0.11*
5	*1886 10 15 02:20*	*Collecchio*	*44*	*6*	*4.70 ±0.24*
5	*1909 01 13 00:45*	*Bassa padana*	*799*	*6-7*	*5.53 ±0.09*
5	*1914 10 27 09:22:36*	*Garfagnana*	*618*	*7*	*5.76 ±0.09*
5	*1916 08 16 07:06*	*Alto Adriatico*	*257*		*6.14 ±0.14*
5-6	*1920 09 07 05:55:40*	*Garfagnana*	*756*	*10*	*6.48 ±0.09*
6	*1923 06 28 15:11:30*	*Formigine*	*22*	*6*	*4.88 ±0.24*
5	*1929 04 19 04:15:22*	*Bolognese*	*82*		
5	*1929 04 20 01:09:46*	*Bolognese*	*109*	*7*	*5.34 ±0.13*
5	*1929 04 29 18:35:59*	*Bolognese*	*45*		
5	*1929 05 11 19:22:48*	*Bolognese*	*64*		
5	*1939 10 15 14:05*	*Garfagnana*	*62*	*6-7*	*5.08 ±0.16*
5	*1971 07 15 01:33:23*	*Parmense*	*229*	*8*	*5.64 ±0.09*
5	*1978 12 25 22:53:42*	*Bassa mantovana*	*28*	*5*	*4.22 ±0.22*
6	*1983 11 09 16:29:52*	*Parmense*	*850*	*6-7*	*5.06 ±0.09*
6	*1987 05 02 20:43:53*	*Reggiano*	*802*	*6*	*4.74 ±0.09*
5-6	*1996 10 15 09:56:02*	*Correggio*	*135*	*7*	*5.41 ±0.09*

Table 15 – Seismic history of Modena (ISIDe), Is ≥ 5

4.3.1.4 Emilia 2012’s Main Events

The earthquake of 2012 in Emilia involved a series of shocks in the seismic district of the Emilia-Po plain, mainly in the provinces of *Modena, Ferrara, Mantova, Reggio Emilia, Bologna and Rovigo*, but also felt over an enormous area, comprising the whole central-northern Italy. The strongest shock, of magnitude M_l 5,9 and magnitude moment M_w 5,86, was recorded on May 20 2012 at 04:03:52 Italian time (02:03:52 UTC), with its epicentre near the town of Finale Emilia (Modena) and hypocentre at a depth of 6.3 km.

On May 29 2012 at 09:00:03 Italian time (07:00:03 UTC), a very strong aftershock, of magnitude M_l 5,8 and M_w 5,66, with its epicentre in the area of *Mirandola*, *Medolla* and *San Felice sul Panaro*, was perceived throughout northern Italy. This shock was followed by other substantial aftershocks: one of magnitude 5 at 12:55 and another of magnitude 5,1 at 13:00.

A further shock, of magnitude 5,1, was felt throughout the same area on June 3 2012 at 21:20:43 Italian time (19:20:43 UTC), with its epicentre in *Novi di Modena*. The maximum intensity of these earthquakes, estimated as the accumulation of the effects of the seismic sequence, was 8,0 on the European Macroseismic Scale.

Table 16 lists the shocks recorded on May-June 2012, excluding those of magnitude <4,0, obtained from ISIDe. The corresponding values (when available) of moment magnitude M_w are shown in brackets. Seismic events of greater severity are shown in bold type.

Date	***Local time***	***Local Magnitude M_l****	***Epicentre***
20-mag-12	*1.13.27*	*4,1 [4,0M_w]*	*Bondeno (Fe)*
20-mag-12	***4.03.52***	***5,9 [5,8M_w]***	***Finale Emilia (Mo) - Bondeno (Fe)***
20-mag-12	*4.06.30*	*4,8*	*Finale Emilia (Mo)*
20-mag-12	*4.07.31*	*5,0*	*Bondeno (Fe)*
20-mag-12	*4.11.46*	*4,3*	*Bondeno (Fe)*
20-mag-12	*4.12.42*	*4,3*	*Finale Emilia (Mo)*
20-mag-12	*4.21.53*	*4,1*	*Mirandola (Mo)*
20-mag-12	*4.35.37*	*4,0*	*Ferrara*
20-mag-12	*4.39.10*	*4,0*	*Finale Emilia (Mo)*
20-mag-12	*5.02.50*	*5,0*	*San Felice sul Panaro (Mo)*
20-mag-12	*11.13.21*	*4,2*	*Finale Emilia (Mo)*
20-mag-12	*15.18.02*	*5,1 [4,9M_w]*	*Vigarano Mainarda (Fe) - Mirabello (Fe)*
20-mag-12	*15.21.06*	*4,1*	*Bondeno (Fe)*
20-mag-12	*19.37.14*	*4,5 [4,2M_w]*	*Bondeno (Fe)*
21-mag-12	*18.37.31*	*4,1*	*Finale Emilia (Mo)*
25-mag-12	*15.14.05*	*4,0 [3,7M_w]*	*Mirandola (Mo)*
27-mag-12	*20.18.45*	*4,0 [3,8M_w]*	*Mirandola (Mo)*
29-mag-12	***9.00.03***	***5,8 [5,6M_w]***	***Medolla (Mo) - Cavezzo (Mo)***
29-mag-12	*9.07.21*	*4,0*	*Cavezzo (Mo)*
29-mag-12	*10.25.51*	*5,0*	*Novi di Modena (Mo)*
29-mag-12	*10.27.23*	*4,6*	*San Felice sul Panaro (Mo)*
29-mag-12	*10.40.58*	*4,2 [4,1M_w]*	*Mirandola (Mo)*
29-mag-12	*11.30.21*	*4,2 [3,7M_w]*	*Concordia sulla Secchia (Mo)*
29-mag-12	***12.55.57***	***5,3Mw***	***San Possidonio (Mo)***
29-mag-12	*13.00.02*	*5,0*	*Cavezzo (Mo)*
29-mag-12	*13.00.25*	*5,1*	*Novi di Modena (Mo) - Moglia (Mn)*
29-mag-12	*13.07.05*	*4,0*	*San Possidonio (Mo)*
31-mag-12	*21.04.04*	*4,2 [3,8M_w]*	*San Possidonio (Mo)*
03-giu-12	***21.20.43***	***5,1 [4,7M_w]***	***Novi di Modena (Mo)***

** - Moment Magnitude M_w is expressed between brackets when present*

Table 16 – Significant Seismic Events of May-June 2012 (FIP INDUSTRIALE)

The city of Modena has two seismic stations: MODE and MDN, more or less equidistant from the *Palazzo dei Musei*. The MODE station, in use since 2007, is situated east of *Palazzo dei Musei*, and is located in the Department of Engineering, University of Modena. The MDN station, in use since 2008, is placed south-west of *Palazzo dei Musei*, and is located in the Leonardo da Vinci school complex (Figure 81).

Figure 81 – Seismic stations near Palazzo dei Musei

Table 17 lists some characteristics of the stations, taken from the accelerometric ITACA 2.0 catalogue (ITalian ACcelerometric Archive).

Both stations lie on subsoil category C. The classification of the MDN station is based on on-field sonic tests (ESAC: Extended Spatial Auto-Correlation Method; FK), and the MODE station is identified according to the geological map. This information matches the results of tests carried out on the *Palazzo dei Musei* site, i.e., classified as subsoil type C.

Details of the characteristics of the four earthquakes of greatest magnitude, recorded during the seismic sequence by ITACA 2.0, are given in Sect. 4.3.1.4.1, 4.3.1.4.2, 4.3.1.4.3, 4.3.1.4.4. In particular, acceleration values recorded in the two Modena stations are listed.

Station	*Code*	*Latitude*	*Longitude*	*Installation date*	*Removal date*	*Network*	*Soil category*
MODENA	*MDN*	*44,647°*	*10,890°*	*23/09/2008*	*/*	*IT-Rete Accelerometrica Nazionale [DPC]*	*C*
MODENA	*MODE*	*44,430°*	*10,949°*	*06/12/2007*	*/*	*IV - Rete Sismometrica Nazionale [INGV]*	*C**

Table 17 – Characteristics of seismometric stations in the city of Modena

4.3.1.4.1 Emilia 1st Mainshock / 2012-05-20 / 02:03:52 (UTC)

The event presents the characteristics summarized in Table 18:

Event Id	*IT-2012-0008*	
Epicentre	***Mirandola (MO)***	
Coordinates	*44,89°* *11,23°*	*Lat* *Long*
Depth	*6,3*	*km*
MI	***5,9***	*(ISIDe)*
Mw	***6,1***	*(RCMT*- INGV)*

(- RCMT: European Mediterrean Regional Centroid Moment Tensors Catalog)*

Table 18 – Main characteristics of the “Emilia 1st Mainshock”

Figure 82 shows the INGV ShakeMap and the INGV Peak Acceleration Map related to this shock (2:03 UTC). In particular, the INGV Peak Acceleration Map allows the immediate assessment of the maximum ground acceleration perceived in the city of Modena.

The PGA values recorded in the two seismometric stations of Modena are reported in Table 19.

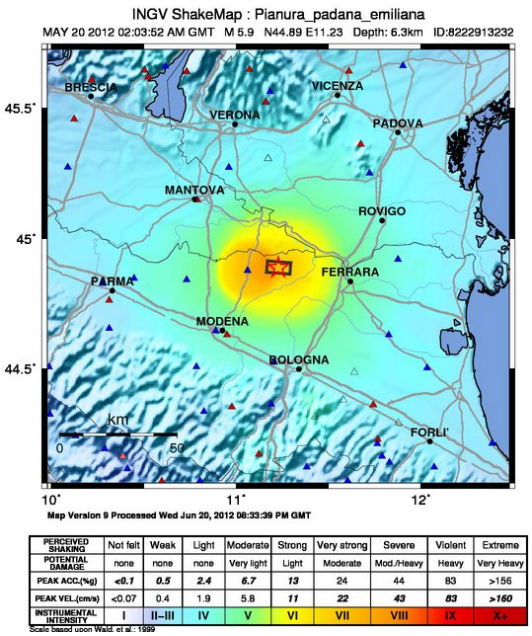

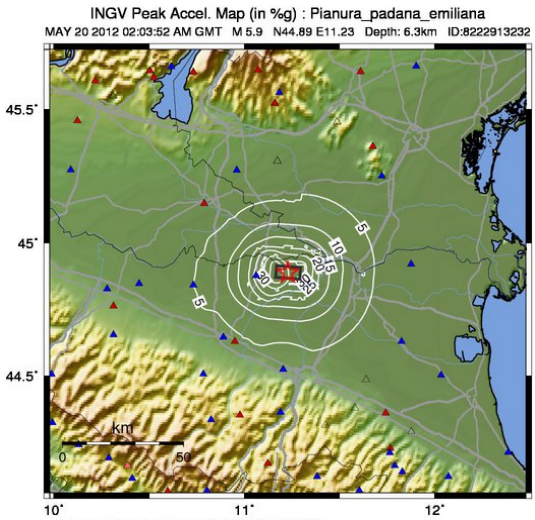

Figure 82 – INGV Shakemap “2012-05-20 02:03:52 – EMILIA 1st MAINSHOCK”

Station	*Code*	*R epicentre[km]*	*Soil category*	*Local Magnitude*	*Moment Magnitude*	*PGA horizontal E-W [cm/s²]*	*PGA horizontal N-S [cm/s²]*	*PGA vertical [cm/s²]*
MODENA	*MDN*	*37,90*	*C*	*5,9*	*6,1*	*36,246*	*32,739*	*28,673*
MODENA	*MODE*	*36,30*	*C**	*5,9*	*6,1*	*26,943*	*41,851*	*32,664*

Table 19 – Recorded data in Modena "2012-05-20 02:03:52 – Emilia 1st Mainshock"

4.3.1.4.2 Emilia 2nd Mainshock / 2012-05-29 / 07:00:03 (UTC)

The event presents the characteristics summarized in Table 20:

Event Id	*IT-2012-0011*	
Epicentre	***Medolla (MO)***	
Coordinates	*44,85°* *11,09°*	*Lat* *Long*
Depth	*10,2*	*km*
MI	***5,8***	*(ISIDe)*
Mw	***6,0***	*(RCMT*- INGV)*

(* - RCMT: European Mediterrean Regional Centroid Moment Tensors Catalog)

Table 20 – Main characteristics of the "Emilia 2nd Mainshock"

Figure 83 shows the INGV ShakeMap and the INGV Peak Acceleration Map related to the event. It can be observed a higher number of monitoring stations compared to that of May 20th, because after the seismic event many temporary seismic stations have been installed throughout the territory. Table 21 resumes the main data relating to the city of Modena.

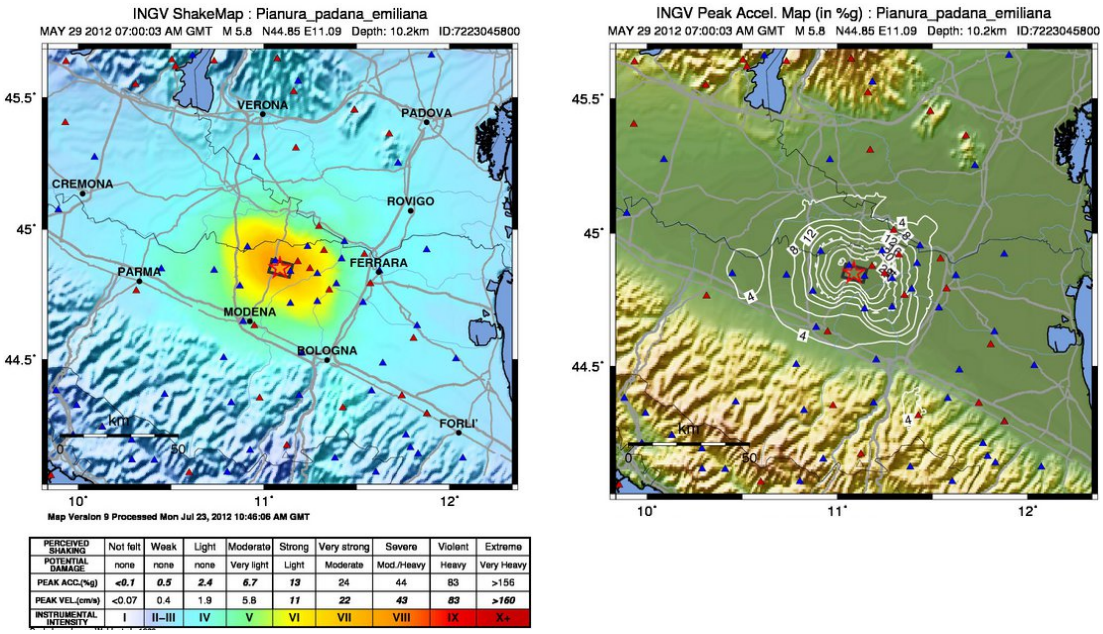

Figure 83 – INGV Shakemap “2012-05-29 07:00:03 – Emilia 2nd Mainshock”

Station	*Code*	*R epicentre[km]*	*Soil category*	*Local Magnitude*	*Moment Magnitude*	*PGA horizontal E-W [cm/s²]*	*PGA horizontal N-S [cm/s²]*	*PGA vertical [cm/s²]*
MODENA	*MDN*	*27,50*	*C*	*5,8*	*6*	*29,601*	*50,520*	*35,142*
MODENA	*MODE*	*26,87*	*C**	*5,8*	*6*	*44,092*	*21,448*	*42,340*

Table 21 – Recorded data in Modena “2012-05-29 07:00:03 – Emilia 2nd Mainshock”

4.3.1.4.3 Emilia 1st Aftershock / 2012-05-29 / 10:55:57 (UTC)

The event presents the characteristics summarized in Table 22:

Event Id	*IT-2012-0010*	
Epicentre	***Mirandola (MO)***	
Coordinates	*44,89°* *11,01°*	*Lat* *Long*
Depth	*6,08*	*km*
MI	***5,3***	*(ISIDe)*
Mw	***5,5***	*(RCMT*- INGV)*

(- RCMT: European Mediterrean Regional Centroid Moment Tensors Catalog)*

Table 22 – Main characteristics of the “Emilia 1st Aftershock”

In Figure 84 and Table 23 INGV ShakeMap and the INGV Peak Acceleration Map related to the event and the main data relating to the city of Modena are reported.

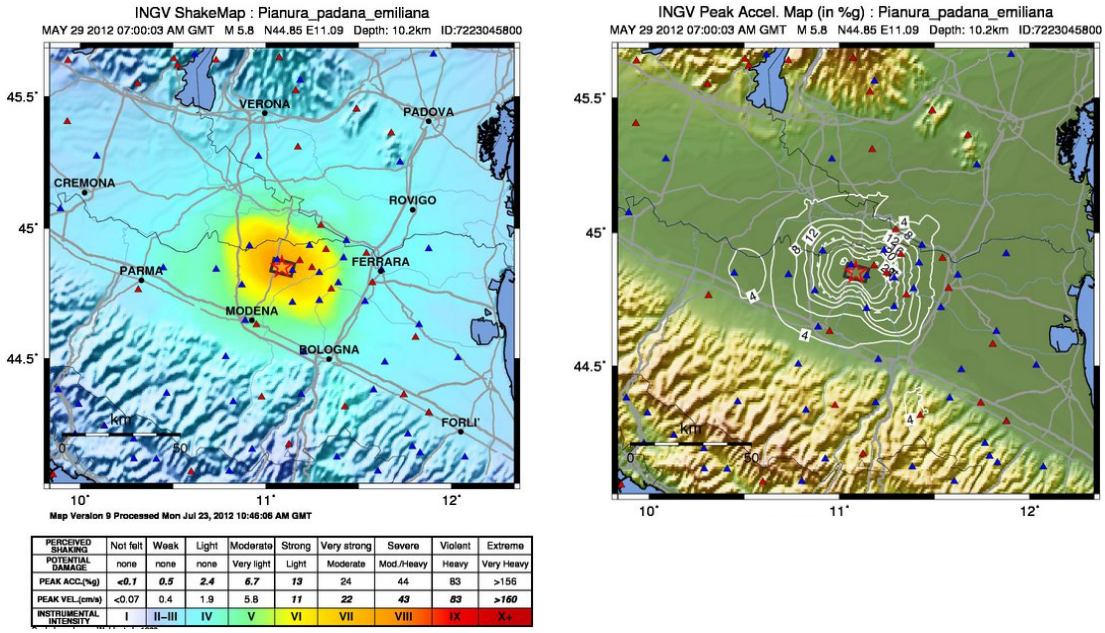

PERCEIVED SHAKING	Not felt	Weak	Light	Moderate	Strong	Very strong	Severe	Violent	Extreme
POTENTIAL DAMAGE	none	none	none	Very light	Light	Moderate	Mod./Heavy	Heavy	Very Heavy
PEAK ACC.(%g)	*<0.1*	*0.5*	*2.4*	*6.7*	*13*	24	44	83	>156
PEAK VEL.(cm/s)	<0.07	0.4	1.9	5.8	*11*	*22*	*43*	*83*	*>160*
INSTRUMENTAL INTENSITY	I	II–III	IV	V	VI	VII	VIII	IX	X+

Figure 84 – INGV Shakemap “2012-05-29 10:55:57 – Emilia 1st Aftershock”

Station	*Code*	*R epicentre[km]*	*Soil category*	*Local Magnitude*	*Moment Magnitude*	*PGA horizontal E-W [cm/s²]*	*PGA horizontal N-S [cm/s²]*	*PGA vertical [cm/s²]*
MODENA	*MDN*	*27,50*	*C*	*5,3*	*5,5*	*18,371*	*30,603*	*24,100*
MODENA	*MODE*	*26,87*	*C**	*5,3*	*5,5*	*19,837*	*16,335*	*23,797*

Table 23 – Recorded data in Modena "2012-05-29 10:55:57 – Emilia 1st Aftershock"

4.3.1.4.4 Emilia 2nd Aftershock / 2012-06-03 / 19:20:43 (UTC)

The event presents the characteristics summarized in Table 24:

Event Id	*IT-2012-0012*	
Epicentre	***Novi di Modena (MO)***	
Coordinates	*44,90°* *10,94°*	*Lat* *Long*
Depth	*9,2*	*km*
MI	***5,1***	*(ISIDe)*
Mw	***4,9***	*(RCMT*- INGV)*

(- RCMT: European Mediterrean Regional Centroid Moment Tensors Catalog)*

Table 24 – Main characteristics of the "Emilia 2nd Aftershock"

In Figure 85 and Table 25 INGV Shakemap and the INGV Peak Acceleration Map related to the event and the main data relating to the city of Modena are reported.

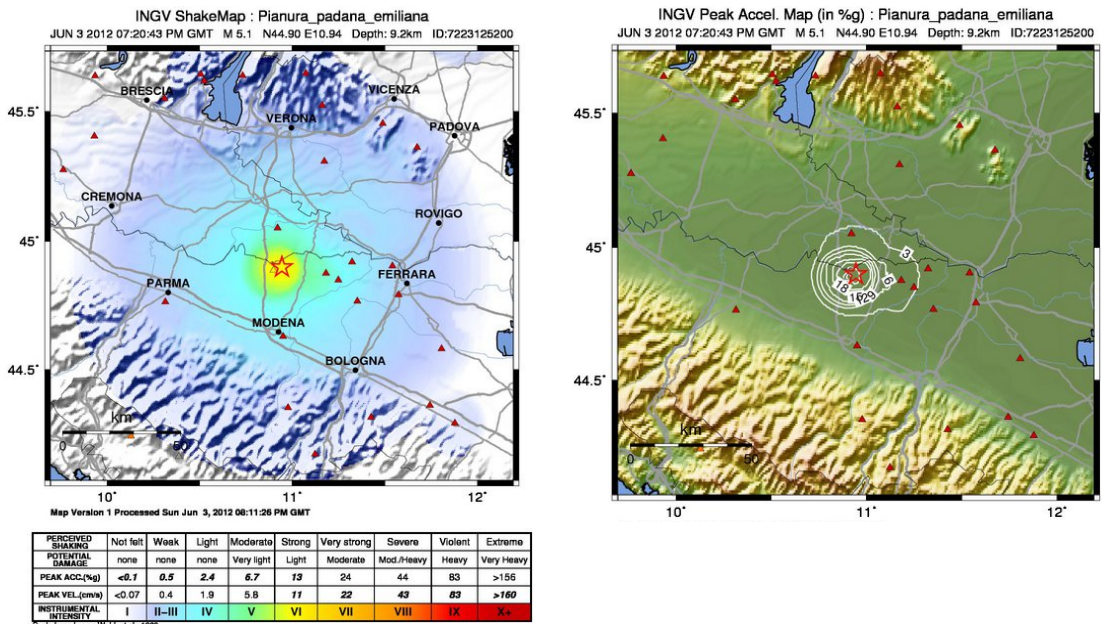

Figure 85 – INGV Shakemap “2012-06-03 19:20:43 – Emilia 2nd Aftershock”

Station	*Code*	*R epicentre[km]*	*Soil category*	*Local Magnitude*	*Moment Magnitude*	*PGA horizontal E-W [cm/s²]*	*PGA horizontal N-S [cm/s²]*	*PGA vertical [cm/s²]*
MODENA	*MDN*	*28,30*	*C*	*5,1*	*4,9*	*8,915*	*12,292*	*10,204*
MODENA	*MODE*	*29,93*	*C**	*5,1*	*4,9*	*12,998*	*7,304*	*10,213*

Table 25 – Recorded data in Modena “2012-06-03 19:20:43 (UTC) – Emilia 2nd Aftershock”

4.3.1.5 Comments

The examination of the seismic history for the city of Modena indicates that destructive earthquakes are not uncommon phenomena in this area. In the last five centuries, starting from 1474, (see Table 15) at least 30 events with intensity above magnitude of 4 are recorded. In particular, it clearly results from this analysis that at least 15 of these events exceeded the magnitude of 6.

The analysis of the recent seismic events, i.e. the four most destructive earthquakes of 2012, substantially confirms the same characteristics highlighted by the study of the historical series. The four events are characterized by an intensity between 5.1 and 5.9 of magnitude, with the Mainshocks of greater intensity compared to that of the Aftershocks, and with similar intensities to those shown by the historical seismicity. With regard to the recorded accelerations, it has been observed a PGA between 0,042g and 0,012g, less than 0.191g determined by the Technical standards for the site of Modena with return period 712 years, and adopted for the structural analysis.

Even though the low acceleration level occurred during the four main seismic events of 2012, the damage level to the city of Modena is not negligible: this may highlight the important contribution of the amplification of the seismic acceleration due to the height of the building (see Sect. 2.2.5), and of the vertical acceleration.

4.3.2 Evaluation of seismic action at the second floor

In order to evaluate the seismic action at the base of the bust both in terms of acceleration and displacement. The first one is crucial for the assessment of the seismic vulnerability of the statue as well as the design of the isolation devices (with reference to the transmitted force). The second one is crucial for the design of the isolated system (with reference to the admissible stroke). In this paragraph the evaluation of seismic action at the second floor, where the bust is located, is given according to Sect. 2.1.3. In detail both the simplified approaches and the numerical one have been used.

4.3.2.1 Simplified approach

As stated in par. 4.3.3.1, the simplified approach proposed by technical Standards EC8 and NTC 2008 (Italian Building Code) has been adopted to obtain the values of the acceleration and displacement amplification for the object due to the height and the principal vibration mode of the building.

A simplified estimation of the first period of the structure, necessary to evaluate the

spectral displacement $S_d(T_k)$, is given by NTC 2008:

$$T_1 = 0{,}05 \cdot (H)^{\frac{3}{4}} = 0{,}56\ s \qquad (38)$$

4.3.2.1.1 Acceleration floor response spectra: Eurocode 8 / NTC 2008

Maximum acceleration S_a, to which the element is exposed, evaluated according to Eq. (4). In particular, for the case study the "Acceleration Amplification coefficient", Eq. (5), has been evaluated with $z/H = 0{,}58$ (i.e. $H = 25{,}20m$ and $z = 14{,}60m$), and shown in Figure 86 as a function of T_a/T_1.

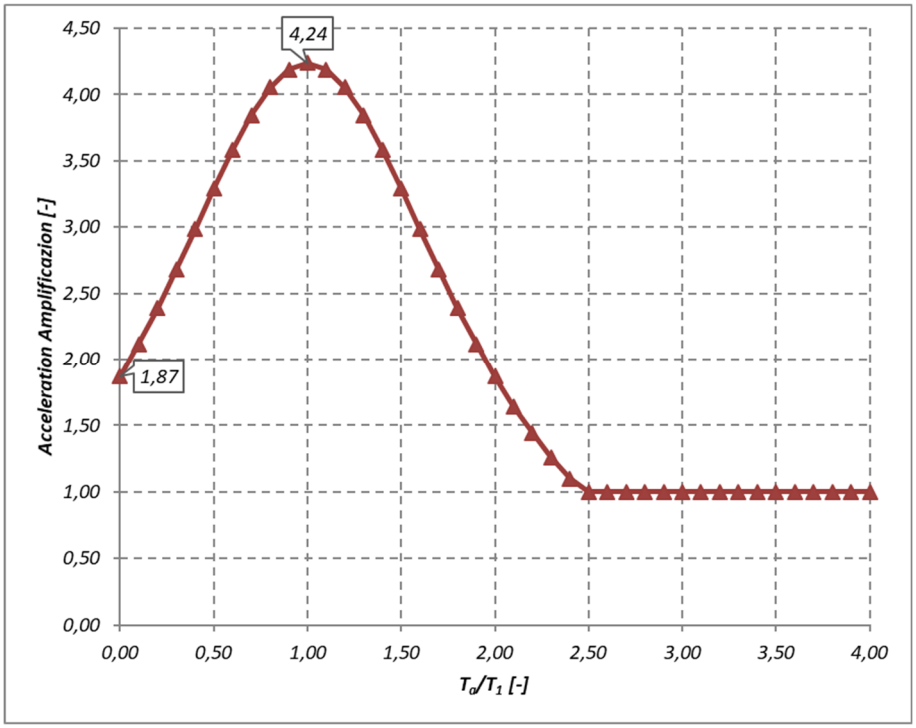

Figure 86 – Amplification coefficient for the acceleration

Assuming the bust and the bust/pedestal as rigid bodies, with $T_a/T_1 = 0$, the coefficient of amplification is equal to $Amp = 1{,}87$. This hypothesis is also confirmed by the results of the modal analysis, performed on the Finite Element models of the bust and bust/pedestal system, which gives a period for the first mode just above 0 s. Concerning the isolation system, assuming as first estimation of the device $T_{is} > T_D = 2{,}36\ s$ with $T_1 = 0{,}56s$, the value of T_a/T_1 is higher than 4, actually not giving any kind of amplification. For this reason, the acceleration spectra at the ground floor can be chosen for the isolation system design.

4.3.2.1.2 Displacement floor response spectra: CNR Guidelines, Lagomarsino (2015)

Concerning the displacement induced by seismic action, the value of the displacement response spectrum $S_d(T)$ is evaluated according to Eq. (6) and (7).

Since the bust is placed at the second floor at $z = 14.60m$, and the height of the building is $H = 25{,}20m$, the mode-shape evaluated according to Eq. (11) becomes: $\psi(z) = 0{,}5793$.

To keep the calculation on the safe side, it is adopted for both the building and the object the conventional 5% damping, accepting an overestimation of the displacement, so $\eta(\xi) = \eta(\xi_b) = 1$, corresponding to $S_d = 0{,}042m$.

Given that one of the goals of this research is the evaluation of the displacement for the design of the seismic isolation system, only the last of the three formulas reported in (7) is considered since $T/T_k > 1{,}9$, which corresponds to the constant branch of the curves represented in Figure 11. With the adopted hypotheses about the damping values such a formula becomes:

$$S_{dZ,k}(T, z) = 3{,}8 \cdot S_d(T_k) \cdot \gamma_k \cdot |\psi_k(z)| \quad [m] \qquad (39)$$

in this case equal to $S_{dT\_k}(T, z) = 0.119m$, independently from the ratio T/T_k. Assuming as first estimation that the period of a seismic isolation device is characterized by $T_{is} > T_D = 2{,}36s$, the corresponding spectral value at ground floor is $S_d = 0{,}177m$, so according to (7) the value of $S_d = 0{,}177m$ evaluated at the ground floor is chosen for designing the isolation device.

4.3.2.2 Numerical approach

In this paragraph the numerical analyses have been performed on the partial model of *Palazzo dei Musei* in order to obtain both the floor seismic signals and the floor response spectra to be used for dynamic and simplified analyses.

In detail, the seismic signals obtained by REXEL (Sect. 4.3.1.2, 4.3.1.2.2) have been applied to the base of the F.E. model of the building, and elastic Time History Analyses have been carried out considering two reference conditions described in Sect. 4.2.2.

Then acceleration time histories are registered at a node of the second floor and used for the input to the friction pendulum isolators.

4.3.2.2.1 Floor seismic signals

Floor seismic signals are obtained considering the 2 different sets of seven couple of spectrum-compatible accelerograms (i.e. *RANGE1*, *RANGE2*). The accelerograms, extracted by means of REXEL software (Sect. 4.3.1.2), are applied in both the direction XY and direction YX. The seismic response of the building in terms of acceleration and displacement time history is registered at the second floor at a node next to the location where the bust is located.

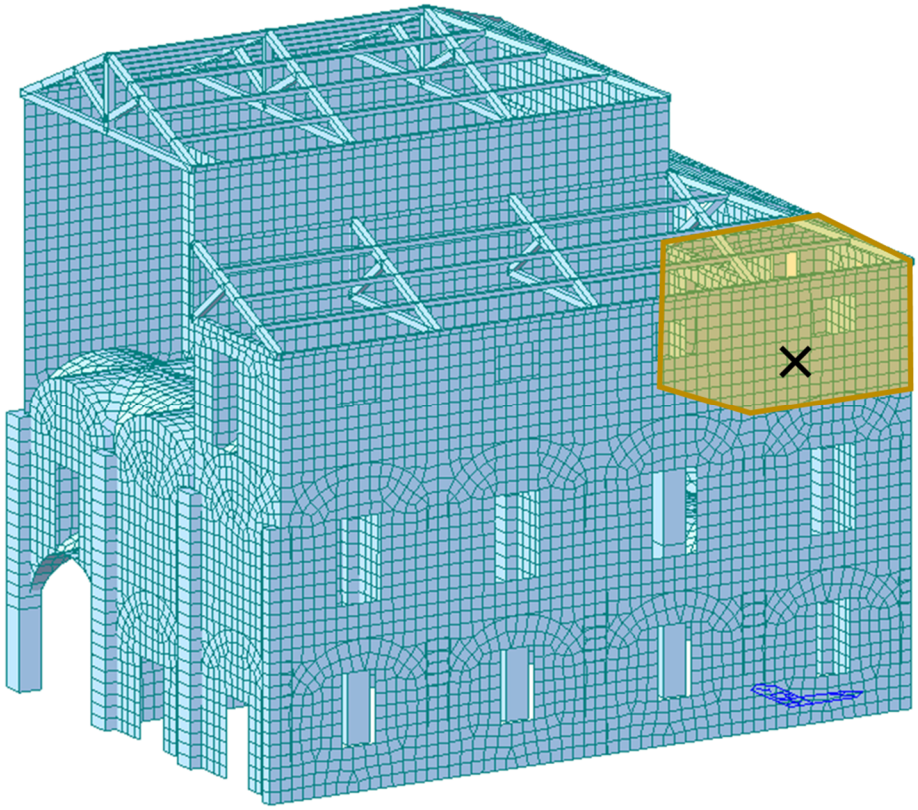

Figure 87 – F.E. Model with indication of the zonewhere the Bust is placed and the control point

With the hypothesis of applying the most demanding couple of accelerograms 6958 – *RANGE1*, first in the XY direction and then in the YX direction, in the following (Figure 88 and Figure 89) the floor accelerograms obtained in the two cases are illustrated, with reference to the F.E. model presented in Figure 67, in both conditions “*DEF*” and “*STIFF*” (introduced in paragraph 4.2.2).

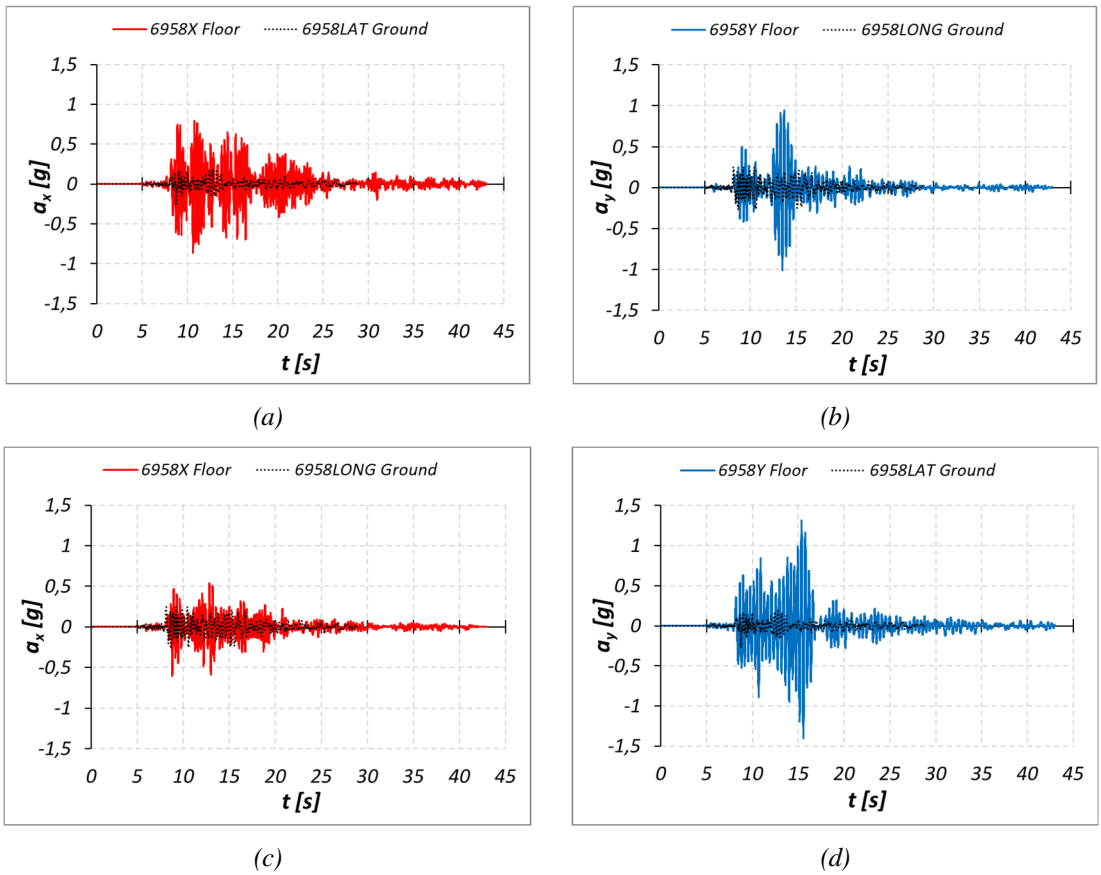

Figure 88 – Floor accelerograms DEF case: (a) x direction (obtained adopting 6958 in XY) (b) y direction (obtained adopting 6958in XY); (c) x direction (obtained adopting 6958 in YX); (d) direction y (obtained adopting 6958 in YX

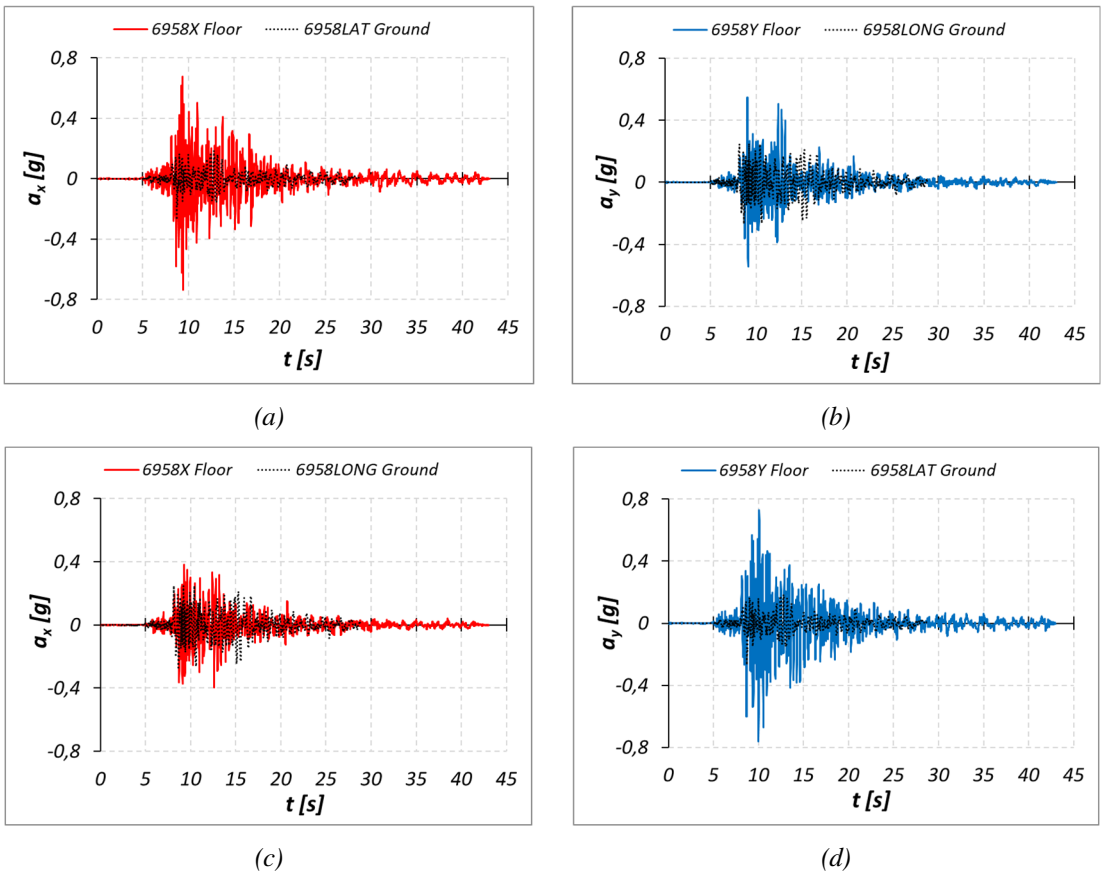

Figure 89 – Floor accelerograms STIFF case: (a) x direction (obtained adopting 6958 in XY) (b) y direction (obtained adopting 6958 in XY); (c) x direction (obtained adopting 6958 in YX); (d) direction y (obtained adopting 6958 in YX)

Similarly, with the hypothesis of applying the most demanding couple of accelerograms 0335 – *RANGE2*, first in the XY direction and then in the YX direction, in the following (Figure 90 and Figure 91) the floor accelerograms obtained in the two cases are illustrated.

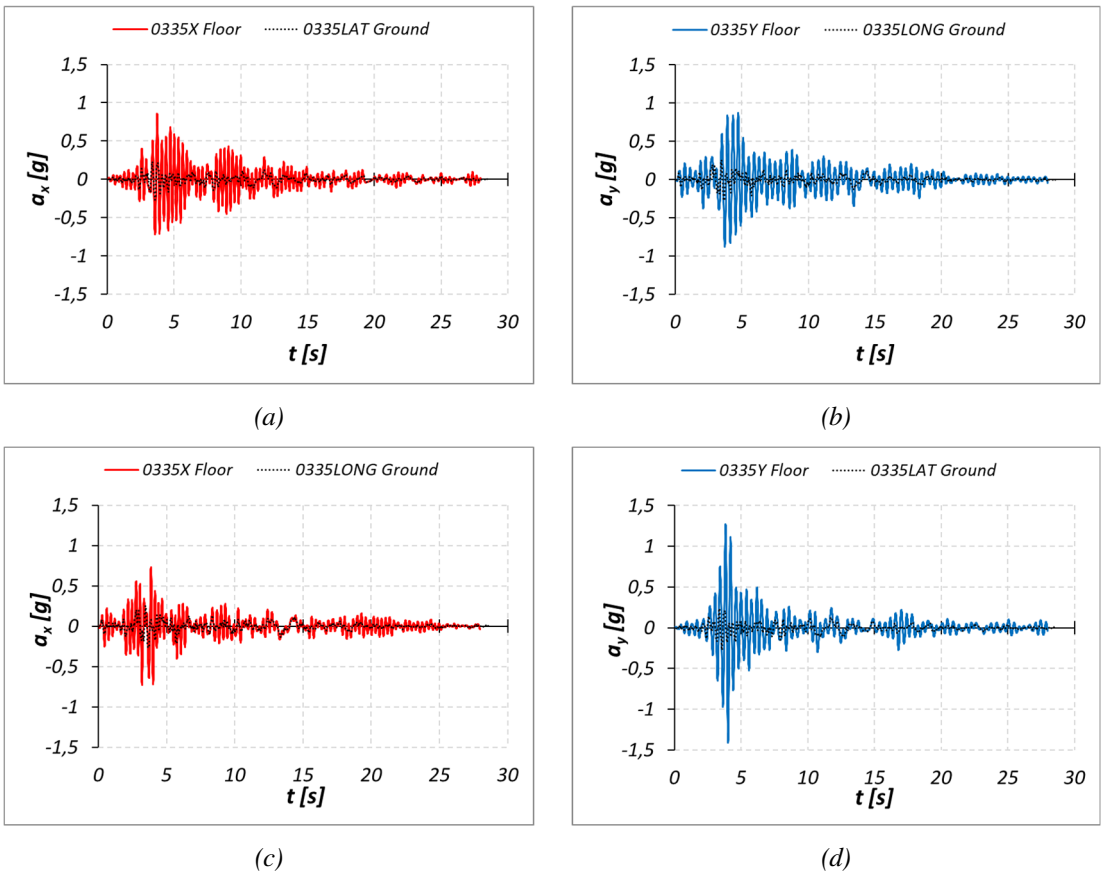

Figure 90 –Floor accelerograms DEF case: (a) x direction (obtained adopting 0335 in XY) (b) y direction (obtained adopting 0335 in XY); (c) x direction (obtained adopting 0335 in YX); (d) direction y (obtained adopting 0335 in YX)

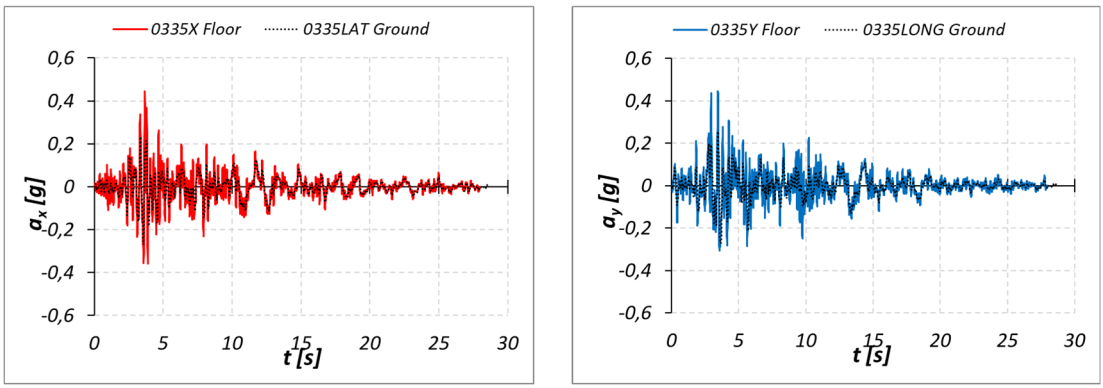

(a)

(b)

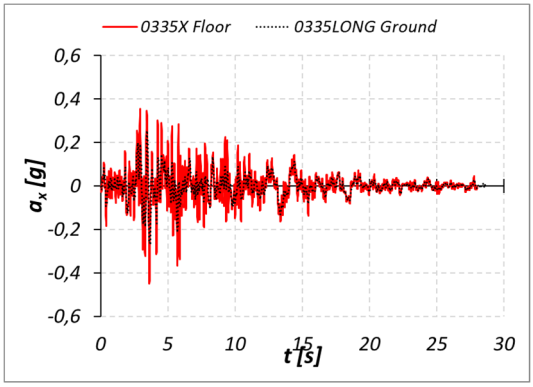

(c)

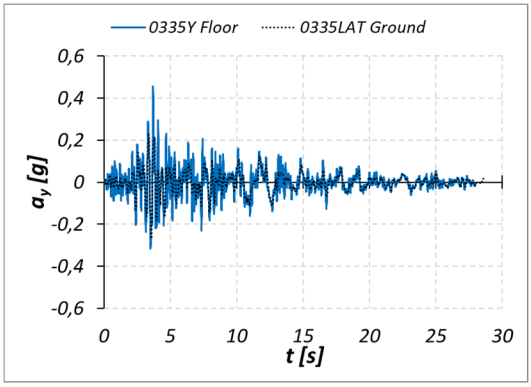

(d)

Figure 91 – Floor accelerograms STIFF case: (a) x direction (obtained adopting 0335 in XY) (b) y direction (obtained adopting 0335 in XY); c) x direction (obtained adopting 0335in YX); (d) direction y (obtained adopting 0335 in YX)

4.3.2.2.2 Floor response spectra

Floor response spectra are obtained from the acceleration time histories registered at the second floor. The signals given by the analyses are processed by Seismosignal software. In this section the results in terms of acceleration and displacement spectra are presented. The results derive from elastic time history analysis of the building in the two reference conditions given in 4.2.2. As example Figure 92 shows for the couple of accelerograms 6958 (the most demanding signal of *RANGE1*), acceleration spectra (Spectral Acceleration S_a) and displacement spectra (Spectral Displacement S_d) for different values of the damping coefficient ξ.

For the two conditions (*DEF* and *STIFF*) and with reference to the accelerograms obtained by applying at the base of the model the couple in the XY direction, the corresponding floor acceleration and floor displacement spectra are shown in Figure 93 and Figure 94, in the X and Y direction, respectively.

Finally, Figure 95 and Figure 96 show average spectra for both floor acceleration and displacement for the first set of accelerograms corresponding to *RANGE1*. In particular Figure 95 shows the spectra for case *DEF* for each direction, obtained by applying the 7 pairs of accelerograms first in XY and then in YX direction. Figure 96 shows the corresponding spectra obtained by considering the case *STIFF*. In both cases, it can be observed as the peak acceleration is positioned in correspondence of the main period of the structure in the examined direction, compare Table 10 and Table 11.

For the sake of comparison, in Figure 97 ground level average spectra for both acceleration and displacement are given, considering the 7 signals corresponding to the 7 couples of accelerograms adopted for the calculation. The comparison between *DEF* and *STIFF* case allows to observe as the increasing stiffness of the building leads to a lower signal amplification because of the "filter effect" of the building.

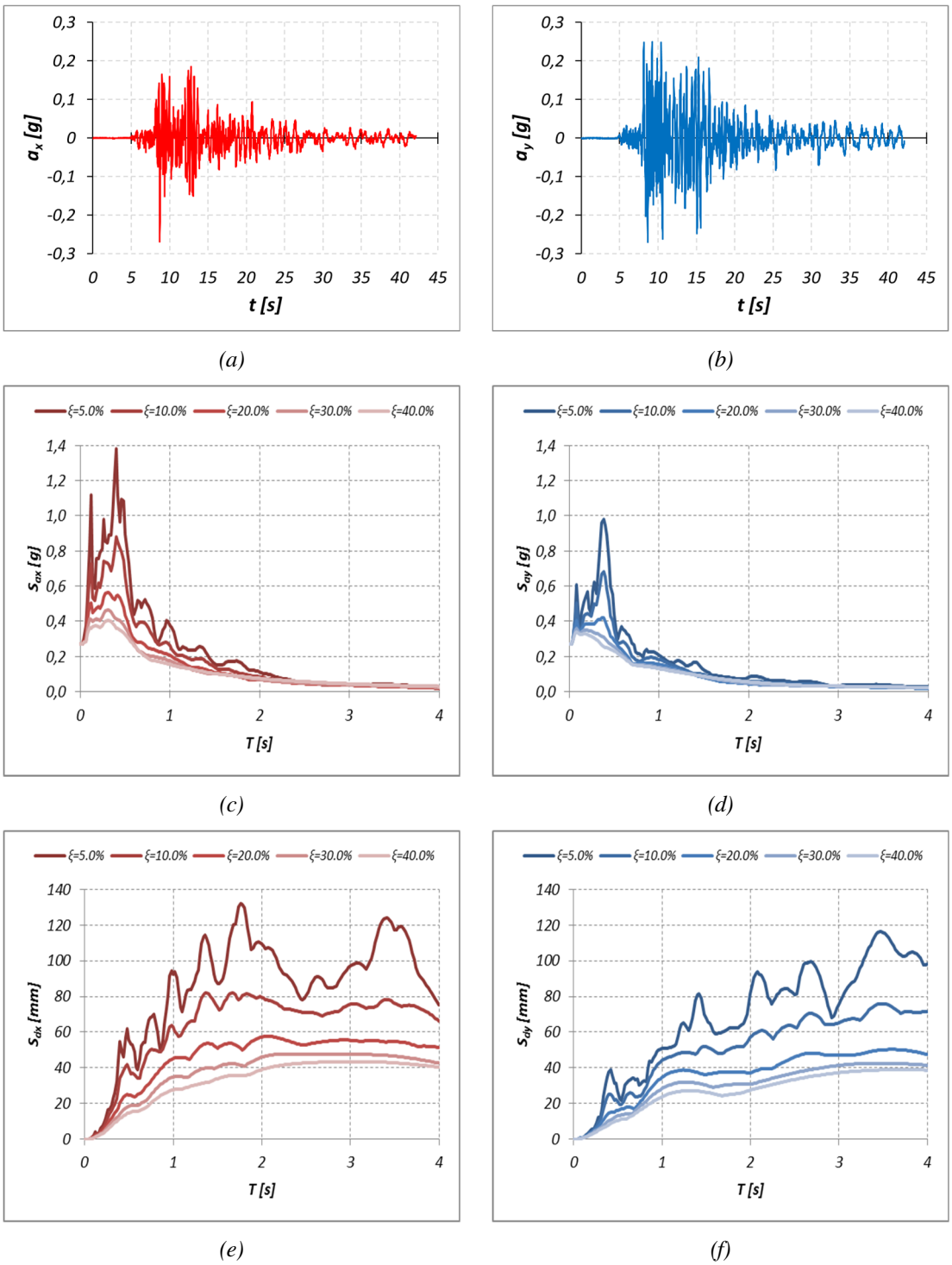

Figure 92 – (a) Accelerogram 6958X x direction at ground floor; (b) Accelerogram 6958Y y direction at ground floor; (c) Acceleration spectrum at ground x direction; (d) Acceleration spectrum at ground floor y direction; (e) Displacement spectrum at ground floor x direction; (f) Displacement spectrum at ground floor y direction

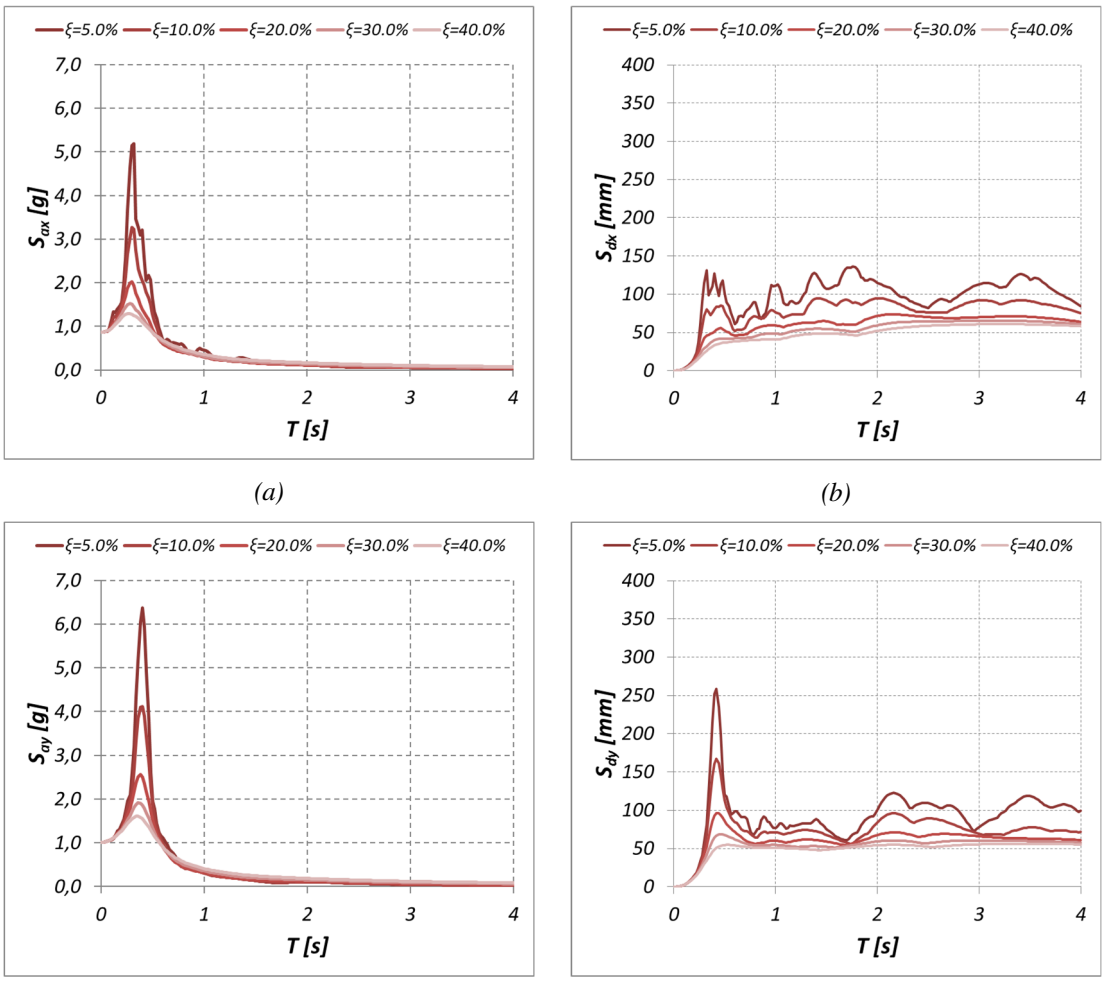

Figure 93 – Floor spectra DEF case (obtained adopting a couple of accelerograms 6958 in XY direction at ground floor): (a) in acceleration x direction; (b) in displacement x direction; (c) in acceleration y direction; (d) in displacement y direction

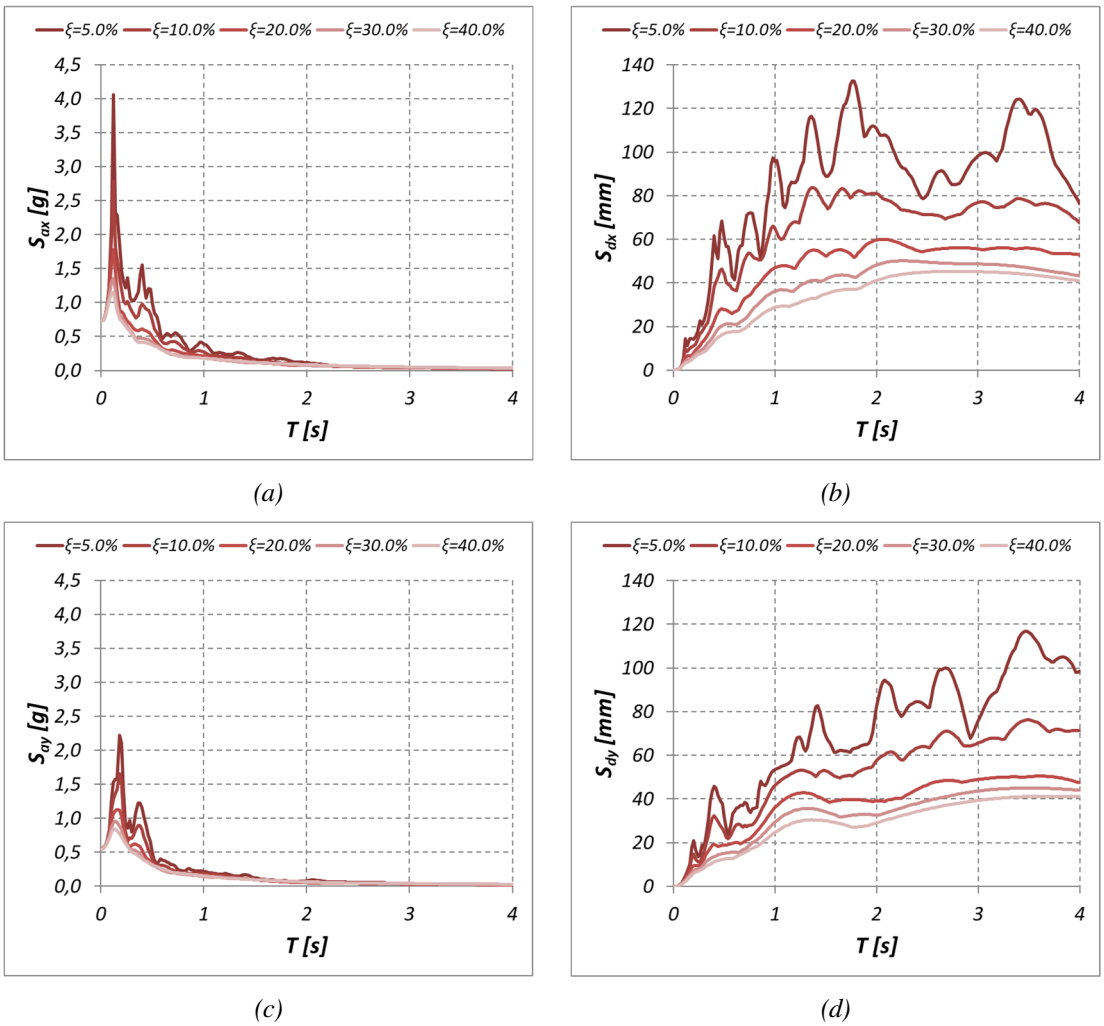

Figure 94 – Floor spectra STIFF case (obtained adopting a couple of accelerograms 6958 in XY direction at ground floor): (a) in acceleration x direction; (b) in displacement x direction; (c) in acceleration y direction; (d) in displacement y direction

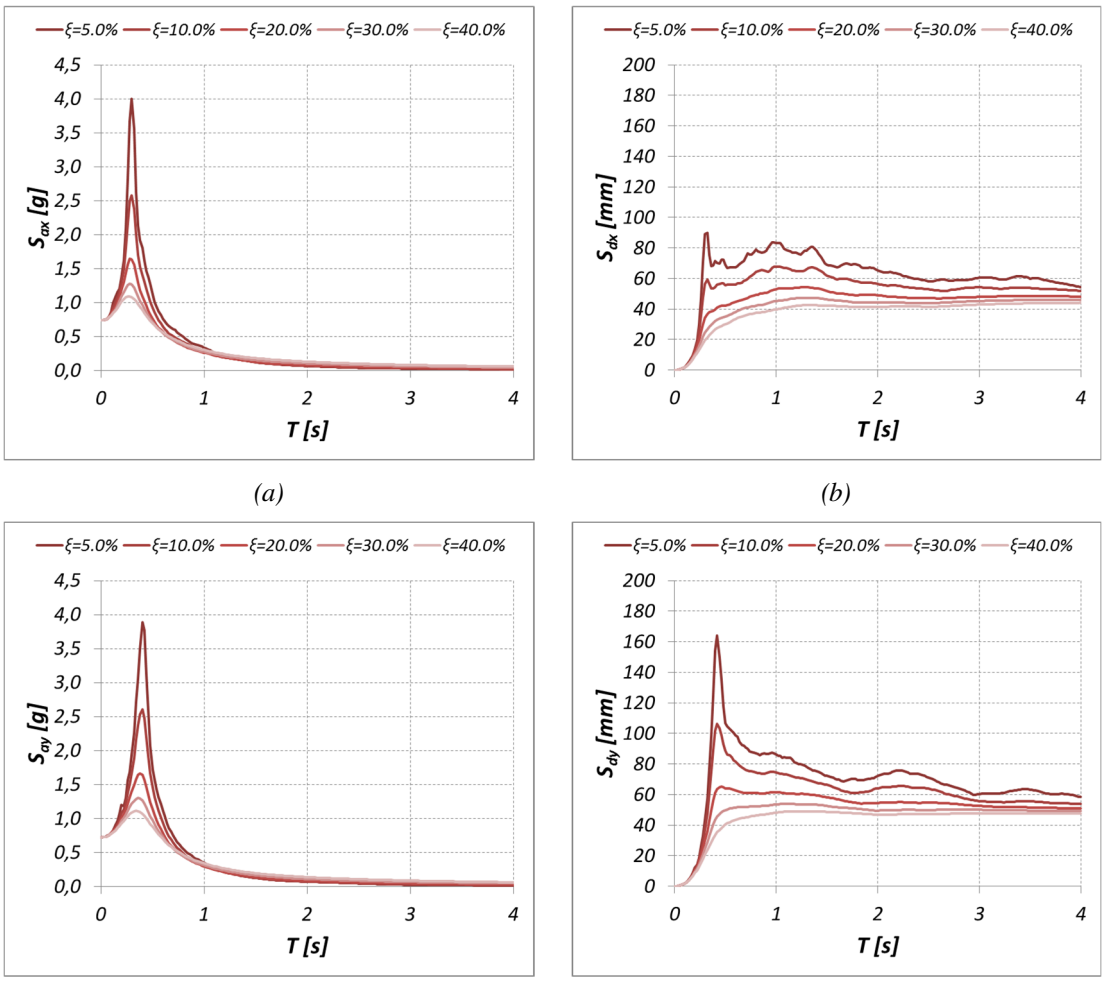

Figure 95 – Average floor spectra DEF case – RANGE1 signals in XY: (a) in acceleration x direction; (b) in displacement x direction: (c) in acceleration y direction; (d) in displacement y direction

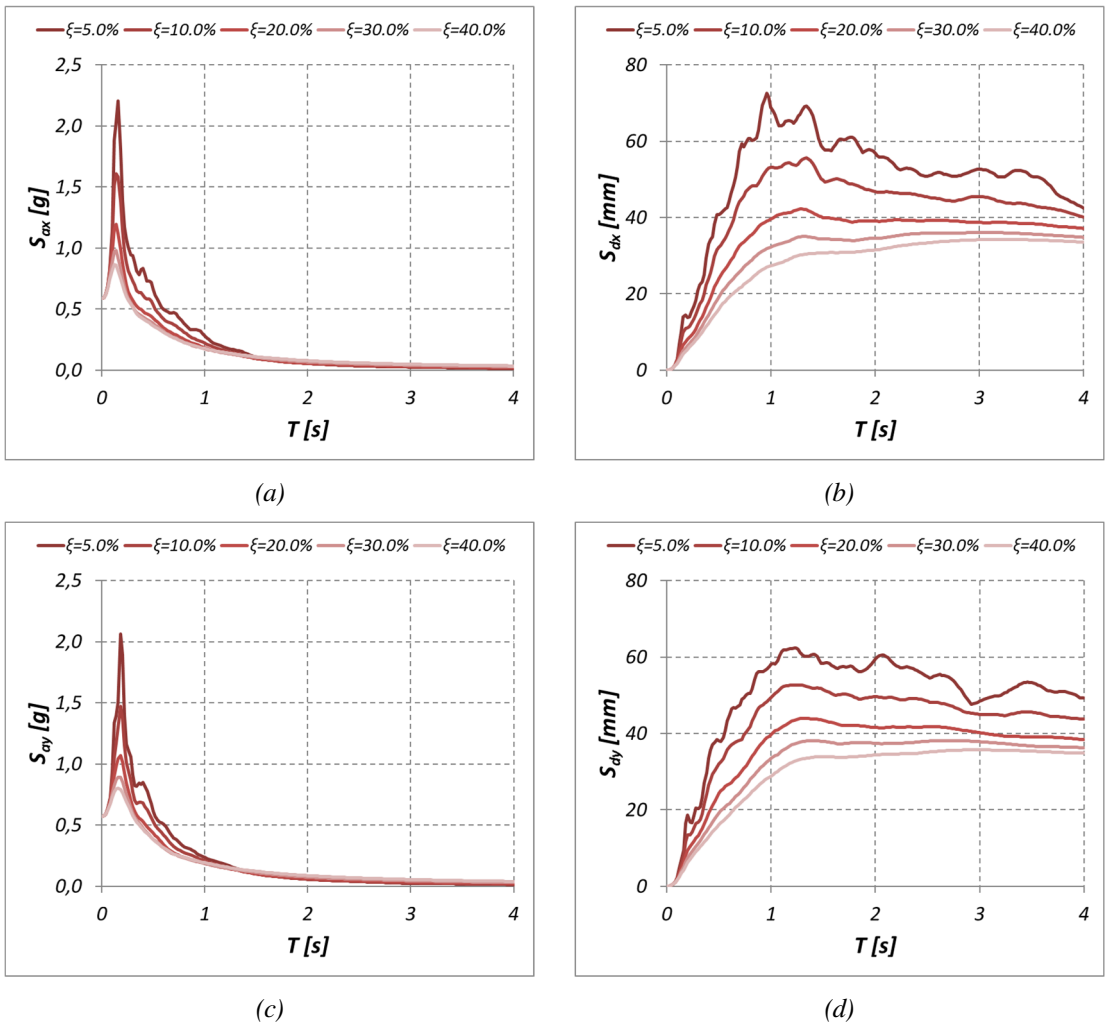

Figure 96 – Average floor spectra STIFF case – RANGE1 signals in XY: (a) in acceleration x direction; (b) in displacement x direction: (c) in acceleration y direction; (d) in displacement y direction

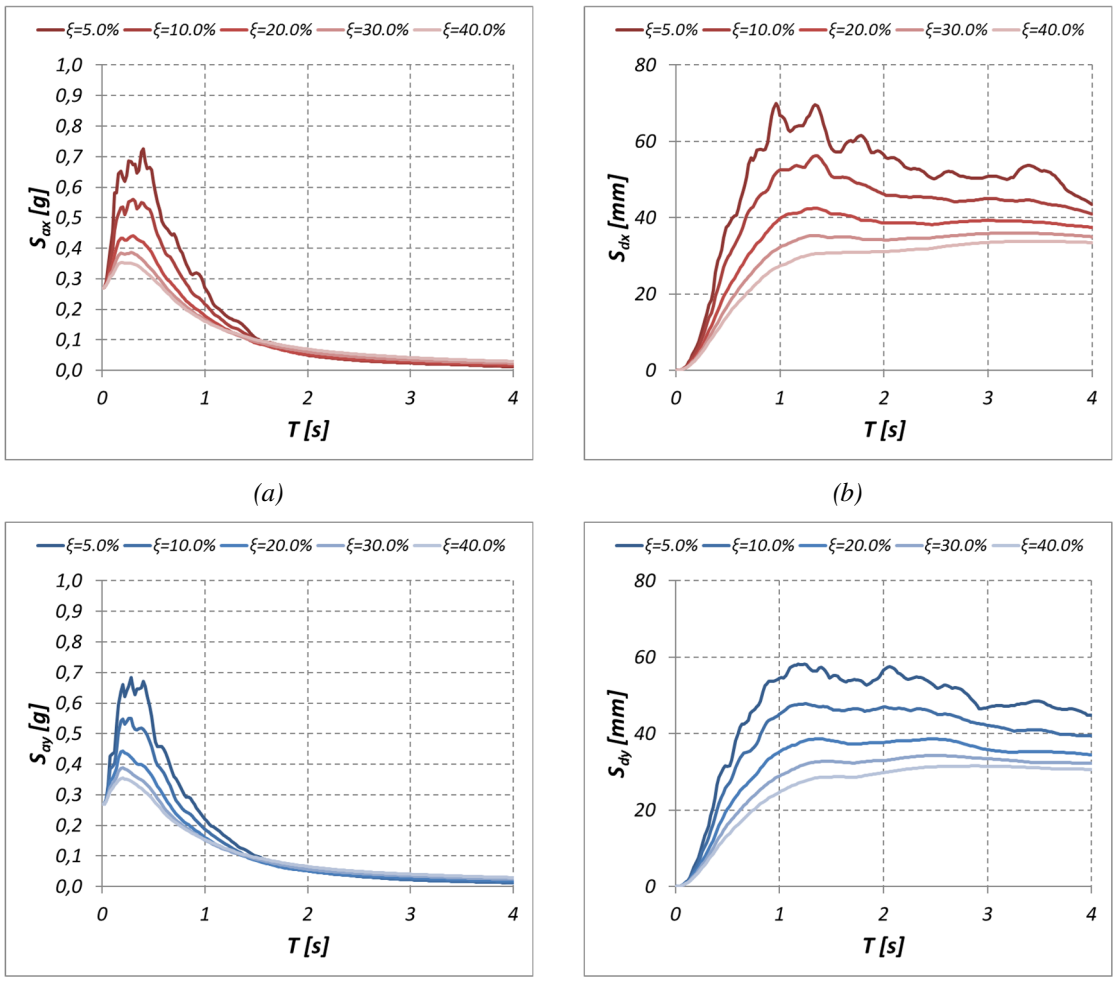

Figure 97 – Average ground spectra – RANGE1: (a) in acceleration x direction; (b) in displacement x direction: (c) in acceleration y direction; (d) in displacement y direction

Figure 98 – Figure 103 present the analogous results obtained considering the accelerograms of *RANGE2*.

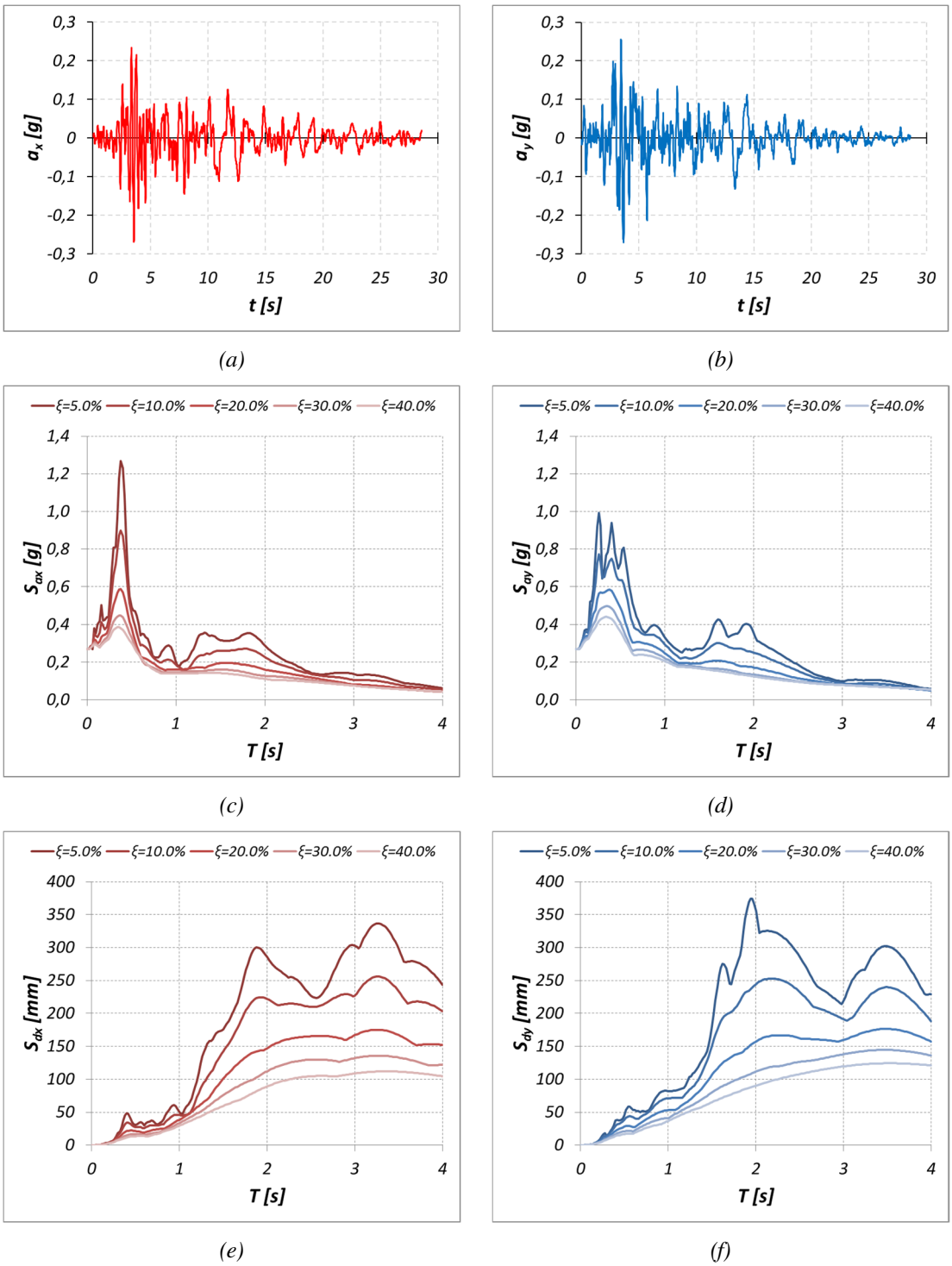

Figure 98 – (a) Accelerogram 0335X x direction at ground floor; (b) Accelerogram 0335Y y direction at ground floor; (c) Acceleration spectrum at ground x direction; (d) Acceleration spectrum at ground floor y direction; (e) Displacement spectrum at ground floor x direction; (f) Displacement spectrum at ground floor y direction

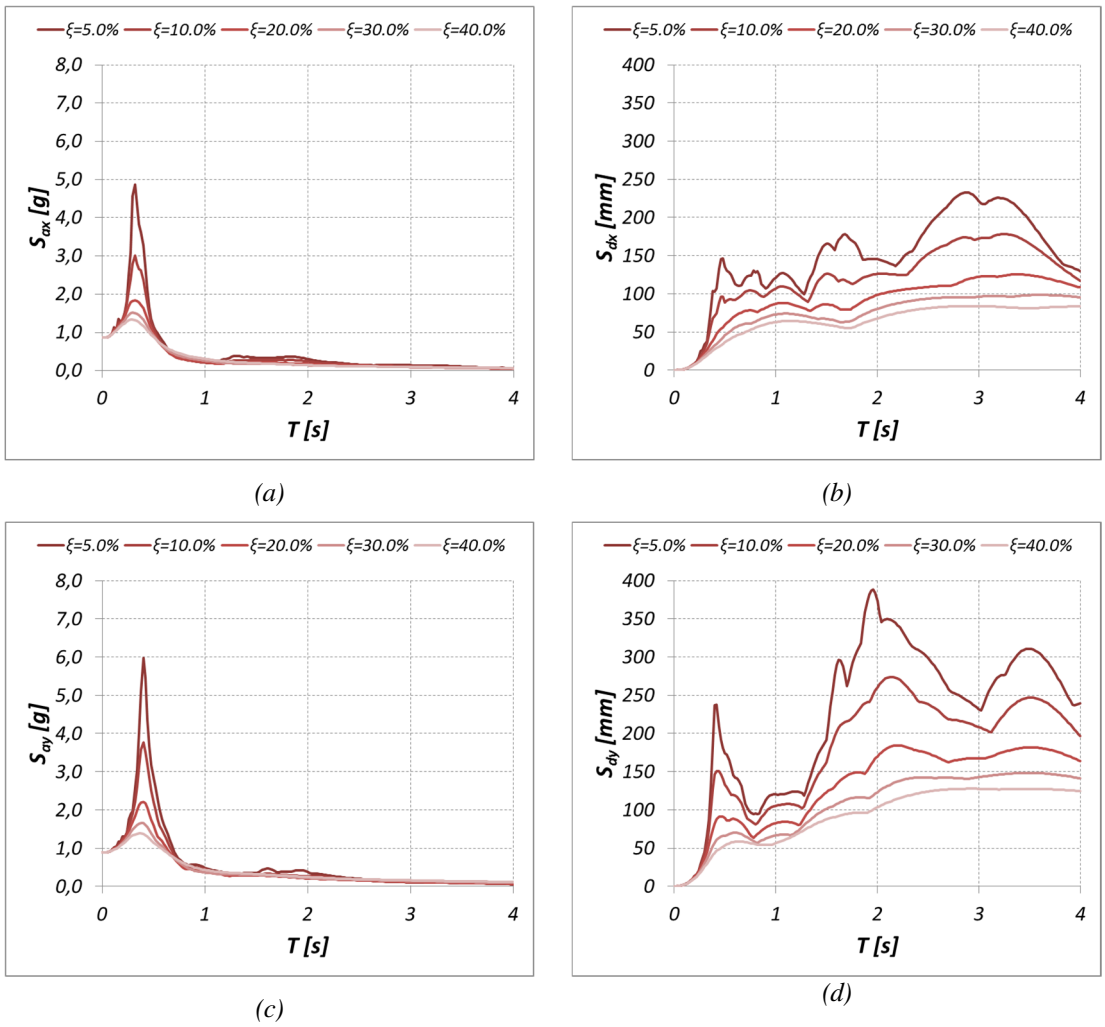

Figure 99 – Floor spectra DEF case (obtained adopting a couple of accelerograms 0335 in XY direction at ground floor): (a) in acceleration x direction; (b) in displacement x direction; (c) in acceleration y direction; (d) in displacement y direction

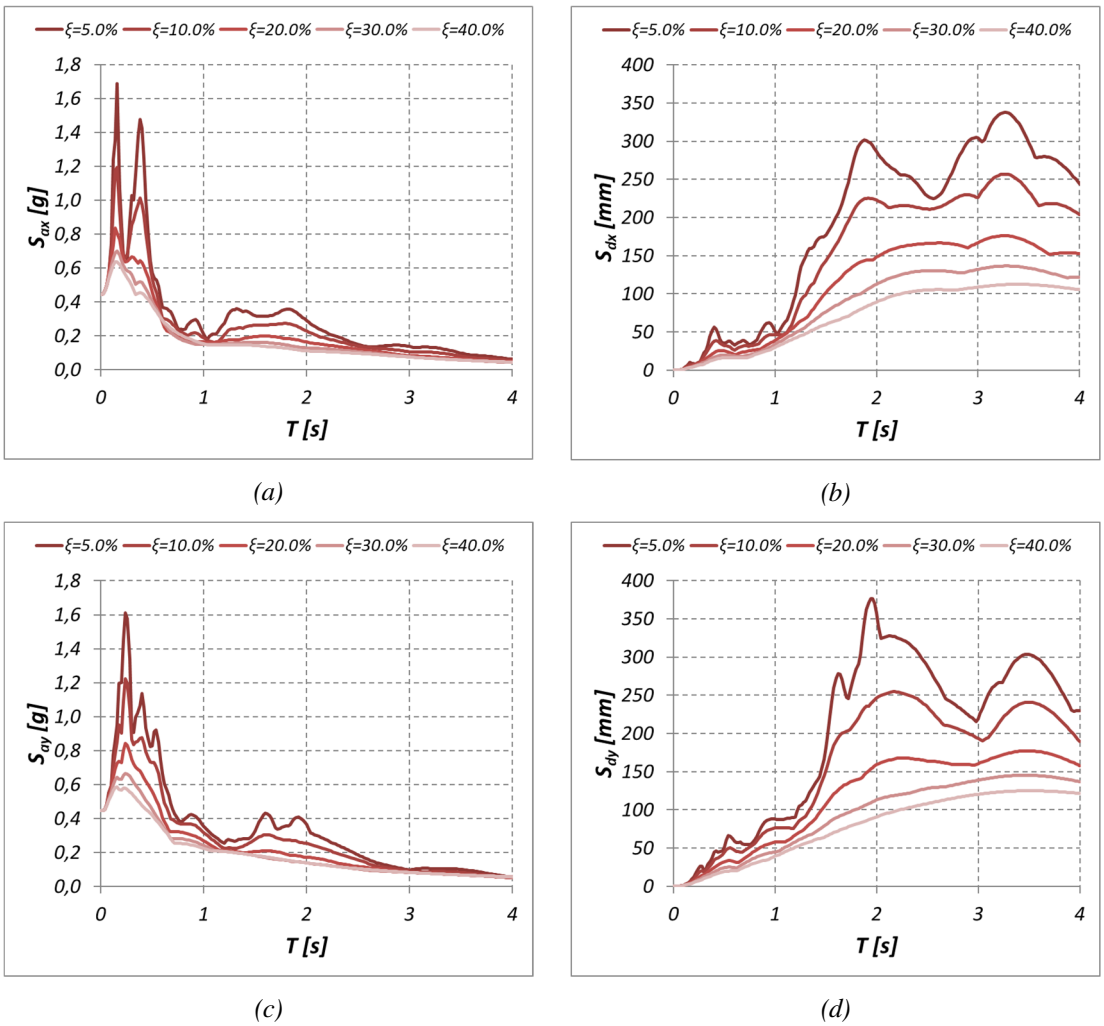

Figure 100 – Floor spectra STIFF case (obtained adopting a couple of accelerograms 0335 in XY direction at ground floor): (a) in acceleration x direction; (b) in displacement x direction; (c) in acceleration y direction; d) in displacement y direction

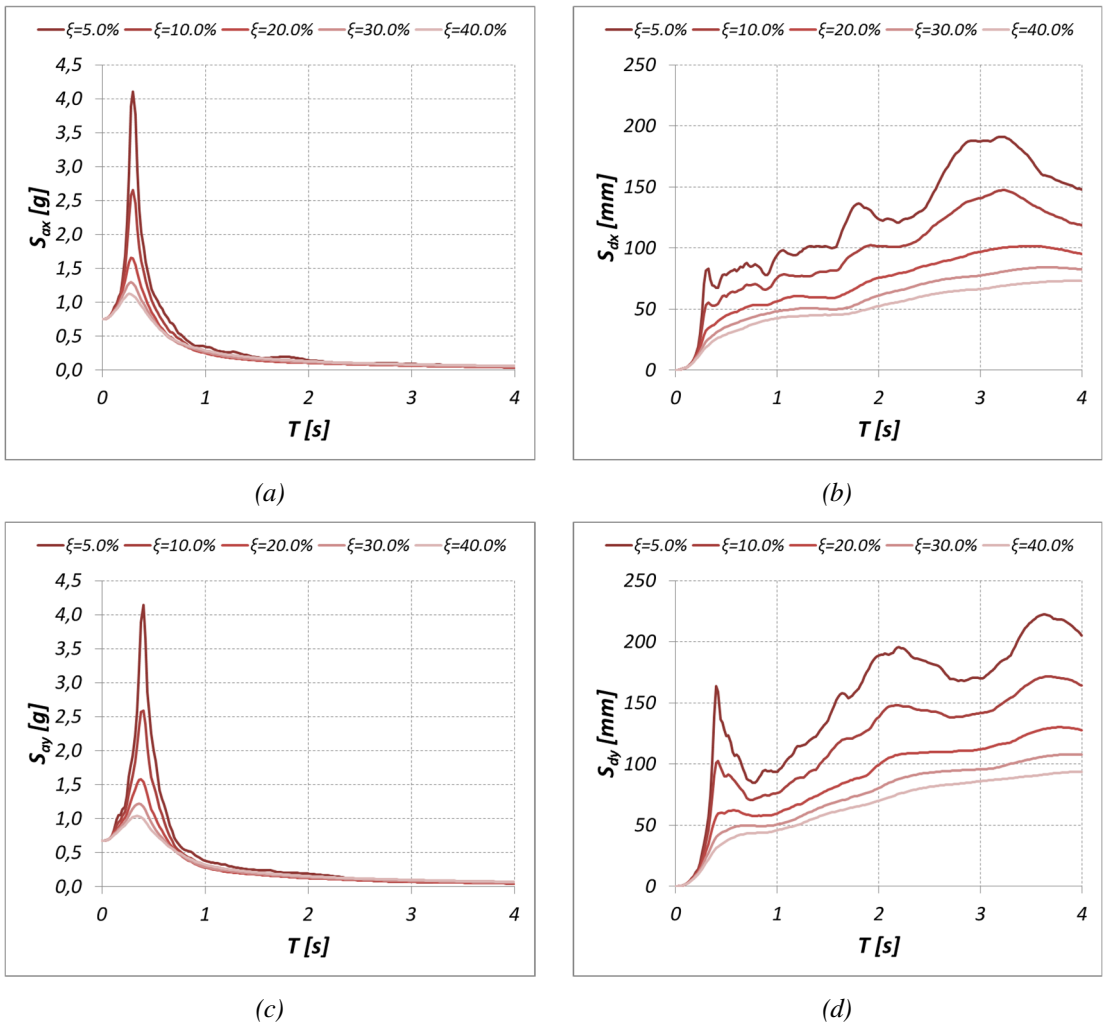

Figure 101 – Average floor spectra DEF case – RANGE2 signals in XY: (a) in acceleration x direction; (b) in displacement x direction: (c) in acceleration y direction; (d) in displacement y direction

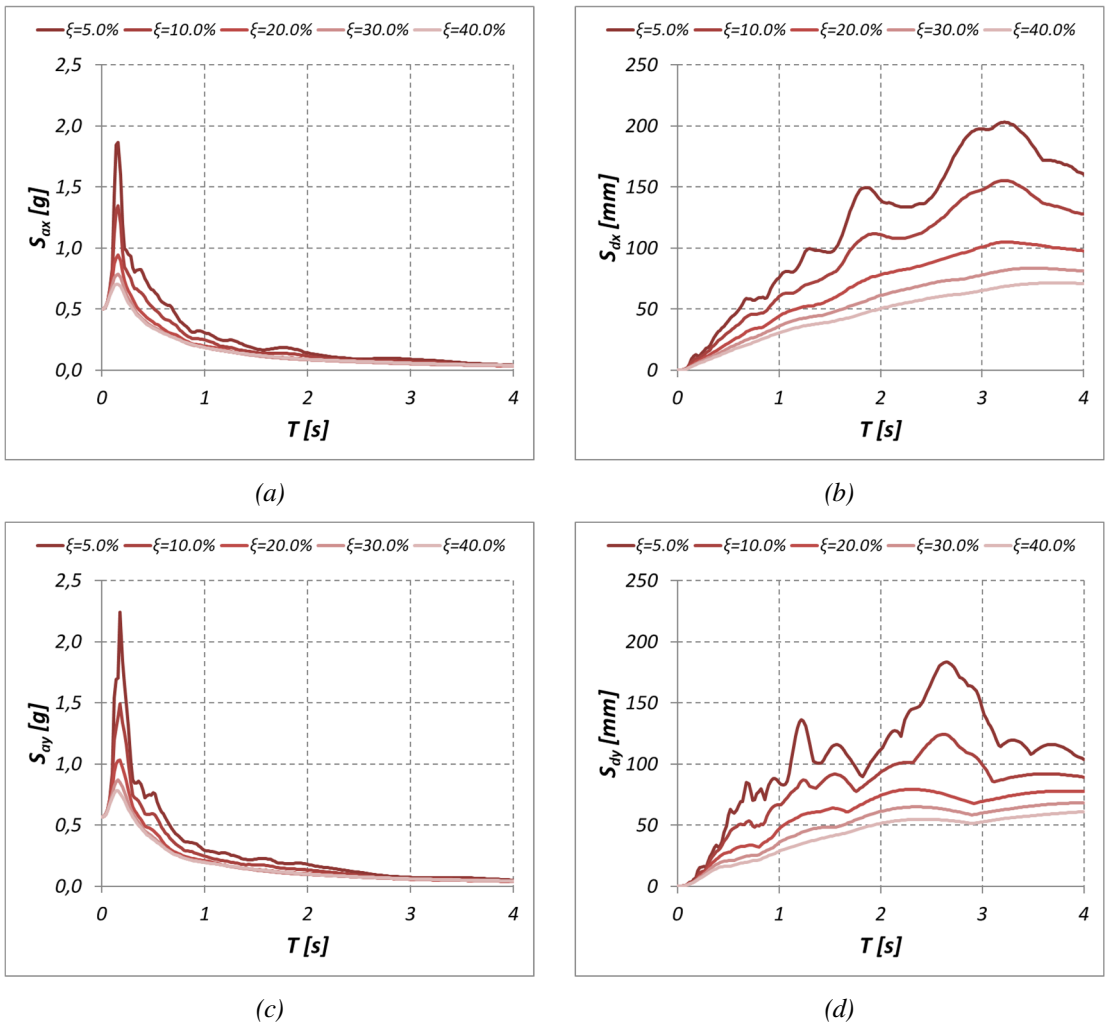

Figure 102 – Average floor spectra STIFF case – RANGE2 signals in XY: (a) in acceleration x direction; (b) in displacement x direction: (c) in acceleration y direction; (d) in displacement y direction

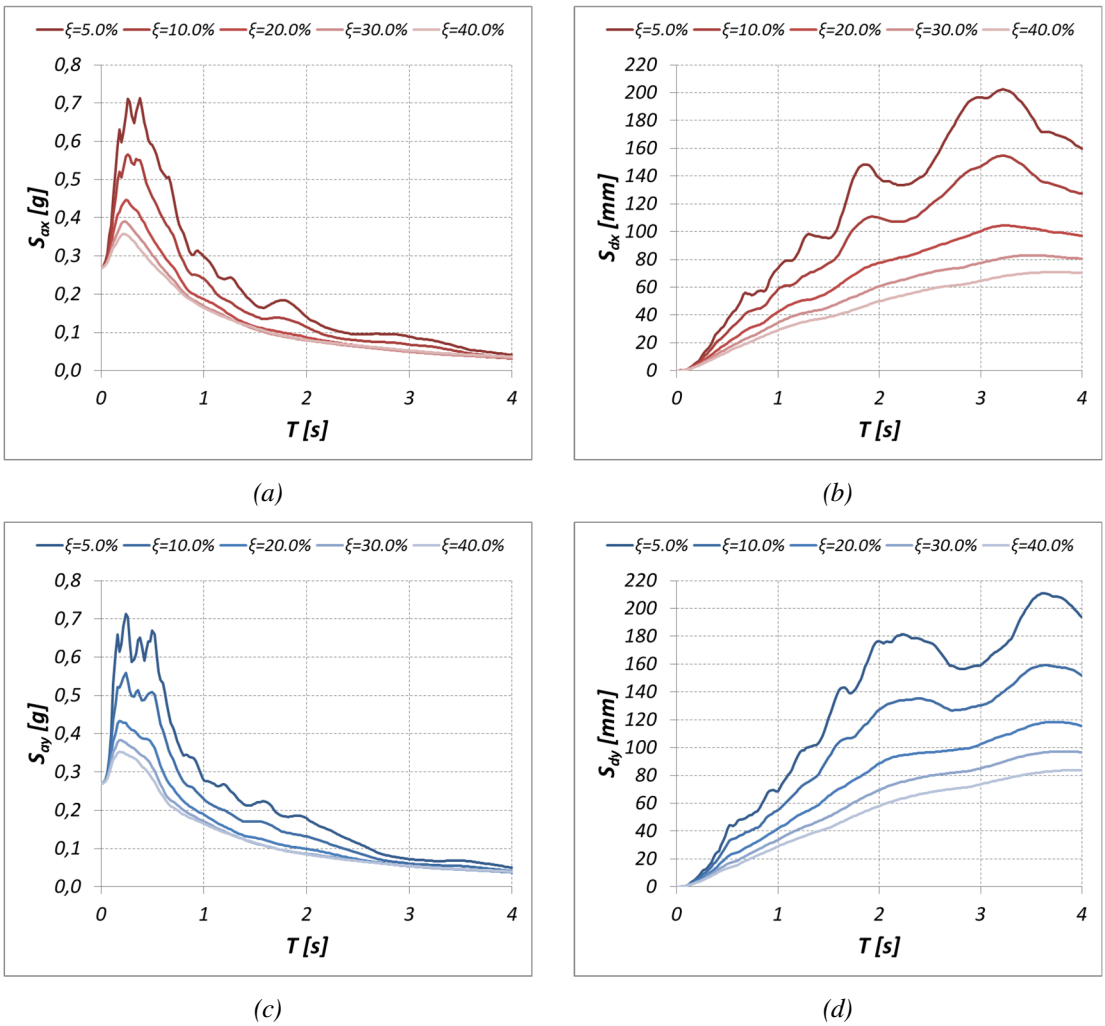

Figure 103 – Average ground spectra – RANGE2: (a) in acceleration x direction; (b) in displacement x direction: (c) in acceleration y direction; (d) in displacement y direction

The comparison between the average floor acceleration spectra for a value of damping equal to 5% and the corresponding spectra obtained with the simplified approach (i.e. EC8) is shown in Figure 104 and Figure 105, respectively for *RANGE1* and *RANGE2* together with the related ground spectrum given by NTC 2008.

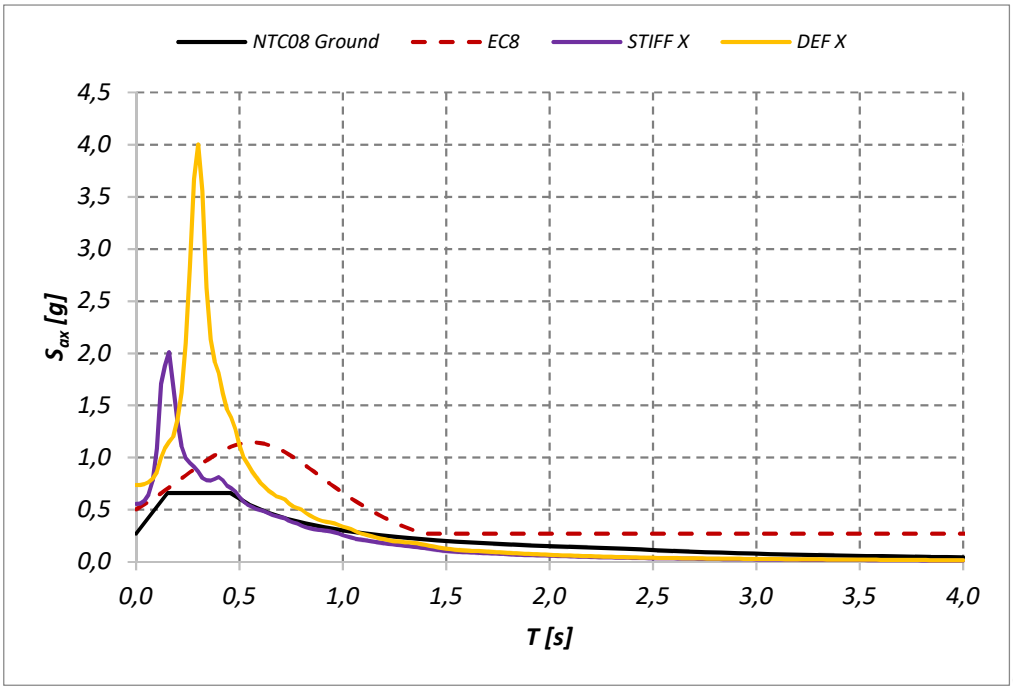

(a)

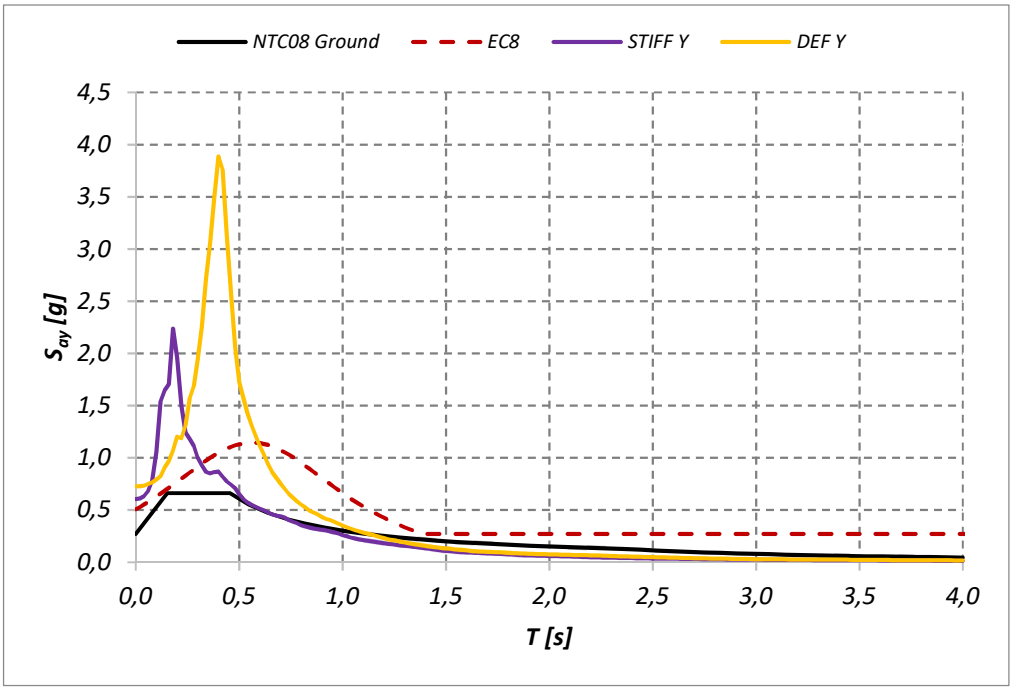

(b)

Figure 104 – Average floor acceleration spectra for RANGE1, and comparison with EC8 Amplification, and NTC 2008 ground spectrum (a) x direction, (b) y direction

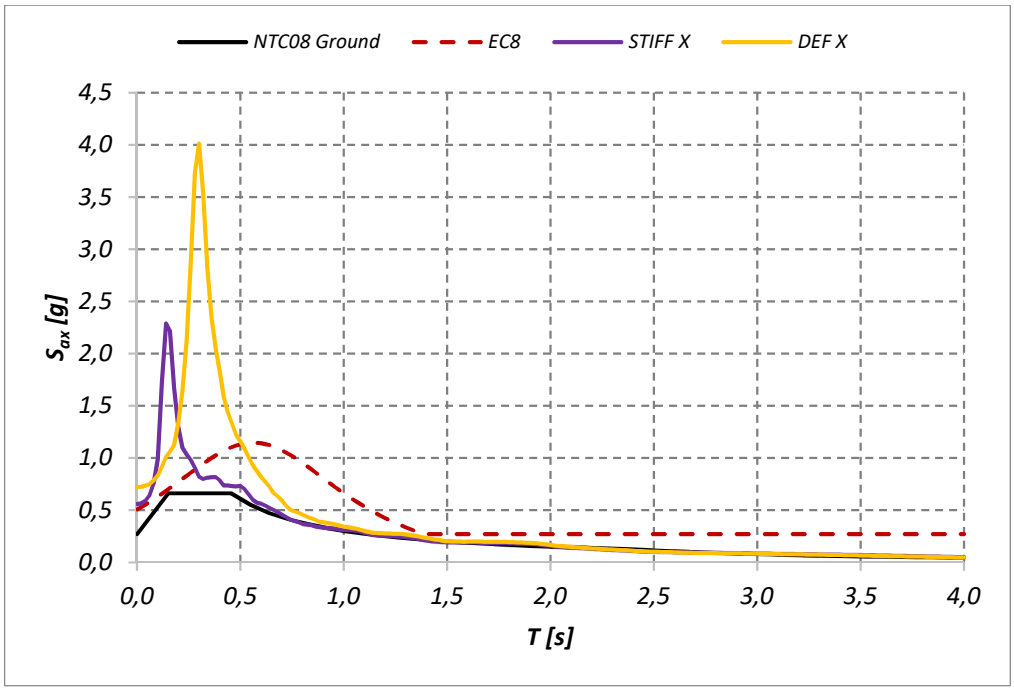

(a)

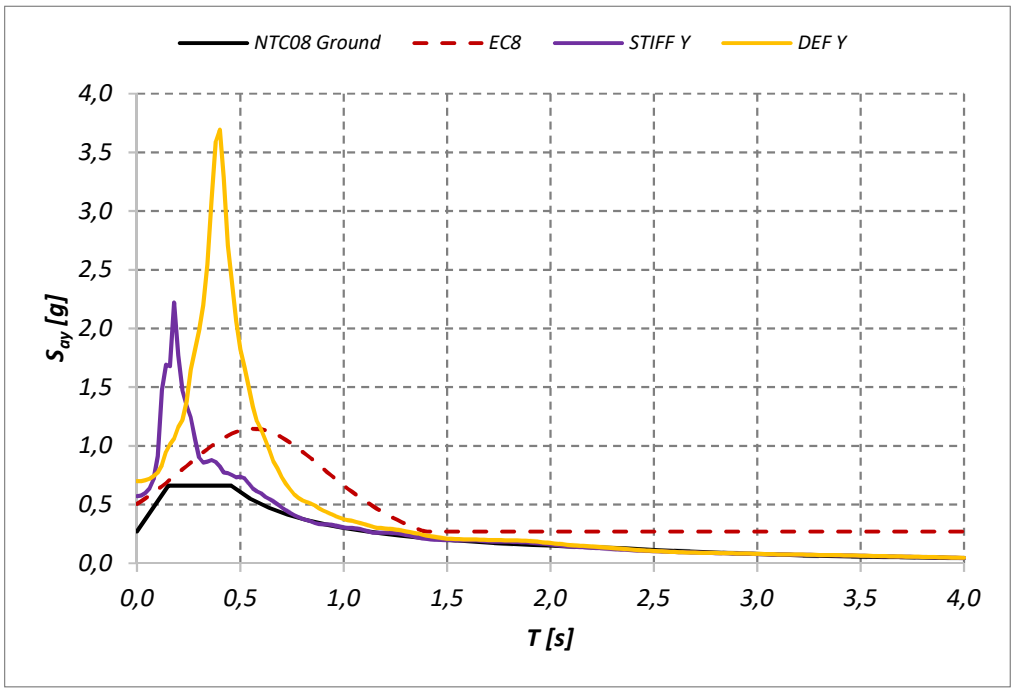

(b)

Figure 105 – Average floor acceleration spectra for RANGE2, and comparison with EC8 Amplification, and NTC 2008 ground spectrum (a) x direction, (b) y direction

The comparison between the average floor displacement spectra for a value of damping equal to 5% and the corresponding spectra obtained with the simplified approach (i.e. CNR Guidelines) is shown Figure 106 and for Figure 107, respectively for *RANGE1* and *RANGE2* together with the related ground spectrum given by NTC 2008.

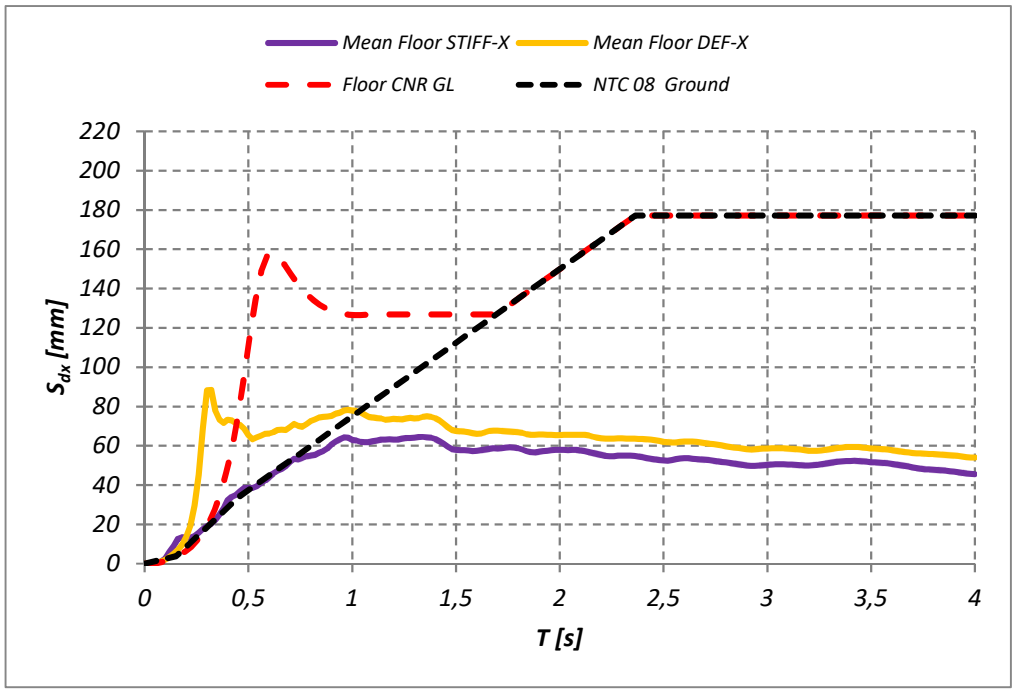

(a)

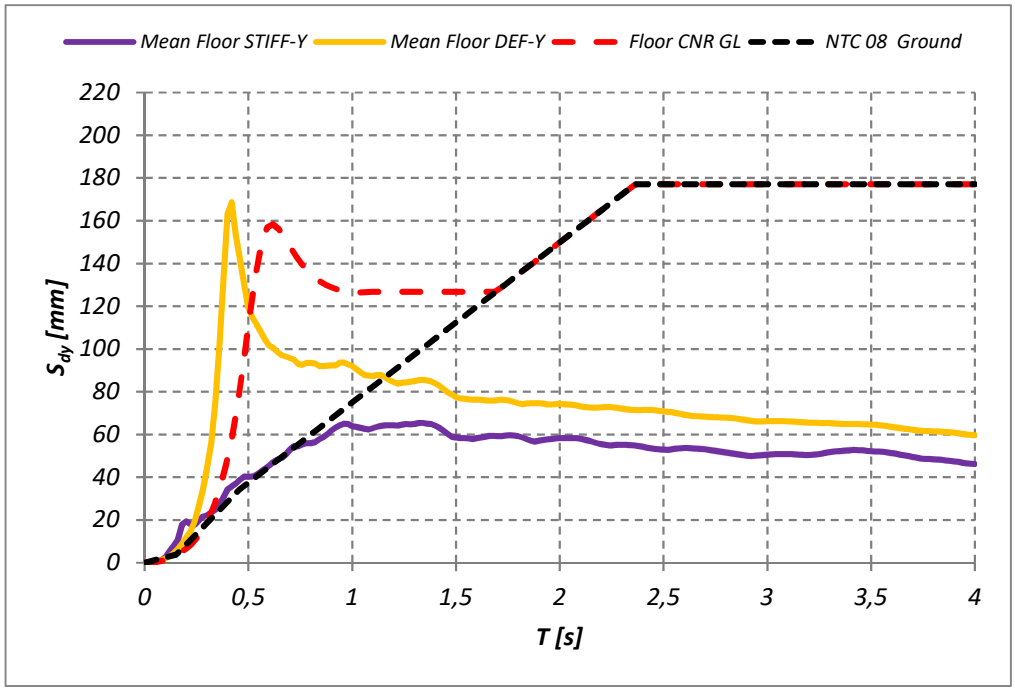

(b)

Figure 106 – Average Displacement floor spectra for RANGE 1 and comparison with the floor spectrum according to CNR Guidelines, and with the Ground spectrum as given by NTC 2008
(a) x direction, (b) y direction

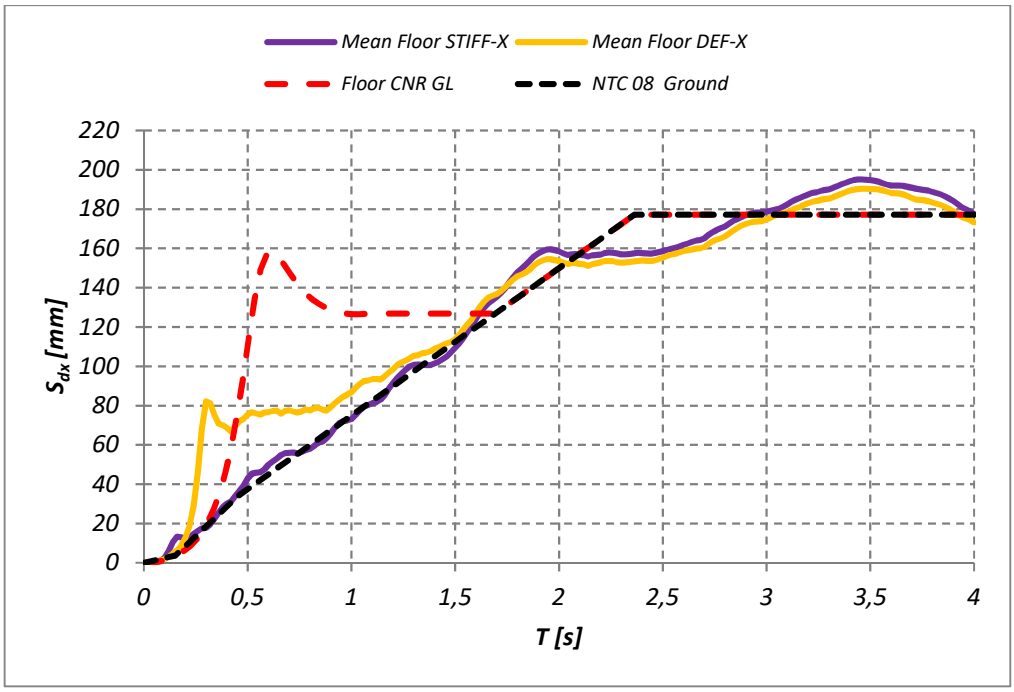

(a)

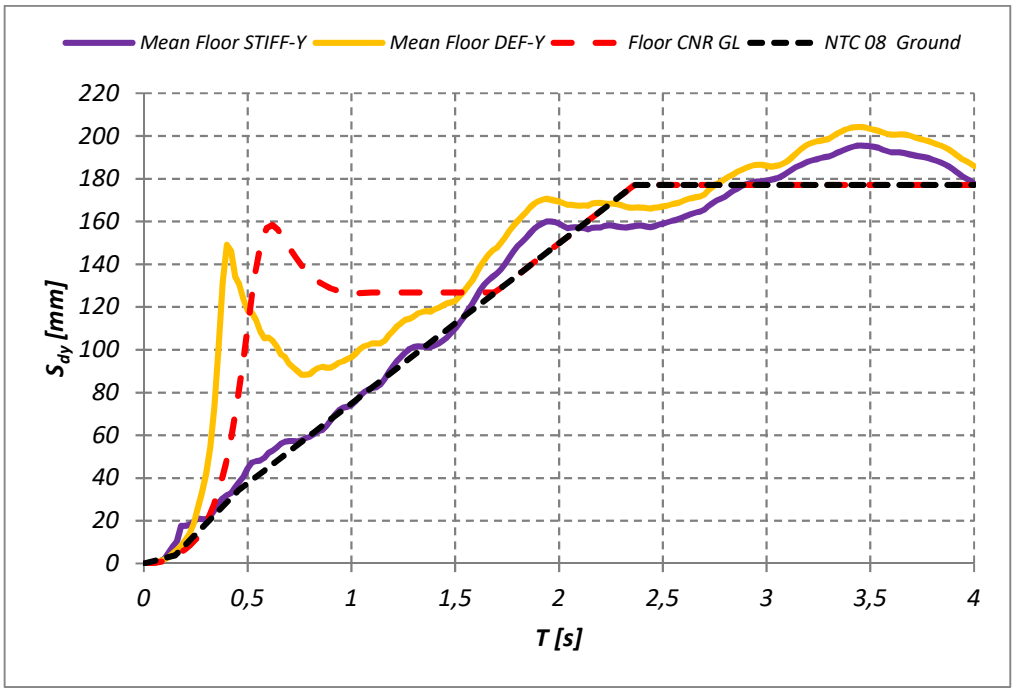

(b)

Figure 107 – Average Displacement floor spectra for RANGE 2 and comparison with the floor spectrum according to CNR Guidelines, and with the Ground spectrum as given by NTC 2008 a) x direction, b) y direction

As regard the acceleration spectra, it is evident that each curve presents the maximum amplification for the corresponding value of the first period of vibration of the structure in the considered direction. For EC8 the simplified value of T_1 obtained by Eq. (38) is adopted. For T=0 the *DEF* case provides the highest value of amplification, with amplification coefficient, evaluated as Sa/PGA, equal to 2,74 and 2,70, respectively along x and y direction greater than 1,7 evaluated according to EC8 (Sect. 4.3.2.1.1). For long

periods the EC8 provides a conservative estimation of the floor acceleration (equal to PGA), higher than the ground spectral acceleration which represent the more plausible value.

As regards the displacement spectra, for the long periods and for both *RANGE1* and *RANGE2*, the numerical floor spectra found for *DEF* case as well for *STIFF* case tend to lay upon the corresponding mean ground spectrum, see Figure 80. It is worth noting that the displacement floor spectrum for *RANGE1* is the least conservative for the long periods due to the strong difference between the corresponding mean ground spectrum and the spectrum given by NTC 2008, as evident in Figure 80. Also the formulation of CNR Guidelines on the long periods overlap on NTC 2008 ground spectrum.

4.4 Bust of Francesco I

4.4.1 Preliminary data

The bust of Francesco I d'Este by Gian Lorenzo Bernini is exhibited at the second floor of *Palazzo dei Musei*, which contains the art collection of the *Galleria Estense*. Some preliminary data relative to the bust and its pedestal have been provided by the *Galleria Estense* and given in Table 26.

Gian Lorenzo Bernini ***Busto ritratto di Francesco I d'Este***	
Bust: *H 100 cm x L 106 cm x P 50 cm* *Base:* *H 14 cm x L 31,5 cm x P 24 cm* *Weight:* *265 kg* *Pedestal:* *H 147,3 cm x L 47,9 cm x P 35,4 cm* *Weight:* *550 kg*	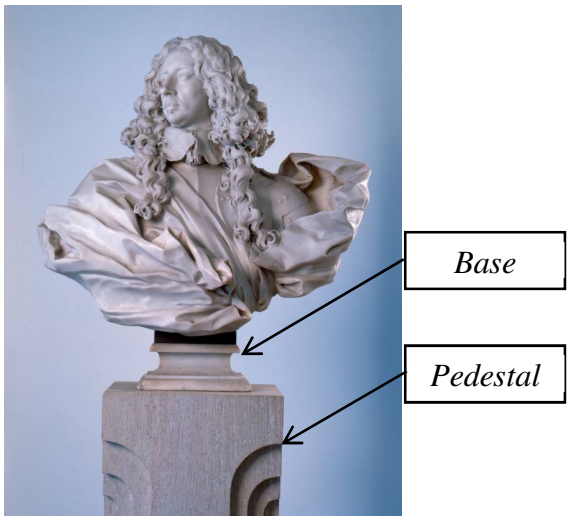

Table 26 – Approximate dimensions of the Portrait Bust of Francesco I d'Este

4.4.1.1 Geometrical and photographic survey

In July 2014, work began on careful examination of the sculpture, after partial removal of its protective crating, made of wood padded out with plastic bubble-pack. The geometric characteristics of the bust were then measured and photographed, in order to create a 3D model. Figure 108 shows some phases of the examination of both bust and pedestal. As the geometry of the pedestal was simpler than that of the bust, direct measurements were taken and graphics produced.

Figure 108 – From top left: first examination, disassembling of the protecting elements, “free” bust, survey on the pedestal

Unlike the bust, which required precise examination, the characteristics and geometry of the pedestal could be studied quite easily. It is a parallelepiped in Istrian stone, with vertical struts at all four corners, terminating with circular volutes to form a capital with a rectangular summit, on which the bust stands. Figure 109 shows the 3D model of the pedestal. Its dimensions are 1473 x 354 x 479 mm (H x L x P).

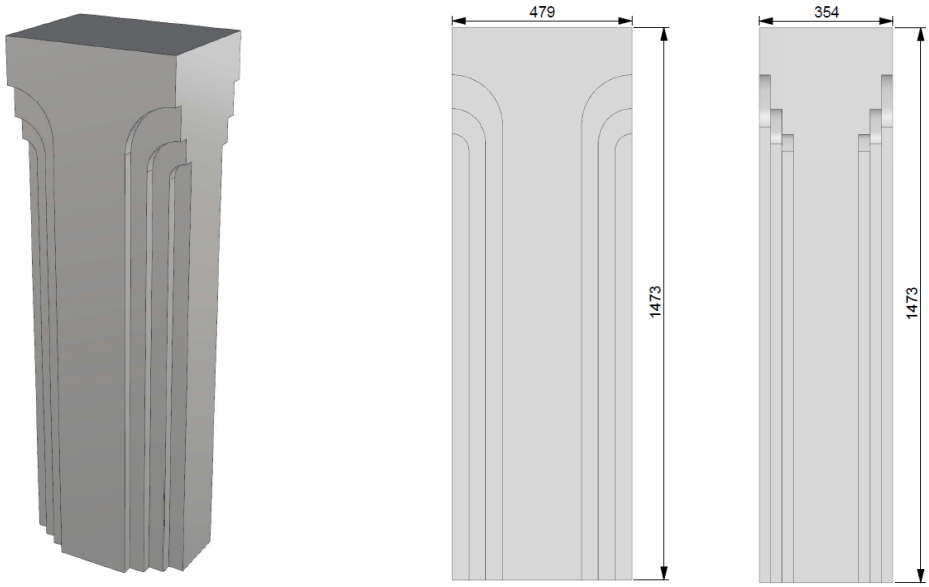

(a) *(b)*

Figure 109 – Pedestal model: 3D view (a) and fronts (b)

4.4.1.2 Numerical modelling

The photographic survey of the bust allowed a 3D model to be reconstructed and, although only approximate with respect to the precision of laser scanning, did allow the necessary data to be obtained.

Autodesk 123D Catch software was used to select and process about 120 photographs round the bust, yielding a preliminary model, and also showing some of the vertical parts of the crate, which was not dismantled. The resulting mesh is thus composed of superficial elements to which a texture was assigned (obtained directly from the photographs). The 360-degree view of the 3D preliminary reconstruction is shown in Figure 110.

Figure 110 –360° view of the preliminary 3D model of the bust (with textures)

The four vertical struts and other parts of the bust were then removed, for proper geometric processing of the solid area. 3D Rhinoceros® modelling software was used. Figure 111 shows the 360° view of the final geometry. Part of the pedestal is also visible. Thus prepared, the solid 3D model could be used to identify the geometric features not only of the bust but also of the Bust/Pedestal (B/P) system. Figure 112 shows the axonometric view of the final refined model.

Figure 111 – 360° view of the refined 3D model of the bust

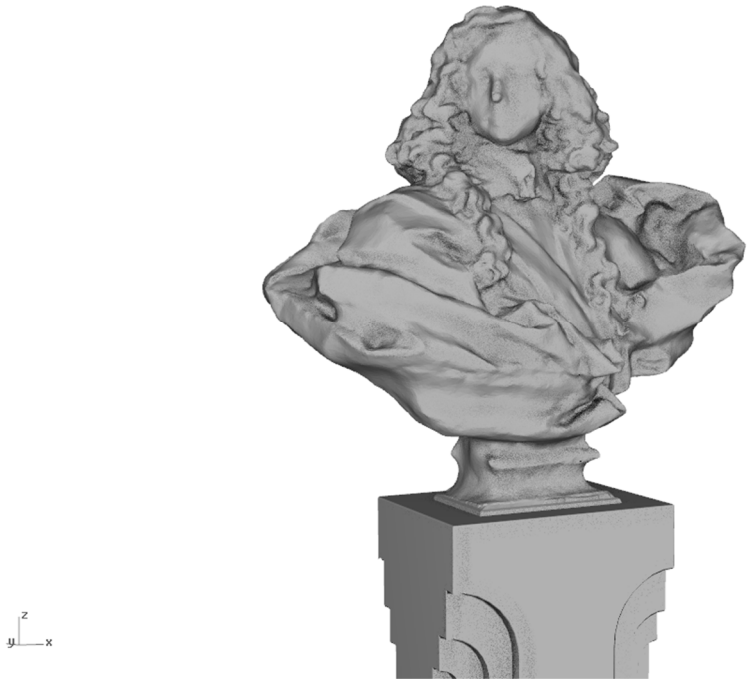

Figure 112 – “Refined” 3D model of the Bust with pedestal

4.4.1.3 Geometrical and inertia characteristics

As the first step in this study of the seismic vulnerability of the bust and its pedestal was to evaluate its tendency to oscillate or overturn, due to horizontal forces, the barycentres of both were ascertained.

The values for the weight of the bust and pedestal are reported in Table 26. Starting from the 3D model, the positions of the barycentres of the Bust, Pedestal and B/P system were calculated. Referring to the symbols in Figure 113, the barycentre coordinates are listed in the first five columns of the Table 27. Figure 113 also shows the origin of reference systems x-y and $\xi - \eta$, used to calculate the baricentres and thus critical accelerations, for oscillatory movements of the bust alone and for the B/P system. In particular, as regards only the bust, reference system $\xi - \eta$ is located on the left front corner of the pedestal (an integral part of the bust), and reference system x-y for the B/P system is located at the left front corner of the rectangle circumscribing the base.

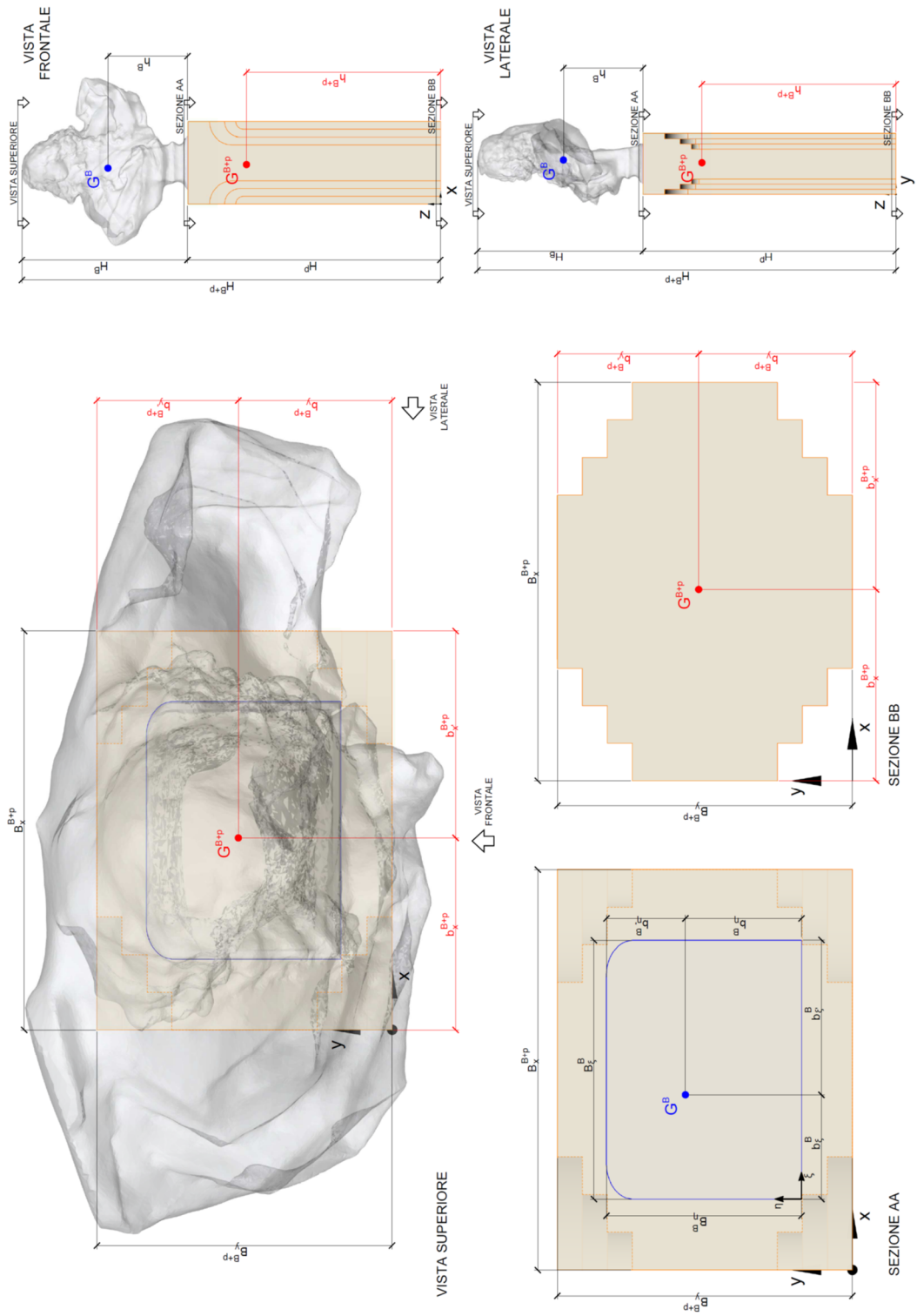

Figure 113 – Geometrical and inertial characteristics of the bust of Francesco I and the pedestal

4.4.2 Vulnerability assessment

In order to allow the assessment of seismic vulnerability of the artwork with regard to the loss of the global equilibrium, it is estimated the return period of the earthquake that corresponds to the attainment of critical values of acceleration $a_{g,c}$, and therefore the onset of rocking. Such an analysis is performed for both the cases of the bust/pedestal system and the bust. It is worth noting that for the calculation of T_{R-C} two situations are considered: object placed at the ground floor and at object placed at the second floor. In addition to the case of soil C, the two soil conditions B and D are also considered, obtaining respectively T_{R-D} and T_{R-D}. Similarly, also for the overturning, the object is considered in both the situations: placed at the ground floor and at the second floor. Finally the return period for the velocity that causes the overturning is calculated for soil type C and for comparison for soil type B and D.

4.4.2.1 Rocking

4.4.2.1.1 Bust located at the ground floor

Table 27 shows the values of the acceleration that induces oscillation obtained by (14), for both the bust and the system bust/pedestal (the meaning of the symbols is reported in Figure 113). With reference to the case of bust, $a_{gc,\xi}$ and $a_{gc,\eta}$ are obtained using the minimum values of b_{ξ}^{B}, $b_{\xi\prime}^{B}$, and respectively b_{η}^{B}, $b_{\eta\prime}^{B}$, while referring to the case of bust/pedestal, $a_{gc,x}$ and $a_{gc,y}$ are obtained using the minimum values of b_{x}^{B+p}, $b_{x\prime}^{B+p}$, and respectively b_{y}^{B+p}, $b_{y\prime}^{B+p}$. Comparing these values with the reference PGA for the site of *Palazzo dei Musei* in Modena, it is observed that the η/y direction are in both cases (i.e. bust and bust/pedestal system) the most vulnerable from the seismic point of view, with a critical acceleration always less than that obtained in the ξ/x direction.

	Model	b_{ξ}^{B} ***(m)***	$b_{\xi\prime}^{B}$ ***(m)***	b_{η}^{B} ***(m)***	$b_{\eta\prime}^{B}$ ***(m)***	h^{B} ***(m)***	$a_{gc,\xi}$ ***(g)***	$a_{gc,\eta}$ ***(g)***	$a_{gc,min}$ ***(g)***	T_{R-B} ***(yrs)***	T_{R-C} ***(yrs)***	T_{R-D} ***(yrs)***
A	*Bust*	*0,125*	*0,186*	*0,139*	*0,095*	*0,464*	*0,269*	*0,204*	*0,204*	*527*	*298*	*192*

	Model	b_{x}^{B+p} ***(m)***	$b_{x\prime}^{B+p}$ ***(m)***	b_{y}^{B+p} ***(m)***	$b_{y\prime}^{B+p}$ ***(m)***	h^{B+p} ***(m)***	$a_{gc,x}$ ***(g)***	$a_{gc,y}$ ***(g)***	$a_{gc,min}$ ***(g)***	T_{R-B} ***(yrs)***	T_{R-C} ***(yrs)***	T_{R-D} ***(yrs)***
B	*Bust + Pedestal*	*0,230*	*0,249*	*0,185*	*0,169*	*1,139*	*0,201*	*0,149*	*0,149*	*238*	*145*	*101*

Table 27 – Critical accelerations and return period for rocking of the bust and Bust/Pedestal system

Currently, it can be stated therefore that the Bust/Pedestal system, because of its slenderness, it is more vulnerable than the sculpture alone, with a critical acceleration

reduced by approximately 25% compared to the configuration with only the bust. In the more severe case, a_{gc} is equal to 0,149 g, that, given soil category C, occurs with a return period of 145 years. This period would be reduced to 101 years if soil D was assumed.
Regarding the sliding of the system, it can be observed that the onset of this type of motion can occur before the triggering of rocking only if the friction coefficient at the interface between pedestal and floor is lower than the minimum $a_{g,c}$ in the two directions, in this case equal to 0,149 g.

4.4.2.1.2 Bust located at the second floor

Considering the amplification coefficient with the height for T_a =0 given by EC8, i.e. 1,87, (see Sect. 4.3.2.1.1), return periods of the earthquake that causes rocking to the object placed at the second floor are calculated and reported in Table 28, for soil category C (same of the site of the building) and for comparison, also for soil category B and D. In particular, for each model and for each direction critical acceleration, the corresponding value of ground acceleration (Sa_g) and corresponding Return period T_R are shown.
Considering the effect of amplification of the seismic signal due to the height of the floor, it can be seen that the return period of the seismic event that triggers rocking diminishes drastically, in the case of soil category C, to the value of 75 years for the case of the Bust and less than 40 years for the Bust/Pedestal system (Table 28). In both cases, the rocking verification is not satisfied for the limit state ULS (712 years). Considering a soil category D, the return period of 50 years for the bust and lower than 30 years for the Bust/Pedestal system is given.
For the sake of comparison, if the amplification coefficient obtained for T=0 in *DEF* case is considered, the values of $Sa_{gc,min}$ become 0,075 g for the Bust and 0,055 g for the Bust/Pedestal system, which correspond respectively to a return period T_{R-C} equal to 32 and <32 years.

	Model	$a_{gc,\xi}$ (g)	$a_{gc,\eta}$ (g)	$Sa_{gc,\xi}$ (ground floor) (g)	$Sa_{gc,\eta}$ (ground floor) (g)	$Sa_{gc,min}$ (ground floor) (g)	$T_{R\text{-}B}$ (years)	$T_{R\text{-}C}$ (years)	$T_{R\text{-}D}$ (years)
A	Bust	0,269	0,204	0,144	0,109	0,109	121	75	50

	Model	$a_{gc,x}$ (g)	$a_{gc,y}$ (g)	$Sa_{gc,x}$ (ground floor) (g)	$Sa_{gc,y}$ (ground floor) (g)	$Sa_{gc,min}$ (ground floor) (g)	$T_{R\text{-}B}$ (years)	$T_{R\text{-}C}$ (years)	$T_{R\text{-}D}$ (years)
B	Bust + Pedestal	0,201	0,149	0,108	0,080	0,080	62	37	< 30

Table 28 – Rocking at the 2nd floor: Critical accelerations and return period for rocking of the Bust and Bust/Pedestal system

4.4.2.2 Overturning

4.4.2.2.1 Bust located at the ground floor

As shown in Sect. 4.4.2.1, two possible configurations bust and Bust/Pedestal are considered for the overturning verification. Table 29 shows the equivalent height h' of the asymmetrical body, evaluated according to (17), while Table 30 shows the critical velocities that determine overturning, assessed according to (16). Equivalent heights and critical velocities are given for the four distances of the projection of the centre of gravity with respect to the corner point of the bust, or pedestal, around which the rotation can take place. With reference to Table 30, it is observed that, unlike rocking verification, in which the bust resulted in the less dangerous condition, in the case of overturning the bust tends to overturn for a Return Period lower than that of the Bust/Pedestal system.

Furthermore, the sensitivity to the soil category is decisive: for the Bust, whereas the ground floor of category B, the T_R for the overturning which occurs with v_{lim} = 0.198 m/s is equal to 1750 years, greater than 712 years (ULS limit state, as defined for the building). Considering soil Type D, the calculation leads to 166 years of return period. Similarly, for the Bust/Pedestal configuration, it is calculated a T_R greater than 2475 (CPLS collapse prevention limit state) for soil type B, until 238 years for the soil type D. With soil type C, a return period equal to 733 years is found for the Bust and of 1262 years for the Bust/Pedestal system, providing in both cases a satisfactory verification.

	Overturning	H' (m)			
		ξ	ξ'	η	η'
A	Bust	0,429	0,404	0,463	0,480

	Overturning	H' (m)			
		X	x'	y	y'
B	Bust/Pedestal	1,085	1,079	1,104	1,108

Table 29 – Equivalent height of Bust and Bust/Pedestal system

	Overturning	v_{lim} (m/s)					T_{RB} (years)	T_{RC} (years)	T_{RD} (years)
		ξ	ξ'	η	η'	min			
A	Bust	0,275	0,424	0,296	0,198	0,198	1750	733	166

	Overturning	v_{lim} (m/s)					T_{RB} (years)	T_{RC} (years)	T_{RD} (years)
		x	x'	Y	y'	min			
B	Bust/Pedestal	0,319	0,347	0,254	0,233	0,233	> 2475	1262	238

Table 30 – Critical velocity for overturning: (a) Bust and (b) Bust/Pedestal

4.4.2.2.2 Bust located at the second floor

Return period for Bust and for Bust/Pedestal are obtained by evaluating an approximate amplification of the velocity equal to that of the acceleration, results of the calculation are reported in Table 31. As can be seen, the Return Period of the event that induces overturning decreases significantly taking up to values of 135 years for the Bust, and up to 220 years for the Bust/Pedestal system, assuming a soil category type C.

	Overturning	v_{lim} (m/s) min	$v_{cr,\ ground\ floor}$ (m/s)	T_{RB} (years)	T_{RC} (years)	T_{RD} (years)
A	Bust	0,198	0,100	290	135	42

	Overturning	v_{lim} (m/s) min	$v_{cr,\ ground\ floor}$ (m/s)	T_{RB} (years)	T_{RC} (years)	T_{RD} (years)
B	Bust/Pedestal	0,233	0,125	500	220	67

Table 31 – Overturning at the 2nd floor: Critical velocity: (a) Bust and (b) Bust/Pedestal

At present, it can be concluded that, because of its slenderness, the system bust/pedestal is the more vulnerable configuration, with a critical acceleration reduced by

approximately 25% compared to the bust. In this case a_{gc} is 0,149g corresponding to a return period of 145 years. Considering also an amplification coefficient of 1,87, the return periods of the earthquake that triggers the oscillation of the object placed at the second floor are evaluated, Table 28. In particular, the critical acceleration, the corresponding acceleration value to the ground (Sa_g) and the return period are summarized. Considering the effect of amplification of the seismic signal, it can be seen that the return period dramatically decreases at a value of 75 years for the bust and less than 40 years for the bust/pedestal. In both cases, for the limit state ULS (712 years) the verification is not satisfied. Similarly, also for overturning, the two configurations of bust and bust/pedestal are considered. Table 30 shows the critical velocity that produces overturning together with the projection of the centre of gravity with respect to the edges of the bust or the pedestal, around which the overturning is possible. It is observed that, on the contrary of the rocking, the bust tends to overturn for a return period lower than that of the bust/pedestal system. The minimum return period is equal to 733 years for the bust and 1262 years for the system bust/pedestal, providing in both cases a safety condition.

In a similar way to the rocking analysis (Sect. 4.4.2.1.2), if the amplification coefficient obtained for T =0 in *DEF* case is considered, the minimum values of $v_{cr,ground\ floor}$ become 0,072 m/s for the Bust and 0,085 m/s for the Bust/Pedestal system, which lead to a return period T_{R-C} equal to 68 and 97 years.

4.4.3 Response to the seismic events of May 2012

In the following, the results obtained by verifying the rocking of the pedestal with reference to maximum accelerations recorded during the main seismic events of Emilia 2012 earthquake are presented. The signals considered for the analyses are registered by the seismographic station "MDN", installed at the Polo School Leonardo da Vinci of Modena, and situated about 6,5 km west of the site of *Palazzo dei Musei*. In Table 32 and Table 33 the results of the rocking verification are summarized respectively for the earthquake of greater magnitude (20 May at 2:03 M_W = 6,1) and that of 29 May (M_W = 6,0). The results are given considering the orientation of the artwork reported in Figure 56 and the amplification of the acceleration due to the height of the building as calculated in 4.3.2.1.1 (simplified approach).

(All)	*Effects envelope [g]*			*Amplified Effects [g]*		
Sign	Pga_X	Pga_Y	Pga_Z	Pga_X	Pga_Y	Pga_Z
(+)	***0,0308***	***0,0318***	***0,0293***	***0,0575***	***0,0594***	***0,0293***
(-)	***-0,0346***	***-0,0371***	~~***-0,0206***~~	***-0,0647***	***-0,0693***	~~***-0,0206***~~
(X)	*Maximum combination in X [g]*			*Amplified Effects [g]*		
Sign	Pga_X	Pga_Y	Pga_Z	Pga_X	Pga_Y	Pga_Z
(+)	***0,0308***	*0,0032*	*-0,0081*	***0,0575***	*0,0059*	*-0,0081*
(-)	***-0,0346***	*-0,0070*	*0,0057*	***-0,0647***	*-0,0132*	*0,0057*
(Y)	*Maximum combination in Y [g]*			*Amplified Effects [g]*		
Sign	Pga_X	Pga_Y	Pga_Z	Pga_X	Pga_Y	Pga_Z
(+)	*-0,0078*	***0,0318***	*-0,0041*	*-0,0147*	***0,0594***	*-0,0041*
(-)	*-0,0075*	***-0,0371***	*-0,0016*	*-0,0139*	***-0,0693***	*-0,0016*
(Z)	*Maximum combination in Z [g]*			*Amplified Effects [g]*		
Sign	Pga_X	Pga_Y	Pga_Z	Pga_X	Pga_Y	Pga_Z
(+)	*0,0034*	*0,0046*	***0,0293***	*0,0063*	*0,0086*	***0,0293***
(-)	*0,0086*	*-0,0325*	***-0,0206***	*0,0160*	*-0,0607*	***-0,0206***

(All)	*Capacity [g]*		*Corrected cap. [g]*		*Capacity/Demand [-]*		*Verification*	
Sign	$a_{gc,X}$	$a_{gc,Y}$	$a_{gc,X}$	$a_{gc,Y}$	*X*	*Y*	*X*	*Y*
(+)	*0,2189*	*0,1486*	*0,2125*	*0,1443*	*3,6963*	*2,4285*	*OK*	*OK*
(-)	*0,2013*	*0,1619*	*0,1954*	*0,1572*	*3,0220*	*2,2685*	*OK*	*OK*
(X)	*Capacity [g]*		*Corrected cap. [g]*		*Capacity/Demand [-]*		*Verification*	
Sign	$a_{gc,X}$	$a_{gc,Y}$	$a_{gc,X}$	$a_{gc,Y}$	*X*	*Y*	*X*	*Y*
(+)	*0,2189*	*0,1486*	*0,2207*	*0,1498*	*3,8384*	*25,2201*	*OK*	*OK*
(-)	*0,2013*	*0,1619*	*0,2002*	*0,1610*	*3,0954*	*12,2407*	*OK*	*OK*
(Y)	*Capacity [g]*		*Corrected cap. [g]*		*Capacity/Demand [-]*		*Verification*	
Sign	$a_{gc,X}$	$a_{gc,Y}$	$a_{gc,X}$	$a_{gc,Y}$	*X*	*Y*	*X*	*Y*
(+)	*0,2189*	*0,1486*	*0,2198*	*0,1493*	*14,9859*	*2,5121*	*OK*	*OK*
(-)	*0,2013*	*0,1619*	*0,2017*	*0,1622*	*14,4680*	*2,3405*	*OK*	*OK*
(Z)	*Capacity [g]*		*Corrected cap. [g]*		*Capacity/Demand [-]*		*Verification*	
Sign	$a_{gc,X}$	$a_{gc,Y}$	$a_{gc,X}$	$a_{gc,Y}$	*X*	*Y*	*X*	*Y*
(+)	*0,2189*	*0,1486*	*0,2125*	*0,1442*	*33,8554*	*16,6876*	*OK*	*OK*
(-)	*0,2013*	*0,1619*	*0,2055*	*0,1653*	*12,8126*	*2,7206*	*OK*	*OK*

Table 32 – Rocking verification of Bust and Bust/Pedestal system – 20 May 2012

(All)	*Effects envelope [g]*			*Amplified Effects [g]*		
Sign	***Pga$_X$***	***Pga$_Y$***	***Pga$_Z$***	***Pga$_X$***	***Pga$_Y$***	***Pga$_Z$***
(+)	*0,0378*	*0,0478*	*0,0359*	*0,0707*	*0,0893*	*0,0359*
(-)	*-0,0306*	*-0,0537*	*~~-0,0330~~*	*-0,0572*	*-0,1004*	*~~-0,0330~~*
(X)	***Maximum combination in X [g]***			***Amplified Effects [g]***		
Sign	***Pga$_X$***	***Pga$_Y$***	***Pga$_Z$***	***Pga$_X$***	***Pga$_Y$***	***Pga$_Z$***
(+)	***0,0378***	*-0,0214*	*-0,0228*	***0,0707***	*-0,0400*	*-0,0228*
(-)	***-0,0306***	*-0,0049*	*-0,0059*	***-0,0572***	*-0,0092*	*-0,0059*
(Y)	***Maximum combination in Y [g]***			***Amplified Effects [g]***		
Sign	***Pga$_X$***	***Pga$_Y$***	***Pga$_Z$***	***Pga$_X$***	***Pga$_Y$***	***Pga$_Z$***
(+)	*-0,0014*	***0,0478***	*0,0156*	*-0,0027*	***0,0893***	*0,0156*
(-)	*0,0046*	***-0,0537***	*-0,0039*	*0,0086*	***-0,1004***	*-0,0039*
(Z)	***Maximum combination in Z [g]***			***Amplified Effects [g]***		
Sign	***Pga$_X$***	***Pga$_Y$***	***Pga$_Z$***	***Pga$_X$***	***Pga$_Y$***	***Pga$_Z$***
(+)	*-0,0030*	*-0,0015*	***0,0359***	*-0,0056*	*-0,0028*	***0,0359***
(-)	*-0,0047*	*0,0084*	***-0,0330***	*-0,0088*	*0,0158*	***-0,0330***

(All)	*Capacity [g]*		*Corrected cap. [g]*		*Capacity/Demand [-]*		*Verification*	
Sign	***$a_{gc,X}$***	***$a_{gc,Y}$***	***$a_{gc,X}$***	***$a_{gc,Y}$***	***X***	***Y***	***X***	***Y***
(+)	*0,2189*	*0,1486*	*0,21101*	*0,1433*	*2,9860*	*1,6041*	*OK*	*OK*
(-)	*0,2013*	*0,1619*	*0,1941*	*0,1561*	*3,3959*	*1,5548*	*OK*	*OK*
(X)	***Capacity [g]***		***Corrected cap. [g]***		***Capacity/Demand [-]***		***Verification***	
Sign	***$a_{gc,X}$***	***$a_{gc,Y}$***	***$a_{gc,X}$***	***$a_{gc,Y}$***	***X***	***Y***	***X***	***Y***
(+)	*0,2189*	*0,1486*	*0,2239*	*0,1520*	*3,1676*	*3,8001*	*OK*	*OK*
(-)	*0,2013*	*0,1619*	*0,2025*	*0,1629*	*3,5430*	*17,6943*	*OK*	*OK*
(Y)	***Capacity [g]***		***Corrected cap. [g]***		***Capacity/Demand [-]***		***Verification***	
Sign	***$a_{gc,X}$***	***$a_{gc,Y}$***	***$a_{gc,X}$***	***$a_{gc,Y}$***	***X***	***Y***	***X***	***Y***
(+)	*0,2189*	*0,1486*	*0,2155*	*0,1463*	*80,6888*	*1,6379*	*OK*	*OK*
(-)	*0,2013*	*0,1619*	*0,2021*	*0,1626*	*23,4147*	*1,6189*	*OK*	*OK*
(Z)	***Capacity [g]***		***Corrected cap. [g]***		***Capacity/Demand [-]***		***Verification***	
Sign	***$a_{gc,X}$***	***$a_{gc,Y}$***	***$a_{gc,X}$***	***$a_{gc,Y}$***	***X***	***Y***	***X***	***Y***
(+)	*0,2189*	*0,1486*	*0,2111*	*0,1433*	*37,3779*	*52,0050*	*OK*	*OK*
(-)	*0,2013*	*0,1619*	*0,2080*	*0,1673*	*23,6944*	*10,6112*	*OK*	*OK*

Table 33 – Rocking verification of Bust and Bust/Pedestal system - 29 May 2012

As it can be observed for both the seismic events (earthquakes), the rocking motion for the system Bust/Pedestal is not triggered as the minimum ratio between capacity and demand in the y direction is at least equal to 1,6.

It should be emphasized, however, that this result was obtained without considering the effect of the vertical acceleration that, reducing the stabilizing effect due to the system own weight, decreases the ratio between capacity and seismic demand to values slightly greater than one.

For the sake of comparison in Table 34 rocking verification is given for the most demanding seismic event (20 May – 1st Mainshock) in which the seismic signals acting at the second floor are evaluated with a more detailed numerical analysis, considering both the reference cases of the building model *DEF* and *STIFF* (see also 4.2.2.3).

Also in this case the verification is satisfied, even if to a lesser extent than that calculated with the simplified method. In particular, in the y direction the maximum calculated floor acceleration is almost twice the measured value using the simplified approach (for which the amplification effect is not affected by the direction).

		Envelope [g]		***Max amplified effects [g]***	
DEF	***Sign***	***Pga_X***	***Pga_Y***	***$a_{max,X}$***	***$a_{max,Y}$***
	(+)	*0,0305*	*0,0317*	*0,0558*	*0,0923*
	(-)	*-0,0345*	*-0,0371*	*-0,0799*	*-0,1132*
		Envelope [g]		***Max amplified effects [g]***	
STIFF	***Sign***	***Pga_X***	***Pag_Y***	***$a_{max,X}$***	***$a_{max,Y}$***
	(+)	*0,0305*	*0,0317*	*0,0609*	*0,0606*
	(-)	*-0,0345*	*-0,0371*	*-0,0610*	*-0,0550*

		Capacity [g]		***Capacity/Demand[-]***		***Verification***	
DEF	***Sign***	***$a_{gc,X}$***	***$a_{gc,Y}$***	***$a_{gc,X}$***	***$a_{gc,Y}$***	***$a_{gc,X}$***	***$a_{gc,Y}$***
	(+)	*0,2189*	*0,1486*	*3,9228*	*1,6103*	*OK*	*OK*
	(-)	*0,2013*	*0,1619*	*2,5189*	*1,4305*	*OK*	*OK*
		Capacity [g]		***Capacity/Demand[-]***		***Verification***	
STIFF	***Sign***	***$a_{gc,X}$***	***$a_{gc,Y}$***	***$a_{gc,X}$***	***$a_{gc,Y}$***	***$a_{gc,X}$***	***$a_{gc,Y}$***
	(+)	*0,2189*	*0,1486*	*3,5968*	*2,4518*	*OK*	*OK*
	(-)	*0,2013*	*0,1619*	*3,2982*	*2,9422*	*OK*	*OK*

Table 34 – Rocking verification of Bust and Bust/Pedestal system, seismic signal of 20 May 2012 with amplification calculated using numerical modelling

4.4.4 Seismic vulnerability mitigation with seismic isolation devices

On the basis of the results of the seismic vulnerability assessment of the artwork (see Sect. 4.4.2) in order to ensure the safety of the bust during the seismic events, it was decided for the realization of an isolation system, such as to prevent the onset of dangerous oscillations or in extreme cases, the overturning of the Bust/Pedestal system.
Given the sensitivity and uniqueness of the artwork, the seismic isolation is a safer solution than other possible measures for mitigation of seismic risk.
In fact, solutions to decrease the tendency of the system to oscillate, such as for example the enlargement of the pedestal or its cut, entail the fact that the work itself, even if protected by the oscillations, would still be subject to a major seismic acceleration, forcing the retention system which connect the bust to its pedestal, and exposing the artwork to probably dangerous localized tensions.
On the other side, seismic isolation transfers to the artwork only a reduced acceleration, much smaller compared to the input, allowing its installation in the context of the new layout of the museum, without heavy modification of the original apparatus.

4.4.4.1 Design of the seismic isolation device

To guarantee the safety of the bust during the seismic events, it is taken into account the implementation of a seismic isolation system, to prevent the trigger of dangerous oscillations or even the overturning of the artwork. For this peculiar application, ISOLART® PENDULUM isolation system is adopted. It comprises double concave curved surface sliders (or pendulum isolators) designed, manufactured and tested by *FIP Industriale*. The well-known technology of pendulum isolators is adapted to the specific needs of the application to art objects, i.e. objects with very small mass if compared to structures such as buildings or bridges. Four isolator devices are placed on a steel platform, properly designed to safely transfer the vertical loads on the perimeter masonry walls without loading the underlying masonry vault. To this aim the structure consists of two parts: the first is a steel deck supported by two main beams on which the isolation devices are placed, the second part is a ribbed steel plate on which the statue is placed, free to slide with the isolation devices during the seismic events.
Both the response spectra obtained at the ground and at the 2nd floor are considered for the design of the isolation system. For the range of periods typically assumed for the isolation devices, no amplifications of the displacement spectra with the height occur, as found in Sect. 4.3.2. Therefore, in the following only the results related to the

displacement ground floor spectra are reported. Concerning the acceleration, the amplification given by EC8 is considered, since, with the prescription that the minimum acceleration must be not lower than PGA, it provides the most conservative estimation of the floor acceleration for long periods, as highlighted in Sect. 4.3.2.2.2.

To proceed with the design of the isolation system it is necessary to define size and weight of the supported object and the characteristics of the seismic demand in terms of expected acceleration and displacement. To find the optimal characteristics of the isolation device, the parameters affecting the performance of the isolated system are defined. From the numerical point of view, the isolator with double concave sliding surface can be treated as a simple pendulum, using the equivalent radius of curvature. Following a linear equivalent approach suggested by (Naeim and Kelly, 1999) it is possible to identify three quantities that defines the performance of the pendulum isolators, respectively effective stiffness, effective period, and effective damping of the equivalent linear elastic system:

$$K_{eff} = \frac{W}{R_{eq}} + \frac{\mu W}{D} \quad [N/m] \tag{40}$$

$$T_{eff} = 2\pi \cdot \sqrt{\frac{1}{g\left(\frac{1}{R_{eq}} + \frac{\mu}{D}\right)}} \quad [s] \tag{41}$$

$$\xi_{eff} = \frac{2}{\pi} \cdot \left(\frac{\mu}{\mu + \frac{D}{R_{eq}}}\right) \quad [\%] \tag{42}$$

The performance of the isolation devices depends on four parameters: the weight W, the equivalent radius of curvature R_{eq}, the friction coefficient μ, and the design displacement D. The weight W is the only parameter known a priori, being determined by the object itself, while R_{eq} is imposed by the designer of the isolation system. As regards the friction coefficient μ, it is necessary to accept some approximations, assuming a range of variability on the basis of design experiences and experimental tests carried out on similar devices. Finally, the design displacement must be evaluated through an iterative process controlling its consistency with the response spectrum of the site. In detail, to determine stiffness, damping, and period of the device, it is necessary to assume a first attempt's design displacement: generally, the spectral displacement for $T = T_D$ (period over which the spectral displacement assumes constant value) and conventional damping ratio ξ=5%, thus obtaining values T_{eff} and ξ_{eff}. With the last one it is possible to express an

additional damped response spectrum, from which a second attempt value of the spectral displacement is taken. According to NTC 2008, the response spectrum is scaled by the quantity η , for ξ greater than 5% up to maximum of 30%, in absence of more in-depth analysis. By applying such an iterative method, a series of charts are obtained (Figure 114-Figure 117), varying both the equivalent radius of curvature R_{eq} (1000÷4000 mm) and the friction coefficient μ (0,005÷0,055). The performance of the seismic isolation system is reported in terms of maximum expected displacement and acceleration, damping and effective period. In the following graphs, the highlighted area indicates the zones obtained selecting the points of the domain that fulfil the requirement imposed by NTC 2008: $\xi \leq 30\%$ (the limit condition is represented in each graph by dotted line), and some other standard-optimization conditions such as $\xi \geq 5\%$, $T > T_D = 2{,}36s$, and the self-centering condition, that occurs for $D/R \leq \mu$. Moreover, in the graphs the dashed lines indicate the points that do not meet the requirement of $T > T_D$, while the symbols "X", for each R_{eq}, correspond to the maximum friction coefficient for which the self-centering can occur. Figure 114 shows the effective period in function of the curvature radius. Considering equation (16) it can be observed that T_{eff} is inversely related to the square root of μ, while directly proportional to the square root of R_{eq} and of D. This means that T_{eff} increases with the increase of R_{eq} and the decrease of μ. The effective damping is reported in Figure 115. The graph shows how the damping of the system is strongly influenced by the friction coefficient and, to a lesser extent from the R_{eq}. Once T_{eff} and the damping are considered, it is possible to observe the expected displacement of the isolation system, Figure 116. Remembering that, for a constant value of μ, effective damping increases with R_{eq}, it is possible to note the progressive decrease of D. Similarly, it is evident as the displacement is reduced with increasing of μ (and therefore of damping). Finally, Figure 117 shows the expected spectral acceleration as function of R_{eq} for different values of μ. The general trend of the curves shows the decrease of the acceleration with R_{eq}, as the radius increases the period. To determine the minimum radius to be adopted for the isolation devices, the acceleration tolerated by the artwork is assumed, i.e. $a_{lim} = a_v = 0{,}149$. As regards the value of μ, it is appropriate to assume a range of study, to derive the maximum acceleration (for the highest value of μ) and the maximum displacement (for the lowest value of μ). Typically, μ has to be low enough to guarantee the occurrence of the sliding motion for low values of S_a, and at the same time high enough to guarantee sufficient damping characteristics, reducing as much as possible

the displacement request of the device.

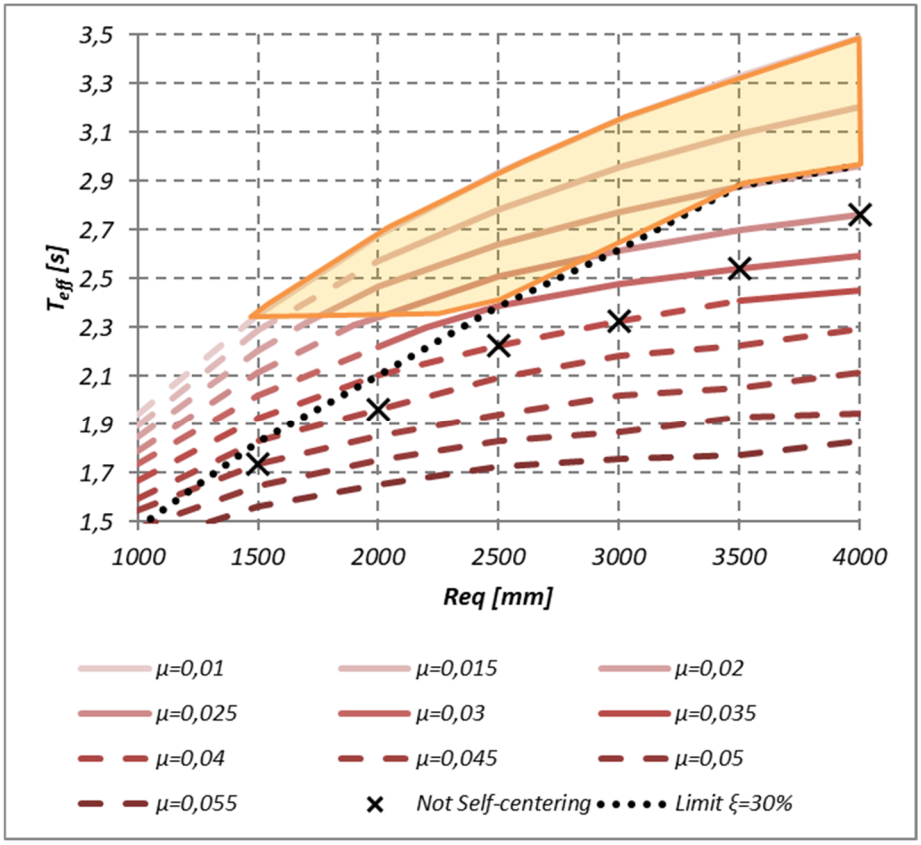

Figure 114 – Effective period

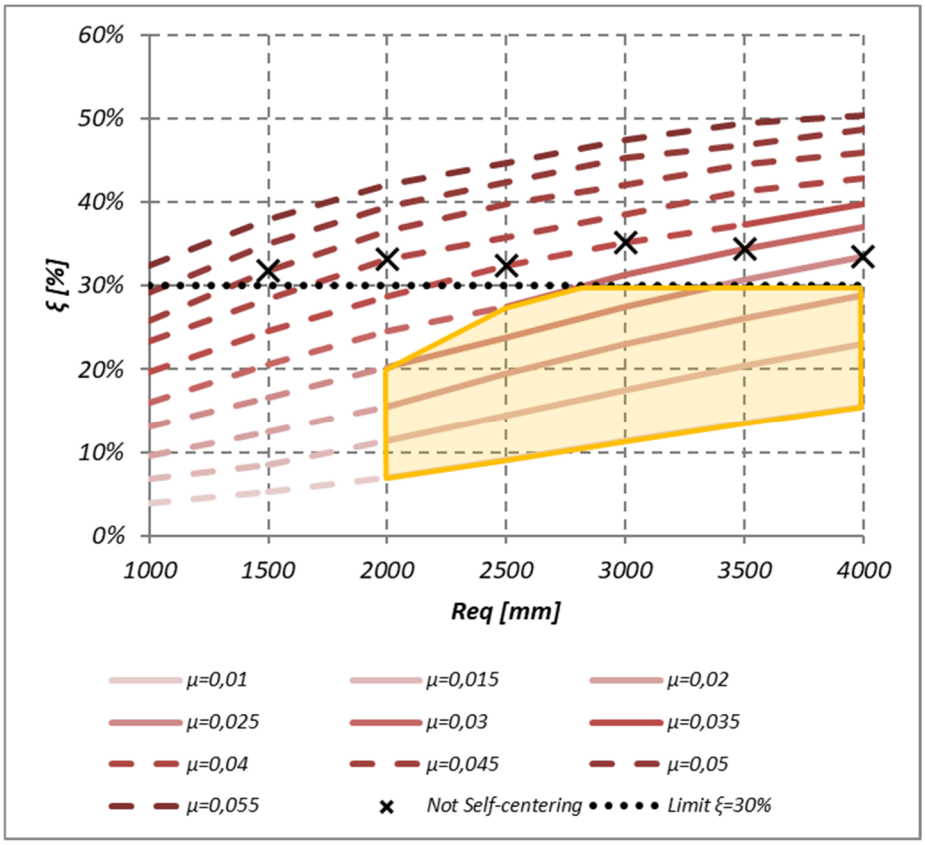

Figure 115 – Effective damping

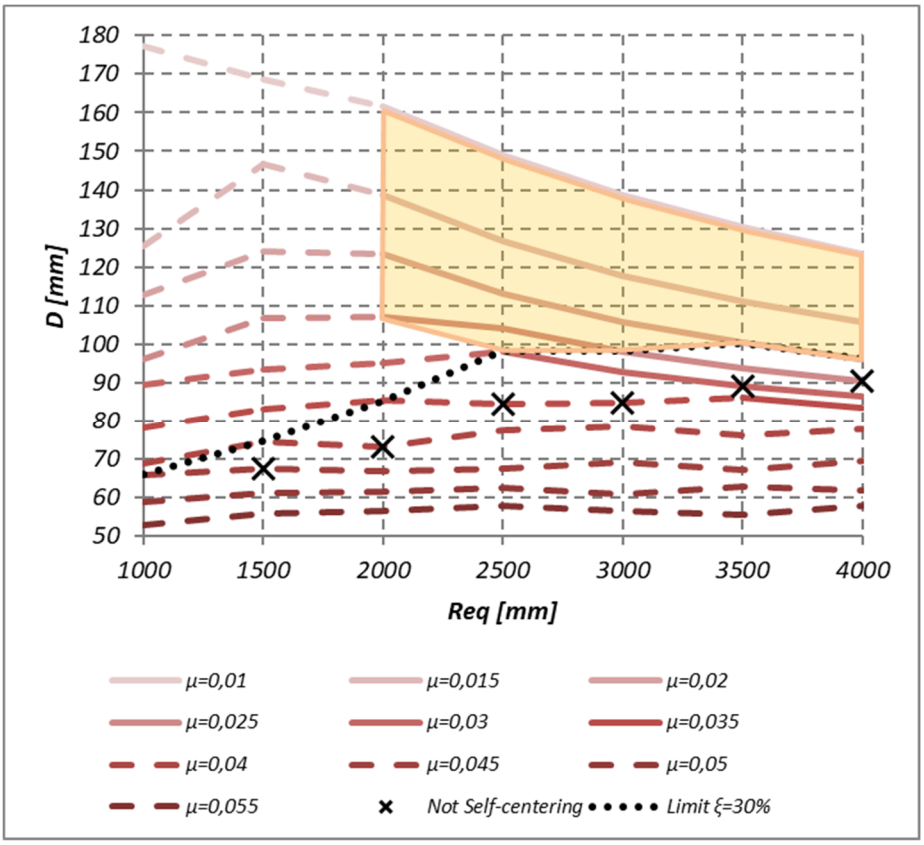

Figure 116 – Displacement

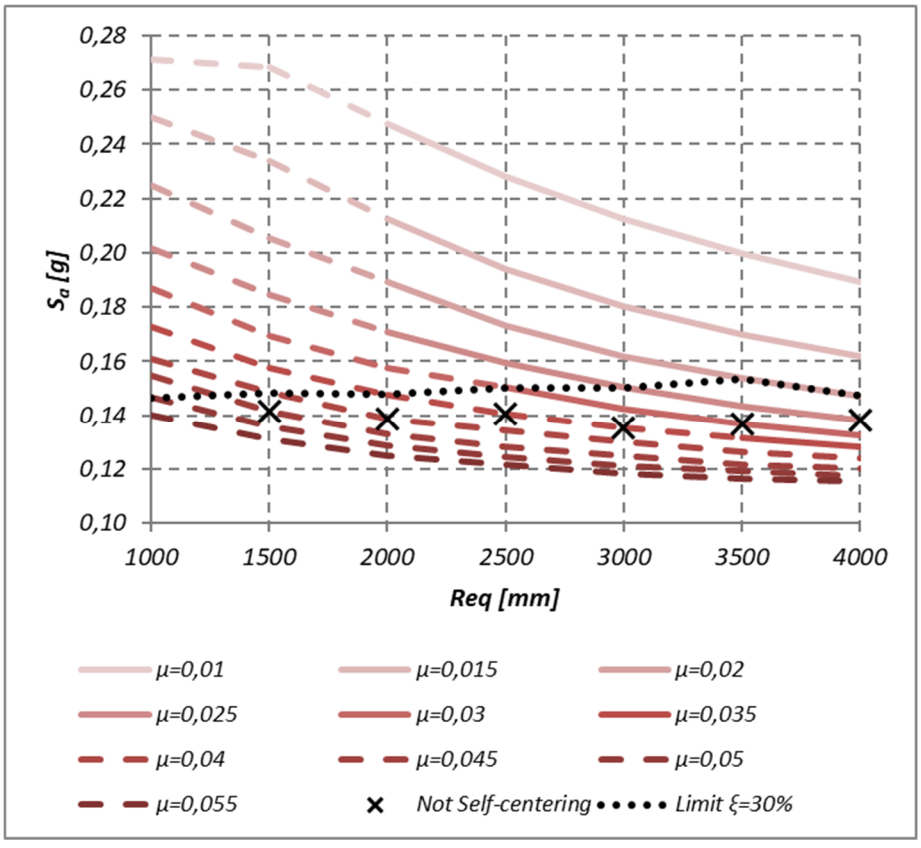

Figure 117 – Spectral acceleration

On the basis of the results of this analysis, an isolator with equivalent radius of curvature $R_{eq}=3500\ mm$ is adopted. The friction coefficient of the interface between steel surface and slider, given the design and experimental experience, is assumed to be in the range 0,035-0,05. Indeed, due to the small weight of the object, the pressure on the sliding surfaces of the isolators is very low, and consequently it is not easy to reach low values of friction coefficient as in isolators for structures. The design displacement for the isolation system is assumed ±180mm, higher than the maximum displacement calculated for the minimum friction coefficient at $R_{eq}=3500\ mm$ (Figure 116), for the sake of safety.

4.4.4.2 Experimental tests on the isolation system

In order to verify the performance, the isolation system is tested in collaboration with *FIP Industriale*. The qualification tests performed are described in Castellano et al. (2016). The description there reported are fully reproduced in the following for clarity and completeness.

The tests are carried out according to European Standard EN 15129 (2009) Anti-seismic devices. The only variation is that the horizontal tests are carried out on the four isolators all-together, due to the small vertical load acting on them and the resulting very small horizontal force. The global mass is carried by the four isolators, and the horizontal displacement is applied through an actuator. The isolators are subjected to a series of sinusoidal movements along two primary axes, at different amplitude, frequency and vertical load. The complete test methods and results will be presented elsewhere. However, the first results show a value of μ generally around the upper value of the considered range, around 5%. As an example, Figure 118 reports the hysteretic cycles measured during one of the tests performed, at the maximum vertical load, maximum displacement and frequency 0,266 Hz.

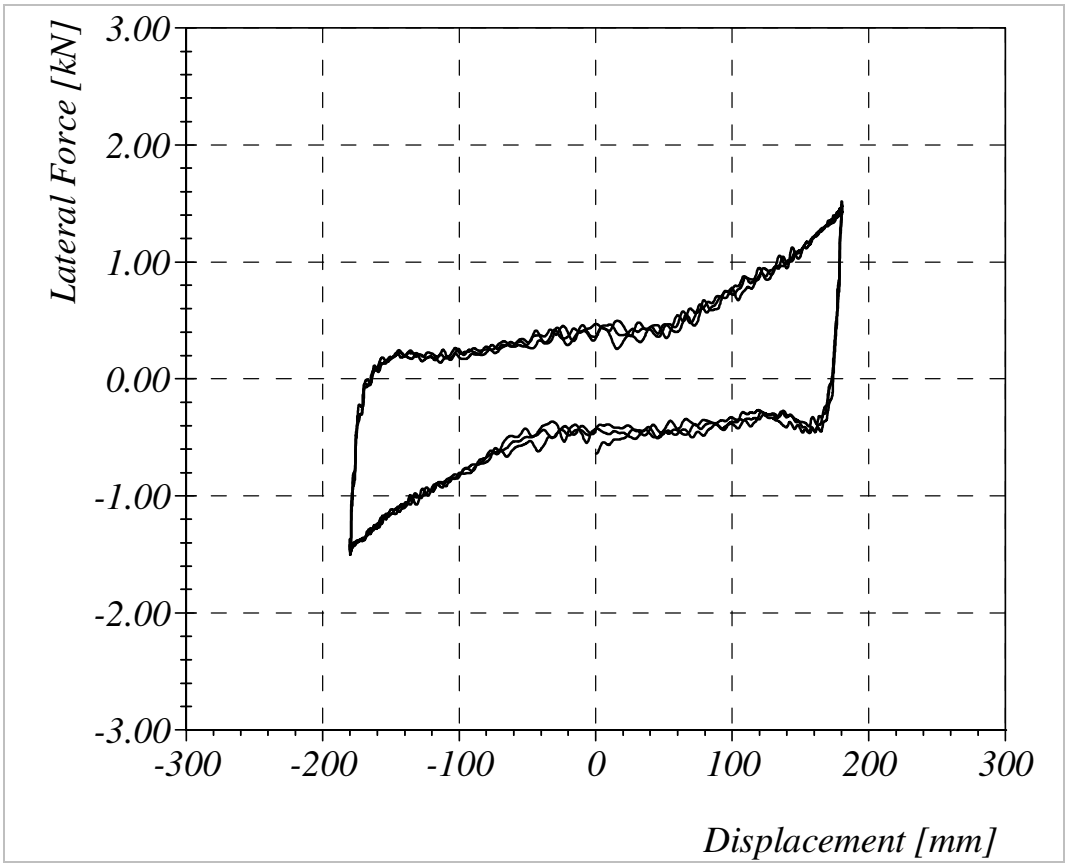

Figure 118 – Preliminary Tests results

To verify the performance of the isolation system, it is tested in the Testing Laboratory of *FIP Industriale*. The tests are carried out as Type Tests according to the European Standard EN 15129:2009 Anti-seismic devices.

A series of static and dynamic sliding tests, with sinusoidal movements applied along the two primary axes, at different amplitude, frequency and vertical load, were performed.

Before and after the sliding testing procedure, the four isolators were tested separately subjected to a 10-minute pre-loading with an axial load equal to the design load N_{sd} (PT1 and PT2 test, see Table 35). A load bearing capacity test was performed on each isolator after the PT1 test (BC test in Table 35) in order to verify the overload capacity of each pendulum when the load is equal to $2N_{Sd}$, applied at zero displacement.

This paper presents the procedure and the results of the dynamic sliding isolation tests, in which case the four isolators were tested all-together, assessing the sliding isolation behaviour of the final system’s configuration.

Test Name		*Label*	*Main DOF*	*Amp. [m]*	*Max Velocity [m/s]*	*Frequency [Hz]*	*Load Shape*	*Vertical Load [kN]*	*No. Cycles*
Pre-test		*PT1*	*vert*	-	-	-	*constant*	*2,24 (8,98)* (*)	-
Load Bearing Capacity		*BC*	*vert*	-	-	-	*constant*	*4,49 (17,95)* (*)	-
Frictional Resistance		*FR*	*long*	*±0,006*	*0,000*	*0,0027*	*triangular*	*8,98*	*1*
Sliding Isolation Tests	*Service*	*S*	*long*	*±0,025*	*0,005*	*0,0320*	*sine*	*8,98*	*20*
	Benchmark	*P1*	*long*	*±0,180*	*0,050*	*0,0440*	*sine*	*8,98*	*3*
	Dynamic 1	*D1*	*long*	*±0,045*	*0,301*	*1,0660*	*sine*	*8,98*	*3*
	Dynamic 2	*D2*	*long*	*±0,090*	*0,301*	*0,5330*	*sine*	*8,98*	*3*
	Dynamic 3	*D3*	*long*	*±0,180*	*0,301*	*0,2660*	*sine*	*8,98*	*3*
	Seismic 1	*E1*	*long*	*±0,180*	*0,301*	*0,2660*	*sine*	*7,85*	*3*
	Seismic 2	*E2*	*long*	*±0,180*	*0,301*	*0,2660*	*sine*	*10,20*	*3*
	Seismic 3	*E3*	*long*	*±0,180*	*0,301*	*0,2660*	*sine*	*11,53*	*3*
	Seismic 4	*E4*	*long*	*±0,180*	*0,301*	*0,2660*	*sine*	*13,68*	*3*
	Seismic 5	*E5*	*long*	*±0,180*	*0,301*	*0,2660*	*sine*	*21,43*	*3*
	Bi-directional	*B*	*long*	*±0,180*	*0,301*	*0,2660*	*sine*	*8,98*	*3*
	Property Verification	*P2*	*long*	*±0,180*	*0,301*	*0,2660*	*sine*	*8,98*	*3*
Post-test		*PT2*	*vert*	-	-	-	*constant*	*2,24 (8,98)* (*)	-

(*) The value in parentheses represent the equivalent vertical load for all four units.

Table 35 – Test matrix for Type Tests on FIP-D XL 10/360(3500) devices

4.4.4.2.1 Test set-up

For the Sliding Isolation Tests the 2000 kN Dynamic Test System of *FIP Industriale* (Infanti et al. 2015) was used. The test system was hydraulically powered, feedback controlled and governed by an MTS Flex Test 60 controller by means of the MTS MPT 793.10 software. The actuator characteristics are: Maximum load ± 2000 kN; maximum displacement ± 300 mm; maximum nominal velocity 200 mm/s at maximum load.

The four isolators were tested together, anchored between an upper and a lower platen. The lower platen was fixed to the base of the test rig frame, while the upper one was fixed on the top of the devices, connected to the piston actuator by means of a steel rod, as shown in photo in Figure 119 and in the test set-up scheme in Figure 120. The upper platen was also used for the application of the vertical load (platen dead load). Depending on the vertical load test requirement, steel platens were removed or added. Horizontal

load and displacement measurements were carried out using a 50 kN load cell and an SSI 650 mm (0,002 mm resolution) displacement transducer, respectively, both connected to the MTS Control System. All measuring chain devices used were HBM.

The tests were conducted by monitoring and recording load and displacement in real time using the DIA-Dem (National Instruments) data acquisition and processing software. The same software was used for data post-processing. All tests were performed at room temperature.

During the data elaboration the inertial effects were evaluated considering the average acceleration of the horizontal movement, in order to depurate the horizontal force signal measured from the load cell.

Figure 119 – Test set-up. ISOLART® PENDULUM devices under dynamic sliding testing.

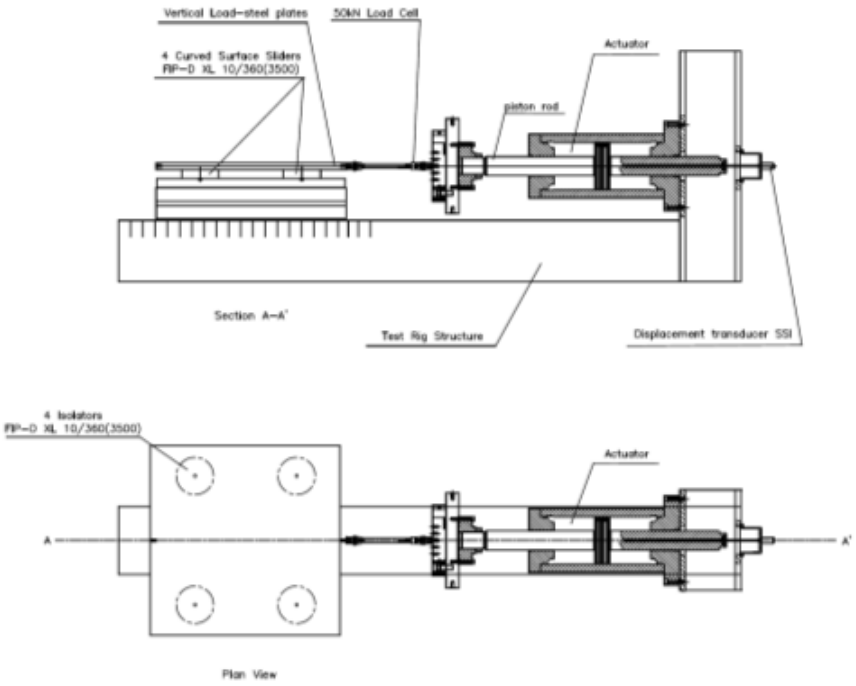

Figure 120 – 2000kN Dynamic Test set-up scheme.

4.4.4.2.2 Test procedure

The Type Tests were performed according to EN15129, in several steps, as illustrated in Table 35. The tests are described in detail in the following paragraphs.

4.4.4.2.3 Frictional resistance (FR)

To verify the maximum lateral force developed by the isolators under service conditions in their final configuration (tested together), the vertical load equal to the design load N_{sd} = 8,98kN (2,24kN x 4 isolators) was imposed at zero displacement, by means of a steel platen placed on the top of the isolator, for 30 minutes. Then a constant sliding velocity was imposed of v ≤ 0,1 mm/s for 1 min.

4.4.4.2.4 Sliding isolation tests

The scope of these tests was to verify the dynamic behaviour of the curved surface sliders (tested together) in terms of frictional resistance (coefficient of friction), damping capacity, as well as stability under repeated cycling. The sliding tests were conducted in accordance with the test matrix provided in Table 35.

The first test (Service-S) was aimed at evaluating the maximum horizontal force developed by the isolation system at maximum non-seismic movement (peak velocity 5mm/s, 20 cycles) under a vertical load equal to the design load N_{sd}. Then maintaining the same vertical load, 3 cycles were imposed to the design seismic displacement d_{bd} =±180 mm and at a peak sliding velocity of 50 mm/s (Benchmark Test: P1).

The dynamic behaviour was verified measuring the force-displacement curves for three values of displacement (Dynamic Tests – 25, 50 and 100% of the design seismic displacement) and for five values of vertical load (Seismic Tests), applying in each of said tests 3 fully reversed cycles at the peak velocity (301 mm/s). According to the European Standards the seismic tests should be performed applying the minimum (7,85kN) and maximum (10,20kN) design vertical load, corresponding to the increase or decrease of vertical load on the single isolator due to the overturning effect of the statue and its basement during the maximum design earthquake. In this case, for research purposes, and with reference to other possible applications of the same isolation system, a series of three additional tests were performed increasing the vertical load up to 21,43kN.

The displacement input waveform was sinusoidal of the type $d_{(t)} = d_x \cdot sin(2\pi \cdot f_x \cdot t)$. The frequency f_x was chosen in relation to the displacement d_x in order to keep the peak

velocity specified value v_{Ed} ($f_x = \frac{v_{Ed}}{2 \cdot \pi \cdot d_x}$). The main frequency f_0 has been calculated as the reverse of the period associated to the restoring stiffness equal to $T = 2\pi \cdot \sqrt{R/g}$, in which R is the equivalent radius of curvature of the pendulum isolators R_{eq} and g is the gravity acceleration. So, the peak velocity was considered as $v_{Ed} = \sqrt{\frac{g}{R}} \cdot d_{bd}$.

The verification of the bi-directional dynamic behaviour of the isolator was carried out at maximum displacement and maximum velocity (Bidirectional test). The device was rotated at 90° and 3 cycles were imposed applying the design load $N_{sd.}$

The device's maximum lateral force and friction coefficient were finally verified by imposing 3 cycles at an amplitude equal to the design seismic displacement at peak velocity and by applying the design vertical load (Property Verification test).

4.4.4.2.5 Test results

The device when tested under service conditions at low velocity (Frictional resistance and Service tests) exhibited a stable lateral force during cycling.

Figure 121 gives the hysteretic cycles of the isolators under service testing (20 cycles), demonstrating the stable cycling behaviour obtaining a maximum lateral force of 0,50 kN. The breakaway force measured in the frictional resistance test is about 1 kN, guaranteeing a sufficient resistance to movement due to unexpected forces that could be applied during maintenance operations of the statue.

The dynamic sliding isolation tests were performed in 3 fully reversed cycles, thus the dynamic coefficient of friction μ_{dyn} was calculated as:

$$\mu_{dyn} = \frac{1}{3} \cdot \sum_{i=1}^{3} \frac{A_{h,i}}{4 \cdot N_s \cdot d_x} \quad [\%] \qquad (43)$$

where, according to EN 15129, $A_{h,i}$ is the area of a single hysteresis cycle, N_s is the vertical load to which the devices are tested, and d_x is the total displacement of the tested apparatus.

Figure 122 presents the force-displacement curves obtained when the isolation system was tested at different frequencies and displacements, but at the same peak velocity and under the design vertical load (Dynamic Tests). The maximum horizontal force F_{max} exhibited by the device was 0,42 kN, 0,82 kN and 1,37 kN at each amplitude, respectively, obtaining a dynamic coefficient of friction μ_{dyn}=5,3% at the design seismic displacement (Test D3). The secondary stiffness of the isolators (restoring stiffness K_R) at maximum displacement was found K_R=2,74kN/m, substantially equal to the theoretical value K_R=

N_{sd}/R.

The frictional resistance behaviour of the isolators tested under different vertical loading conditions (seismic tests) is shown in Figure 123, including the Dynamic test D3 (design vertical load). In the range of load corresponding to this application (tests D3, E1 and E2), the friction values ranges between 5,10% ÷ 5,50%. When the load is doubled (test E5) the friction decrease is noticeable (μ_{dyn}=4,80%), confirming the well-known decrease of friction coefficient at the increase of vertical load. The maximum dynamic friction variation between the minimum and maximum vertical loads of such application (E1 and E2 tests) compared to the design vertical load (D3 test) was about 7%.

Figure 124 compares the hysteretic cycles obtained at each loading condition. The devices demonstrate a constant maximum lateral force at each test for all three cycles. The F_{max} ranges from 1,22 kN (for 7,85 kN vertical load) up to 2,28 kN (for 21,43 kN vertical load).

The bi-directional test provided a difference between the two orthogonal directions of 9,4% on the dynamic coefficient of friction and 0,8% on the equivalent viscous damping. This demonstrates the substantial independence on behaviour of the isolation devices relative to the direction of movement, even after a large number of cycles during the whole test procedure (Figure 125). The maximum force obtained was 1,37kN for Dynamic test D3 and 1,39kN for the Bi-directional test.

Upon final inspection performed after disassembly of all four pendulum isolators, the units were undamaged and the sliding material did not show signs of wear.

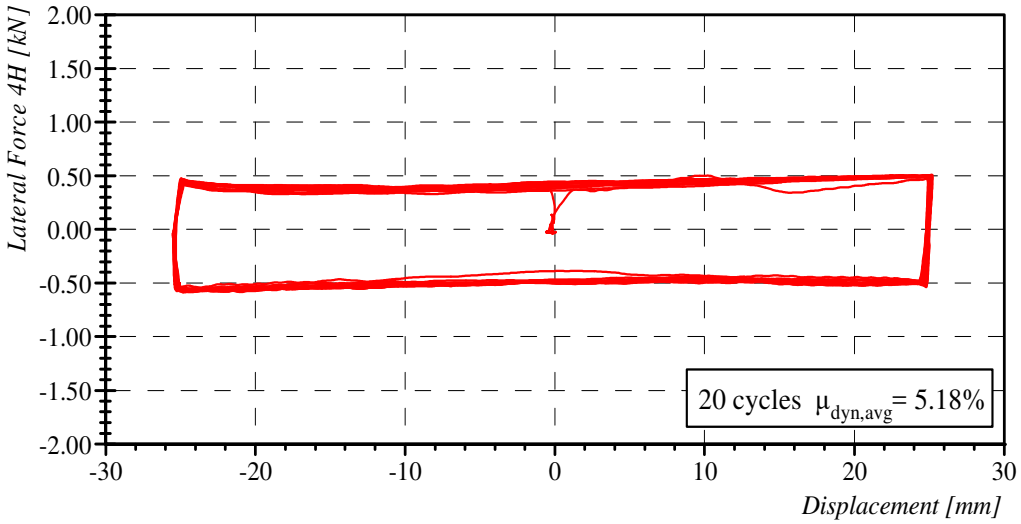

Figure 121 – 20 Hysteretic cycles during Service Test

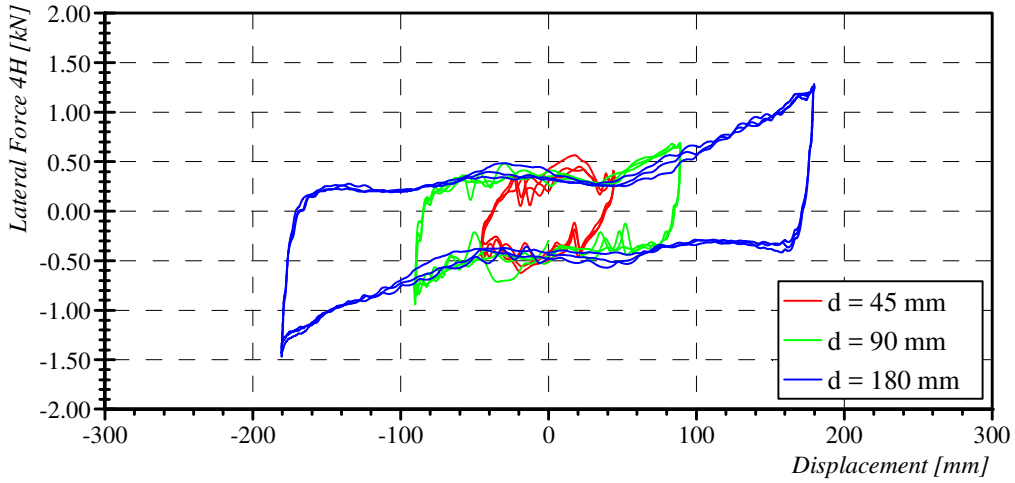

Figure 122 – Hysteretic cycles obtained during the Dynamic Tests. Four isolators FIP-D XL 10/360(3500) tested at peak velocity and with three amplitudes equal to 25%, 50% and 100% of the design seismic displacement.

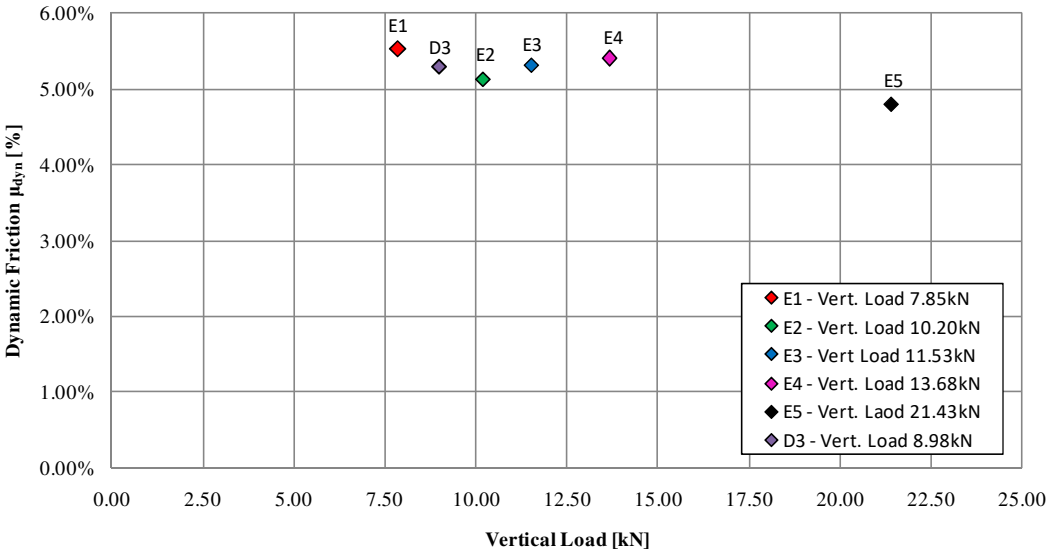

Figure 123 – Dynamic friction coefficient vs. Vertical load (test at maximum displacement at peak velocity).

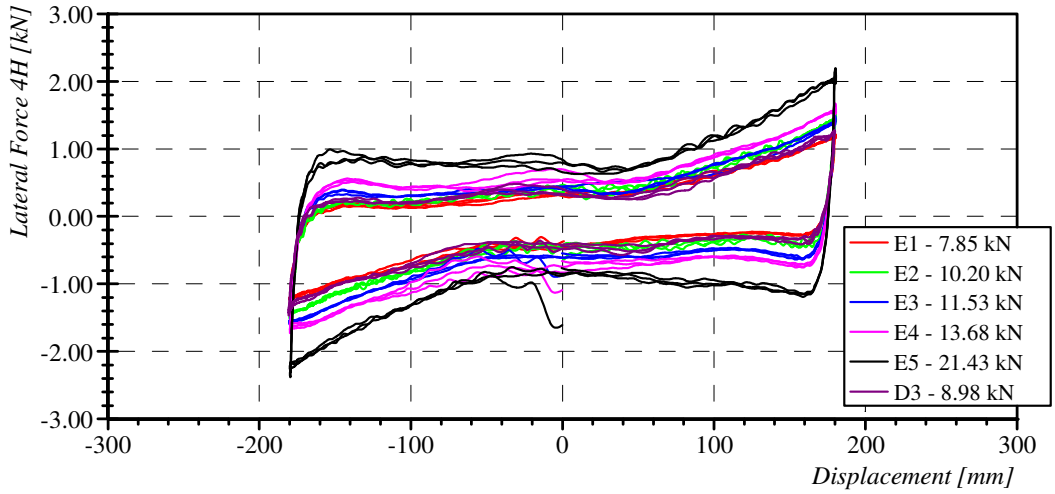

Figure 124 – Hysteretic cycles obtained during the Seismic Tests and Dynamic Test D3. Isolators tested at max. displacement and peak velocity under different vertical loading conditions.

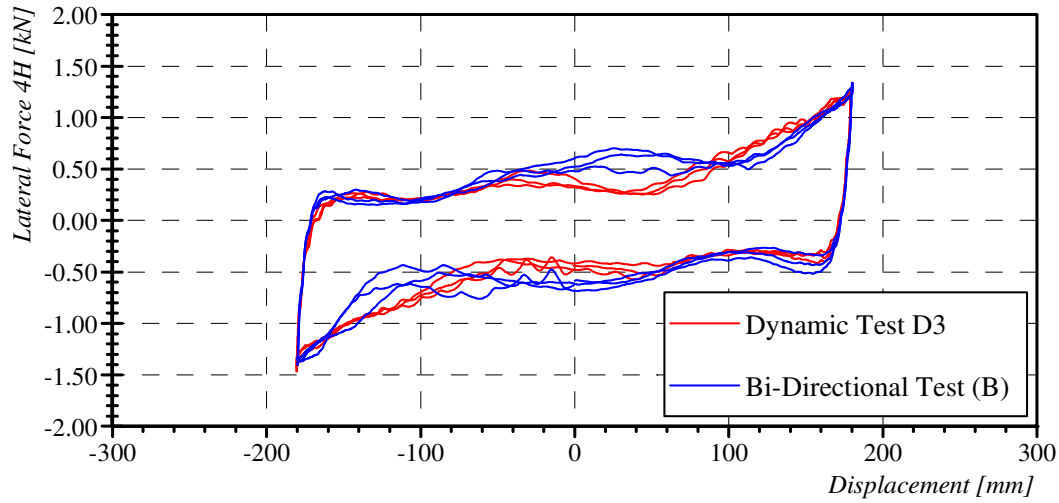

Figure 125 – Comparison of the hysteretic behaviour obtained at maximum load and displacement during Dynamic Test (D3) and Bi-directional Test (B)

4.4.4.3 Numerical analyses

On the basis of the test results, more detailed non-linear analyses are carried out. A series of non-linear time histories analyses is performed, carefully taking into consideration the effect of the amplification and modification of the seismic input due to the height and the frequency of the building.

For each set of spectrum compatible accelerograms (*RANGE1* and *RANGE2*), the 7 couples of floor seismic signals are considered (see Sect. 4.3.2.2.1). With such signals, 7 time histories analyses are performed, by using the Friction pendulum link (*midas GEN* 2015), whose parameters are calibrated according to (Berto et al., 2013, Baggio et al., 2015a, Baggio et al. 2015b).

Initial stiffness of the isolator	$K_1 = 65\ N/mm$
Friction coefficient at low velocity	$\mu_{slow} = 0{,}0528$
Friction coefficient at high velocity	$\mu_{fast} = 0{,}0528$
Velocity evolutive ratio	$r = 0{,}01$
Equivalent Curvature Radius	$R_{eq} = 3500\ mm$

Table 36 – Parameters of Link Friction Pendulum (midas GEN 2015)

The results of these analyses show a general efficiency of the isolator system in reducing the acceleration acting at the base of the pedestal to a value compatible with the safety of the artwork, while respecting the maximum tolerable displacement for the isolation device (+/- 180mm).

In particular, the critical acceleration that induces rocking to the Bust/Pedestal system in the post-cutting pedestal condition was equal to 0,176 g which, even considering a confidence factor FC equal to 1,35, it becomes 0,13g.

4.4.4.3.1 First set of accelerograms – *RANGE1*

Considering the first set of accelerograms, corresponding to *RANGE1* set, Figure 126, Figure 127, Figure 128, Figure 129, show the hysteresis loops for the 7 pairs of accelerograms for both the longitudinal direction and for the lateral one for both the application of combinations of signals.

It is worth noting that, in the more difficult situation (6958), the maximum value for the acceleration is 0,08 g, much lower than the one tolerated by the artwork. Furthermore, the total magnitude of the shift amounts at most around 180 mm.

The good behaviour of the isolated system is shown by the hysteresis cycles given in Figure 126, Figure 127, Figure 128, Figure 129, for which the results of the application of seven seismic bidirectional inputs are given in the longitudinal and lateral direction. It can be seen that the maximum value registered for the acceleration is 0,063g, lower than the acceleration tolerated by the artwork. Also the displacement ranges within the tolerable stroke – 360mm – with maximum values around 90mm.

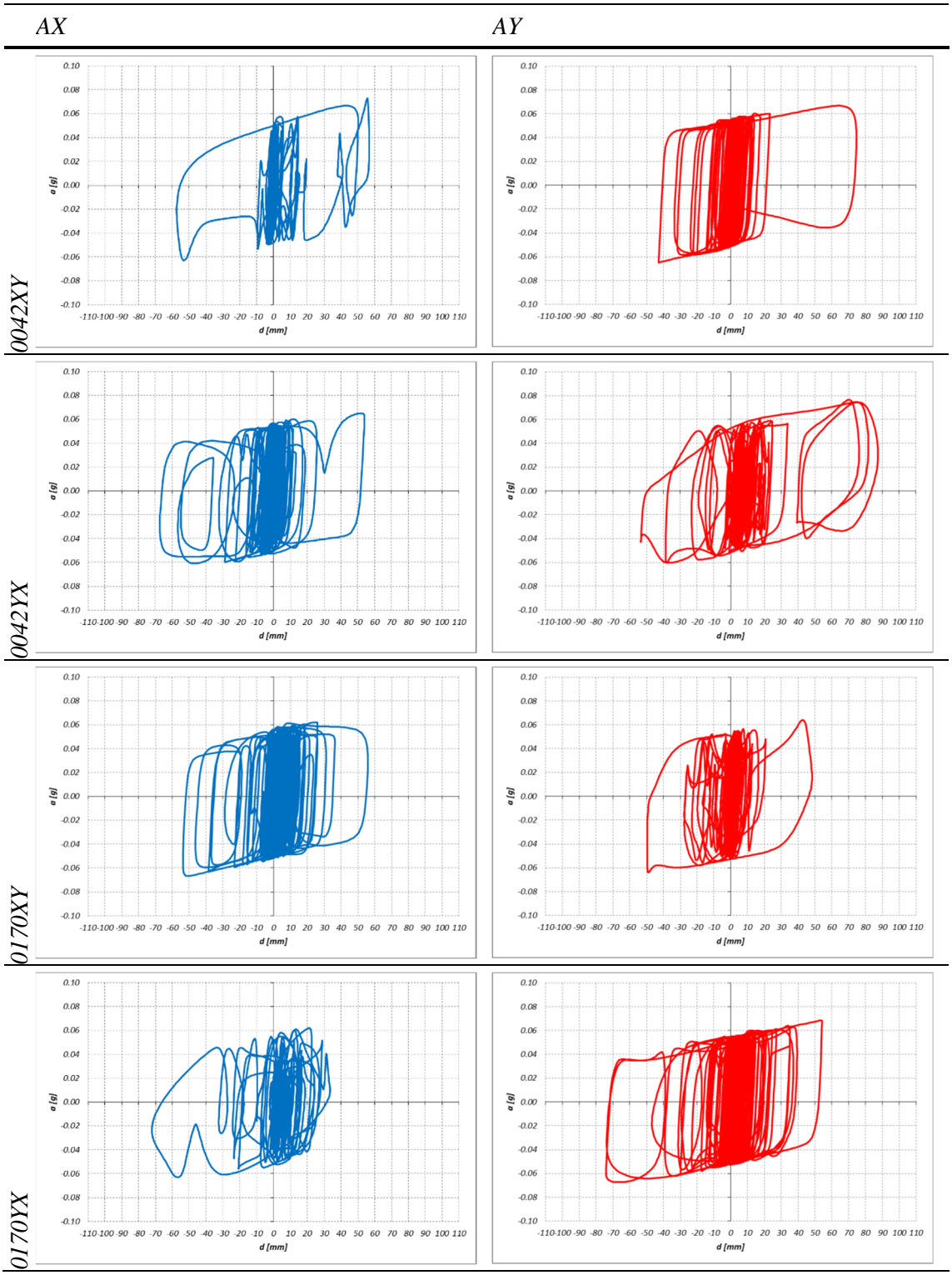

Figure 126 – Hysteresis loops for signals 0042 e 0170 in x e y directions, for both the two possible combinations of application

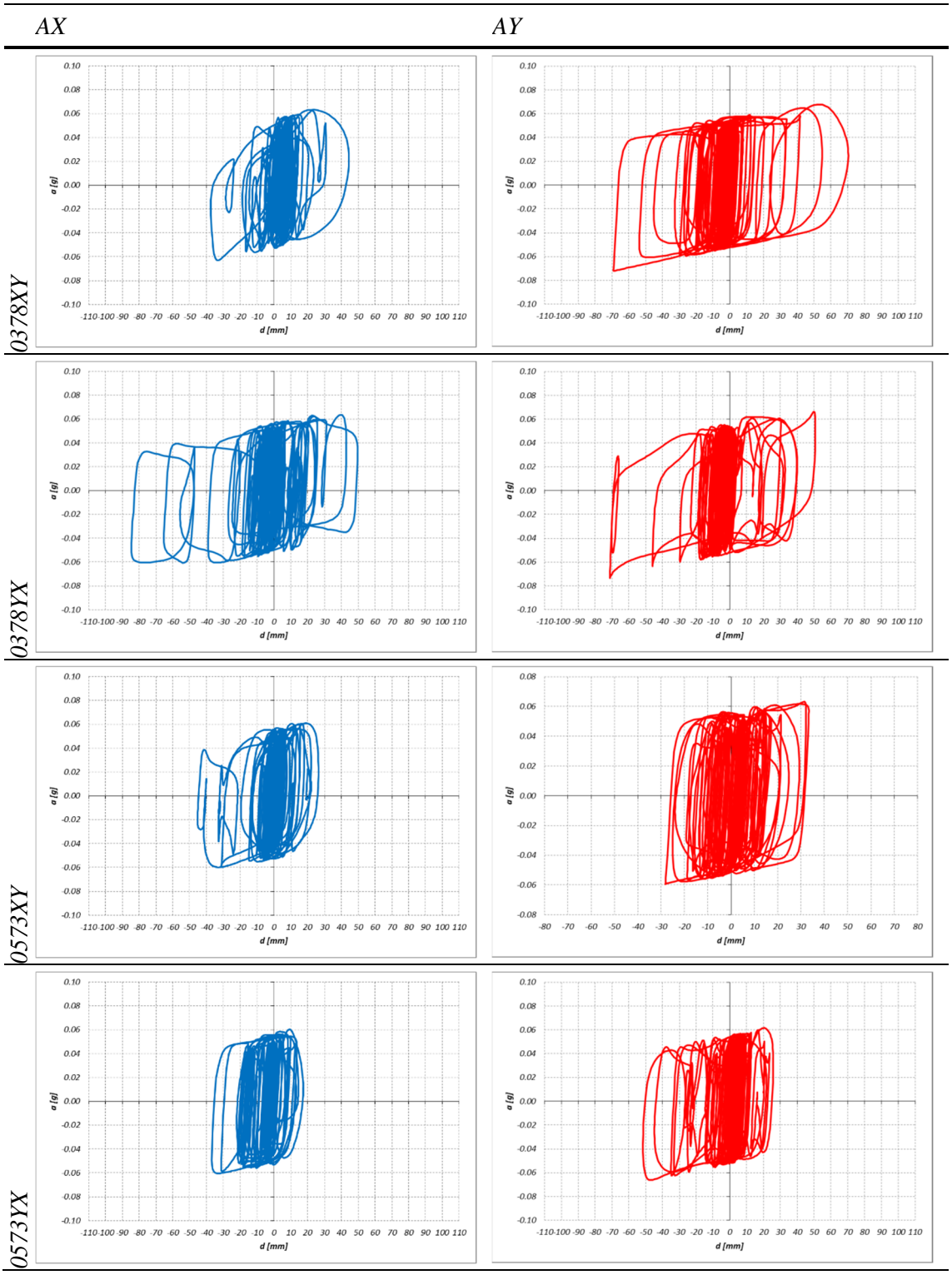

Figure 127 – Hysteresis loops for signals 0378 e 0573 in x e y directions, for both the two possible combinations of application

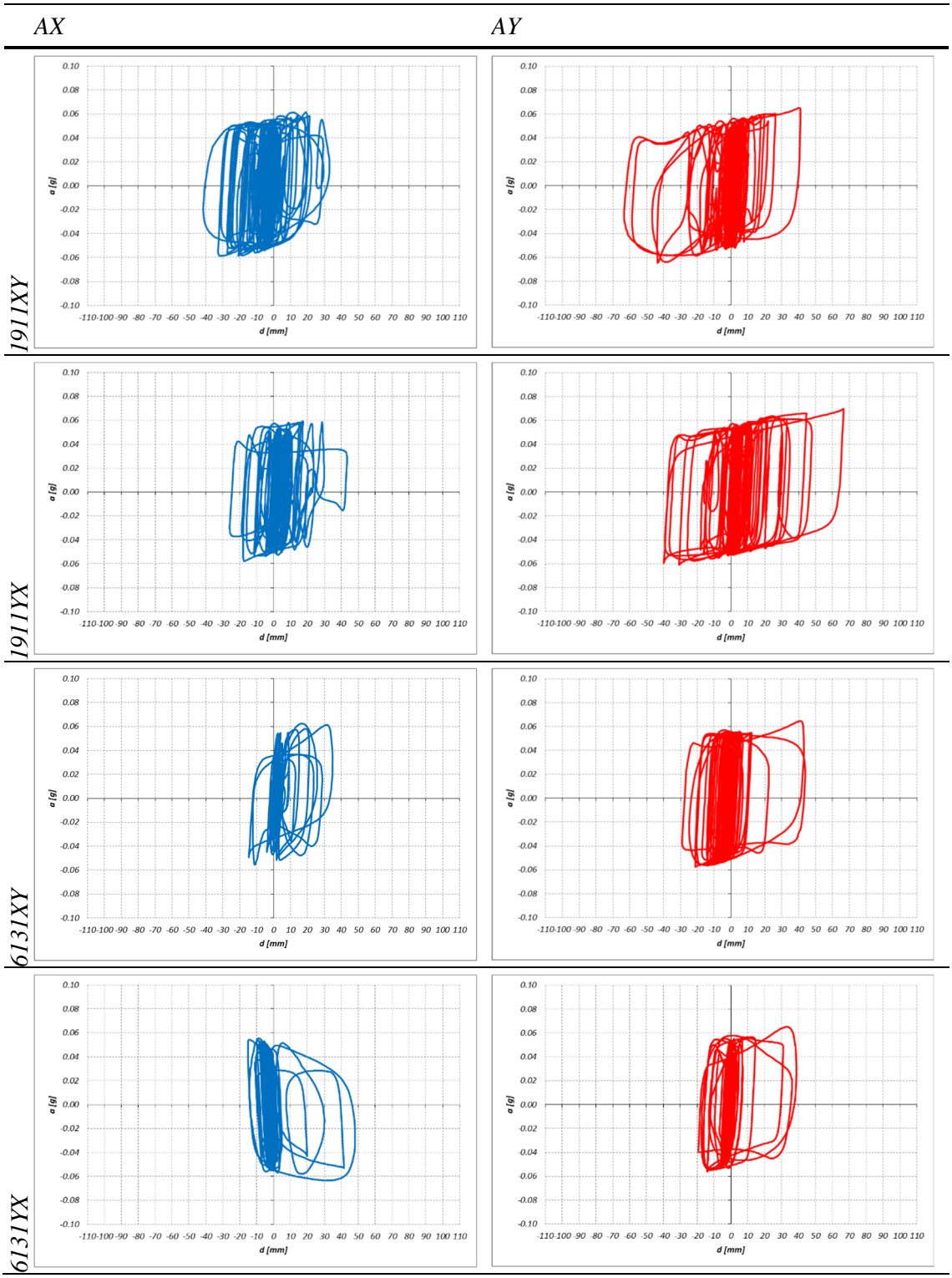

Figure 128 – Hysteresis loops for signals 1911 e 6131 in x e y directions, for both the two possible combinations of application

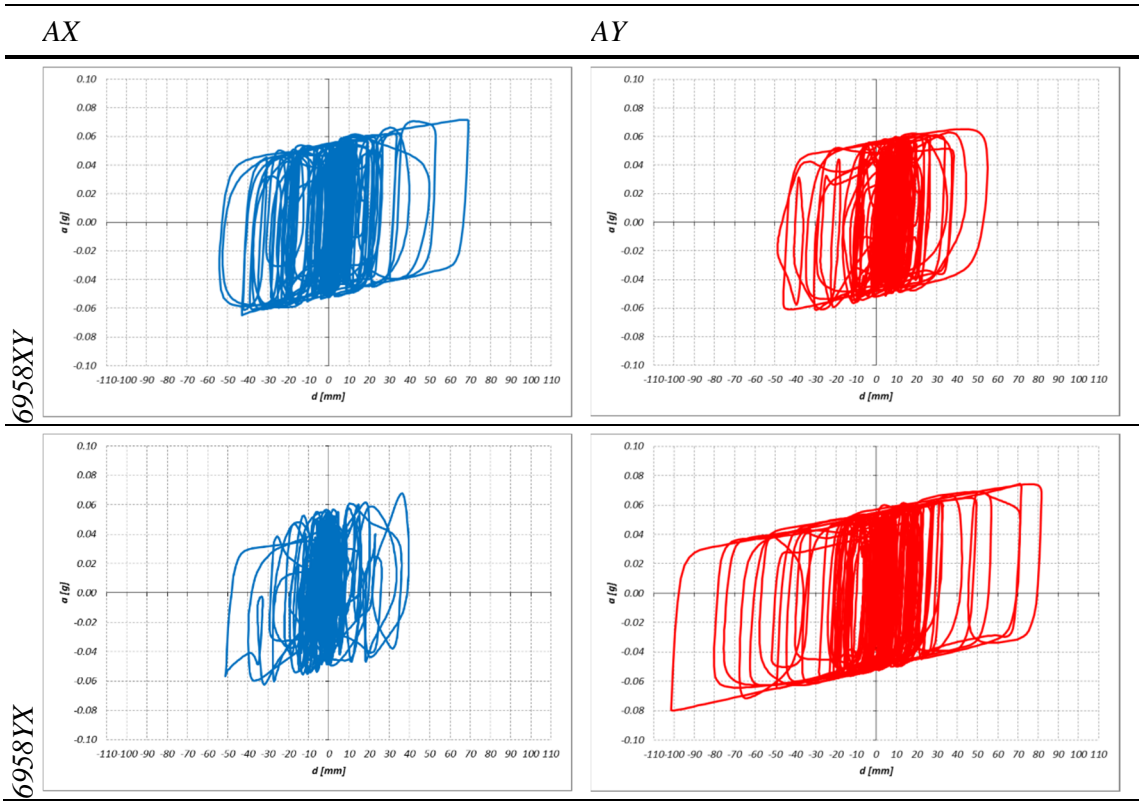

Figure 129 – Hysteresis loops for signals 6958 in x e y directions, for both the two possible combinations of application

4.4.4.3.2 Second set of accelerograms – RANGE2

The numerical analyses of the seismically isolated system are also performed with the second set of spectrum compatible accelerograms (see Sect. 4.3.1.2 and 4.3.1.2.2). Hysteresis cycles for the set are given in Figure 130, Figure 131, Figure 132, Figure 133.

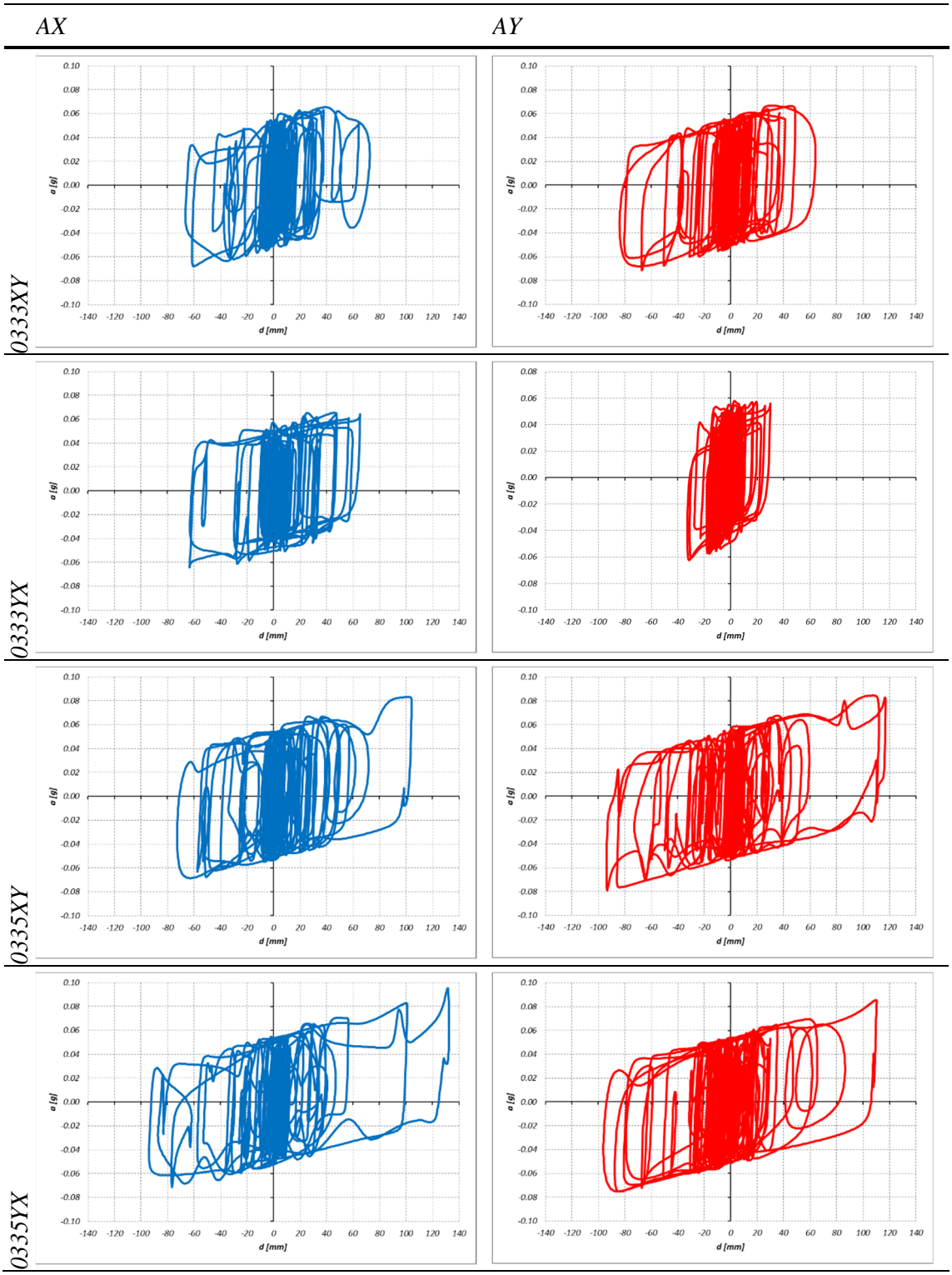

Figure 130 – Hysteresis loops for signals 0042 e 0170 in x e y directions, for both the two possible combinations of application

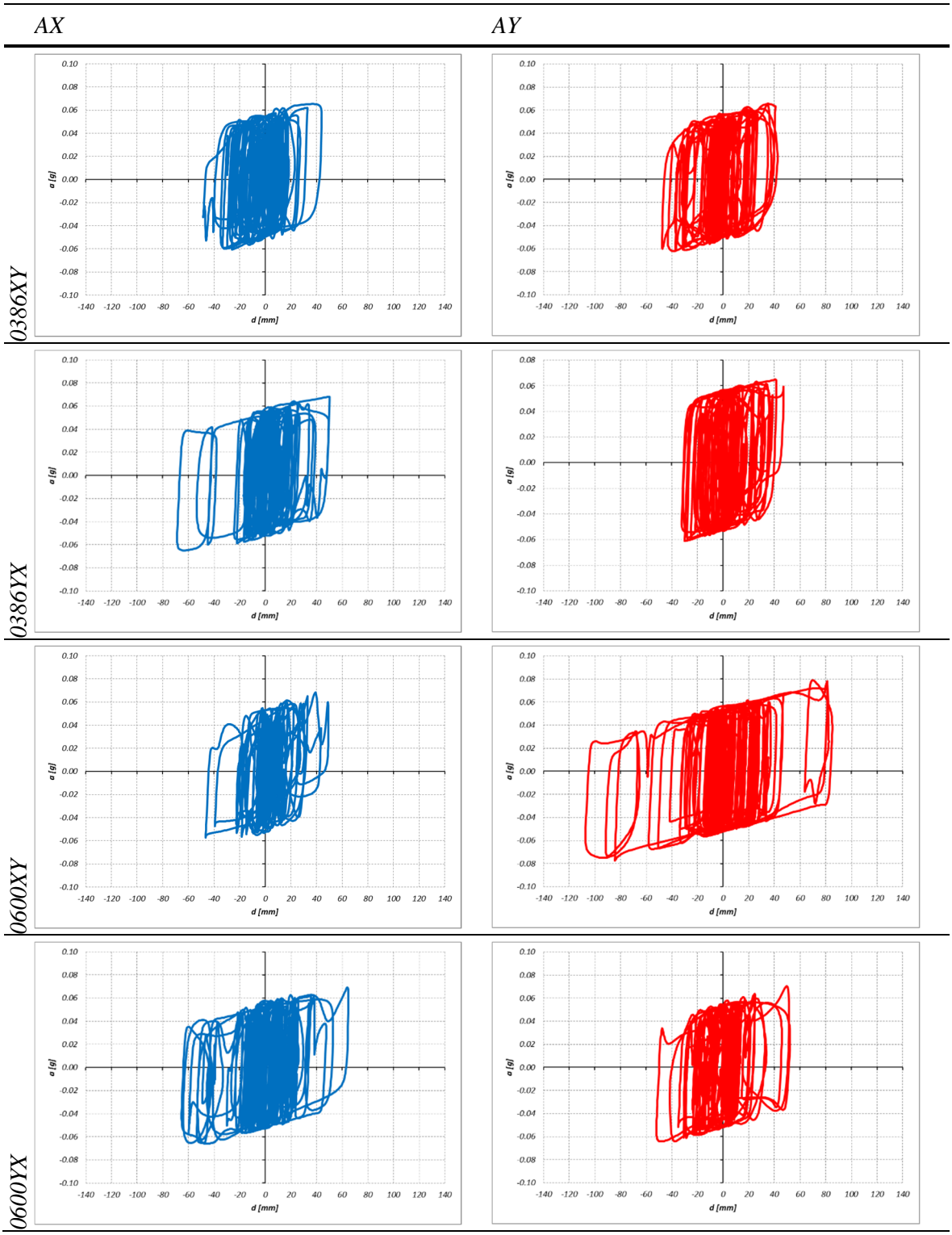

Figure 131 – Hysteresis loops for signals 0378 e 0573 in x e y directions, for both the two possible combinations of application

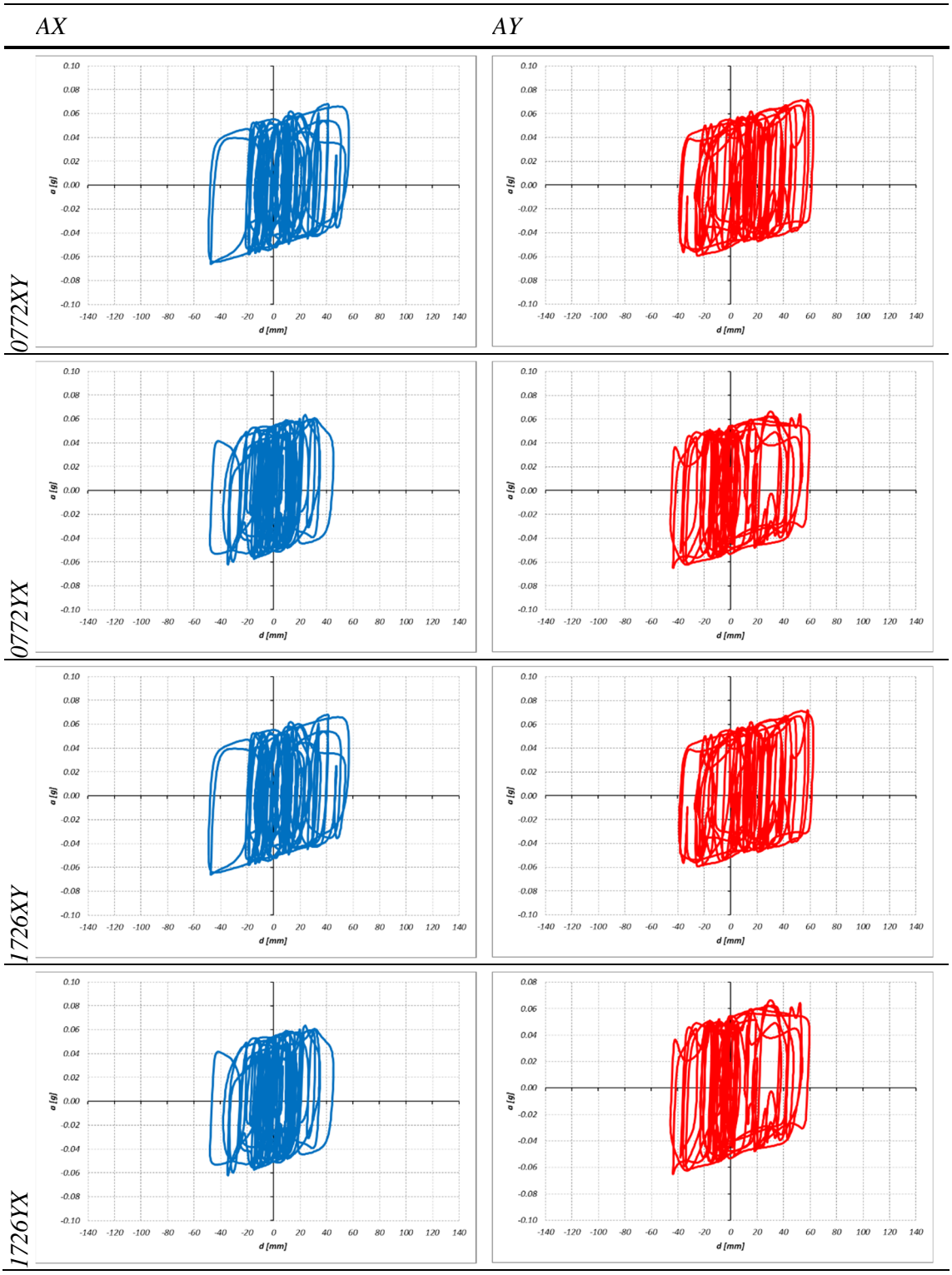

Figure 132 – Hysteresis loops for signals 1911 e 6131 in x e y directions, for both the two possible combinations of application

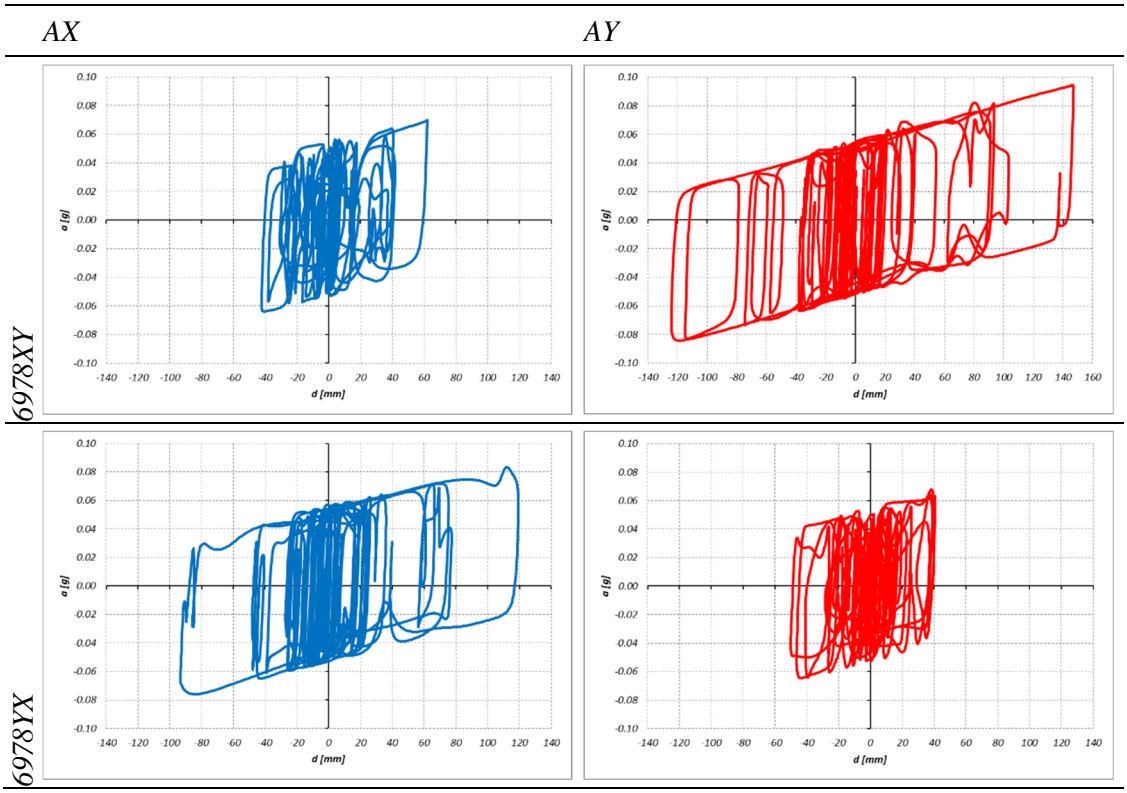

Figure 133 – Hysteresis loops for signals 6958 in x e y directions, for both the two possible combinations of application

4.4.4.4 Comments and conclusion

The results of this preliminary study indicate that the bust of Francesco I d'Este, due to the geometric and inertial characteristics, and to the presence of the pedestal, may be subjected to dangerous oscillations even for low intensity earthquakes. For this reason, it follows the opportunity to proceed with an intervention of seismic isolation at the base of the art object to reduce its seismic vulnerability. To this aim four ISOLART® PENDULUM devices produced by *FIP Industriale*, Figure 134, are placed on a steel platform, which transfer the loads on the perimeter masonry walls, Figure 135.

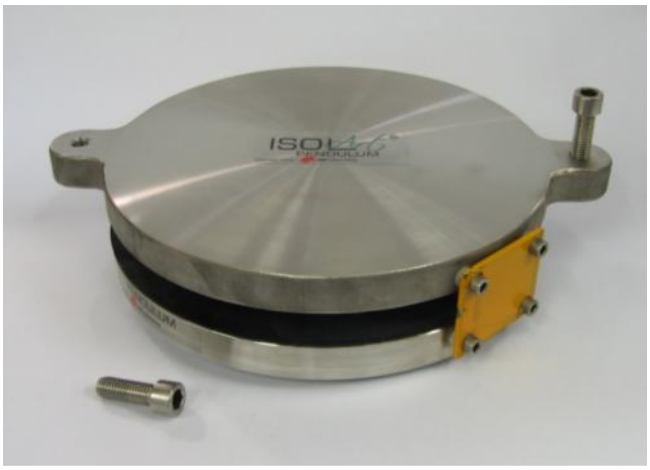

Figure 134 – One of the ISOLART® PENDULUM

Figure 135 – Final installation (courtesy of Galleria Estense)

5 Review of the results and the developed procedures

5.1 Foreword

This chapter presents the review of the main innovations and developed methodologies introduced in the previous chapters re-interpreted and discussed in light of the results obtained by the application of the proposed framework to the case study of seismic isolation intervention for the Bust of Francesco I D'Este..

First of all, the calibration procedure for numerical modelling of DCCSS, described in Sect. 3.3. is briefly recalled in its main and original aspects and discussed.

Then some observations about the assessment of the seismic action at the higher floors, are highlighted.

Finally, the application of the proposed framework of Seismic Risk Mitigation to the Case Study presented in Sect. 4.4.4 is briefly summarized, evidencing the main original aspects.

5.2 Calibration methods for DCCSS seismic isolators

As described in Sect. 3.3, the calibration phase precedes the modelling phase and it is essential for checking whether the existing numerical models for friction pendulum isolator can fit the behaviour of the re-sized device under study. Correct evaluation of the governing parameters is indeed fundamental for the correct design of devices, that otherwise could be unsuitable for the proposed application. The first phase of calibration, concerning an extensive experimental campaign performed in Caltrans Laboratories in University of California – San Diego (see 3.3), involved the following parameters:

- K_1, which is the value of the initial stiffness of the system;
- μ_f, μ_s that are the values of the coefficient of friction and represent respectively the coefficient of friction for high and low sliding velocity, (e.g. Constantinou et al. 1990);
- ξ, which is the value of the numerical damping to assume in the analyses.

In this phase, the sensitivity analyses highlighted the influence of each single parameter on the response and pointed out that their accurate evaluation allows to reach results that describe the global response of the devices in terms of maximum force and displacement. One of the main results of the calibration procedure concerns the modification of the

formula proposed by Naeim & Kelly (1999) to assess the initial stiffness for bilinear modelling of the DCCSS. In comparison to traditional friction pendulum isolator, implemented in civil structures, stiffness K_1 is proportionally higher. Initial stiffness K_1 is related to secondary stiffness $K_2 = W/R$ according to:

$$K_1 = \alpha K_2 \qquad (44)$$

In which α is a multiplying factor usually equal to 51. The proposed correction, which takes into account the reduced dimensions of the new devices, recommends a higher value of "α", equal to 150.

Two different numerical damping ratios for the analyses are proposed: $\xi = 5\%$ was assumed for modeling the physical models used in the experimental tests (made by superposition of concrete blocks), while a value $\xi = 0{,}5\%$ can be considered more reasonable for modeling the statues.

Concerning the coefficient of friction, the values $\mu_{fast} = 2{,}5\%$ and $\mu_{slow} = 1{,}5\%$ were assumed for the analyses, while in a first phase of the research, the effect of a variation of the velocity evolutive ratio "r" is neglected assuming a constant value $r = 0{,}04$, found in literature.

Among the three investigated parameters, the friction coefficient was identified as the most important parameter influencing the behavior of the isolation system in terms of energy dissipation and, on the numerical side, decisive for the correspondence between experimental tests and simulation. Therefore a deeper investigation in the calibration of this parameter was needed. Moreover, an additional research for the improvement of calibration of the friction coefficient is performed, including the evolutive ratio "r" of the formula (N).

The enhanced calibration led to a new set of friction parameter that led to a better simulation of experimental tests. The comparison of such supplementary series of numerical simulations for different values of friction parameters confirmed the role of μ_{fast} and μ_{slow} and furthermore highlights the relevance of the parameter r. A marked variation in energy dissipated per cycle, maximum displacement and maximum value of transmitted shear, are observed also considering for the velocity evolutive ratio r a wider range than that assumed in the first phase.

It is worth mentioning that the simulation performed on HCM (High Centre of Mass – Cfg#4) and HCME (High Centre of Mass and Eccentricity – Cfg#5) models provided good results, proving that the enhanced calibration was suitable for the numerical analysis of such kind of isolated structure.

Finally, the work performed led to a reliable representation of seismically isolated statues and provided a solid basis to further studies and to design seismic isolation intervention based on DCCSS friction isolators.

5.3 Floor response spectra and seismic inputs at the higher floor

The generation of floor seismic accelerogram and floor response spectrum is a challenging problem, which has to be dealt with due to the mutual interaction of the two systems, i.e. the structure of the building and the object at the floor, with different dynamic behaviour..

To obtain the value of the seismic action (expressed in acceleration and displacement), both simplified and more accurate approaches are followed. In particular seismic acceleration and displacement are calculated according to the simplified approach given in NTC 2008/EC8, and Lagomarsino (2014)/CNR-DT 212/2013, and to the more accurate non-linear time history analyses.

Concerning this last issue the choice of a spectrum compatible set of seismic accelerograms need a deep study due to the implementation of seismic isolation system, as the one designed for the Bust of Francesco I. Given that no specific prescriptions are reported in NCT 2008 or EC8 about the spectrum compatibility requirements in case of isolated systems which are located at upper floors of a non-isolated structure, two different ranges of periods are chosen: the first considers only the prescription given by the Technical Standards about the building and results in a narrow range, the second is obtained by considering also the presence of the seismic isolation system and results in a much wider range of periods. With the ground floor seismic action, several time histories analyses are performed and results in terms of acceleration and displacement time histories are extracted.

To this aim, concerning the case study, an appropriate model of the structure of *Palazzo dei Musei* was carefully created, taking in consideration the particular condition of the building in terms of boundary conditions and uncertainties in the material characterization. To overtake this problem, the substructure of *Palazzo dei Musei* in which the Bust of Francesco I is hosted, was analysed with different boundary conditions and different stiffness levels. The observation of the ripened results highlighted two possible limit behaviours: stiff (*STIFF*) and deformable (*DEF*).

Finally, with the acceleration obtained from the time histories analyses, seismic floor spectra are evaluated for each of the aforementioned conditions: stiff and deformable

building, narrow and wide spectrum-compatible ground accelerograms. The given spectrum compatible accelerograms are also compared to the acceleration floor spectra given by NTC 2008/EC8 and the displacement floor spectra given by Lagormarsino (2014) and CNR-DT 212/2013.

5.4 Proposed methodology's assessment: the Case Study

The work presented in this thesis proposes a specific framework for seismic vulnerability assessment of art objects and the suitable design of a seismic mitigation intervention by means of DCCSS isolators. The proposed methodology is successfully applied to the Case Study of seismic isolation intervention for the Bust of Francesco I D'Este. In order to realize the intervention, all the four steps of the proposed framework are carried out: 1) knowledge path; 2) characterization of the seismic action of the site; 3) development of specific methods of analysis; 4) design of the suitable intervention for seismic protection. More in detail, for first phase, the correct assessment of the seismic vulnerability of the art object, the preliminary survey of the building and the object itself has been carried out. This crucial phase can be accomplished with different levels of accuracy. In this work the geometrical and inertial data of the bust are given by the elaboration of a huge photographic campaign with Autodesk 123D Catch software. This method proved to be adequate for the needs of this study, maintaining a proper level of accuracy without the computational efforts that a more complex laser scan survey could produce. The use of this software opens up to proficient applications in the field of conservation of cultural objects. For the building a highly accurate laser scan survey has been performed.
For the second phase, the characterization of the seismic action, three main data sources are considered:

- the seismic history, that considered ancient events;
- the registrations of the seismic events of May 2012, in particular in terms of acceleration.
- the normative prescriptions, expressed as seismic spectra and spectrum compatible accelerograms;

This study is thus very helpful to identify the conditions under which the artwork has been subject in the past, and the most likely seismic demand for future events.
In the third phase, with the data obtained from previous step, the vulnerability of the Bust is assessed, by comparing the seismic demand with the capacity of the object itself. In this regard, since the position of the statue at the second floor of *Palazzo dei Musei*, the

definition of specific analysis tools was needed. To this aim, the prescriptions given by NTC 2008, EC8, CNR-DT 212/2013 and Lagomarsino (2014) for the assessment of the amplification of the seismic demand of non-structural component with the height are profitably extended to the art objects and in particular to the case of the Bust of Francesco I D'Este. An examination of such prescriptions is performed, also with the help of numerical simulations. The amplification in terms of accelerations calculated by means of numerical simulations, in fact, underlined the shortcomings of the normative prescription, especially regarding the value of the maximum amplification obtained in correspondence of the principal vibration period of the building. Anyway, for the purpose of this work, since the period of the isolation system is placed far from the maximum amplification, the NTC 2008 and CNR Guidelines proved to be conservative solution for the assessment of seismic acceleration and displacement.

In the fourth phase of the framework, which regards the design of a specific mitigation intervention, specific design charts, based on linear analyses of the isolation system, are developed for *FIP Isolart*®, the DCCSS devices produced by *FIP Industriale*, and specifically devoted to match the stringent requirements of museum exhibition as the limitation on the maximum overall dimension.

The charts help the Designer of the isolation intervention to determine the values of R_{eq} and d_{bd} to be adopted for the device, while matching also an adequate level of seismic protection in terms of tolerated transmitted acceleration. The designed devices are then validated with experimental tests (aimed to the assessment of the friction coefficient), and non-linear numerical simulations (aimed to control the correspondence with the linear analyses).

It is believed that the outcomes of this research may be successfully extended to a wide variety of art objects, aiming to correctly assess the seismic vulnerability of the artistic assets and proposing suitable mitigation interventions.

6 References

Abaqus http://www.3ds.com/products-services/simulia/products/abaqus/

Advances in the Protection of Museum Collections from Earthquake Damage, Symposium Held at the J. Paul Getty Museum at the Villa on May, Editor: Jerry Podany, J. Paul Getty Trust Publications, May 2008.

Agbabian M.S., Ginell W.S., Masri S.F., Nigbor R.L.. Evaluation of earthquake damage mitigation methods for museum objects, Studies in conservation, 36 (1991), 111-120

Ansys http://www.ansys.com/

Applied Technology Council. Tentative provisions for the development of seismic regulations for buildings. Report No. ATC3-06, Applied Technology Council, Palo Alto, CA, 1978

Augusti G., Ciampoli M. (1996) Guidelines for Protection of Museum Contents, in Proceedings of 11th World Conference on Earthquake Engineering, Acapulco, Messico, Giugno 1996, Paper No. 1668 (CD-ROM)

Autodesk 123D http://www.123dapp.com/

Baggio S., Berto L., Favaretto T., Saetta A. (2013) Mitigazione del rischio sismico per beni artistici mobili: un sistema di isolamento sismico. In Proceedings of XV convegno ANIDIS. L'ingegneria Sismica in Italia, Padova, 30 June - 4 July 2013.

Baggio, S., Berto, L, Favaretto, T., Saetta, A., Vitaliani, R. (2015a). Seismic isolation technique of marble sculptures at the Accademia Gallery in Florence: numerical calibration and simulation modelling, Bull. of Earth. Eng., 13(9): 2719-2744

Baggio, S., Berto, L., Castellano, M.G., Faccio, P., Marcolin, L., Infanti, S., Rocca, I., Saetta, A. (2015b). Seismic vulnerability and risk reduction interventions for art goods: the bust of Francesco I d'Este in Modena. In Proc. ANIDIS Conference L'Ingegneria Sismica in Italia, L'Aquila, Italy.

Berto L., Faccio P., Fain E., Saetta A. (2011a) Valutazione del Rischio Sismico di Beni Mobili. In Proceedings of XIV convegno ANIDIS. L'ingegneria Sismica in Italia, Bari: digilabs, 2011.September 18 - 22

Berto L., Favaretto T., Saetta A. (2011b) Seismic Vulnerability of art objects: Statues of the Galleria dei Prigioni - Galleria dell'accademia of Firenze. In Proceedings of XIV convegno ANIDIS. L'ingegneria Sismica in Italia, Bari: digilabs, 2011. September, 18 - 22.

Berto L., Favaretto T., Saetta A., Antonelli F., Lazzarini L. (2012) Assessment of seismic vulnerability of art objects: The "Galleria dei Prigioni" sculptures at the Accademia Gallery in Florence. Journal of Cultural Heritage, Volume 13, Issue 1, pp. 7–21.

Berto L., Favaretto T., Saetta A. (2013) Seismic risk mitigation technique for art objects: experimental evaluation and numerical modeling of double concave curved surface sliders, Bulletin of Earthquake Engineering, Volume 11, Issue 5, pp 1817-1840

Bommer JJ, Ruggeri C, (2002), The specification of acceleration time-histories in seismic design codes, *European Earthquake Engineering*, Vol: 16, Pages: 3-17, ISSN: 0394-5103

Bommer J.J., Elnashai A.S., Weir A.G., Compatible acceleration and displacement spectra for seismic design codes. In: Proceedings of the Twelfth World Conference on Earthquake Engineering, 2000 Auckland, Paper No. 207

Caliò I., Marletta M. (2004) On the Mitigation of Seismic Risk of Art Objects: Case Studies. In proceedings 13th World Conference on Earthquake Engineering, Vancouver, (Canada), August 1-6. Paper no. 2828

Calvi G.M., Convegno: "Sisma ed elementi non strutturali – Approcci, Stati Limite e Verifiche Prestazionali" – S.A.I.E. – Bologna, 2014

C.A.S.E., (2010) L'Aquila: Il progetto C.A.S.E., Pavia: IUSS Press.

Castellano, M.G. & Infanti, S. 2010. Seismic Isolation of Buildings in Italy with Double Concave Curved Surface Sliders. In Proc. 14th European Conference on Earthquake Engineering, Ohrid, FYROM.

Castellano M.G., Pigouni AE, Marcolin L, Infanti S, Baggio S, Berto L, Faccio P, Rocca I, Saetta A (2016). Testing of the seismic isolation system for the bust of Francesco I d'Este in Modena, Italy. In Proceedings: SACH 2016

CEN, European Standard EN 15129:2009 – E Anti-seismic devices, Bruxelles, November 2009.

Chen, Y., Soong, T.T. (1988). State-of-the-art-review: Seismic response of secondary systems. Engineering Structure, 10, 218-228.

Cheng F. Y., Jiang H., Lou K. (2008) Smart Structures: Innovative Systems for Seismic Response Control. CRC Press, Taylor and Francis.

CNR-DT 212/2013 "Istruzioni per la Valutazione Affidabilistica della Sicurezza Sismica di Edifici Esistenti", in Italian

Constantinou M., Mokha A., Reinhorn A. (1990) Teflon Bearings in Base Isolation Part II: Modeling. Journal of Structural Engineering, 116(2), pp. 455–474

D.P.C.M. 2011 Direttiva Presidenza del Consiglio dei Ministri 12 ottobre 2007 per la valutazione e riduzione del rischio sismico del patrimonio culturale tutelato, S.O. n. 25 alla G.U. n. 24 del 29 gennaio 2008, update 9 febbraio 2011, (GU n. 47 del 26.02.11)

Earthquake Protection Systems Inc. (2003) Technical Characteristics of Friction Pendulum Bearings. http://www.earthquakeprotection.com/TechnicalCharacteristicsofFPBearngs.pdf.

EN 1998-1:2004 Eurocode 8: Design of structures for earthquake resistance. Part 1-1: General rules – Seismic actions and general requirements for structures

Favaretto T. (2012) Assessment and reduction of seismic vulnerability of art objects. Dissertation. Università di Firenze, T.U. Braunschweig

Fenz D., Constantinou M. (2006) Behaviour of the double concave Friction Pendulum bearing. Earthquake Engineering and Structural Dynamics, Issue 35. 1403–1424

Forni M., Martelli A., Indirli M. (2003) Seismic isolation and other seismic vibrations control techniques of structures in Europe. In proceedings Fourth International Conference of Earthquake Engineering and Seismology 12-14 May 2003 Tehran, Islamic Republic of Iran.

Gasparini D. A., Vanmarcke E. H., "Simulated earthquakes compatible with prescribed response spectra", Massachusetts Institute of Technology, Publication No. R76-4, Cambridge, Massachusetts, January 1976.

Housner W.G., The behaviour of inverted pendulum structures during earthquake, Bull. Seismol. Soc. Amer., 53 (1963), 403-417

Iervolino I. and Cornell C. A. (2005) Record Selection for Nonlinear Seismic Analysis of Structures. Earthquake Spectra: August 2005, Vol. 21, No. 3, pp. 685-713.

Iervolino I., Maddaloni G., Cosenza E., (2009) A Note on Selection of Time-Histories for Seismic Analysis of Bridges in Eurocode 8, Journal Earthquake Eng. 13(8):1125-1152

Iervolino I., Galasso C., Cosenza E., (2010) REXEL: computer aided record selection for code-based seismic structural analysis, Bull. Earthquake Eng. 8 (2) 339–362.

Infanti S., Benzoni G., Castellano M. (2011) Dynamic testing of Double Concave curved surface sliders. In proceedings 7th World Congress on Joints, Bearings and Seismic Systems for Concrete Structures, Las Vegas, Nevada October 2-6, 2011.

Infanti, S., De Toni, S., Pigouni A.E. (2015). Dynamic Testing Protocols for Seismic Protection Devices: Challenges for Test Facilities. In Proc. 14th World Conf. on Seismic Isolation, Energy Dissipation and Active Vibration Control of Structures, San Diego, USA.

INGV National Institute for Geophysics and Volcanology, http://esse1-gis.mi.ingv.it/

Ishiyama Y., Motion of rigid bodies and criteria for overturning by earthquake excitations, Earthq.Eng. Struct. Dyn, 10, 5 (1982), 630-650

ISIDe – Italian Seismological Instrumental and parametric Database – ISIDe working group (2016) version 1.0, DOI: 10.13127/ISIDe (http://iside.rm.ingv.it/)

ITACA 2.0 (http://itaca.mi.ingv.it; Luzi et al., 2008; Pacor et al., 2011)

Koumousis V.K., Design of the Seismic Isolation System for the Statue of Hermes at the New Museum of Olympia, in: Proceedings of 10th World Conference on Seismic Isolation, Energy Dissipation and Active Vibrations Control of Structures, Istanbul, Turkey, May 28-31, 2007.

Lagomarsino S. (2014), Seismic Assessment of rocking masonry structures, Bull. Earthquake Eng. 8(2) 339-362

Lam, N., J. Wilson, G Hutshinson (2000). Generation of synthetic accelerograms using seismological modelling: a review. Journal of Earthquake Engineering 4(3), 321-354

Lowry M., Armendariz D., Farra, B. J., Podany J. (2008) Seismic Mount Making: A Review of the Protection of Objects in the J. Paul Getty Museum from Earthquake Damage. In: Advances in the Protection of Museum Collections from Earthquake Damage, Symposium Held at the J. Paul Getty Museum at the Villa on May3-4, 2006. Los Angeles: J. Paul Getty Museum Trust.

Matteini M., Exploring David. Diagnostic tests and state of conservation, Ed. Giunti, Firenze, 2004.

Midas GEN. User's Guide, Getting Started & Tutorials

midas GEN (2015) Ver. 1.2 Integrated solution system for buildings and general structures, MIDAS Information Technology, Co., Ltd. http://www.MidasUser.com

Mokha, A., Constantinou, M., Reinhorn, A., and Zayas, V. (1991). ”Experimental Study of Friction-Pendulum Isolation System.” *J. Struct. Eng.*, 117(4), 1201–1217.

Naeim, F. and Lew, M., (1995), On the Use of Design Spectrum Compatible Time Histories, Earthquake Spectra, Vol. 11, 1, EERI, Feb.

Naeim F., Kelly J. (1999) Design of Seismic isolated Structures: from theory to practice. John Wiley and Sons, Inc.

National Institute for Geophysics and Volcanology (INGV), http://esse1-gis.mi.ingv.it/

NTC 2008: Norme Tecniche per le Costruzioni, D.M. 14/1/2008, SO n.30 G.U. n.29 del 4/2/2008

O.P.C.M. 3274 Ordinanza Presidenza del Consiglio dei Ministri 3274 del 20/03/2003 – Primi elementi in materia di criteri generali per la classificazione sismica del territorio nazionale e di normative tecniche per le costruzioni in zona sismica

Rhinoceros®, 3-D modeling software, developed by Robert McNeel & Associates

Seismosignal http://www.seismosoft.com/seismosignal

Shenton H.W., Criteria for initiation of slide, rock, slide-rock rigid-body modes, J. Engrg Mech ASCE, 122(7) (1996) 690-693

SIMQKE_GR http://gelfi.unibs.it/software/simqke/simqke_gr.htm

Tsai C., Chiang T., Chen B. (2005) Experimental evaluation of piecewise exact solution for predicting seismic responses of spherical sliding type isolated structures. Earthquake Engineering and Structural Dynamics, Issue 34, pp. 1027-1046.

Yim C.S., Chopra A., Penzien J., Rocking response of rigid blocks to earthquakes, Earthq. Eng. Struct. Dyn. 8 (1980), 565-587

Zayas, V., Low, S., and Mahin, S. (1987). "The FPS system: Experimental report." Report No. UCB/EERC-87-O1, Earthquake Engr. Res. Ctr., Berkeley, Calif.

Zayas, V., Low, S., Bozzo, L., and Mahin, S. (1989). "Feasibility and performance studies on improving the earthquake resistance of buildings using the friction pendulum system." Report No. UCB/EERC-89-09, Earthquake Engrg. Res. Ctr., Berkeley, Calif.